Mathematical Engineering

Ahmer Mehmood

Viscous Flows

Stretching and Shrinking of Surfaces

Springer

Mathematical Engineering

Series editors

Today, the development of high-tech systems is unthinkable without mathematical modeling and analysis of system behavior. As such, many fields in the modern engineering sciences (e.g. control engineering, communications engineering, mechanical engineering, and robotics) call for sophisticated mathematical methods in order to solve the tasks at hand.

The series Mathematical Engineering presents new or heretofore little-known methods to support engineers in finding suitable answers to their questions, presenting those methods in such manner as to make them ideally comprehensible and applicable in practice.

Therefore, the primary focus is—without neglecting mathematical accuracy—on comprehensibility and real-world applicability.

To submit a proposal or request further information, please use the PDF Proposal Form or contact directly: *Dr. Jan-Philip Schmidt, Publishing Editor (jan-philip.schmidt@springer.com)*.

More information about this series at http://www.springer.com/series/8445

Ahmer Mehmood

Viscous Flows

Stretching and Shrinking of Surfaces

Springer

Ahmer Mehmood
Mathematics and Statistics
International Islamic University Islamabad
(IIUI)
Islamabad
Pakistan

ISSN 2192-4732 ISSN 2192-4740 (electronic)
Mathematical Engineering
ISBN 978-3-319-55431-0 ISBN 978-3-319-55432-7 (eBook)
DOI 10.1007/978-3-319-55432-7

Library of Congress Control Number: 2017936904

Printed on acid-free paper

This Springer imprint is published by Springer Nature
The registered company is Springer International Publishing AG
The registered company address is: Gewerbestrasse 11, 6330 Cham, Switzerland

To my respected Parents and beloved Family

Preface

The boundary-layer flow past bodies of finite lengths has a long history as old as the concept of boundary-layer itself. Such kind of flows had completely been explored till the completion of first fifty years of the boundary-layer theory. In contrast, the boundary-layer flow due to moving continuous surfaces was first introduced in 1961, almost six decades later to the idea of boundary-layer. Besides the interesting nature of this flow, it has so far not been explored in complete. Even the two-dimensional self-similar case of this flow cannot be claimed to be fully explored and understood, despite the presence of hundreds of published research papers on this flow. The biggest misfortune with this flow is that it had never been studied completely; rather, the developments on this flow had been contributed in bits. The situation is far worse in the cases of axisymmetric and three-dimensional flows of this class. Only the self-similar laminar flows of this type have so far been investigated in literature, and no attention has been given to the non-similar and turbulent flows at all.

A critical review of the published literature on this topic reveals the presence of huge number of those published research papers which do involve incorrect and misleading analyses. Unfortunately, after getting published, such researches become an authentic reference regarding the further propagation and justification of such misleading erroneous analyses. In this way, the research on this topic has, by a lot, went rotten because of the publication of huge number of erroneous research papers. Unfortunately, the published wrong results are immediately adopted by the others instead of correcting them. In such a messy situation, it is really quite hard to correct all such erroneous literature by making all the audience aware of such mistakes.

A thorough review of the available literature on this topic concludes that the majority of the errors have arose due to the incorrect self-similar formulation of the governing systems; examples can be given of the problems concerning shrinking surfaces or those involving local parameters in the governing equations. Therefore, it seems that if the concept of self-similarity could be explained in detail and the construction of self-similar variables of these flows could be made available, then the errors are expected to be minimized to an appreciable extent. Such an

elaboration can further be expected to be helpful to the researchers in the exploration of further self-similar flows of this class.

After having a realization of the above facts, the author had continuously been worried, since last few years, regarding the correction of aforementioned incorrect analyses. Writing a correction or comment to every such paper was, however, quite inconvenient in this regard. Finally, it was decided to identify the root causes of such incorrect analyses and the way out toward their correction and to report this all in the form of a book at once. In this regard, the incomplete understanding of the self-similarity was identified to be the major root cause behind all such incorrect analyses, at the most, as pointed out in the above paragraph. In view of these facts, the primary objective of this book is threefold: first, to elaborate the general criterion of self-similarity by reporting the general self-similarity criterion for the planar and the axisymmetric cases; second, the presentation of correct shrinking surface flow analysis which could negate most of the "mysterious" facts associated with this flow; and third, to introduce the non-similar flows of this class in the said two cases, namely the planar and the axisymmetric ones. In this regard, the self-similarity criterion for this class of flows has completely been determined and the associated self-similar governing systems have been developed. Correct self-similar formulation of the shrinking sheet flow has been reported, and the self-similar shrinking sheet flow has been discussed in detail. A comparison between the current and the already existing formulations has been made in order to clarify the situation. The non-similar flows of this class have been formulated in general; some particularly chosen non-similar flows in the planar and axisymmetric cases have also been discussed. The identification of temporal self-similarity and the criterion of semi-similarity have been included. Finally, the turbulent flow due to stretching surfaces has also been considered.

Fundamental knowledge of fluid mechanics and the boundary-layer theory is essential for the understanding of the presented material. This book particularly focuses the students and the initial researchers in this field. Therefore, the presentation of the material is quite straightforward with a bit detail and sufficient explanation. However, the presented material is also expected to be of equal importance for the specialized and established researchers in this field.

This book has mainly been distributed into four major parts. The first part includes some fundamental essential knowledge and the explanation of the concept of self-similarity. Part II contains the self-similar flows due to moving continuous surfaces including the planar and axisymmetric flows. Spatial and temporal non-similarity has been modeled in Part III, whereas the turbulent flows due to moving continuous surfaces have been considered in Part IV.

First four chapters constitute the Part I of this book. Boundary-layer character of the flows due to moving continuous surfaces has been explained in Chap. 1. The governing boundary-layer equations and the momentum integral equations corresponding to the planar and axisymmetric flows have been developed in Chap. 2. The concept and restrictions of self-similarity have been explained in detail in Chap. 3, whereas an introduction to the suitable solution techniques has been given in Chap. 4. The criterion of self-similarity for the wall velocities has been

determined in detail for both the planar and axisymmetric flows in Chap. 5. Flows due to stretching and shrinking surfaces have been discussed in Chaps. 6 and 7, respectively. The restriction on the wall suction/injection velocities and on the variable thickness of the continuous surfaces, in view of self-similarity criterion determined in Chap. 5, has also been determined in these chapters. Similarity criterion of the unsteady flows due to moving continuous surfaces has been derived in Chap. 8. The aforementioned Chaps. 5–8 have been included in Part II. Non-similar flows due to moving continuous surfaces have been introduced in Part III consisting of Chaps. 9–11. The planar and axisymmetric non-similar flows have been considered in Chaps. 9 and 10, respectively, whereas the temporal non-similarity has been considered in Chap. 11. The Part IV includes only one chapter (Chap. 12) concerning the turbulent flow due to moving and stretching continuous surfaces.

Islamabad, Pakistan Ahmer Mehmood

Acknowledgements

Ultimate thanks are to the ALLAH almighty, the source of all knowledge and the creator of the universe in a great systematic way. Thanks are also due to the Holy Prophet Muhammad (PBUH) who introduced the God to the humanity and always prayed for the growth of knowledge. Because of his introduction to God, it became possible for me to realize the creative powers of God whenever I understood any complex flow phenomena, more especially the boundary-layer mechanism or the shock-wave phenomena.

The successful completion of this book was never ever possible without diverse contributions of several kind people. The first major contribution toward the completion of this book is due to Mr. Usman who had continuously been assisting me in multiple manners. Majority of the graphs and tables have been produced by him in addition to the manuscript typing. His pleasant company, utmost availability, and sincere support are highly acknowledged. I am also highly indebted to Prof. Weigand for motivating me to write this book. His keen interest in the topic and the contents of the book and continuous support are sincerely admitted. Kind cooperation of Dr. Munawar is also greatly acknowledged regarding the production of some figures of Chap. 11.

Kind support from the Department of Mathematics and Statistics and hence from the International Islamic University, Islamabad (IIUI) is also acknowledged. I am thankful to the President (IIUI) for relaxing my official workload for one semester. Fruitful efforts by the Chairman (Maths & Stats) and the Dean (FBAS) in this regard are highly acknowledged. Sincere support and great appreciation from the department colleagues can never be forgotten and are sincerely admired.

At last but never the least, I am very much thankful to my parents and my family for everything. Selfless prayers and best wishes from my parents had always been a source of success of mine in every aspect of my life. Just before receiving the proofs of this book my father passed away; May his soul rest in heaven. Long sittings at the department and continuous work on the weekends made my family to suffer a lot. In this regard, my wife really deserves praise for managing the home and the children during my every day absence. I am really thankful to her for her

understanding and great support throughout this project. Love is due to the little Hassan and Fatima who had always been waiting for my return even till late at night. May they grow well and become noble personalities.

In addition to this all, there are definitely several other people who deserve formal acknowledgement but could not be named individually. I am thankful to all those whoever supported me in this project, either directly or indirectly. I am also thankful to my brothers and sisters and my in-laws for their moral support.

January 2017 Ahmer Mehmood
Islamabad

Contents

List of Figures

List of Tables

Introduction

The history of fluid mechanics is as old as the history of human beings. Every human in his life solves so many fluid mechanics problems whether consciously or unconsciously. But the manner he solves his daily life problems, such as dissolving sugar in the cup of tea by stirring a spoon in it or blowing the lump of hot food before taking it to mouth, is exactly in accordance with the scientific laws of fluid mechanics in convective phenomena. Similar examples can also be found in the Stone Age era when man had been using long, slim, and even fin-stabilized arrows for hunting the animals and birds. His understanding about the water flow from high level to low, in the process of irrigation, is also an example of utilizing the potential energy of water to make it to flow. Numerous similar examples can further be found from the practices of present and the history of ancient man where the above constitute only a few glimpses from it. Thus, the unconscious understanding of the human about the fluid flow and heat and mass transfer phenomena continuously turned into his conscious efforts toward the scientific exploration of the flow phenomena because of his day by day increasing problems of fluid mechanics.

The first, on the record, scientific theory in fluid mechanics is due to the Archimedes in which he presented his research as postulates of buoyancy. The viscous resistance in fluids was scientifically interpreted by Sir Isaac Newton in 1687 when he stated his famous law of viscosity. The law of fluid motion was first proposed by Daniel Bernoulli in 1730 and was further improved by Leonhard Euler in 1755. It is important to note that although the Newton's law of viscosity was discovered in 1687 and the Bernoulli's equation, after Euler's modification, in 1755, but they intentionally ignored the fluid friction. The fluid friction was taken into account by Navier and Stokes independently where they introduced the viscous terms to the equation of motion in 1827 and 1845, respectively. Consequently, the resulting equations were named as Navier–Stokes equations and are still recognized by this name. These equations are equally applicable to gasses and liquids following the Newton's law of viscosity. Later, the Osborn Reynolds distinguished the viscous flows into two categories on the basis of velocity magnitude. However, he also explored that this differentiation does not depend strictly upon the fluid velocity only but obviously upon the viscosity of fluid and the pipe radius also.

On the basis of this argument, he developed the famous *Reynolds number* which has great practical importance in laminar and turbulent flows having velocities less than the speed of sound.

In 1749, a French mathematician Jean le Rond D'Alembert, while working on the flow drag on a solid surface, concluded that "it seems to me that the theory (potential flow), developed in all possible rigor, gives, at least in several cases, a strictly vanishing resistance, a singular paradox which I leave to future Geometers (i.e., mathematicians—the two terms were used interchangeably at that time) to elucidate." On the other hand, the experimental results reflected significant viscous drag for the flows in water and air at that time. Based on the failure of the theory regarding the prediction of viscous drag, D'Alembert stated his results in the form of a famous paradox in 1752 which stayed unresolved till the year 1904. The D'Alembert's paradox states that "for incompressible and inviscid potential flow—the drag force is zero on a body moving with constant velocity relative to the fluid." At this stage, the reader is asked to realize that the D' Alembert's paradox stayed unresolved even after the development of the Navier–Stokes equations which completely incorporate the contribution of viscous forces to the momentum transport equation. The misfortune with the D'Alembert and the other scientists of that time was that they used to ignore the "little" air friction in the theoretical calculations causing them to reach the wrong conclusion of zero drag. On the other hand, such "little" air friction was impossible to be ignored in the experiments where it kept on resulting in significant viscous drag. This fact was actually realized by Ludwigs Prandtl, in his series of experiments, that in such flows, with less friction, the viscous effects are negligible in most of the flow domain but are in-ignorable in a very thin region near the solid surface. This observation made him able to split the entire flow domain into two major parts: a potential flow region where there is no flow resistance at all and the near wall region where the effects of viscous resistance are prominent. He called this thin region as the *thin shear layer* or the *boundary-layer*. This thin, near wall, region was actually being ignored by the previous scientists, thus preventing them to reach the correct results. The development of a concrete theory for the accommodation of this fact was another difficult step for which Prandtl himself introduced the order of magnitude analysis. He calculated the magnitude of every term in the Navier–Stokes equations and identified the contributing/surviving and vanishing/ignorable terms. The process is strictly based on his clear understanding of exact nature of the flow within the boundary-layer. This theory revealed that most of the terms in viscous part of the Navier–Stokes equation are ignorable, as did by the previous scientists, but not the all. Thus, the identification of surviving and non-surviving terms does mainly based on the order of magnitude analysis which is actually due to the Ludwigs Prandtl.

Before Prandtl, there were two divergent branches of fluid dynamics, namely the theoretical *hydrodynamics* and the *hydraulics*. In the era of D'Alembert, it was misbelieved that the theoretical hydrodynamics does not apply to many practical situations, such as air or water flows, where the viscous drag does play important role in actual. On this basis, the engineers of that time started developing their own

theory based largely on the experimental data in order to meet the rapidly increasing technological demands and named their new theory as *hydraulics*. In the Prandtl's era, the theory of hydraulics was also so developed having nothing common with the theoretical hydrodynamics. Prandtl therefore also has a credit of joining these two important branches of fluid mechanics due to his famous theory of boundary-layers. Due to this theory, it became possible to investigate, theoretically, the viscous flow involving very small friction where the obtained results do match sufficiently with the experiment. After the introduction of this theory, it was further developed very rapidly, initially by the people at Göttingen and later on worldwide. It then quickly became a solid foundation for the modern fluid dynamics which also gave birth to the two new and important branches of fluid dynamics the *aerodynamics* and the *gas dynamics*. Furthermore, the development in these modern areas created a gap for another intelligent branch of fluid dynamics which is known as the *computational fluid dynamics*. This all has happened in the last eleven decades which has raised the man from the pedestrian stage to the hypersonic speeds, where the Prandtl kept on standing behind all this development.

Immediate after the introduction of Prandtl's theory of boundary-layers, there were huge things to be done, several questions to be answered, many levels to be attained, and hence a long way to go. The complete understanding of flow behavior within the boundary-layer was the first task for which the simple flows were the ultimate choice. The first test case, in this regard, was the two-dimensional boundary-layer flow which was considered by Hartman Blasius under the supervision of Ludwigs Prandtl. Later on, the two-dimensional Blasius flow was extended to the self-similar wedge flow by Falkner and Skan. Further extension to the three-dimensional and axisymmetric flows was done by several other renowned researchers of the time. Among these flows, the flat plate boundary-layers had been given great attention by the subsequent researchers and almost all (eventually not all) related flows have been studied in detail for this case. Most importantly, the classification of similar and non-similar flows has been done, and interesting non-similar flows have also been studied in detail by the pioneers of the time. Example can be given of Howarth's retarded flow where the calculation of separation had been the major issue. Interestingly, all such flows, either self-similar or non-similar, have only been studied in the cases where the external potential flow was assumed to be essentially there whether the solid surface stays stationary or continues to move. In all such investigations, the other way situation had completely been ignored where the solid surface moves in a static fluid. This flow was first modeled by Sakiadis for the two-dimensional and axisymmetric cases and was solved subsequently by Sakiadis himself in a series of two famous papers. In his flow problem, Sakiadis assumed a continuous solid surface of infinite length moving uniformly through a fluid at rest, just opposite to the Blasius flow in the sense that in the Blasius flow the fluid moves and the plate stays at rest. In his analysis, Sakiadis found that in comparison with the Blasius flow the viscous drag is larger in this case and other physical parameters of boundary-layer flow such as the momentum thickness and the displacement thickness did also differ from the Blasius flow. Finally, he concluded that the boundary-layers due to the moving

continuous surfaces are entirely different from those of Blasius-type flows and are therefore required to be investigated independently because the Blasius solution does not apply there. Similar to Blasius flow, self-similar solution also exists for the Sakiadis flow. Sakiadis designated such flows as the *viscous flows due to moving continuous surfaces*.

After Sakiadis, self-similar solution to this problem was further extended by Crane and Banks to the cases when the wall velocity varies linearly or obeys the power-law profile, respectively. Magyari and Keller extended the Sakiadis flow for the case of exponential wall velocity. These flows are usually categorized as the stretching sheet flows in literature. They contribute another interesting class of viscous flows, commonly known as the shrinking sheet flows, when the stretching wall velocity is reversed in direction by multiplying it by -1. The self-similar solutions to the moving plate boundary-layer equations have almost been explored completely for the two-dimensional case. However, very little is known about the three-dimensional and axisymmetric cases, to the best of our knowledge. Furthermore, non-similar flows due to moving continuous surfaces are also very rare in the three cases such as the two-dimensional, three-dimensional, and axisymmetric flows. Therefore, in comparison with the finite surfaces, the viscous flows due to moving continuous surfaces have not been explored completely and require proper consideration.

With the availability of this huge gap in literature, we take the privilege to fill it, to some extent, by giving general criterion for the self-similarity and non-similarity in view of the necessary conditions on the wall profiles in all the aforementioned cases. In this book, we derive completely (in a sense, see Chaps. 3 and 5) the wall velocity profiles for which the self-similar solutions are possible in two-dimensional, three-dimensional, and axisymmetric cases. The related similarity transformations and hence the transformed similarity boundary-layer equations have also been derived in detail. It is concluded (with some exceptions, see Chaps. 3 and 5) that all the wall velocities other than the derived ones, for the similarity solution, make the flow non-similar. The non-similar flow equations have in general been developed, and some selected non-similar flows have also been discussed in this book. This all above is concerned with the laminar flows only. Turbulent flow equations for three-dimensional and axisymmetric cases have also been developed in integral form. Two-dimensional and axisymmetric turbulent flows due to moving or linearly stretching continuous surfaces have been investigated theoretically.

In addition to the stretching surface flows, the flows due to shrinking surfaces are also very popular among the researchers in this field. However, this is very much unfortunate that all the literature concerning the shrinking sheet flow is incorrect because of the utilization of incorrect self-similar equations and the insufficient analysis. This mistake has trapped a large number of researchers who have contributed huge number of research papers to this topic within the last few years. The mistake in the existing self-similar modeling of this flow has been addressed in detail in Chap. 7 of this book. The wrong conclusions regarding the shrinking sheet flow have been disproved by presenting the correct self-similar modeling and

the correct analysis of shrinking sheet flow. The axially symmetric flow due to shrinking cylinder and shrinking disk is also included in the same chapter.

Scaling group of symmetries has been utilized in the derivation of similarity transformations and for the identification of similarity criterion in all the above-mentioned cases. With the particularly chosen group of scalings, it can be claimed that we have derived all the self-similar solutions, but this does not deny the existence of any other similarity solution (see Chaps. 3 and 5). Most of the newly modeled three-dimensional and axisymmetric flows have been left uninvestigated, for the subsequent researchers to explore, because the author finds it inconvenient for him to explore all of them in full detail. Particular cases from each class have, however, been investigated with sufficient detail.

In summary, the major purpose of this book is to present the criterion for self-similarity and non-similarity for the considered class of flows; the correction of incorrect shrinking sheet flows, the introduction of non-similar flows, the concept of self-similarity and non-similarity in the non-steady flows, and finally the consideration of turbulent flows due to moving continuous surfaces.

Part I
Essential Fundamental Material

Chapter 1
Viscous Flow Due to Moving Continuous Surfaces

Soon after the inception of boundary-layer concept, introduced by Prandtl [1], the first formal attempt toward the understanding of boundary-layer character was made by Blasius [2]. Blasius considered steady-state two-dimensional boundary-layer flow past a semi-infinite flat plate at zero incidence (see Fig. 1.1). He assumed a constant potential flow approaching the leading edge of the flat plate, with continued motion past the plate surface, and studied the flow within the so-formed boundary-layer at the plate surface. The Blasius equation was further investigated by Bairstow [3], Goldstein [4], Töpfer [5], Howarth [6], and Meksyn [7] under different circumstances. Experimental investigations, in order to confirm the theory, were conducted by Burgers [8], van der Hegge Zijnen [9], Hansen [10], and the Nikuradse [11]. The novelty of the idea and the curiosity of the flow character within the boundary-layer attracted several renowned scientists of the time who greatly contributed to the topic and raised the topic to the heights where it is seen today. A detailed account to this topic has been given in the glorious book by Schlichting [12] where all the major contributions have possibly been cited. The other important notable contributions to this topic are due to Goldstein [13], Rosenhead [14], and Batchelor [15] where huge fundamental knowledge has been gathered under one cover. The subject then went on developing day by day, but all the research concerning the flat-plate boundary-layers was limited to the situation when the fixed plate is attacked by a stream of potential flow, till 1961. In 1961, Sakiadis [16] introduced the viscous flow, owing the boundary-layer character caused due to the motion of a continuous solid surface within a quiescent fluid otherwise at rest.

The correct reasons for ignoring this flow, for a long time, are unknown to the author, but it seems that the pioneers of the boundary-layer theory had been more inclined toward the applications of boundary-layer theory in aerodynamics for the calculation of surface drag, in particular. In this perspective, the consideration of Blasius' like situation served as an appropriate theoretical model for the two-dimensional flow on the straight wing of an air craft and having great resemblance with the situation established in the wind tunnel experiments. The extension

A. Mehmood, *Viscous Flows*, Mathematical Engineering,
DOI 10.1007/978-3-319-55432-7_1

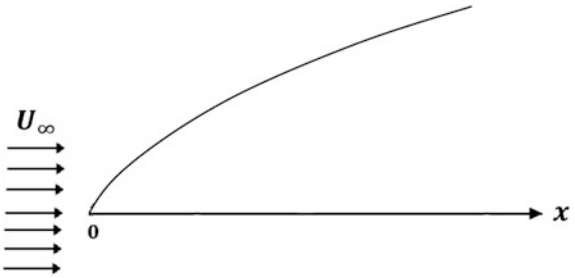

Fig. 1.1 Schematic of the Blasius flow

of the Blasius' model to the three-dimensional case applies to the situations when the potential flow attacks the swept-back wing, for example. With these sophisticated initiations, the development in the boundary-layer theory provided a very sound base to the modern aerodynamics. However, the theory of boundary-layers is not limited to the aerodynamic phenomena only but applies, in general, to every physical flow following the boundary-layer character. It is, sometimes, also misunderstood that the boundary-layer exists in the external flows only. This is, however, not the case; the boundary-layer is also formed in the internal flows such as in pipes and ducts, and also in the free surface flows, such as in free jets.

1.1 Sakiadis Flow

Let us consider the schematic of the Blasius flow once again (Fig. 1.1). Notice that the constant stream of potential flow attacks the leading edge and hence forms the boundary-layer starting right from the leading edge and growing downstream. In contrast, let us assume that the potential flow is absent and the plate moves with a constant velocity U_0 in the $-$ve x-direction as shown in Fig. 1.2.

In this case, as the plate continues to move, the fluid experiences disturbance right from the leading edge and is continuously being disturbed at the intermediate locations on the moving plate. The boundary-layer then develops in the direction of increasing x as the plate penetrates in the fluid in $-$x-direction. In this case too, the boundary-layer develops in the direction from the leading edge to the trailing edge, as shown in Fig. 1.2, similar to the Blasius flow. Therefore, the flow situations described in Figs. 1.1 and 1.2 can be regarded as equivalent where one can easily be transformed to the other by the use of simple Galilean transformations. In these two situations, the boundary-layer is actually formed due to the leading edge of the plate. Now the question arises: How the "moving plate boundary-layers" are different if the two flows, shown in Figs. 1.1 and 1.2, are the same? The answer is: when the moving surface moves in the $+$ ve x-direction instead of –ve x-direction having no edges. Then, the two flows are entirely different from each other, and it becomes impossible to recover one from the other. Such a situation exists in diverse practical applications; example can be given of polymer industry.

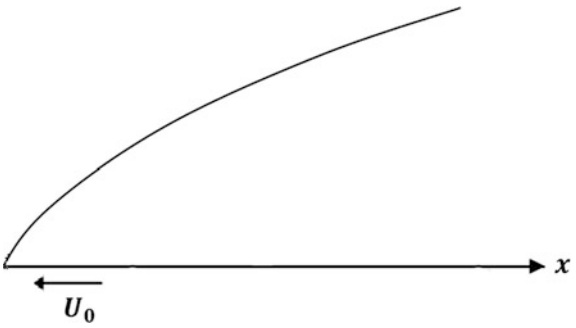

Fig. 1.2 Reverse of Blasius flow situation shown schematically

In the manufacturing of polymer sheets, the polymer melt issues continuously from a slit and travels a wind-up roll as shown in Fig. 1.3. In such a course of sliding past a wind-up roll, the sheet is, sometimes, also being stretched to attain the desired thickness and is cooled simultaneously. In order to obtain the final product of desired characteristic, the process of stretching and cooling requires to be controlled, which in turn gives rise to a fluid mechanics problem. Notice that, as the polymer sheet filament issues from the slit and travels downstream, the disturbance starts penetrating in the ambient fluid right from the slit and continues to grow subsequently downstream, hence forming the boundary-layer on the moving surface. This situation is also referred to as the "moving plate" in a fluid, but is quite different from the situation shown in Fig. 1.2 because of the absence of any leading edge. In such a senior the boundary-layer starts developing from the slit and grows in the direction of motion of the moving surface.

Unlike Fig. 1.2, the continued issuance of polymer filament from the slit provides the reason for the boundary-layer to develop downstream in the direction of motion of the moving sheet or the thread. Based on the similar reasoning, Sakiadis [16] introduced the boundary-layer flow due to a moving surface and essentially associated the word "continuous" as the prefix to the word "surface" just to clear the absence of any leading edge. With these assumptions, his equations of motion for two-dimensional flow due to a moving continuous surface are exactly the same as those of Blasius, i.e.,

$$\frac{\partial u}{\partial x} + \frac{\partial v}{\partial y} = 0, \tag{1.1a}$$

$$u\frac{\partial u}{\partial x} + v\frac{\partial u}{\partial y} = \nu\frac{\partial^2 u}{\partial y^2}, \tag{1.1b}$$

where the involved quantities bear their usual meanings. Like Blasius, Sakiadis was also lucky enough to get the self-similar solution for this flow. Fortunately, the self-similar formulation of Blasius is also applicable to this case and Eqs. (1.1a, 1.1b) readily transform to the Blasius equation in dimensionless form, given by

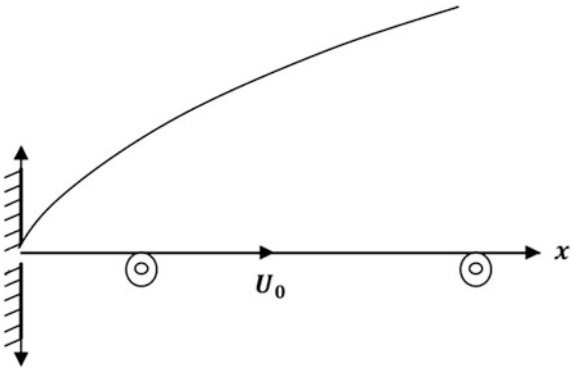

Fig. 1.3 Schematic of moving continuous sheet

$$\frac{1}{2}ff'' + f''' = 0, \tag{1.2}$$

where $\eta = \sqrt{\frac{U_0}{vx}}y$ and $f(\eta) = \frac{1}{\sqrt{vxU_0}}\psi(x,y)$ are the Blasius' similarity variables. However, the boundary conditions are entirely different in this case and read as

$$\left.\begin{array}{lll} \text{at } \eta = 0, & f = 0, & f' = 1 \\ \text{at } \eta = \infty, & & f' = 0 \end{array}\right\}, \tag{1.3}$$

which makes the Sakiadis flow sufficiently different from the Blasius flow admitting the boundary conditions of the form

$$\left.\begin{array}{lll} f = 0, & f' = 0, & \text{at } \eta = 0 \\ f' = 1, & & \text{at } \eta = \infty \end{array}\right\}. \tag{1.4}$$

Sakiadis [17, 18] showed that the moving (continuous) surface boundary-layers contribute a new class of boundary-layers where the results of finite (semi-infinite) plate boundary-layer flow do not apply anyway. After his name, the boundary-layer flow due to a moving continuous surface with a uniform speed is referred to as the Sakiadis flow. In the rest of the text, we shall not always write the word "continuous" but occasionally, and the flow due to a moving continuous surface will then be written as moving surface/plate boundary-layer flow.

1.2 Stretching Sheet Flow

Sakiadis considered constant wall velocity $u_w = U_0$ in [17] and [18] while discussing the two-dimensional and axially symmetric cases, respectively. However, the moving plate boundary-layers are not limited to the constant wall velocity only;

rather, one may also take the variable wall velocity, such as $u_w = u_w(x)$. The variable wall velocity of the solid surface is then interpreted as the stretching/shrinking wall velocity, depending upon the sign of $u_w(x)$.

1.2.1 Crane's Flow

This has already been mentioned, in the preface, that despite the novelty and interesting features of the Sakiadis flow, it stayed deprived almost for a decade and was not attracted by the renowned scientists of the time till 1970. Lawrence J. Crane [19] was the first who extended the Sakiadis flow of constant wall velocity to variable wall velocity by taking $u_w = u_w(x) = ax$, where a denotes the constant stretching rate having the dimension of T^{-1}. Crane utilized the same equation as by Sakiadis, namely Blasius' Eqs. (1.1a, 1.1b), and introduced the similarity variables of the form

$$\eta = \sqrt{\frac{a}{\nu}}y, \quad u = axf'(\eta), \quad v = -\sqrt{a\nu}f(\eta). \tag{1.5}$$

Consequently, his equation of motion in dimensionless form came out of the form

$$f''' + ff'' - f'^2 = 0, \tag{1.6}$$

subject to the boundary conditions (1.3). Equation (1.6) is totally different from Eq. (1.2), but is exactly the same as that of Falkner and Skan [20] for $m = 1$. Again the difference between the Crane's and Falkner–Skan flow is the boundary conditions (1.3) and (1.4). It is important to start noting the similarity between the Falkner–Skan and the moving sheet flow; the Sakiadis flow is governed by the Blasius' equation which is actually the Falkner–Skan equation (for $m = 0$), and the Crane's flow is also governed by the Falkner–Skan' equation (for $m = 1$). So far, the difference between the two flows, due to moving continuous surface and on the finite surface, is only due to the boundary conditions. Crane reported a closed form solution to his problem and calculated the heat transfer coefficient analytically.

1.2.2 Power-Law and Exponential Stretching Velocities

After Crane [19], thirteen more years of ignorance passed and the moving plate boundary-layers enjoyed no significant advancement. In 1983, Banks [21] introduced the power-law stretching velocity of the Falkner–Skan form $u_w = ax^m$ and reported similarity solution to this case. Banks utilized the similarity transformations of the form

$$\eta = \sqrt{\frac{a}{\nu}} x^{\frac{m-1}{2}} y, \quad u = a x^m f'(\eta), \quad v = -\sqrt{a\nu} x^{\frac{m-1}{2}} \left(\frac{m+1}{2} f + \frac{m-1}{2} \eta f' \right), \tag{1.7}$$

and transformed Eqs. (1.1a, 1.1b) to the form

$$f''' + \frac{m+1}{2} f f'' - m f'^2 = 0, \tag{1.8}$$

subject to the boundary conditions (1.3). Again, in this case too, self-similar Eq. (1.8) is the same as that of Falkner–Skan [20] for the potential flow $u_\infty(x) = ax^m$, but the only difference is of the boundary conditions. At this stage, it has now become clear that the two flows are governed by the same self-similar equation but own different boundary conditions. The similarity transformations applicable to the cases of finite surfaces are equally applicable to the corresponding cases of continuous surface flows. Later in 1999, Magyari and Keller [22] introduced the self-similar flow due to an exponentially stretching continuous surface. They assumed the wall velocity of the form $u_w = U_0 e^{\frac{x}{L}}$ and utilized the following similarity transformations

$$\eta = \left(\frac{Re_L}{2} \right)^{1/2} \frac{y}{L} e^{x/2L}, \quad u = U_0 e^{x/L} f'(\eta), \quad v = -\frac{\nu}{L} \left(\frac{Re_L}{2} \right)^{1/2} e^{x/2L} (f + \eta f'), \tag{1.9}$$

to reduce Eqs. (1.1a, 1.1b) to the self-similar form

$$f''' + f f'' - 2 f'^2 = 0. \tag{1.10}$$

In addition to the two-dimensional case, the axially symmetric and the three-dimensional cases regarding the boundary-layer flow on continuous surfaces have also been reported in the literature. The axially symmetric case includes the flow due to a uniformly moving/stretching cylinder [18, 23] and uniformly stretching circular flat disk [24]. The credit of stretching disk case also goes, indirectly, to Crane who extended the idea of stretching surface flow to the axisymmetric case in 1975. The three-dimensional flow due to a stretching sheet has been investigated by stretching the sheet uniformly [25] or exponentially [26] in the two lateral directions. The case of three-dimensional flow due to linear bilateral stretching of the sheet was considered by Wang [25] in 1984, whereas the exponential form of stretching wall velocity, in three-dimensional flow, was considered by Liu et al. [26] in 2013.[1]

[1]However, the author is not sure if the three-dimensional flow due to exponentially stretching sheet was actually first introduced by [26].

In second part of this book, it will be shown that the two-dimensional case of stretching sheet flow has almost been explored completely,[2] in the existing literature, with some deficiency in the exponential stretching case. However, a very little has been done for the axially symmetric and three-dimensional cases and a big class of self-similar solutions associated with these cases is yet unexplored. The complete[3] self-similar criterion for the three cases, namely the two-dimensional, three-dimensional and axially symmetric flows, has been derived in detail in Chap. 5.

1.3 Shrinking Sheet Flow

In addition to the stretching sheet flows, there is another important, perhaps, interesting class of self-similar flows which is commonly referred to as the shrinking sheet flows. These flows correspond to the situations when the stretching wall velocity (discussed in the previous section) is given the '–ve' sign. Such a shrinking sheet flow was first introduced by Miklavcic and Wang [27] in 2006 where they assumed the wall velocities of the form

$$u = -ax, \quad v = -a(M-1)y, \tag{1.11}$$

with $a > 0$ for a steady three-dimensional flow due to bilateral motion (shrinking) of the flexible sheet and M being 0 or 1. For this flow, they developed the self-similar momentum equation of the form

$$f''' + Mff'' - f'^2 = 0, \tag{1.12}$$

which is the same as for the corresponding stretching sheet flow, but the only difference arose in the boundary conditions: For this case, they obtained $f'(0) = -1$ instead of $f'(0) = 1$ and the ambient condition stayed the same as it does in the stretching sheet flow. With this modeling, they reached a conclusion that the solution to this problem does not exist in the absence of sufficient wall suction.

Following Miklavcic and Wang [27], number of researchers got impressed by this flow and went involved in studying this flow for various flow situations. Consequently, they contributed a great number of research papers in the last decade on this flow. But there happened a very big misfortune with this case that the pioneer authors [27] committed a little mistake in the dimensionless self-similar

[2]Although the developed procedures of finding the self-similar solutions, either systematic or ad hoc, are actually based on the group theoretical approach explained in Chap 3, it is, however, mentioned there that finding some similarity solutions does not mean that one has explored all the similarity solutions and the existence of any other self-similar solution can never be denied.

[3]Complete in a sense, and this completeness does not deny the existence of any other self-similar solution.

formation of this flow and also a little bit mishandling, which was further followed by the other researchers in toto. Consequently, they obtained wrong results and tried to justify them with the help of non-physical reasoning. This mistake committed by the authors of [27] and the subsequent authors[4] is explained in detail in Chap. 7 where the correct self-similar formulation to this case with appropriate interpretation of the wall velocities is also presented.

References

1. L. Prandtl, Über Flüssigkeits bewegung bei sehr kleiner Reibung, in *Proceedings of 3rd International. Mathematical Congress* (Heidelberg, 1904) pp. 484–491
2. H. Blasius, Grenzschichten in Flüssigkeiten mit kleiner Reibung. Z. Math. u. Phys. **56**, 1–37 (1908)
3. L. Bairstow, Skin friction. J. Roy. Aero. Soc. **19**, 3 (1925)
4. S. Goldstein, Concerning some solutions of the boundary-layer equations in hydrodynamics. Proc. Cambr. Phil. Soc. **26**, 1–30 (1930)
5. C. Töpfer, Bemerkungen zu dem Aufsatz von H. Blasius, "Grenzschichten in Flüssigkeiten mit kleiner Reibung", Z. Math. u. Phys., **60**, 397–398 (1952)
6. L. Howarth, On the solution of the laminar boundary layer equations. Proc. Roy. Soc. London A **164**, 547–579 (1938)
7. D. Meksyn, New methods in laminar boundary layer theory (London, 1961)
8. J.M. Burgers, in *Proceedings of 1st International Congress Application Mechanism*., (Delft, 1924)
9. B.G. van der Hegge Zijnen, Measurements of the velocity distribution in the boundary layer along a plane surface, Thesis, (Delft, 1924)
10. M. Hansen, Die Geschwindigkeitsverteilung in der Granzschicht an einer eingetauchten Platte, ZAMM, **8** (1928) 185–199; NACA TM 585 (1930)
11. J. Nikuradse, *Laminare Reibungsschichten an der längsangetrömten Platte, Manograph* (Zentrale f. wiss. Berichtswesen, Berlin, 1942)
12. H. Schlichting, Boundary-Layer theory, 6th edition McGraw-Hill Book Company, 1968. Translated by J. Kestin
13. S. Goldstein, *Modern Developments in Fluid Dynamics*, vol. 1 (Clarendon Press, Oxford, 1938)
14. L. Rosenhead, *Laminar Boundary Layers* (Dover publication Inc., New York, 1963)
15. G.K. Batchelor, in *An Introduction to the Fluid Dynamics* (Cambridge University Press, 1967)
16. B.C. Sakiadis, Boundary-layer behavior on continuous solid surface: I. Boundary-layer equations for two-dimensional and axisymmetric flow. AIChE **7**(1), 26–28 (1961)
17. B.C. Sakiadis, Boundary-layer behavior on continuous solid surfaces: II. The boundary-layer on a continuous flat surface. AIChE **7**(2), 221–225 (1961)
18. B.C. Sakiadis, Boundary-layer behavior on continuous solid surfaces: III. The boundary-layer on a continuous cylindrical surface. AIChE **7**(3), 467–472 (1961)
19. L.J. Crane, Flow past a stretching sheet. Z. Angew. Math. Phys. **21**, 645–647 (1970)

[4]Here we intentionally avoid the citation of any such paper because the literature on shrinking surface flow is great in number and it is impossible to cite all those studies over here. Therefore, the author is of the opinion that citing few of them is as bad as ignoring the rest of them.

20. V.M. Falkner, S.W. Skan, Some approximate solutions of the boundary-layer equations. Phil. Mag. **12**, 865–896 (1931)
21. W.H.H. Banks, Similarity solution of the boundary-layer equations for a stretching wall. J. Mecanique Theorique et Appliquee **2**(3), 375–392 (1983)
22. E. Magyari, B. Keller, Heat and mass transfer in the boundary layers on an exponentially stretching continuous surface. J. Phys. D Appl. Phys. **32**(5), 577–585 (1999)
23. L.J. Crane, Boundary layer flow due to a stretching cylinder. ZAMP **26**, 619–622 (1975)
24. T. Fang, Flow over a stretchable disk, Phys. Fluids. **19**, 12805 (1–4) (2007)
25. C.Y. Wang, The three-dimensional flow due to a stretching surface. Phys. Fluids **27**, 1915–1917 (1984)
26. I.C. Liu, H.H. Wang, Y.F. Peng, Flow and heat transfer for three-dimensional flow over an exponentially stretching surface. Chem. Eng. Comm. **200**, 253–268 (2013)
27. M. Miklavcic, C.Y. Wang, Viscous flow sue to a shrinking sheet. Quart. Appl. Math. **64**(2), 283–290 (2006)

Chapter 2
Governing Equations

In the present and the subsequent chapters, we shall, either directly or indirectly, be concerned with the boundary-layer flow of an incompressible viscous fluid without any involvement of heat and mass transfer. Therefore, our governing laws will be the conservation of mass and momentum only which are commonly known as the equations of continuity and the Navier–Stokes equations, respectively. In usual notation, they are written as (in Cartesian coordinates):

$$\frac{\partial u}{\partial x}+\frac{\partial v}{\partial y}+\frac{\partial w}{\partial z}=0, \tag{2.1}$$

$$\rho\left(\frac{\partial u}{\partial t}+u\frac{\partial u}{\partial x}+v\frac{\partial u}{\partial y}+w\frac{\partial u}{\partial z}\right)=-\frac{\partial p}{\partial x}+\mu\left(\frac{\partial^2 u}{\partial x^2}+\frac{\partial^2 u}{\partial y^2}+\frac{\partial^2 u}{\partial z^2}\right)+F_x, \tag{2.2}$$

$$\rho\left(\frac{\partial v}{\partial t}+u\frac{\partial v}{\partial x}+v\frac{\partial v}{\partial y}+w\frac{\partial v}{\partial z}\right)=-\frac{\partial p}{\partial y}+\mu\left(\frac{\partial^2 v}{\partial x^2}+\frac{\partial^2 v}{\partial y^2}+\frac{\partial^2 v}{\partial z^2}\right)+F_y, \tag{2.3}$$

$$\rho\left(\frac{\partial w}{\partial t}+u\frac{\partial w}{\partial x}+v\frac{\partial w}{\partial y}+w\frac{\partial w}{\partial z}\right)=-\frac{\partial p}{\partial z}+\mu\left(\frac{\partial^2 w}{\partial x^2}+\frac{\partial^2 w}{\partial y^2}+\frac{\partial^2 w}{\partial z^2}\right)+F_z, \tag{2.4}$$

and in cylindrical coordinates:

$$\frac{\partial v_r}{\partial r}+\frac{v_r}{r}+\frac{1}{r}\frac{\partial v_\theta}{\partial \theta}+\frac{\partial v_z}{\partial z}=0, \tag{2.5}$$

$$\begin{aligned}&\rho\left(\frac{\partial v_r}{\partial t}+v_r\frac{\partial v_r}{\partial r}+\frac{v_\theta}{r}\frac{\partial v_r}{\partial \theta}-\frac{v_\theta^2}{r}+v_z\frac{\partial v_r}{\partial z}\right)\\&\quad=-\frac{\partial p}{\partial r}+\mu\left(\frac{\partial^2 v_r}{\partial r^2}+\frac{1}{r}\frac{\partial v_r}{\partial r}-\frac{v_r}{r^2}+\frac{1}{r^2}\frac{\partial^2 v_r}{\partial \theta^2}-\frac{2}{r^2}\frac{\partial v_\theta}{\partial \theta}+\frac{\partial^2 v_r}{\partial z^2}\right)+F_r,\end{aligned} \tag{2.6}$$

A. Mehmood, *Viscous Flows*, Mathematical Engineering,
DOI 10.1007/978-3-319-55432-7_2

$$\rho\left(\frac{\partial v_\theta}{\partial t}+v_r\frac{\partial v_\theta}{\partial r}+\frac{v_\theta}{r}\frac{\partial v_\theta}{\partial \theta}+\frac{v_r v_\theta}{r}+v_z\frac{\partial v_\theta}{\partial z}\right)$$
$$=-\frac{1}{r}\frac{\partial p}{\partial \theta}+\mu\left(\frac{\partial^2 v_\theta}{\partial r^2}+\frac{1}{r}\frac{\partial v_\theta}{\partial r}-\frac{v_\theta}{r^2}+\frac{1}{r^2}\frac{\partial^2 v_\theta}{\partial \theta^2}+\frac{2}{r^2}\frac{\partial v_r}{\partial \theta}+\frac{\partial^2 v_\theta}{\partial z^2}\right)+F_\theta, \quad (2.7)$$

$$\rho\left(\frac{\partial v_z}{\partial t}+v_r\frac{\partial v_z}{\partial r}+\frac{v_\theta}{r}\frac{\partial v_z}{\partial \theta}+v_z\frac{\partial v_z}{\partial z}\right)=-\frac{\partial p}{\partial z}+\mu\left(\frac{\partial^2 v_z}{\partial r^2}+\frac{1}{r}\frac{\partial v_z}{\partial r}+\frac{1}{r^2}\frac{\partial^2 v_z}{\partial \theta^2}+\frac{\partial^2 v_z}{\partial z^2}\right)+F_z, \quad (2.8)$$

where $\boldsymbol{F}=\left(F_x,F_y,F_z\right)$ or $=(F_r,F_\theta,F_z)$ denotes the body force. However, the flows considered in the subsequent chapters do not involve any body force because of which $\boldsymbol{F}$ will be taken identically equal to zero in all those chapters.

2.1 Boundary-Layer Equations

2.1.1 The Boundary-Layer Assumption

In the study of viscous flow due to the motion of a continuous surface, a natural question arises "whether the boundary-layer assumptions considered by Prandtl are applicable to this case where the flow is established by the motion of the solid surface in the absence of any potential flow?" The same question arose in the mind of Sakiadis [1] in 1960 and he first confirmed the boundary-layer character of the viscous flow established by the motion of a continuous surface. This question, however, finds some crude justification from Sect. 1.1 of Chap. 1, where the Sakiadis flow has been explained, but a theoretical proof or experimental evidence is still required. In this connection, Sakiadis [1] performed an experiment and confirmed the formation of boundary-layer near the surface of the moving continuous surface in accordance with the explanation given in Sect. 2.1. He considered the rectangular Lucite acrylic resin tank and filled it with a water-based solution of milling yellow. He passed two parallel threads issuing from the little holes in the blocks immersed completely in the tank as shown in Fig. 2.1.

For the sake of comparison, he moved the left-hand thread from top to bottom and kept the right one fixed within the tank. After a while, when the steady state reached, the photograph (see Fig. 2.2) shows the formation of the boundary-layer near the moving thread, starting right from the hole and thus developing in the direction of motion of the thread.

This experiment confirms that the viscous flow established by the motion of a continuous surface does exhibit the boundary-layer character. Therefore, the Prandtl's boundary-layer assumptions are equally valid in this case and the order of magnitude analysis also works in the same manner as in the case of finite surfaces.

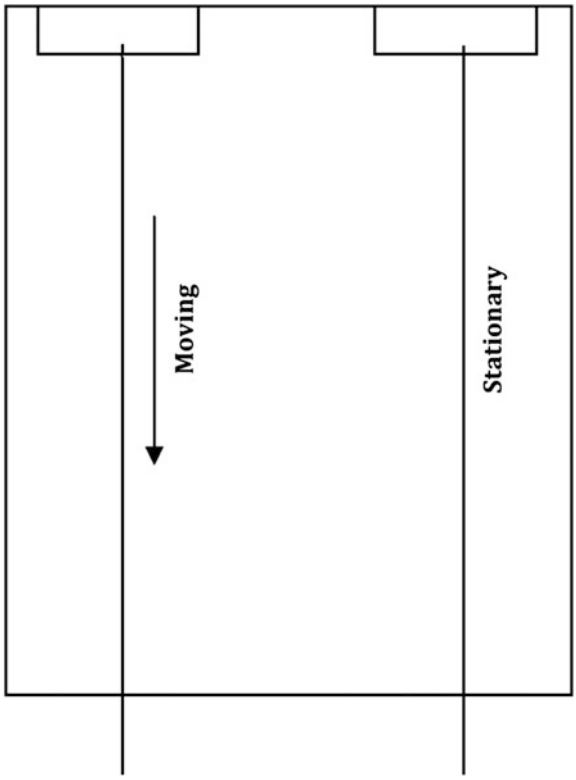

Fig. 2.1 Schematic of experimental setup of Sakiadis [1]

Fig. 2.2 Photograph of the Sakiadis' experiment [1]

2.1.2 The Pressure Gradient Term

According to the Prandtl's boundary-layer theory, the pressure within the boundary-layer does not become very much different from the pressure in the inviscid potential flow. That is, there are no significant changes in pressure across the boundary-layer because of which the term $\partial p/\partial y$ is simply ignored in the two-dimensional case; however, the changes in pressure along the lateral directions can be of any significance. Therefore, the pressure variation along the lateral directions within the boundary-layer is assumed to be the same as they are in the inviscid potential flow outside the boundary-layer and are determined with the use of Bernoulli's equation, for example, in the two-dimensional steady-state case, as

$$\frac{\mathrm{d}p}{\mathrm{d}x} = u_\infty \frac{\mathrm{d}u_\infty}{\mathrm{d}x}$$

Thus, the constancy or absence of the external potential flow makes the pressure gradient term equal to zero in the boundary-layer equations governing the flow due to a moving continuous solid surface. The external pressure in the subsequently studied flows will be considered absent, thus making the pressure gradient term equal to zero, i.e.,

$$\frac{\partial p}{\partial s_l} = 0, \tag{2.9}$$

where s_l denotes any lateral coordinate.

2.1.3 Boundary-Layer Equations in Cartesian Coordinates

However, it has now been established that the boundary-layer equations, present already in the literature, for the two-dimensional and three-dimensional flows are equally applicable to the flows due to moving continuous surfaces too. Therefore, the derivation of these equations here again does not make any sense. We, therefore, prefer to follow Schlichting [2] and write the boundary-layer equations directly here

$$\frac{\partial u}{\partial x} + \frac{\partial v}{\partial y} + \frac{\partial w}{\partial z} = 0, \tag{2.10}$$

$$\frac{\partial u}{\partial t} + u\frac{\partial u}{\partial x} + v\frac{\partial u}{\partial y} + w\frac{\partial u}{\partial z} = \nu\frac{\partial^2 u}{\partial y^2}, \tag{2.11}$$

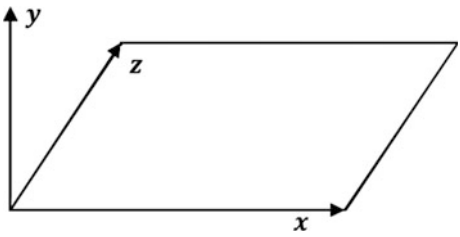

Fig. 2.3 Cartesian coordinate system

$$\frac{\partial w}{\partial t}+u\frac{\partial w}{\partial x}+v\frac{\partial w}{\partial y}+w\frac{\partial w}{\partial z}=v\frac{\partial^2 w}{\partial y^2}, \tag{2.12}$$

where the system of coordinates is shown in Fig. 2.3. The velocity components u, v and w have been taken along the x-, y-, and z-axes, respectively.

2.1.4 Boundary-Layer Equations in Cylindrical Coordinates

The geometrical objects, of our interest, owing to the axial symmetry are the continuous circular cylinder and the circular disk of infinite radius. The schematic of the flow due to a continuous circular cylinder and the associated system of coordinates is shown in Fig. 2.4.

Since there is no circular rotation in the flow therefore, the boundary-layer equations in this case look like

$$\frac{\partial}{\partial z}(ru)+\frac{\partial}{\partial r}(rv)=0, \tag{2.13}$$

$$\frac{\partial u}{\partial t}+u\frac{\partial u}{\partial z}+v\frac{\partial u}{\partial r}=v\frac{1}{r}\frac{\partial}{\partial r}\left(r\frac{\partial u}{\partial r}\right), \tag{2.14}$$

whereas in the case of circular disk, the governing system takes the form

$$\frac{\partial}{\partial r}(ru)+\frac{\partial}{\partial z}(rw)=0, \tag{2.15}$$

$$\frac{\partial u}{\partial t}+u\frac{\partial u}{\partial r}+w\frac{\partial u}{\partial z}=v\frac{\partial^2 u}{\partial z^2}. \tag{2.16}$$

The chosen system of coordinates, corresponding to the disk geometry, is shown in Fig. 2.5.

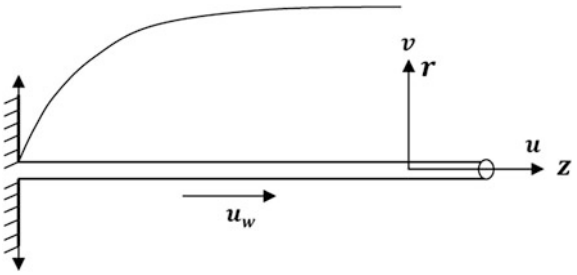

Fig. 2.4 Schematic of the continuous cylinder and the associated coordinate system

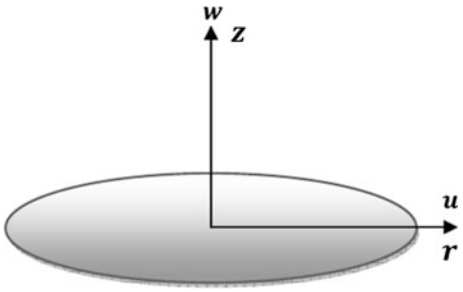

Fig. 2.5 Coordinate system for the axially symmetric disk geometry

2.2 Momentum Integral Equations

The integral form of the momentum boundary-layer equations, either in Cartesian coordinates or in cylindrical coordinates, comes directly from their respective differential forms, such as Eqs. (2.10)–(2.12), (2.13)–(2.14), (2.15)–(2.16) corresponding to the planner two- or three-dimensional flow, axially symmetric flow near a cylinder and disk, respectively.

2.2.1 In Cartesian Coordinates

Consider a steady three-dimensional flow caused due to the bilateral motion of a flexible continuous flat sheet. The appropriate boundary conditions for this flow read as:

$$\left.\begin{array}{ll} u = u_w(x,z), w = w_w(x,z), v = v_w(x,z), & \text{at } y = 0 \\ u = 0, w = 0, & \text{at } y = \infty \end{array}\right\}, \tag{2.17}$$

where $u_w(x,z)$ and $w_w(x,z)$ denote the stretching/shrinking wall velocities in x- and z-directions, respectively. In the case of porous flexible sheet, suction/injection may also be allowed through the sheet surface which is denoted by $v_w(x,z)$. Outside the boundary-layer, the fluid is supposed to be at rest in the absence of any potential

flow. The momentum integral equations in this case are derived by the integration of Eqs. (2.10)–(2.12) w.r.t. y between the limits 0 and $\delta(x,z)$, where $\delta(x,z)$ denotes the boundary-layer thickness. Integration of Eq. (2.10) w.r.t. y yields

$$v = v_w - \int_0^y \left(\frac{\partial u}{\partial x} + \frac{\partial w}{\partial z}\right) \mathrm{d}y. \tag{2.18}$$

Integration of Eqs. (2.11) and (2.12) with respect to y between the limits $0 \leq y \leq \delta$ results in the following integral equations:

$$\int_0^\delta \left(u\frac{\partial u}{\partial x} + v\frac{\partial u}{\partial y} + w\frac{\partial u}{\partial z}\right) \mathrm{d}y = \frac{1}{\rho}\tau_{x,0}, \tag{2.19}$$

$$\int_0^\delta \left(u\frac{\partial w}{\partial x} + v\frac{\partial w}{\partial y} + w\frac{\partial w}{\partial z}\right) \mathrm{d}y = \frac{1}{\rho}\tau_{z,0}, \tag{2.20}$$

where

$$\tau_{x,0} = -\mu \left.\frac{\partial u}{\partial y}\right|_{y=0} \quad \text{and} \quad \tau_{z,0} = -\mu \left.\frac{\partial w}{\partial y}\right|_{y=0}. \tag{2.21}$$

Substituting Eq. (2.18) in Eqs. (2.19) and (2.20) by noting that

$$\left[u \int_0^y \left(\frac{\partial u}{\partial x} + \frac{\partial w}{\partial z}\right) \mathrm{d}y\right]_0^\delta = 0, \tag{2.22}$$

and

$$\left[w \int_0^y \left(\frac{\partial u}{\partial x} + \frac{\partial w}{\partial z}\right) \mathrm{d}y\right]_0^\delta = 0, \tag{2.23}$$

we finally arrive at

$$\frac{\partial}{\partial x}\int_0^\delta u^2 \mathrm{d}y + \frac{\partial}{\partial z}\int_0^\delta uw \mathrm{d}y = v_w u_w + \frac{1}{\rho}\tau_{x,0}, \tag{2.24}$$

$$\frac{\partial}{\partial x}\int_0^{\delta} uw\mathrm{d}y + \frac{\partial}{\partial z}\int_0^{\delta} w^2\mathrm{d}y = v_w w_w + \frac{1}{\rho}\tau_{z,0}. \tag{2.25}$$

The system (2.24)–(2.25) represents the momentum integral equations for the steady three-dimensional viscous flow due to a moving continuous porous sheet. For the two-dimensional case, Eq. (2.25) just vanishes out and Eq. (2.24) in the absence of wall suction/injection simplifies to

$$\frac{\mathrm{d}}{\mathrm{d}x}\int_0^{\delta} u^2\mathrm{d}y = \frac{1}{\rho}\tau_{x,0}, \tag{2.26}$$

which is the same as derived by Sakiadis [1].

2.2.2 *In Cylindrical Coordinates*

In Sect. 2.1.4, the axial flow due to a moving continuous surface has been represented in cylindrical coordinates by splitting it into two particular flow geometries, namely the circular cylinder and the circular flat disk. The integral formulation for the said two cases follows immediately by the integration of Eqs. (2.13), (2.14), (2.15), and (2.16), respectively. Following the same procedure (of Sect. 2.1.4), we derive integral momentum equations for these two cases separately. The appropriate boundary conditions for a uniformly stretching/shrinking long continuous cylinder, as shown in Fig. 2.4, with porous surface read as

$$\left.\begin{array}{ll} u = u_w(z),\ v = v_w(z), & \text{at } r = R \\ u = 0, & \text{at } r = \infty \end{array}\right\}, \tag{2.27}$$

where R denotes the radius of cylinder. Integrating Eq. (2.13) w.r.t. r, we readily get

$$v = \frac{R}{r}v_w - \frac{1}{r}\int_0^{r}\frac{\partial u}{\partial z}r\mathrm{d}r. \tag{2.28}$$

Substituting Eq. (2.28) in Eq. (2.14) and integrating between the limits $R \le r \le \delta(z)$, we have

$$\frac{\mathrm{d}}{\mathrm{d}z}\int_0^{\delta} u^2 r\mathrm{d}r = R\left(u_w v_w + \frac{\tau_{z,0}}{\rho}\right), \tag{2.29}$$

which is the momentum integral equation for the uniformly stretching/shrinking cylinder. This equation immediately reduces to that, first, derived by Sakiadis [1] for a continuous cylinder of impermeable solid wall by substituting $v_w = 0$. Here, $\tau_{z,0} = -\mu \frac{\partial u}{\partial r}\big|_{r=R}$ is the tangential shear stress at the cylindrical surface. The similar procedure applies to the continuous circular disk of infinite radius. In this case, the describing conditions at the disk surface should be of the form

$$\left.\begin{array}{ll} u = u_w(r),\ w = w_w(r), & \text{at } z = 0 \\ u = 0, & \text{at } z = \infty \end{array}\right\}, \tag{2.30}$$

for a permeable stretching/shrinking disk. Notice that, Eq. (2.16) in steady-state form can be rewritten, with the utilization of Eq. (2.15), as:

$$\frac{\partial}{\partial r}\left(ru^2\right) + \frac{\partial}{\partial z}(ruw) = vr\frac{\partial^2 u}{\partial z^2}, \tag{2.31}$$

which upon integration between the limits $0 \le z \le \delta(r)$, in view of Eq. (2.30), simplifies to

$$\frac{1}{r}\frac{\mathrm{d}}{\mathrm{d}r}\left[r\int_0^{\delta} u^2 \mathrm{d}z\right] = u_w v_w + \frac{\tau_{r,0}}{\rho}, \tag{2.32}$$

where $\tau_{r,0} = -\mu \frac{\partial u}{\partial z}\big|_{z=0}$ is the radial component of wall tangential shear stress. Equation (2.32) constitutes the momentum integral equation for a radially stretching/shrinking disk.

References

1. B.C. Sakiadis, Boundary-layer behavior on continuous solid surface: I boundary-layer equations for two-dimensional and axisymmetric flow. AIChE **7**(1), 26–28 (1961)
2. H. Schlichting, Boundary-Layer theory, 6th edn. (McGraw-Hill Book Company, 1968). Translated by J. Kestin

Chapter 3
The Concept of Self-similarity

One of the important classes of boundary-layer flows comprises the self-similar flows. The concept of self-similarity is equally important in mathematical as well as physical point of views. Normally, the boundary-layer flow problems are modeled in the form of partial differential equations (*pdes*) involving two or more independent variables in addition to the involved physical parameters or constants. If, under certain conditions, it becomes possible to reduce the number of independent variables, in a particular problem, to one by combining all the independent variables suitably, then the problem under consideration is called *self-similar* or *auto-model*. Consequently, the governing partial differential equations are transformed to ordinary differential equations *(odes)* which are completely in the form of new variables and free from the previous variables. A useful example could be the steady, two-dimensional flow past a static wedge governed by the system (1.1) which are *pdes* in two independent variables. In this flow, the boundary-layer is formed at the wedge surface due to the presence of external potential flow, having velocity $u_\infty(x)$. The self-similar solutions for this flow exist if the external potential velocity is of the form, but not limited to, $u_\infty(x) = ax^m$ where a is a constant having suitable dimensions and m is a pure number. Consequently, the system (1.1) completely transforms to an ordinary differential equation (Eq. 1.8) and becomes free from previous variables.

Dimensional analysis, based upon the Buckingham Pi-theorem,[1] is one of the fundamental approaches for reducing the number of independent variables, while dealing with the partial differential equations, by combining them suitably to construct the new variables. The criterion of Buckingham Pi-theorem guides in this regard completely and not only tells, exactly, what number of independent variables can be reduced but also guides toward the construction of new variables. Following

[1]Buckingham Pi-theorem is of fundamental importance in dimensional analysis. The interested readers is recommended to consult the Ref. [1].

A. Mehmood, *Viscous Flows*, Mathematical Engineering,
DOI 10.1007/978-3-319-55432-7_3

its criterion, the dimensional analysis determines suitable new fundamental dimensions which come out to represent the problem in the form of new variables. This actually is done by the suitable scaling of the involved physical quantities.

The existence of self-similarity in a particular flow problem is usually a consequence of the non-existence of a characteristic length along one or more space directions. Such a problem, therefore, have a capacity of absorbing more than one variables into a single one, thus forming the new self-similar (independent) variable. The construction of new variables is, sometimes, also guided/restricted by the involved boundary and initial conditions. However, there is a systematic approach of constructing the new self-similar variables which will be discussed in detail in Sect. 3.3 and will be utilized in Chap. 5. Another important aspect of similarity solutions is that they usually exhibit asymptotic behavior; the same is true with the boundary-layer flows as the velocity within the boundary-layer also exhibits the asymptotic character. This actually is the reason that the family of self-similar solutions to the boundary-layer equations constitutes a big class of important flows in the fluid dynamics.

3.1 In View of Group Theoretic Approach

The application of dimensional analysis does always not result in the reduction of independent variables even if the reduction is possible. Sometimes, it happens that the dimensional analysis fails in finding those new fundamental dimensions which could be used to describe the original problem in self-similar variables. Consequently, the stuck guy is forced to think about any other strategy (method). The way out to this situation comes directly from the notion/concept of invariance of *pdes* under the scaling of variables in the frame work of Group Theoretic approach. A partial differential equation can actually be transformed to an ordinary differential equation, completely, due to the use of some suitable transformations only if the original *pde* is invariant under the Lie group of scaling transformations [1]. A detailed account to this topic can be found in [1], and the interested reader is referred to follow the Chap. 1 of [1].

Hence, the determination of new variables in the framework of dimensional analysis is actually attributed to the invariance property of the original equation(s) under the scaling group of involved variables, whereas the dimensional analysis actually does not implement the criterion of invariance, in complete, to the given *pde* under the utilized group of scaling transformations and thus stays unable to capture the self-similarity in many cases. There are examples, as we already mentioned above, where the dimensional analysis does not find any new fundamental dimensions due to which the original problem cannot be transformed to the self-similar form, but the Group Theoretic approach via one- or multi-parameter group of scaling transformations successfully determines the self-similar variables

in the same problem.[2] Therefore, the Group Theoretic approach can be regarded as the most generalized one, which successfully determines the criterion of self-similarity for a particularly chosen problem. However, the determination of self-similarity criterion via a one-parameter Lie group of scaling transformations does not deny the existence of any other self-similar solution(s) because the determined self-similar solutions represent all those concerning to the particularly utilized group of scaling transformations. Besides the Group Theoretic procedure, there are several other, ad hoc, approaches which can be utilized to determine the self-similarity in a particular problem. However, the underlying property, working behind all such approaches, is the requirement of invariance of the original *pde*. Worth mentioning other techniques are the determination of self-similarity through separation of variables and through the conservation laws, etc.

In the above discussion, we have repeatedly been using the word "problem" by which we mean the given partial differential equation(s) and the associated initial and boundary conditions which subsequently will be called as auxiliary data. The author's experience with the 'similarity' reveals that the existence of self-similarity is strongly dependent upon the nature of auxiliary data. For example, if a certain *pde* admits a similarity solution under the constraints of one auxiliary data, it may not be admitting the self-similarity for the other auxiliary data. The existence of dual (or more) similarity variables for certain problems and the fundamental reason behind the non-uniqueness of the similarity variables is basically the nature of auxiliary data.[3] Particular to the boundary-layer flows past flat surfaces, self-similar solutions are possible in those cases where the reference velocities follow the power-law or exponential form as did in the Falkner–Skan flow.[4] The dependence of the self-similarity on the auxiliary data can further be explained due to the following example. Let us consider the Stokes first problem described by the system of equations

$$\frac{\partial u}{\partial t} = \nu \frac{\partial^2 u}{\partial y^2}, \tag{3.1}$$

$$u(0, y) = 0, \quad y \geq 0 \tag{3.2a}$$

$$u(t, 0) = U_0, \quad t > 0 \tag{3.2b}$$

$$u(t, \infty) = 0. \tag{3.2c}$$

[2]For further detail on this account the reader is referred to follow [1].

[3]As in the Falkner–Skan flow, the similarity variables take different forms for different values of m, though the nature of the flow is the same, that is the potential flow past a wedge.

[4]This fact can be confirmed in Chap. 5 which, however, does not deny the possibility of any other form.

The system (3.1)–(3.2a) admits a similarity solution of the form

$$u = U_0 f(\eta), \quad \eta = \frac{y}{2\sqrt{\nu t}} = \frac{y t^{-1/2}}{2\sqrt{\nu}}, \tag{3.3}$$

which transforms Eq. (3.1) to an ordinary differential equation of the form

$$f'' + 2\eta f' = 0, \tag{3.4}$$

subject to the transformed boundary conditions

$$f(0) = 1, \quad f(\infty) = 0. \tag{3.5}$$

Notice that the original three constraints (the auxiliary conditions) have now been reduced to two in number. Both of these are the boundary conditions, and the initial condition has completely been vanished. To understand this fact the definition of $\eta = \frac{y t^{-1/2}}{2\sqrt{\nu}}$ is important and the fact that the initial and boundary data are described at $t = 0$, $y = 0$ and $y = \infty$ only. In view of the definition of η and the critical values of y and t where the boundary and initial data have been described, we note that $\eta = 0$ at $y = 0$ only but $\eta = \infty$ either at $y = \infty$ or at $t = 0$, simultaneously. This means that in the transformed system the condition $f(\infty) = 0$ at $\eta = \infty$ must, simultaneously, represent the initial and boundary conditions defined at $t = 0$ and $y = \infty$, respectively. This can only be achieved if the said initial and boundary conditions do coalesce, that is

$$u(0, y) = u(t, \infty). \tag{3.6}$$

This means that if such a coalition of the initial and the boundary conditions is not possible, then the similarity variable η, defined above, can never be utilized in order to get the transformed *ode* (Eq. 3.4). Fortunately, the condition (3.6) is met by the auxiliary data (3.2a) due to which the similarity solution exists for this problem. Otherwise, it was impossible to achieve any way. In this perspective, regarding the existence of similarity solutions, few of the auxiliary conditions, defined at different points in the domain of interest, must coalesce to one. Such a situation is only possible if the new variables are constructed from the original variables by raising them to suitable powers. Such a power-law product of the original variables, in the construction of similarity variables, can never be achieved without having the reference velocity of the similar form. This is one of the important reasons behind the fact that the self-similar solutions follow the power-law form of the reference velocities. However, such a coalition is always not necessary, especially in those cases where the auxiliary conditions are already very few.

Based upon the number of auxiliary data, interesting conclusions regarding the number of similarity variables are drawn here:

- If the problem is well-posed[5], then a unique similarity variable will exist provided the problem admits a self-similar solution. For an ill-posed[6] problem, the uniqueness of the similarity variable is not guaranteed; the problem may admit one or more similarity variables if the self-similar solution is possible.
- If the given problem, whether well-posed or ill-posed, does not admit a self-similar solution then the solution will be called non-similar.

3.2 Physical Meanings

The concept of self-similarity is a little bit hard to explain in words, on one hand or seems to be explainable in a single sentence, on the other hand. In view of physical meanings of self-similarity the author is more inclined to the latter opinion because, in words, to-the-point explanation of self-similarity is hard to extend beyond few lines and one ultimately requires the assistance of mathematical language. Based upon the second opinion, we shall start trying to understand the physics of self-similarity from the mathematical view point and will try to become more and more less mathematical, gradually.

In the start of this chapter we explicitly stated that a problem is self-similar if the total number of involved independent variables can be reduced to one. Obviously, this can only be done by a suitable mixing of the original independent variables to form a single new variable, as discussed in the previous section. Ultimately, the resulting (new) single variable is called the similarity variable. Another important ingredient of this discussion is the scaling of variables which is a common base line among the dimensional analysis and the Group Theoretic method. Thus the mathematical sense of developing the similarity variables is based upon the suitable mixing of the original variables or more formally the suitable scaling of the original variables. At this stage it seems very useful to pick a particular example so that the concept of self-similarity can more conveniently be explained. For this purpose the Falkner–Skan flow (1.7)–(1.8) would be the best choice.

Let us concentrate on the definition of η and $f'(\eta)$ in Eq. 1.7 by ignoring the constant coefficient $\sqrt{\frac{a}{\nu}}$, for instance. Such constant coefficients have actually nothing to do with the self-similarity and are present just to non-dimensionalize the system. Notice that the Falkner–Skan problem is defined for $x > 0$ and $0 \leq y < \infty$ with the boundary conditions

[5]If for a given differential equation, sufficient numbers of auxiliary conditions are known to make the unique solution sure and the solution thus obtained depends continuously upon the given auxiliary data.

[6]If for a given differential equation, at least one or more auxiliary conditions are missing, the problem is ill-posed.

$$u(x,0)=0, \quad v(x,0)=0, \tag{3.7}$$

$$u(x,\infty)=u_\infty(x)=ax^m, \tag{3.8}$$

including no condition at any x-location. Since the independent variables are only x and y, the construction of η by combining x and y does not require any boundary conditions to coalesce. In this particular flow $\eta=\sqrt{\frac{a}{\nu}}x^{\frac{1-m}{2}}y$ having the domain [0, ∞) derived directly from the domain of y. Clearly, in the construction of η, y has simply been transformed to become η after a suitable scaling by an appropriate scale factor, namely $\sigma(x)=x^{\frac{1-m}{2}}$. Similarly, the construction of $f'(\eta)$ is also a consequence of suitable scaling of u by an appropriate scale factor which is obviously the external potential velocity $u_\infty(x)$. Hence, the function $\sigma(x)=x^{\frac{1-m}{2}}$ is the suitable scale factor in y and the reference velocity $u_\infty(x)=ax^m$ is the suitable scale factor in u.

Let us assume that we have calculated the velocity $f'(\eta)$ at $\eta=1$ which is $f'(1)=0.3298$ for $m=0$. Notice that, in Fig. 3.1a, the velocity $f'(1)=0.3298$ is the same at the locations x_1 and x_2, but differs in scale factors ax_1^0 and ax_2^0 in u and by $\sqrt{x_1}$ and $\sqrt{x_2}$ in y at the two locations. Mathematically, this fact can be expressed as

$$\frac{u\left(x_1,\frac{y_1}{\sqrt{x_1}}\right)}{ax_1^0}=\frac{u\left(x_2,\frac{y_2}{\sqrt{x_2}}\right)}{ax_2^0}. \tag{3.9}$$

Similar situation can be seen in Fig. 3.1b for the case $m=1$. If η is taken arbitrary for some fixed x_1 and x_2, then y must also be taken as arbitrary. Consequently, Eq. (3.9) modifies as, for $m=0$

$$\frac{u\left(x_1,\frac{y}{\sqrt{x_1}}\right)}{ax_1^0}=\frac{u\left(x_2,\frac{y}{\sqrt{x_2}}\right)}{ax_2^0}, \tag{3.10}$$

and for $m=1$

$$\frac{u(x_1,y)}{ax_1}=\frac{u(x_2,y)}{ax_2}. \tag{3.11}$$

Now, for the arbitrary m, Eqs. (3.9)–(3.11) unify as

$$\frac{u(x_1,y/\sigma(x_1))}{u_\infty(x_1)}=\frac{u(x_2,y/\sigma(x_2))}{u_\infty(x_2)}. \tag{3.12}$$

Thus if the solution is self-similar, then the x-component of velocity differs only by a scale factor in u and y, at any two different x-locations. In other words, the nature of the velocity profile does not depend upon x at all. The reason behind this

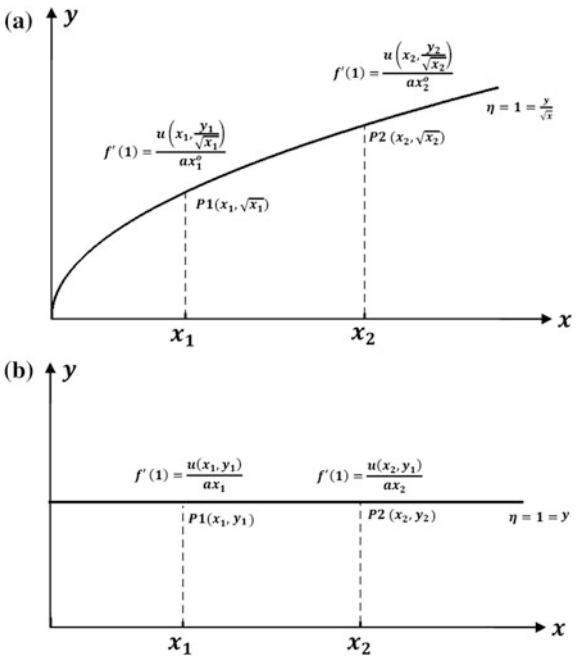

Fig. 3.1 **a** and **b** Graphical description of self-similarity

fact is the allowance, by the governing system, of the construction of η due to x and y in which x and y are so suitably combined. Such an allowance by the governing system is in fact recognized as the invariance of the system. The appropriate mixing of x and y in the construction of η generates a family of curves in the xy-plane. When a numerical code iterates to compute the solution at different η-nodes (say η_i), it actually computes the solution at $y = \eta_i\sqrt{x}$ curves in the physical/actual domain as shown in Fig. 3.2. This property, actually, lifts the requirement of computing the solution at various x-nodes, meaning that the solution is "self-similar" at all x-locations and only differs by a constant scale factor. Hence, if the solution is known at any x-location, the solution at any other x-location can easily be determined from the already known solution. The independence of the velocity from the variable x guarantees the absence of any length scale in the x-direction. In contrast, the Howarth's retarded flow [2] does involve flow separation and thus involves a definite length in x-direction, namely the distance of the point of separation from the leading edge, hence reacting as non-similar in nature.

Here, x-component of velocity has particularly been mentioned and the y-component of velocity has not been named at all. Actually, within the boundary-layer, only the lateral component(s) of velocity constitutes the main flow and the normal component of velocity is usually determined from the equation of continuity in the form of lateral velocity component. Moreover, the variation in velocity across the boundary-layer is more significant than that in the lateral direction. This could also be said a reason for similarity in x because the role of x within the

boundary-layer is somewhat like a slack variable; and the slack has to leave the system, ultimately.

3.3 General Theory

The simplification of a given differential equation via some transformation of involved variables based on the criterion of invariance is actually credited to Sophous Lie [3, 4]. Lie introduced the procedure of finding the infinitesimal transformations which leave the given differential equation invariant and result in significant simplification of the original equation, either by reducing the order of the original equation or by reducing the number of independent variables in it. The process of finding the infinitesimal symmetries of a differential equation is quite hectic but is highly algorithm and is easy to implement in a computer code. However, regarding the determination of self-similar solutions one does not need to follow the Lie's algorithm of finding the point symmetries, because the number of independent variables in a *pde* can be reduced through a group of scaling transformations. It is therefore straightforward to utilize the scaling group of transformations directly for finding the similarity solution. Morgan [5] utilized the general theory of invariance and developed a straightforward procedure for constructing the similarity variables. The procedure developed by Morgan was further utilized in fluid dynamics problems by [6–10].

Consider a system of n *pdes*, $E_j = 0$ in n unknowns u_j, $(j = 1, 2, \ldots, n)$ depending upon m number of independent variables x_i $(i = 1, 2, \ldots, m)$. A one-parameter group G of scaling transformations is assumed for the involved variables, of the form

$$\bar{x}_i = k^{\alpha_i} x_i, \bar{u}_j = k^{\gamma_j} u_j \quad (i = 1, 2, \ldots, m), \quad (j = 1, 2, \ldots, n), \tag{3.13}$$

where $k \neq 0$ is the continuous real parameter and the α_i and γ_j are the real exponents to be determined. The group (3.13) is applied to the given system of equations where the condition of invariance of the transformed system results in a system of simultaneous linear equations in the exponents α_i and γ_j. The non-trivial solution of this system is then utilized in the construction of (new) similarity variables which actually are the invariants of the scaling group G. At a time, only one independent variable can be reduced through one-parameter group. Let us assume that the linear system in α_i and γ_j admits a non-trivial solution and the variable x_1 is to be eliminated; there arise two cases for the exponent α_1, namely for $\alpha_1 \neq 0$ or $\alpha_1 = 0$.

Case I $(\alpha_1 \neq 0)$
If $\alpha_1 \neq 0$ the similarity (or new) variables (or invariants of G) are constructed as

$$\eta_r = \frac{x_r}{x_1^{\frac{\alpha_r}{\alpha_1}}}, \quad (r = 2, \ldots, m), \tag{3.14a}$$

and

$$f_j(\eta_2, \eta_3, \ldots, \eta_m) = \frac{u_j(x_1, x_2, \ldots, x_m)}{x_1^{\gamma_j/\alpha_1}}, \quad (j = 1, 2, \ldots, n). \tag{3.14b}$$

Case II ($\alpha_1 = 0$)
If $\alpha_1 = 0$, the similarity variables are constructed as

$$\eta_r = \frac{x_r}{e^{\alpha_r x_1}}, \quad (r = 2, 3, \ldots, m), \tag{3.15a}$$

and

$$f_j(\eta_2, \ldots, \eta_m) = \frac{u_j(x_1, x_2, \ldots, x_m)}{e^{\gamma_j x_1}}, \quad (j = 1, 2, \ldots, n). \tag{3.15b}$$

In the following, this procedure has been employed to a simple problem in fluid dynamics which will further help to understand the utility of the above procedure.

Example Consider the Stokes first problem which we already considered in Sect. 3.1 (Eqs. 3.1–3.2a) in some different context. Equation (3.1) admits a similarity solution for which the corresponding similarity variables are defined in Eq. (3.3). Let us derive Eq. (3.3) with the help of above described general theory of constructing the similarity variables. Consider the scaling group G of the form (for the variables involved in Eqs. (3.1)–(3.2a)).

$$G : \bar{t} = k^{\alpha_1} t, \quad \bar{y} = k^{\alpha_2} y, \quad \bar{u} = k^{\gamma_1} u. \tag{3.16}$$

Substitution of Eq. (3.16) in Eq. (3.1) and the requirement of invariance of the original *pde* result in the following linear equation:

$$\alpha_1 - \gamma_1 = 2\alpha_2 - \gamma_1. \tag{3.17a}$$

The initial condition (3.2a) and the boundary condition (3.2c) contribute nothing to the system, whereas the boundary condition (3.2b) gives

$$\gamma_1 = 0. \tag{3.17b}$$

The non-trivial solution of the simultaneous system (3.17a) reads as

$$\frac{\alpha_2}{\alpha_1} = \frac{1}{2}; \quad \alpha_1 \neq 0. \tag{3.18}$$

Therefore, the similarity variables, according to Eq. (3.14a), are constructed as

$$\eta = \frac{y}{t^{\frac{\alpha_2}{\alpha_1}}} = \frac{y}{t^{1/2}} = yt^{-1/2}, \tag{3.19a}$$

and

$$f(\eta) = \frac{u}{t^{\frac{\gamma_1}{\alpha_1}}} = \frac{u}{t^0} = u. \tag{3.19b}$$

Thus, $u = f(\eta)$ and $\eta = yt^{-1/2}$ are the (new) similarity variables which transform governing Eq. (3.1) to the self-similar form. The presence of the factors U_0 and $\frac{1}{\sqrt{\nu}}$ in Eq. (3.3) with $f(\eta)$ and $yt^{-1/2}$, respectively, is just for the sake of non-dimensionalization; also the presence of a factor $\frac{1}{2}$ in the definition of η (in Eq. 3.3) is simply to manipulate the constant coefficient in the transformed Eq. (3.4). These are actually the niceties and have nothing to do with the process of determining the similarity variables. For further examples and a bit more detail on this topic, the interested reader is referred to follow a very nice book by Ames [11]. The method will be applied to the boundary-layer equations in Chap. 5 where a detailed account on the construction of similarity variables is presented.

References

1. G.W. Bluman, S.C. Anco, *Symmetry and Integration Methods for Differential Equations* (Springer, Berlin, 2002)
2. L. Howarth, On the solution of the laminar boundary layer equations. Proc. R. Soc. Lond. A **164**, 547–579 (1938)
3. S. Lie, Über die Integration durch bestimmte Integrale von einer klasse linearer partialler Differentialgleichungen. Arch. Math. **6**, 328–368 (1992); also *Gesammelte Abhandlungen*, vol. III, pp. 492–523, B.G. Teubner, Leipzig, 1922. Originally in 1881
4. S. Lie, *Theorie der Transformationsgruppen*, vol. III (B.G. Teubner, Leipzig, 1893)
5. A.J.A. Morgan, The reduction by one of the number of independent variables in some systems of partial differential equations. Q. J. Math. Oxford **3**, 250–259 (1952)
6. R. Manohar, Some similarity solutions of partial differential equations of boundary-layer equations. Math. Res. Center (Uni. Wis.) Tech. Summar Rept. No. 375 (1963)
7. H. Schuh, in *Über the ähnlichen Lösungen der instalionaren Laminares Granzschichtgleichungen in inkompressiblen Strömungen*, ed. by H. Görtler, W. Tollmien. 50 Jahre Grenzschichtforschung (Vieweg, Braunschweig, 1955), p. 149
8. T. Geis, in *Ähnliche Grenzschichten an Rotationskörpern*, ed. by H. Göstler, W. Tollmien. 50 Jahre Grenzschichtforschung (Vieweg, Braunschweig, 1955), p. 294
9. A.G. Hansen, Possible similarity solutions of the laminar, incompressible, boundary-layer equations. Trans. ASME **80**, 1553–1559 (1958)
10. A.J.A. Morgan, Discussion of "possible similarity solutions of the laminar, incompressible, boundary-layer equations". Trans. ASME **80**, 1559–1562 (1958)
11. W.F. Ames, *Nonlinear Partial Differential Equations in Engineering* (Academic Press, 1965)

Chapter 4
Solution Techniques

The inherited nonlinear character of the boundary-layer equations is the great barrier in finding their exact analytic solution. The boundary-layer equations do not get linearized in any boundary-layer flow, assumed however simple, except the Stokes' unidirectional flow. The level of difficulty increases sufficiently if one switches from two-dimensional to three-dimensional flow or takes the unsteadiness into account simultaneously. The fundamental reason behind this fact is the non-vanishing character of the inertial part of the (Navier–Stokes equations) boundary-layer equations, where the nonlinearity actually comes from. On the other hand, it is also required to be realized that the boundary-layer equations are developed after the great simplification of the original Navier–Stokes equations. For example, in the steady two-dimensional boundary-layer flow the second component of the Navier–Stokes equations vanishes completely giving only $\partial p/\partial y = 0$. The constancy of the pressure across the boundary-layer and the applicability of the Bernoulli's equation inside the boundary-layer regarding the pressure gradient term also resolve the important issue of pressure gradient term in these flows. However, the material presented in this Book is strictly limited to the incompressible fluid having constant properties in the laminar and turbulent flow situations where almost more than three quarters of the Book are devoted to the laminar flow only. Therefore, most of the problems presented in this Book do not pose a significant level of difficulty to the investigator, but still they could not be taken so easy as of biting the soft cake. Regarding the solution point of view, the involved laminar problems can be classified into two categories, namely the self-similar and the non-similar flows.

As explained in the previous chapter the self-similar flows allow transformation of the governing partial differential equations to ordinary differential equations, thus reducing the difficulty in solution quite significantly. However, the non-similar flows do not offer such facility; consequently, a nonlinear *pde* is to be solved for these flows. Series solution techniques presented in Sect. 4.1 and the numerical techniques presented in Sect. 4.2.1 are recommended for the former case in order to obtain the analytic and numerical solutions, respectively. For the latter case, the

A. Mehmood, *Viscous Flows*, Mathematical Engineering,
DOI 10.1007/978-3-319-55432-7_4

implicit finite-difference scheme commonly known as the Keller's Box method is highly recommended which has unconditional quadratic convergence of the solution procedure. A brief introduction to this scheme is given in Sect. 4.2.2. The turbulent flows discussed in Part D can equally be studied either analytically or numerically. Usually, the theoretical analysis, either analytic or numerical, most often, requires the availability of experimental data. The numerical treatment involves the selection of appropriate turbulent model, whereas the integral methods require the velocity ansatz and the appropriate modeling of Reynolds stresses. On the basis of comparison made between the experimental and numerical or theoretical solution, the selection of the appropriate model in the numerical computations or the velocity ansatz in the integral methods can be made. Without the availability of experimental data the reliability of solution is hard to achieve.

Along with the previously described feelings of being deprived, another important proof of negligence of the flows due to the moving continuous solid surfaces is the non-availability of the experimental data for the turbulent flows. In the absence of such experimental data it is not easy to claim for the approximate solution to be sufficiently correct as the uncertainty remains always there. In this Book, the turbulent flow has been studied with the help of integral method just for the sake of mathematical beauty and of course because of its easy treatment. A detailed account on integral methods has been given in Sect. 4.3.

4.1 Series Solution

The idea of obtaining the solution of a differential equation in the form of a series is very old where the famous power-series methods had continuously been utilized in finding the solution of linear ordinary differential equations with variable coefficients since too long. Such type of methods is of equal importance for the solution of nonlinear equations also. Perturbation methods constitute an important class of approximate series solution methods. The perturbation methods are usually particular to the power-series expansion in the form of a parameter so deemed as small or large. Mostly, the boundary-layer problems do not involve any small or large parameter which could be considered small or large to construct the asymptotic perturbation series. In such situations the idea of representing the solution in the form of a series, without requiring the presence of small or large parameter in the system, is of fundamental importance.

Blasius [1], while solving his famous Blasius flow Eqs. (1.2) and (1.4), utilized the idea of series solution and obtained a complete solution in the form of a series. Since then, this solution is commonly referred as the Blasius series solution. The Blasius method of series solution was further explained by Prandtl [2] and strengthened by Bairstow [3] and Goldstein [4]. However, the Blasius' series solution served as accurate method for the Blasius flow but failed completely in the case of cylinder in cross-flow. In this case the Blasius series requires sufficient upgradation in order to produce acceptable results. Howarth [5] developed another,

similar, method of series solution for the calculation of boundary-layer separation in the retarded flow past a flat-plate. The Howarth's series solution happened to be very accurate and calculated the flow separation quite exactly. Similarly, Seban and Bond [6], Curle [7], and Wang [8] also utilized the series method in order to capture the effects of transverse curvature in the axisymmetric viscous flow along a long slim cylinder. A thorough review of literature reveals that such series solution methods, as developed and utilized in the above studies, are of ad hoc nature and do not have their wider applicability. The reason for this is their typical construction, which actually is the object oriented, based on the particular information of the flow under consideration. This is the reason behind the fact that such a so-constructed series solution method applies successfully to one problem but blows away for the other.

The above-cited few references [1–4, 6–8] are just a few glimpses from the history of boundary-layers in view of solution methods. It is now easy to understand that such ad hoc methods, though rich in mathematics, based strictly on the physics of flow, found no wider acceptance and hence became outdated nowadays. In comparison with these methods the general series solution methods, namely the power-series and the perturbation methods, are still alive and are utilized in diverse areas of science and engineering. In this section we intend to introduce the reader a series solution method having less limitations and wider applicability, namely the homotopy analysis method (HAM). This method has widely been applied to the boundary-layer equations, and quite exact solutions have been obtained because of it. Important related studies are mentioned in [9–27] where the interested reader is referred to consult.

Homotopy analysis method is actually an extension of the conventional perturbation methods depending upon no small or large parameter. This method has been developed due to the idea of *homotopy*, an important concept in topology. For a given nonlinear problem, the method assumes an initial linear problem (admitting the giving boundary conditions) and constructs a homotopy between the assumed initial linear problem and the actual nonlinear problem involving an embedding parameter p (say) such that $0 \leq p \leq 1$. As p varies from 0 to 1 continuously, the problem so-constructed deforms uniformly from initial solution to the final solution. The idea of HAM was first introduced by Liao [9] in his doctoral thesis and was further improved and applied to various differential equations in [10]. However, the homotopy analysis method is quite popular in the solution of laminar self-similar boundary-layer equations and the people already in the field are very well aware of it. But a brief description of the method seems necessary here just to familiarize the reader with the HAM.

Consider a nonlinear differential equation $\mathcal{N}(u(x)) = 0$ where x denotes the independent variable and u is the dependent variable. Corresponding to this nonlinear equation we choose a linear differential operator $\mathcal{L}$ such that $\mathcal{L}f = 0$, whenever $f = 0$. Liao [10] defined homotopy between the original nonlinear equation and the newly selected linear one as:

$$(1-p)\mathcal{L}[\bar{u}(x,p,\hbar,H)-u_0(x)]=p\hbar H(x)\mathcal{N}(\bar{u}(x,p,\hbar,H)), \tag{4.1}$$

with $p\in[0,1]$ such that $\bar{u}(x,p=0)=u_0(x)$ and $\bar{u}(x,p=1)=u(x)$. This means that the initial solution $u_0(x)$ continuously deforms to become the final solution $u(x)$ as p varies from 0 to 1. The parameter $\hbar$ denotes the auxiliary parameter, and $H(x)$ is designated as the auxiliary function. Equation (4.1) is called the zero-order deformation equation, whereas the mth-order deformation is obtained due to the m times differentiation of Eq. (4.1) with respect to p at $p=0$ and is given by

$$\mathcal{L}[u_m(x)-\chi_m u_{m-1}(x)]=\hbar H(x)R_m(x), \tag{4.2}$$

where

$$R_m(x)=\sum_{k=1}^{m}\gamma_{m-k}(x);\quad \gamma_n(x)=\frac{1}{n!}\frac{\partial^n\mathcal{N}(\bar{u}(x,p))}{\partial p^n}\bigg|_{p=0}, \tag{4.3}$$

and

$$\chi_k=\begin{cases}0 & \text{for} \quad k\le 1,\\ 1 & \text{for} \quad k>1.\end{cases} \tag{4.4}$$

According to the Taylor series, expansion of $\bar{u}(x;p)$ about $p=0$ is given by

$$\bar{u}(x,p)=u_0(x)+\sum_{m=1}^{\infty}u_m(x)p^m;\quad u_m(x)=\frac{\partial^m\bar{u}(x,p))}{\partial p^m}\bigg|_{p=0}. \tag{4.5}$$

If the series (4.5) converges as $p\to 1$, then $\bar{u}(x;\ 1)$ represents the solution of the nonlinear equation $N(u(x))=0$ where the mth term of the solution series is obtained by solving mth-order deformation equation (4.2).

The convergence of the solution series, with sufficient number of terms, depends strongly upon the auxiliary parameter $\hbar$. The determination of the interval of admissible values of $\hbar$ for which the solution series converges is of fundamental importance. However, with an interval of admissible values of $\hbar$ in hand it is still crucial to decide for the appropriate value of $\hbar$ so that the solution is accurate. In this regard the calculation of residual error is the best approach to make the solution accurate. The m terms of the solution series can easily be calculated with the aid of some suitable computing software such as the Mathematica, MATLAB, or Maple. There are several other versions of homotopy analysis method with certain modifications or simplifications contributed by others or Liao himself which are of equal importance within the limits of their applicability. Such progresses can be found in Refs. [28–37].

4.2 Numerical Methods

The tremendous development in the field of fluid dynamics in general and in aerodynamics in particular can simply be indebted to the development of modern numerical techniques toward the computation of flow and heat transfer phenomena in complex flows involving complicated geometries. The foundation of an entirely new branch of modern fluid dynamics, namely the computational fluid dynamics (CFD), is obvious evidence in the support of this fact. The creation of the state-of-the-art sophisticated subsonic to hypersonic space vehicles, ranging from the commercial aircrafts to the high-speed jets and the missile systems, is directly attributed to the impressive achievements of the modern CFD. Therefore, the importance of numerical techniques in the study of fluid dynamics problems can never be denied. Due to the availability of the high-performance computing machines and the development of computation-oriented computer software, the computation of numerical solution to the nonlinear differential equations is not that costly now, as it was a few decades back. Due to these facts, the accuracy of numerical methods has so been improved to an extent that they are now usually called as the "numerical exact solutions."

Under these circumstances the numerical solution of the fluid dynamics problems is highly appreciated and is widely acceptable with no hesitation. The scarce of the analytic or approximate methods in the turbulent flows is so severe where the numerical methods are the ultimate choice. Based on the levels of difficulty and the convenience of the user, diverse CFD softwares have been developed by utilizing the modern CFD tools. Such CFD softwares are widely being used by the engineers in industry as well as the researchers in academia. As far as the requirement of this Book is concerned, the considered problems can successfully be handled by implementing the following (but not essentially these) numerical methods on a desktop computer in a simple computing software such as Mathematica, Maple, MATLAB, or Mathcad.

4.2.1 RK Methods/Built-in Packages

However, the majority of the problems presented in this Book are those which can be classified as similar or non-similar in nature. The self-similar flows have been modeled in the form of boundary value problems involving ordinary differential equations, whereas the non-similar flow modeling results in a partial differential equation. A boundary value problem involving ordinary differential equation can simply be solved with the help of famous Runge–Kutta method. This method transforms the given *ode,* having order ≥ 2, into a system of first-order initial value problems, and then integrates it numerically. This method has widely been used in the study of self-similar boundary-layer flows. This method also has the great capacity of finding the dual or multiple solutions to the Falkner-Skan equations

whether the flow is past the wedge or due to the stretching/shrinking surface. The details of this method can easily be found in any text book on numerical methods or in [38] where the information on the other numerical methods has also been given.

Alternatively, one can also utilize the easily available *ode* solving packages in the above-mentioned software such as Mathematica, MATLAB, or Mathcad. However, it is important to emphasize that the solution of the self-similar problems is not limited to the RK methods only rather they can also be solved with the aid of any suitable numerical scheme such as finite-difference schemes.

4.2.2 Keller's Box Method

The mathematical modeling of non-similar boundary-layer flows results in the form of boundary value problems involving the partial differential equations. Such *pdes* cannot be solved with the help of aforementioned series solution method (HAM) or the RK methods, in general. In this regard an implicit finite-difference scheme, commonly known as the Keller's Box scheme, is highly recommended. This method was first developed by Herbert B. Keller [39] and was improved further by Keller and Cebeci. The method was first employed to the boundary-layer equations by Keller and Cebeci [40, 41] and Cebeci and Keller [42, 43]. Because of these studies the method was found to be very appropriate for the solution of boundary-layer equations. They (Cebeci and Keller) concluded that the method converges unconditionally for these flows having convergence rate of order two. They further pointed out that the method is quite easier to program and executes much faster. Further details on this method can be found in [44, 45] and the references therein.

The utilization of Keller's Box method first transforms the given *pde* to a system of first-order differential equations. The resulting first-order nonlinear system is then solved using Newton's method with the aid of block-tridiagonal factorization technique. The computations are carried out on an arbitrary rectangular grid where the derivatives are approximated by central difference quotients averaged at the middle of the net blocks. As mentioned above, this scheme is very useful in the integration of non-similar flow equations and the author's personal experience with this scheme is also very good. This scheme can equally be employed to the self-similar equations with no extra labor.

4.3 Integral Methods

Most of the practical boundary-layer flows are comprised of the turbulent flows because of their abundant occurrence in almost all real physical phenomena. Because of their complex nature no complete theory has yet been developed to explain their behavior in general. The most crucial step in the handling of turbulent

flows is the modeling of Reynolds stresses. Based upon empirical and semi-empirical information several turbulent models have been developed which are applicable within their limited domains. Due to this fact, it is generally postulated that all solutions available for turbulent flows are the approximate solutions. However, with the development of modern CFD tools, the simulated results, which are quite trustworthy and helpful in the development of modern technologies, are possible, but the theory has been stuck here. The improvement in the simulated results is continuously being brought by the introduction of new empirical or semi-empirical turbulent models. Under these circumstances the approximate integral methods are the only option for the theoretical study of turbulent boundary-layers because of the availability of universal wall laws and the velocity ansatz.

The most fundamental integral methods are due to von Karman [46] and Pohlhausen [47], developed for the study of viscous flow past a flat-plate. The Pohlhausen method was improved significantly by Holstein and Bohlen [48] in addition to the other contributors. For details on review of developments in Pohlhausen method the reader is referred to follow [49]. Another important integral method is due to Thwaites [50] which calculates the laminar flow separation quite exactly. Besides these very few methods there are various other diverse integral methods available in the literature, but it is impossible to cite all of them here. It is important to remember that the integral methods are strongly dependent upon certain assumptions among which most frequent are the velocity profiles. Because of such assumptions they usually do not provide acceptable results in the laminar flows. This is the primary reason for their negligence in these flows. However, with the availability of universal wall laws and universal velocity profiles, they provide quite reasonable approximation with fewer efforts for the turbulent flows. Because of this reason they did not become outdated even yet besides the tremendous improvements in the simulation techniques. This actually proves their applicability and acceptability in the calculation of turbulent boundary-layers. A detailed account on the integral methods for turbulent boundary-layers can be found in [49] and [51].

The turbulent boundary-layer flows have been presented in the last part of this Book. First integral method for the turbulent flows due to moving continuous surfaces is because of Sakiadis [52, 53] for the two-dimensional and axisymmetric flows. The Sakiadis' solution has been extended to $1/n$th power-law profile, and the Crane's flow has also been investigated in Chap. 12.

References

1. H. Blasius, Grenzschichten in Flüssigkeiten mit kleiner Reibung. Z. Math. u Phys. **56**, 1–37 (1908)
2. L. Prandtl, The mechanics of viscous fluids, ed. By W.F. Durand, in *Aerodynamic Theory III* (1935), pp. 34–208
3. L. Bairstow, Skin friction. J. Roy. Aero. Soc. **19**, 3 (1925)

4. S. Goldstein, Concerning some solutions of the boundary-layer equations in hydrodynamics. Proc. Cambr. Phil. Soc. **26**, 1–30 (1930)
5. L. Howarth, On the solution of the laminar boundary layer equations. Proc. Roy. Soc. London A **164**, 547–579 (1938)
6. R.A. Seban, R. Bond, Skin-friction and heat-transfer characteristics of a laminar boundary layer on a cylinder in axial incompressible flow. J. Aeronuat. Sci. **18**, 671 (1951)
7. S.N. Curle, Calculation of the axisymmetric boundary layer on a long thin cylinder. Proc R Soc Lond A Math. Phys. Sci. **372**(1751), 555–564 (1980)
8. C.Y. Wang, Fluid flow due to a stretching cylinder. Phys. Fluids **31**, 466–468 (1988)
9. S.J. Liao, The proposed homotopy analysis technique for the solution of nonlinear problems, PhD Thesis, Shanghai Jiao Tong University, 1992
10. S.J. Liao, *Beyond perturbation: introduction to the homotopy analysis method* (Chapman & Hall/CRC, 2004)
11. S.J. Liao, K.F. Cheung, Homotopy analysis of nonlinear progressive waves in deep water. J. Eng. Math. **45**, 105–116 (2003)
12. S.J. Liao, I. Pop, Explicit analytic solution for similarity boundary layer equations. Int. J. Heat Mass Tranf. **47**(1), 75–85 (2004)
13. C. Wang, J.M. Zhur, S.J. Liao, I. Pop, On the explicit analytic solutions of Cheng-Chang equations. Int. J. Heat Mass Transf. **46**(10), 1855–1860 (2003)
14. F.M. Allan, M.I. Syam, On analytic solution of the non-homogeneous Blasius problem. J. Comp. Appl. Math. **182**, 355–365 (2005)
15. S.J. Liao, A uniformly valid analytic solution of 2D viscous flow past a semi infinite flat plate. J. Fluid Mech. **385**, 101–128 (1999)
16. S.J. Liao, A. Campo, Analytic solutions of the temperature distribution in Blasius viscous flow problem. J. Fluid Mech. **453**, 411–425 (2002)
17. S.J. Liao, On the analytic solution of magnetohydrodynamics flows of non-Newtonian fluids over a stretching sheet. J. Fluid Mech. **488**, 189–212 (2003)
18. A. Mehmood, A. Ali, Analytic homotopy solution of generalized three-dimensional channel flow due to uniform stretching of the plate. Acta. Mech. Sin. **23**, 503–510 (2007)
19. A. Mehmood, A. Ali, Analytic solution of three-dimensional viscous flow and heat transfer over a stretching flat surface by homotopy analysis method. J. Heat. Transf.-Trans. ASME **130**, 121701 (2008). (1–7)
20. A. Mehmood, A. Ali, An explicit analytic solution of steady three-dimensional stagnation point flow of second grade fluid towards a heated plate. J. Appl. Mech.-Trans. ASME **75**, 061003 (2008). (1–8)
21. M. Sajid, T. Hayat, The application of homotopy analysis method for MHD viscous flow due to a shrinking sheet. Chaos Solutions Fractals **39**, 1317–1323 (2009)
22. T. Hayat, M. Khan, M. Ayub, On the explicit analytic solution on Oldroyd 6-constant fluid. Int. J. Eng. Sci. **42**, 123–135 (2004)
23. T. Hayat, M. Khan, S. Asghar, Homotopy analysis of MHD flows of an Oldroyd 8-constant fluid. Acta Mech. **168**, 213–232 (2004)
24. S. Abbasbandy, The application of homotopy analysis method to nonlinear equations arising in heat transfer. Phy. Lett. A **360**, 109–113 (2006)
25. Y. Liu, Z. Li, The homotopy analysis method for approximating the solution of the modified Korteweg-de Vries equation. Chaos Solution Fractals **39**, 1–8 (2009)
26. T. Hayat, Z. Abbas, T. Javed, M. Sajid, Three-dimensional rotating flow induced by a shrinking sheet for suction. Chaos Solution Fractals **39**, 1615–1626 (2009)
27. S. Abbasbandy, F.S. Zakaria, Soliton solution for the fifth-order KdV equation with the homotopy analysis method. Nonlinear Dyns. **51**(1), 83–87 (2008)
28. J.H. He, An approximate solution technique depending upon an artificial parameter. Commun. Nonlinear Sci. Numer. Simmulat. **3**, 92–97 (1998)
29. J.H. He, Newton-like iteration method for solving algebraic equation. Commun. Nonlinear Sci. Numer. Simmulat. **3**, 106–109 (1998)

30. E.I. Grigolyuk, V.I. Shalashilin, *Problems of nonlinear deformation: the continuation method applied to nonlinear problems in solid mechanics* (Kluwer Academic Publishers, Dordrecht, 1991)
31. J.C. Alexander, J.A. Yorke, A homotopy continuation method: numerically implementable topological procedures. Trans. Amer. Math. Soc. **242**, 271–284 (1978)
32. J.H. He, Some asymptotic methods for strongly nonlinear equations. Int. J. Modern Phys. B **20**(10), 1141–1199 (2006)
33. V. Marinca, N. Herisanu, L. Nemes, Optimal homotopy asymptotic method with application to thin film flow. Cent. Eur. J. Phys. **6**(3), 648–653 (2008)
34. K. Yabushita, M. Yamashita, K. Tsuboi, An analytic solution of projectile motion with the quadratic resistance law using the homotopy analysis method. J. Phys. A: Math. Theor. **40**, 8403–8416 (2007)
35. Z. Niu, C. Wang, A one-step optimal homotopy analysis method for non-linear differential equations. Commun. Nonlinear Sci. Numer. Simulat. **15**, 2026–2036 (2010)
36. S.J. Liao, An optimal homotopy analysis approach for strongly nonlinear differential equations. Commun. Nonlinear Sci. Numer. Simulat. **15**, 2003–2016 (2010)
37. S. Munawar, A. Mehmood, A. Ali, Effects of slip on flow between two stretchable disks using optimal homotopy analysis method. Can. J. Appl. Sci. **1**(2), 50–68 (2011)
38. T.Y. Na, *Computational methods in engineering boundary value problems* (Academic Press, New York, 1979)
39. H.B. Keller, in *A New Difference Scheme for Parabolic Problems. Numerical Solution of Partial Differential Equations, II,* ed. By J. Bramble (Academic Press, New York, 1970)
40. H.B. Keller, T. Cebeci, Accurate numerical methods for boundary-layer flows-I. Two-dimensional laminar flows. AIAA J. **10**, 1193 (1971)
41. H.B. Keller, T. Cebeci, Accurate numerical methods for boundary-layer flows-II. Two-dimensional turbulent flows. AIAA J. **10**, 1193 (1972)
42. T. Cebeci, H.B. Keller, *On the computation of unsteady boundary layers, Recent research on unsteady boundary layers* (IUTAM Symp. 1971), vol. I, p. 1082, Les Presses de I' Universitė Laval, Quebee, Canada
43. T. Cebeci, H.B. Keller, *Laminar boundary layers with assigned wall shear*, Lecture Notes in Physics (Proc. Int. Conf. Numer. Methods Fluid Dynam., 3rd), vol. 19 (Springer, Berlin and New York, 1973)
44. T. Cebeci, A.M.O. Smith, *Analysis of turbulent boundary layers* (Academic Press Inc., New York, 1974)
45. T. Cebeci, P. Bradshaw, *Momentum transfer in boundary layers* (Hemisphere Publishing Company, UK, 1977)
46. Th. von. Karman, Über laminare und turbulente Reibung, ZAMM, 1 (1921) 233–252; NACA TM 1092 (1946)
47. K. Pohlhausen, Zur näherungsweisen Integration der Differentialgleichung der laminaren Reibungsschicht. ZAMM **1**, 252–268 (1921)
48. H. Holstein, T. Bohlen, Ein einfaches Verfahren zur Berechnung lamimarer Reibungsschichten, die dem Näherungsansatz von. K. Pohlhausen genügen, Lilienthal-Bericht S 10 (1940), pp. 5–16
49. H. Schlichting, *Boundary-layer theory*, 6th edn. (McGraw-Hill Book Company, 1968). Translated by J. Kestin
50. B. Thwaites, Approximate calculation of the laminar boundary layer. Aero. Q. **1**, 245–280 (1949)
51. I.V. Shevchuk, *Convective heat and mass transfer in rotating disk systems* (Springer, Heidelberg, 2009)
52. B.C. Sakiadis, Boundary-layer behavior on continuous solid surfaces: II. The boundary-layer on a continuous flat surface. AIChE **7**(2), 221–225 (1961)
53. B.C. Sakiadis, Boundary-layer behavior on continuous solid surfaces: III. The boundary-layer on a continuous cylindrical surface. AIChE **7**(3), 467–472 (1961)

Part II
Self-similar Flows

Chapter 5
The Criterion of Self-similarity for Wall Velocities

The laminar boundary-layer flows can mainly be subdivided into two subclasses, namely the self-similar flows and the non-similar flows, as mentioned previously. Among these two classes, the self-similar flows had been more popular and studied extensively in the previous decades. The reason behind their wider acceptance is twofold: first, because of their governing boundary-layer equations, which are *pdes* actually, but readily reduce to ordinary differential equations by means of the similarity transformations, thus facilitating greatly toward their solution exploration; second, such self-similar flows help greatly toward the understanding of flow character within the boundary-layer. Because of these advantages, the self-similar boundary-layer flows, especially two-dimensional, have extensively been studied not only for the finite plate but also for the continuous sheet. The theory can almost be considered as complete for the self-similar flows past finite surfaces, but is still pending for the continuous surfaces. In this particular class of flows, the development had neither been quick nor been complete; rather, it had been contributed in bits. For example, Sakiadis [1] first introduced the self-similar solution for the continuous flat surface moving with uniform velocity. Crane [2] introduced the self-similar solution for variable wall velocity by restricting it to the linear form and referred it as the linear wall stretching. Later, the nonlinear stretching wall velocity was introduced by Banks [3] and Magyari and Keller [4] for the power-law and exponential wall velocities, respectively. This development is strictly restricted to the two-dimensional case; in view of these developments, the (two-dimensional) self-similar flows due to power-law wall velocities can be regarded as explored completely,[1] but the flows due to exponential wall velocities still require further exploration. The situation is far more adverse in the cases of three-dimensional and axisymmetric flows.

The available literature on three-dimensional flows is mainly restricted to the linear stretching velocities in two lateral directions. Some self-similar solutions

[1]Complete in a sense (see Sect. 3.1). This statement does not deny the existence of any other self-similar solution.

A. Mehmood, *Viscous Flows*, Mathematical Engineering,
DOI 10.1007/978-3-319-55432-7_5

corresponding to the exponential bilateral wall velocities have also been reported without covering the whole class. In this regard, three-dimensional self-similar flow due to a stretching sheet was introduced by Wang [5] in which he considered linear stretching in the two lateral directions. The axially symmetric case of self-similar flow due to a stretching cylinder was also introduced by Wang [6] where he again assumed the linear stretching velocity at the surface of the cylinder. Another type of axis-symmetric flow, due to a stretching surface, is the case of stretching disk flow which was introduced by Fang [7] by considering the linear radial stretching of the flexible circular disk. In all the aforementioned cases of three-dimensional and axisymmetric flows, the criterion of self-similarity has not been explored completely, thus requiring a thorough investigation regarding the identification of self-similar wall velocities in these cases. After having done all this, one will be more quite in claiming that the criterion of self-similarity in view of the stretching/shrinking wall velocities has completely been determined for the continuous surfaces. This will in turn help to complete the theory of self-similar laminar boundary-layers due to moving continuous surfaces.

In view of above-cited history regarding the, in bits, development of the self-similar boundary-layer flows due to moving continuous surfaces, a student or a new researcher in this area misleadingly perceives that the identification of such particular wall velocities for which the similarity solution exists is just by luck or due to the hit-and-trial method. This is the reason behind the fact that whenever a new self-similar solution was introduced in this area, it was immediately adopted by almost all the researchers involved with this topic. The same is the fact with the "shrinking sheet flow" which has also been adopted by a huge number of researchers despite the fact that the self-similar modeling introduced by Miklavcic and Wang [8] is, somewhat, wrong. But even then, the involved authors are continuously following the incorrect formulation and are publishing wrong results on this topic. A detail account on this issue is given in Chap. 7.

Therefore, keeping these facts in mind the systematic approach toward the determination of self-similar criterion for any flow situation has been explained and employed to the two-dimensional, three-dimensional, and axisymmetric flow situations in this chapter. The allowed wall velocities in the aforementioned cases for which the self-similar solutions exist have been determined, and the corresponding self-similar governing systems have also been derived.

5.1 Two-Dimensional Flow

Consider a flexible impermeable flat sheet emerging from a slit (situated at the point $(0, 0)$) in the positive x-direction with velocity $u_w(x)$. The x-axis has been taken aligned to the sheet, and the y-axis goes deep into the fluid vertically upward by fixing the origin of the coordinate system at the orifice. The fluid is assumed to be viscous and incompressible following the Newton's law of viscosity. Outside the boundary-layer, the fluid velocity is denoted by u_∞ and is assumed to be zero.

Because of the absence of any potential flow and the utility of the boundary-layer assumption, the pressure gradient within the boundary-layer, formed on the moving continuous sheet, is zero. In this situation, the flow is steady and two-dimensional in nature. A schematic of the flow is shown in Fig. 5.1.

Based on the flow assumptions, the appropriate velocity vector reads as:

$$\boldsymbol{V} = [u(x,y), v(x,y), 0]. \tag{5.1}$$

Consequently, the governing boundary-layer system (2.10)–(2.12) reduces to

$$\frac{\partial u}{\partial x} + \frac{\partial v}{\partial y} = 0, \tag{5.2}$$

$$u\frac{\partial u}{\partial x} + v\frac{\partial u}{\partial y} = \nu\frac{\partial^2 u}{\partial y^2}, \tag{5.3}$$

subject to the boundary conditions [due to Eq. (2.17)]

$$\left.\begin{array}{lll} u = u_w(x), v = 0, & \text{at} & y = 0 \\ u = 0, & \text{at} & y = \infty \end{array}\right\}. \tag{5.4}$$

Further simplification to the system (5.2)–(5.4) can be achieved by introducing the stream function $\psi(x,y)$ owing to the following relation with the velocity components:

$$u = \frac{\partial \psi}{\partial y}, \quad v = -\frac{\partial \psi}{\partial x}. \tag{5.5}$$

Due to Eq. (5.5), the equation of continuity (5.2) is satisfied identically and Eqs. (5.3) and (5.4) take the form

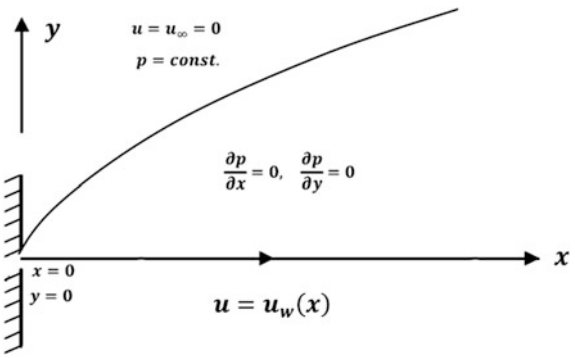

Fig. 5.1 Schematic of the two-dimensional flow and the coordinate system

$$\frac{\partial\psi}{\partial y}\frac{\partial^2\psi}{\partial x\partial y}-\frac{\partial\psi}{\partial x}\frac{\partial^2\psi}{\partial y^2}=\nu\frac{\partial^3\psi}{\partial y^3}, \tag{5.6}$$

$$\left.\begin{array}{lll}\frac{\partial\psi}{\partial y}=u_w(x),\frac{\partial\psi}{\partial x}=0, & \text{at} & y=0\\ \frac{\partial\psi}{\partial y}=0, & \text{at} & y=\infty\end{array}\right\}, \tag{5.7}$$

respectively. Equations (5.6) and (5.7) are the representative equations for the considered two-dimensional flow with certain possible simplifications to be determined.

These equations shall now be applied the procedure of group theoretical approach in obtaining the similarity transformations, as explained in Sect. 3.3. According to the general theory, we need to introduce the scaling of all the variable quantities involved in the system (5.6)–(5.7). Therefore, we choose a scaling group of the form:

$$\bar{x}=k^{\alpha_1}x,\ \ \bar{y}=k^{\alpha_2}y,\ \ \bar{\psi}=k^{\alpha_3}\psi,\ \ \bar{u}_w=k^{\alpha_4}u_w, \tag{5.8}$$

where k is the scaling parameter and $\alpha_i(i=1,\ldots,4)$ denote the scaling exponents. Utilization of the group (5.8) transforms the system (5.6)–(5.7) in the form of new variables as

$$k^{\alpha_1+2\alpha_2-2\alpha_3}\frac{\partial\bar{\psi}}{\partial\bar{y}}\frac{\partial^2\bar{\psi}}{\partial\bar{x}\partial\bar{y}}-k^{\alpha_1+2\alpha_2-2\alpha_3}\frac{\partial\bar{\psi}}{\partial\bar{x}}\frac{\partial^2\bar{\psi}}{\partial\bar{y}^2}=\nu\,k^{3\alpha_2-\alpha_3}\frac{\partial^3\bar{\psi}}{\partial\bar{y}^3}, \tag{5.9}$$

$$\left.\begin{array}{llll}k^{\alpha_2-\alpha_3}\frac{\partial\bar{\psi}}{\partial\bar{y}}=k^{-\alpha_4}\bar{u}_w, & \frac{\partial\bar{\psi}}{\partial\bar{y}}=0, & \text{at} & \bar{y}=0\\ \frac{\partial\bar{\psi}}{\partial\bar{y}}=0, & & \text{at} & \bar{y}=\infty\end{array}\right\}. \tag{5.10}$$

The restriction of invariance of the system (5.6)–(5.7) under the action of scaling group (5.8) requires that all the constant coefficients in (5.9) must have the same powers of k and the same applies to Eq. (5.10) also. This gives rise to a system of algebraic equations in $\alpha_i(i=1,..,4)$ of the form

$$\alpha_1+2\alpha_2-2\alpha_3=3\alpha_2-\alpha_3,\alpha_2-\alpha_3=-\alpha_4. \tag{5.11}$$

Before we solve the system (5.11), it is important to decide, first, about the variable to be eliminated among the original independent variables x and y. In this case, the obvious choice is x. This gives rise the consideration of two cases regarding the zero and nonzero character of α_1, the scaling exponent of x:

Case I $(\alpha_1\neq 0)$
In this case, the division by α_1 to the system (5.11) is possible and results in the system

$$1+2\frac{\alpha_2}{\alpha_1}-2\frac{\alpha_3}{\alpha_1}=3\frac{\alpha_2}{\alpha_1}-\frac{\alpha_3}{\alpha_1},\frac{\alpha_2}{\alpha_1}-\frac{\alpha_3}{\alpha_1}=-\frac{\alpha_4}{\alpha_1},$$

admitting the non-trivial solution of the form

$$\frac{\alpha_3}{\alpha_1}=1-\frac{\alpha_2}{\alpha_1},\frac{\alpha_4}{\alpha_1}=1-2\frac{\alpha_2}{\alpha_1}.$$

The ratio $\frac{\alpha_2}{\alpha_1}$ has appeared as the free variable and will be treated as an arbitrary constant in the subsequent process. Based on this solution, the new variables are constructed as follows (see Eq. 3.14):

$$\eta=\frac{y}{x^{\alpha_2/\alpha_1}},\ f(\eta)=\frac{\psi(x,y)}{x^{\alpha_3/\alpha_1}},\ a\equiv\text{const.}=\frac{u_w(x)}{x^{\alpha_4/\alpha_1}}. \tag{5.12}$$

Let us say

$$1-2\frac{\alpha_2}{\alpha_1}=m(\text{an arbitrary constant}), \tag{5.13}$$

due to which Eq. (5.12) takes the form

$$\eta=x^{\frac{m-1}{2}}y,\ \ \psi=x^{\frac{m+1}{2}}f(\eta),\ \ u_w=ax^m, \tag{5.14}$$

where η and $f(\eta)$ are the new independent and dependent variables, respectively, and a is a pure constant having suitable dimensions. These variables shall be called the similarity variables if they successfully transform the system (5.6)–(5.7) of partial differential equations to an equivalent system of ordinary differential equations. The utilization of Eq. (5.14) in the system (5.6)–(5.7) immediately gives the self-similar system of the form

$$mf'^2-\left(\frac{m+1}{2}\right)ff''=vf''', \tag{5.15}$$

$$f(0)=0,\ \ f'(0)=1,\ \ f'(\infty)=0, \tag{5.16}$$

where the previous variables have successfully been removed. Therefore, the variables η and $f(\eta)$ (given in Eq. 5.14) can safely be regarded as the similarity variables. Notice that in Eq. (5.14), the wall velocity follows the form $u_w=ax^m$ which is of the power-law type. Thus, the case $\alpha_1\neq 0$ results in the power-law wall velocity criterion of the moving continuous surface for which the resulting system (5.15)–(5.16) is self-similar. Notice that Eq. (5.15) is exactly the same as it is for the Falkner–Skan [9] flow. This can also be written as

$$\frac{2m}{m+1}f'^2 - ff'' = vf''', \tag{5.17}$$

if the variable η is scaled by a factor of $\sqrt{\frac{m+1}{2}}$.

Case II ($\boldsymbol{\alpha_1 = 0}$)
In this case, the system (5.11) reduces to the form

$$2\alpha_2 - 2\alpha_3 = 3\alpha_2 - \alpha_3, \quad \alpha_2 - \alpha_3 = -\alpha_4,$$

which admits a non-trivial solution, given by

$$\alpha_3 = -\alpha_2, \quad \alpha_4 = -2\alpha_2.$$

Here α_2 serves as the free variable, whereas α_3 and α_4 are determined using α_2. Let us put $-2\alpha_2 = m$, where m is an arbitrary constant and is local to this case, due to which the above solution is modified as

$$\alpha_2 = -\frac{m}{2}, \quad \alpha_3 = \frac{m}{2}, \quad \alpha_4 = m. \tag{5.18}$$

For the case $\alpha_1 = 0$, the similarity variables are constructed as (see Eq. 3.15):

$$\eta = \frac{y}{e^{\alpha_2 x}}, \quad f(\eta) = \frac{\psi(x,y)}{e^{\alpha_3 x}}, \quad a \equiv \text{const.} = \frac{u_w(x)}{e^{\alpha_4 x}}. \tag{5.19}$$

Substituting the values of $\alpha_i (i = 2, 3, 4)$ from Eq. (5.18) into Eq. (5.19), one gets the new variables of the form

$$\eta = ye^{\frac{m}{2}x}, \quad \psi = e^{\frac{m}{2}x} f(\eta), \quad u_w = ae^{mx}, \tag{5.20}$$

which transform the system (5.6)–(5.7) to the form

$$m\left(f'^2 - \frac{1}{2}ff''\right) = vf''', \tag{5.21}$$

$$f(0) = 0, \quad f'(0) = 1, \quad f'(\infty) = 0. \tag{5.22}$$

Evidently, Eqs. (5.21) and (5.22) are independent of the previous (original) variables. Therefore, the transformations (5.20) can be regarded as similarity transformations and the system (5.21)–(5.22) as the self-similar one. In this case, the wall velocity came out of the exponential form, i.e., $u_w = ae^{mx}$, where m is an arbitrary constant exponent. Thus, the case $\alpha_1 = 0$ leads to another type of similarity solutions for this problem caused by the exponentially varying motion of the continuous surface.

In the available literature, only the case for $m = 1$ has been discussed in the case of exponentially stretching or shrinking wall velocities. The consideration of other

values of m finally completes this class of self-similar flows. This, ignorance of the other values of m, was actually the "incompletion" which we have pointed out in the start of this chapter regarding the two-dimensional flows due to moving continuous surfaces. However, it is again emphasized that, besides the use of the word "complete," we do not claim the nonexistence of any other self-similar solution to this case. The meanings of this completion over here are in the sense that we have explored the self-similar solutions completely, corresponding to the chosen group of scalings.

At the end of this section, it is quite important to summarize that the implementation of group theoretical procedure resulted in two self-similar forms of the two-dimensional boundary-layer equations with the restriction that the wall velocity $u_w(x)$ must either follow the power-law form $(u_w = ax^m)$ or the exponential form $(u_w = ae^{mx})$. That is, if the wall velocity is taken either of the forms the flow will be self-similar; otherwise, it will be non-similar. Such a restriction on the form of variable wall velocity is actually regarded as the criterion of self-similarity to this case.

5.2 Three-Dimensional Flow

In the continuation of above, two-dimensional case, it is again assumed that the fluid of our interest is viscous and incompressible following the Newton's law of viscosity. A semi-infinite body of fluid is assumed to be occupying the upper half space and bounded by an infinite flexible sheet situated at $y = 0$. The flow is assumed to be caused by the variable motion of the sheet surface in two lateral directions. The flow geometry and the chosen system of coordinates are shown in Fig. 5.2.

This type of flow was first considered by Wang [5] in 1984 where he assumed uniform stretching velocities in the two lateral directions and obtained a self-similar solution. Unsteady case of this flow due to an impulsively started stretching sheet was considered by Takhar et al. [10]. Another three-dimensional flow due to a

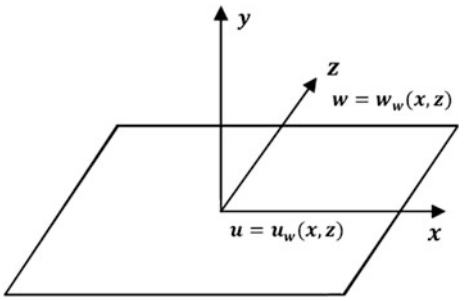

Fig. 5.2 Three-dimensional flow schematic and the associated system of coordinates

stretching sheet was also considered by Wang [11] where he considered unidirectional stretching of the sheet in a rotating fluid. Recently, Liu et al. [12] assumed the exponential stretching wall velocities in the two lateral directions and obtained a self-similar solution to this case. This had been very much unfortunate that the three-dimensional flow due to nonlinear (power-law) wall velocities and the other powers (other than 1) of the exponential wall velocities have not been given any attention, so far. It is therefore important to consider a flow in which the lateral wall velocities have been assumed to be the general functions of x and z coordinates, that is $u_w(x,z)$ and $w_w(x,z)$. The group theoretical procedure will be employed to determine the similarity criterion for the wall velocities by determining the explicit forms of the functions $u_w(x,z)$ and $w_w(x,z)$.

Based on the above assumptions, the flow is essentially three-dimensional owing to the boundary-layer character. Therefore, the velocity vector for such a steady three-dimensional flow reads as

$$\boldsymbol{V} = [u(x,y,z), v(x,y,z), w(x,y,z)]. \tag{5.23}$$

Compatible to this velocity vector, the governing system comprises of Eqs. (2.10)–(2.12) and the appropriate boundary conditions are described as

$$\left.\begin{array}{lll} u = u_w(x,z), v = 0, w = w_w(x,z), & \text{at} & y = 0 \\ u = 0,\ w = 0, & \text{at} & y = \infty \end{array}\right\}. \tag{5.24}$$

Similar to the previous section, the continuity equation can be made satisfied identically by introducing the two stream functions $\psi(x,y,z)$ and $\phi(x,y,z)$ which have the following relations with velocity components:

$$u = \frac{\partial \psi}{\partial y}, \quad w = \frac{\partial \phi}{\partial y}, \quad v = -\left(\frac{\partial \psi}{\partial x} + \frac{\partial \phi}{\partial z}\right). \tag{5.25}$$

The above stream functions were first introduced by Moore [13] and were further refined by Geis [14] for the rectangular Cartesian coordinates. Due to (5.25), the equation of continuity (2.10) satisfies identically by reducing the number of unknowns from three to two. Consequently, Eqs. (2.11), (2.12), and (5.24) readily transform to the new form

$$\frac{\partial \psi}{\partial y}\frac{\partial^2 \psi}{\partial x \partial y} - \frac{\partial \psi}{\partial x}\frac{\partial^2 \psi}{\partial y^2} - \frac{\partial \phi}{\partial z}\frac{\partial^2 \psi}{\partial y^2} + \frac{\partial \phi}{\partial y}\frac{\partial^2 \psi}{\partial y \partial z} = \nu \frac{\partial^3 \psi}{\partial y^3}, \tag{5.26}$$

$$\frac{\partial \psi}{\partial y}\frac{\partial^2 \phi}{\partial x \partial y} - \frac{\partial \psi}{\partial x}\frac{\partial^2 \phi}{\partial y^2} - \frac{\partial \phi}{\partial z}\frac{\partial^2 \phi}{\partial y^2} + \frac{\partial \phi}{\partial y}\frac{\partial^2 \phi}{\partial y \partial z} = \nu \frac{\partial^3 \phi}{\partial y^3}, \tag{5.27}$$

and

$$\left.\begin{array}{lll} \frac{\partial\psi}{\partial y} = u_w(x,z),\ \ \frac{\partial\phi}{\partial y} = w_w(x,z),\ \ \frac{\partial\psi}{\partial x} + \frac{\partial\phi}{\partial z} = 0, & \text{at} & y = 0 \\ \frac{\partial\psi}{\partial y} = 0,\ \ \frac{\partial\phi}{\partial y} = 0, & \text{at} & y = \infty \end{array}\right\}. \tag{5.28}$$

Let us consider a one-parameter group of scalings, of all the involved independent and dependent variables, of the form

$$\bar{x} = k^{\alpha_1}x,\ \bar{y} = k^{\alpha_2}y,\ \bar{z} = k^{\alpha_3}z,\ \bar{\psi} = k^{\alpha_4}\psi,\ \bar{\phi} = k^{\alpha_5}\phi,\ \bar{u}_w = k^{\alpha_6}u_w,\ \bar{w}_w = k^{\alpha_7}w_w, \tag{5.29}$$

where k is the scaling parameter and $\alpha_i (i = 1, \ldots, 7)$ are the scaling exponents. In this case too, the procedure is exactly the same as was implemented in the previous section. The details of the procedure can, therefore, be skipped by retaining the major steps. However, the author feels it necessary and useful, especially for the students, to proceed with a bit more detail in order to facilitate the reader. Moreover, this chapter in general and this section in particular include the crux of this book; therefore, a bit more detail seems not that costly. The extra burden of this chapter will be compensated in the forthcoming chapters. The substitution of (5.29) into the system (5.26)–(5.28) results in the following system in bared notation:

$$\begin{aligned} &k^{\alpha_1+2\alpha_2-2\alpha_4}\left(\frac{\partial\bar{\psi}}{\partial\bar{y}}\frac{\partial^2\bar{\psi}}{\partial\bar{x}\partial\bar{y}} - \frac{\partial\bar{\psi}}{\partial\bar{x}}\frac{\partial^2\bar{\psi}}{\partial\bar{y}^2}\right) - k^{2\alpha_2+\alpha_3-\alpha_4-\alpha_5}\left(\frac{\partial\bar{\phi}}{\partial\bar{z}}\frac{\partial^2\bar{\psi}}{\partial\bar{y}^2} - \frac{\partial\bar{\phi}}{\partial\bar{y}}\frac{\partial^2\bar{\psi}}{\partial\bar{y}\partial\bar{z}}\right) \\ &= \nu k^{3\alpha_2-\alpha_4}\frac{\partial^3\bar{\psi}}{\partial\bar{y}^3}, \end{aligned} \tag{5.30}$$

$$\begin{aligned} &k^{\alpha_1+2\alpha_2-\alpha_4-\alpha_5}\left(\frac{\partial\bar{\psi}}{\partial\bar{y}}\frac{\partial^2\bar{\phi}}{\partial\bar{x}\partial\bar{y}} - \frac{\partial\bar{\psi}}{\partial\bar{x}}\frac{\partial^2\bar{\phi}}{\partial\bar{y}^2}\right) - k^{2\alpha_2+\alpha_3-2\alpha_5}\left(\frac{\partial\bar{\phi}}{\partial\bar{z}}\frac{\partial^2\bar{\phi}}{\partial\bar{y}^2} - \frac{\partial\bar{\phi}}{\partial\bar{y}}\frac{\partial^2\bar{\phi}}{\partial\bar{y}\partial\bar{z}}\right) \\ &= \nu k^{3\alpha_2-\alpha_5}\frac{\partial^3\bar{\phi}}{\partial\bar{y}^3}, \end{aligned} \tag{5.31}$$

and

$$\left.\begin{array}{lll} k^{\alpha_2-\alpha_4}\frac{\partial\bar{\psi}}{\partial\bar{y}} = k^{-\alpha_6}\bar{u}_w, k^{\alpha_2-\alpha_5}\frac{\partial\bar{\phi}}{\partial\bar{y}} = k^{-\alpha_7}\bar{w}_w, k^{\alpha_1-\alpha_4}\frac{\partial\bar{\psi}}{\partial\bar{x}} + k^{\alpha_3-\alpha_5}\frac{\partial\bar{\phi}}{\partial\bar{z}} = 0, & \text{at} & \bar{y} = 0 \\ \frac{\partial\bar{\psi}}{\partial\bar{y}} = 0,\ \ \frac{\partial\bar{\phi}}{\partial\bar{y}} = 0, & \text{at} & \bar{y} = \infty \end{array}\right\}. \tag{5.32}$$

The requirement of invariance of the system (5.26)–(5.28), under the group of scalings (5.29), requires that the system (5.30)–(5.32) must be free from the constant coefficients appearing in the powers of k. This is certainly possible if the following linear system of equations holds:

$$\alpha_1 + 2\alpha_2 - 2\alpha_4 = 2\alpha_2 + \alpha_3 - \alpha_4 - \alpha_5 = 3\alpha_2 - \alpha_4, \tag{5.33}$$

$$\alpha_1 + 2\alpha_2 - \alpha_4 - \alpha_5 = 2\alpha_2 + \alpha_3 - 2\alpha_5 = 3\alpha_2 - \alpha_5, \tag{5.34}$$

$$\alpha_2 - \alpha_4 = -\alpha_6, \alpha_2 - \alpha_5 = -\alpha_7, \alpha_1 - \alpha_4 = \alpha_3 - \alpha_5. \tag{5.35}$$

Note that this case involves three independent variables; in order to transform the system (5.26)–(5.28) to an equivalent system of ordinary differential equations, one must eliminate two independent variables from the original three. Before solving the system (5.33)–(5.35), it is, therefore, quite important to decide for the variable to be eliminated first. Being slack within the boundary-layer, one among the x and z can equally be chosen and this choice will not affect the final result. We prefer to choose x to be eliminated first. In this way, two cases arise corresponding to the zero and nonzero character of the scaling exponent α_1.

Case I $(\alpha_1 \neq 0)$

Dividing the system (5.33)–(5.35) by $\alpha_1 (\neq 0)$ throughout and solving subsequently, one finds

$$\frac{\alpha_2}{\alpha_1} = A, \quad \frac{\alpha_3}{\alpha_1} = B, \quad \frac{\alpha_4}{\alpha_1} = 1 - A, \quad \frac{\alpha_5}{\alpha_1} = B - A, \quad \frac{\alpha_6}{\alpha_1} = 1 - 2A, \quad \frac{\alpha_7}{\alpha_1} = B - 2A, \tag{5.36}$$

due to which the new variables are constructed as:

$$\xi = \frac{z}{x^{\alpha_3/\alpha_1}}, \quad \eta = \frac{y}{x^{\alpha_2/\alpha_1}}, \quad F(\xi,\eta) = \frac{\psi(x,y,z)}{x^{\alpha_4/\alpha_1}}, \quad G(\xi,\eta) = \frac{\phi(x,y,z)}{x^{\alpha_5/\alpha_1}},$$
$$F_w = \frac{u_w(x,z)}{x^{\alpha_6/\alpha_1}}, \quad G_w = \frac{w_w(x,z)}{x^{\alpha_7/\alpha_1}}. \tag{5.37}$$

Assuming that $1 - 2A = m$ (an arbitrary constant), we finally get

$$\xi = x^{-B} z, \quad \eta = x^{\frac{m-1}{2}} y, \quad \psi = x^{\frac{m+1}{2}} F(\xi,\eta), \quad \phi = x^{B-\frac{m-1}{2}} G(\xi,\eta), \tag{5.38}$$

with

$$u_w(x,z) = x^m F_w(\xi), \quad w_w(x,z) = x^{B-(m-1)} G_w(\xi), \tag{5.39}$$

where B is also an arbitrary constant which can also be chosen equal to zero. For the sake of generality, B will be treated as nonzero in the further proceedings.

At this stage, the variables x has been absorbed in the new independent variables ξ and η which are now $2(= 3 - 1)$ in number. The above new variables (5.38) and (5.39) transform the system (5.26)–(5.28) to the form

$$m\left(\frac{\partial F}{\partial \eta}\right)^2 - B\xi\frac{\partial F}{\partial \eta}\frac{\partial^2 F}{\partial \xi \partial \eta} - \left(\frac{m+1}{2}\right)F\frac{\partial^2 F}{\partial \eta^2} + B\xi\frac{\partial F}{\partial \xi}\frac{\partial^2 F}{\partial \eta^2} - \frac{\partial G}{\partial \xi}\frac{\partial^2 F}{\partial \eta^2} + \frac{\partial G}{\partial \eta}\frac{\partial^2 F}{\partial \xi \partial \eta} = v\frac{\partial^3 F}{\partial \eta^3}, \tag{5.40}$$

$$(B+m-1)\frac{\partial F}{\partial \eta}\frac{\partial G}{\partial \eta} - B\xi\frac{\partial F}{\partial \eta}\frac{\partial^2 G}{\partial \xi \partial \eta} - \left(\frac{m+1}{2}\right)F\frac{\partial^2 G}{\partial \eta^2} + B\xi\frac{\partial F}{\partial \xi}\frac{\partial^2 G}{\partial \eta^2} - \frac{\partial G}{\partial \xi}\frac{\partial^2 G}{\partial \eta^2} + \frac{\partial G}{\partial \eta}\frac{\partial^2 G}{\partial \xi \partial \eta} = v\frac{\partial^3 G}{\partial \eta^3}, \tag{5.41}$$

and

$$\left.\begin{array}{llll} \frac{\partial F}{\partial \eta} = F_w(\xi), \ \ \frac{\partial G}{\partial \eta} = G_w(\xi), & \left(\frac{m+1}{2}\right)F - B\xi\frac{\partial F}{\partial \xi} + \frac{\partial G}{\partial \xi} = 0, & \text{at} & \eta = 0 \\ \frac{\partial F}{\partial \eta} = 0, \ \ \frac{\partial G}{\partial \eta} = 0, & & \text{at} & \eta = \infty \end{array}\right\}. \tag{5.42}$$

Evidently, the variable x has been eliminated successfully indicating that the process can be continued further for the elimination of one more independent variable. For doing so, we again assume a one-parameter group of scalings of the variables involved in the system (5.40)–(5.42):

$$\bar{\xi} = k^{\beta_1}\xi, \ \ \bar{\eta} = k^{\beta_2}\eta, \ \ \bar{F} = k^{\beta_3}F, \ \ \bar{G} = k^{\beta_4}G, \ \ \bar{F}_w = k^{\beta_5}F_w, \ \ \bar{G}_w = k^{\beta_6}G_w, \tag{5.43}$$

where $\beta_i (i = 1, \ldots, 6)$ are the scaling exponents to be determined. The group (5.43) transforms the system (5.40)–(5.42) to the form

$$k^{2\beta_2-2\beta_3}\left[m\left(\frac{\partial \bar{F}}{\partial \bar{\eta}}\right)^2 - B\bar{\xi}\frac{\partial \bar{F}}{\partial \bar{\eta}}\frac{\partial^2 \bar{F}}{\partial \bar{\xi}\partial \bar{\eta}} - \left(\frac{m+1}{2}\right)\bar{F}\frac{\partial^2 \bar{F}}{\partial \bar{\eta}^2} + B\bar{\xi}\frac{\partial \bar{F}}{\partial \bar{\xi}}\frac{\partial^2 \bar{F}}{\partial \bar{\eta}^2}\right] - k^{\beta_1+2\beta_2-\beta_3-\beta_4}\left[\frac{\partial \bar{G}}{\partial \bar{\xi}}\frac{\partial^2 \bar{F}}{\partial \bar{\eta}^2} - \frac{\partial \bar{G}}{\partial \bar{\eta}}\frac{\partial^2 \bar{F}}{\partial \bar{\xi}\partial \bar{\eta}}\right] = vk^{3\beta_2-\beta_3}\frac{\partial^3 \bar{F}}{\partial \bar{\eta}^3}, \tag{5.44}$$

$$k^{2\beta_2-\beta_3-\beta_4}\left[(B+m-1)\frac{\partial \bar{F}}{\partial \bar{\eta}}\frac{\partial \bar{G}}{\partial \bar{\eta}} - B\bar{\xi}\frac{\partial \bar{F}}{\partial \bar{\eta}}\frac{\partial^2 \bar{G}}{\partial \bar{\xi}\partial \bar{\eta}} - \left(\frac{m+1}{2}\right)\bar{F}\frac{\partial^2 \bar{G}}{\partial \bar{\eta}^2} + B\bar{\xi}\frac{\partial \bar{F}}{\partial \bar{\xi}}\frac{\partial^2 \bar{G}}{\partial \bar{\eta}^2}\right] - k^{\beta_1+2\beta_2-2\beta_4}\left[\frac{\partial \bar{G}}{\partial \bar{\xi}}\frac{\partial^2 \bar{G}}{\partial \bar{\eta}^2} - \frac{\partial \bar{G}}{\partial \bar{\eta}}\frac{\partial^2 \bar{G}}{\partial \bar{\xi}\partial \bar{\eta}}\right] = vk^{3\beta_2-\beta_4}\frac{\partial^3 \bar{G}}{\partial \bar{\eta}^3}, \tag{5.45}$$

and

$$\left.\begin{array}{ll} k^{\beta_2-\beta_3}\frac{\partial \bar{F}}{\partial \bar{\eta}} = k^{-\beta_5}\bar{F}_w, \quad k^{\beta_2-\beta_4}\frac{\partial \bar{G}}{\partial \bar{\eta}} = k^{-\beta_6}\bar{G}_w, & \\ k^{-\beta_3}\left[\left(\frac{m+1}{2}\right)\bar{F} - B\bar{\xi}\frac{\partial \bar{F}}{\partial \bar{\xi}}\right] + k^{\beta_1-\beta_4}\frac{\partial \bar{G}}{\partial \bar{\xi}} = 0, & \text{at} \quad \bar{\eta} = 0 \\ \frac{\partial \bar{F}}{\partial \bar{\eta}} = 0, \quad \frac{\partial \bar{G}}{\partial \bar{\eta}} = 0, & \\ & \text{at} \quad \bar{\eta} = \infty \end{array}\right\}. \tag{5.46}$$

The requirement of invariance of the system (5.40)–(5.42) under the group (5.43) leads to the system of linear algebraic equations in $\beta_i (i = 1, \ldots, 6)$ given as

$$2\beta_2 - 2\beta_3 = \beta_1 + 2\beta_2 - \beta_3 - \beta_4 = 3\beta_2 - \beta_3, \tag{5.47}$$

$$2\beta_2 - \beta_3 - \beta_4 = \beta_1 + 2\beta_2 - 2\beta_4 = 3\beta_2 - \beta_4, \tag{5.48}$$

$$\beta_2 - \beta_3 = -\beta_5, \beta_2 - \beta_4 = -\beta_6, \beta_1 - \beta_4 = -\beta_3. \tag{5.49}$$

Again, before solving the system (5.47)–(5.49) the selection of the leaving variable is mandatory. In view of the expressions of ξ and η given in Eq. (5.38), the natural choice is ξ. In the group of scalings (5.43), β_1 is the scaling exponent of the variable ξ. The zero and nonzero character of β_1 is again of particular importance in the construction of new variables. Before we continue with the solution of the system (5.47)–(5.49), it is worth remembering that we are already proceeding the Case I ($\alpha_1 \neq 0$) and the ongoing process is actually a part of Case I. Therefore, the cases $\beta_1 \neq 0$ and $\beta_1 = 0$ need to be designated as the subcases of Case I. Thus, from now onward the cases $\beta_1 \neq 0$ and $\beta_1 = 0$ shall, respectively, be designated as

Case I; Subcase I ($\alpha_1 \neq 0;\ \beta_1 \neq 0$),
Case I; Subcase II ($\alpha_1 \neq 0;\ \beta_1 = 0$).

Case I; Subcase I ($\alpha_1 \neq 0;\ \beta_1 \neq 0$)
The nonzero character of β_1 allows the division of the system (5.47)–(5.49) by β_1 everywhere. This results in the following system of algebraic equations

$$2\frac{\beta_2}{\beta_1} - 2\frac{\beta_3}{\beta_1} = 1 + 2\frac{\beta_2}{\beta_1} - \frac{\beta_3}{\beta_1} - \frac{\beta_4}{\beta_1} = 3\frac{\beta_2}{\beta_1} - \frac{\beta_3}{\beta_1}, \tag{5.50}$$

$$2\frac{\beta_2}{\beta_1} - \frac{\beta_3}{\beta_1} - \frac{\beta_4}{\beta_1} = 1 + 2\frac{\beta_2}{\beta_1} - 2\frac{\beta_4}{\beta_1} = 3\frac{\beta_2}{\beta_1} - \frac{\beta_4}{\beta_1}, \tag{5.51}$$

$$\frac{\beta_2}{\beta_1} - \frac{\beta_3}{\beta_1} = -\frac{\beta_5}{\beta_1}, \quad \frac{\beta_2}{\beta_1} - \frac{\beta_4}{\beta_1} = -\frac{\beta_6}{\beta_1}, \quad 1 - \frac{\beta_4}{\beta_1} = -\frac{\beta_3}{\beta_1}, \tag{5.52}$$

which ultimately solves as

$$\frac{\beta_3}{\beta_1} = -\frac{\beta_2}{\beta_1}, \quad \frac{\beta_4}{\beta_1} = 1 - \frac{\beta_2}{\beta_1}, \quad \frac{\beta_5}{\beta_1} = -2\frac{\beta_2}{\beta_1}, \quad \frac{\beta_6}{\beta_1} = 1 - 2\frac{\beta_2}{\beta_1}. \tag{5.53}$$

Having this solution in hand, the new variables are thus constructed as

$$\zeta = \xi^{\frac{n-1}{2}}\eta, \quad F(\xi,\eta) = \xi^{\frac{n-1}{2}} f(\zeta), \quad G(\xi,\eta) = \xi^{\frac{n+1}{2}} g(\zeta), \tag{5.54}$$

where the wall profiles read as

$$F_w(\xi) = a\xi^{n-1}, \quad G_w(\xi) = b\xi^n. \tag{5.55}$$

where n denotes an arbitrary (dimensionless) constant constructed as

$$1 - 2\frac{\beta_2}{\beta_1} = n. \tag{5.56}$$

Furthermore, the constants a and b are also arbitrary, having suitable dimensions which are usually referred to as the stretching or shrinking rates. Consequently, the system (5.40)–(5.42) transforms as:

$$(m - B(n-1))f'^2 - \left(\frac{m+1}{2} - B\left(\frac{n-1}{2}\right)\right)ff'' - \left(\frac{n+1}{2}\right)gf'' + (n-1)f'g' = vf''', \tag{5.57}$$

$$(m - 1 - B(n-1))f'g' - \left(\frac{m+1}{2} - B\left(\frac{n-1}{2}\right)\right)fg'' - \left(\frac{n+1}{2}\right)gg'' + ng'^2 = vg''', \tag{5.58}$$

and

$$\left.\begin{array}{llll} f' = a, & g' = b, & \left(\frac{m+1}{2} - B\left(\frac{n-1}{2}\right)\right)f + \left(\frac{n+1}{2}\right)g = 0, & \text{at} \quad \zeta = 0 \\ f' = 0, & g' = 0, & & \text{at} \quad \zeta = \infty \end{array}\right\}, \tag{5.59}$$

where the $'$ denotes differentiation with respect to ζ. Clearly, the system (5.57)–(5.59) is a system of ordinary differential equations from where the, absorbed (previous), independent variables have completely been eliminated.

Since the scaling groups of one-parameter transformations have been utilized, therefore, the reduction in the number of independent variables at each step is also one. This is the reason for the elimination of x and z in two steps. However, it is also possible to eliminate more than one variable at once; for doing so, one must utilize the multi-parameter group of scalings. The details of such a procedure can be found in Refs. [15, 16]. After having determined the suitable similarity transformations due to one-parameter group of scalings, it then stays not necessary to transform the original system (5.26)–(5.28) to the self-similar form (5.57)–(5.59) in two steps, essentially. An integrated set of similarity transformations is possible to obtain by combining Eqs. (5.38) and (5.54) as

$$\zeta = z^{\frac{n-1}{2}} x^{\frac{m-1}{2}-B\left(\frac{n-1}{2}\right)} y, \quad \psi = z^{\frac{n-1}{2}} x^{\frac{m+1}{2}-B\left(\frac{n-1}{2}\right)} f(\zeta), \quad \phi = z^{\frac{n+1}{2}} x^{\frac{m-1}{2}-B\left(\frac{n-1}{2}\right)} g(\zeta), \tag{5.60}$$

which can directly transform the system (5.26)–(5.28) to the self-similar form (5.57)–(5.59) in a single step. Similarly, the obtained wall velocities after combining Eqs. (5.39) and (5.55) in their final form read as

$$\left.\begin{aligned} u_w &= a x^{m-B(n-1)} z^{n-1} \\ w_w &= b x^{m-1-B(n-1)} z^{n} \end{aligned}\right\}. \tag{5.61}$$

Case I; Subcase II $(\alpha_1 \neq 0,\ \beta_1 = 0)$
Substitution of $\beta_1 = 0$ does not affect the system (5.47)–(5.49) by any large. The resulting system does admit a non-trivial solution of the form

$$\beta_3 = -\beta_2, \quad \beta_4 = -\beta_2, \quad \beta_5 = -2\beta_2, \quad \beta_6 = -2\beta_2. \tag{5.62}$$

This solution can also be recovered by multiplying Eq. (5.53) by β_1 and substituting $\beta_1 = 0$ subsequently. In this case, the new variables are constructed as

$$\zeta = \frac{\eta}{e^{\beta_2 \xi}}, \quad f(\zeta) = \frac{F(\xi,\eta)}{e^{\beta_3 \xi}}, \quad g(\zeta) = \frac{G(\xi,\eta)}{e^{\beta_4 \xi}}, \tag{5.63}$$

and the wall velocities come out of the form

$$a \equiv \text{const.} = \frac{F_w(\xi)}{e^{\beta_5 \xi}}, \quad b \equiv \text{const.} = \frac{G_w(\xi)}{e^{\beta_6 \xi}}, \tag{5.64}$$

where a and b are constants having suitable dimensions. With the aid of Eq. (5.62), one explicitly finds from Eqs. (5.63) and (5.64) that

$$\zeta = e^{\frac{n}{2}\xi}\eta, \quad F(\xi,\eta) = e^{\frac{n}{2}\xi} f(\zeta), \quad G(\xi,\eta) = e^{\frac{n}{2}\xi} g(\zeta), \tag{5.65}$$

and

$$F_w(\xi) = a e^{n\xi}, \quad G_w(\xi) = b e^{n\xi}, \tag{5.66}$$

where n is an arbitrary (dimensionless) constant defined by

$$-2\beta_2 = n. \tag{5.67}$$

The use of similarity variables (5.65) transforms the system of partial differential Eqs. (5.40) and (5.41) to the system of ordinary differential equations, given by

$$m f'^2 - \left(\frac{m+1}{2}\right) f f'' - \frac{n}{2} g f'' + n f' g' - B n \xi \left(f'^2 - \frac{1}{2} f f''\right) = \nu f''', \tag{5.68}$$

$$(B+m-1)f'g'-\left(\frac{m+1}{2}\right)fg''-\frac{n}{2}gg''+ng'^2-Bn\xi\left(f'g'-\frac{1}{2}fg''\right)=vg''', \tag{5.69}$$

from which the previous variable ξ has not been eliminated completely. However, the elimination of ξ can be ensured by choosing the arbitrary constant

$$B=0. \tag{5.70}$$

This is important to remember that this particular choice of B is particular to this case only and does not apply to other cases in general. By doing so, the self-similar system reads as:

$$mf'^2-\left(\frac{m+1}{2}\right)ff''-\frac{n}{2}gf''+nf'g'=vf''', \tag{5.71}$$

$$(m-1)f'g'-\left(\frac{m+1}{2}\right)fg''-\frac{n}{2}gg''+ng'^2=vg'''. \tag{5.72}$$

The use of the similarity variables (5.65) and the so determined wall velocity laws (5.66) transform the boundary conditions (5.42) to the form

$$\left.\begin{array}{llll} f'=a, & g'=b, & \left(\frac{m+1}{2}\right)f+\frac{n}{2}g=0, & \text{at} \quad \zeta=0 \\ f'=0, & g'=0, & & \text{at} \quad \zeta=\infty \end{array}\right\}. \tag{5.73}$$

The unified transformations for this case are obtained by combining (5.38) and (5.65) as

$$\zeta=x^{\frac{m-1}{2}}\mathrm{e}^{\frac{n}{2}zx^{-B}}y, \quad \psi=x^{\frac{m+1}{2}}\mathrm{e}^{\frac{n}{2}zx^{-B}}f(\zeta), \quad \phi=x^{B+\frac{m-1}{2}}\mathrm{e}^{\frac{n}{2}zx^{-B}}g(\zeta),$$

which cannot serve as similarity transformation until $B=0$. Owing to Eq. (5.70), the above transformation takes the form

$$\zeta=x^{\frac{m-1}{2}}\mathrm{e}^{\frac{n}{2}z}y, \quad \psi=x^{\frac{m+1}{2}}\mathrm{e}^{\frac{n}{2}z}f(\zeta), \quad \phi=x^{\frac{m-1}{2}}\mathrm{e}^{\frac{n}{2}z}g(\zeta), \tag{5.74}$$

which can directly transform original Eqs. (5.26)–(5.28) to the self-similar form (5.71)–(5.73). Accordingly, the compact form of the wall velocity functions can also be obtained by combining Eq. (5.66) with Eq. (5.39). Consequently, after incorporating Eq. (5.70), one finally obtains

$$u_w=ax^m\mathrm{e}^{nz}, \quad w_w=bx^{m-1}\mathrm{e}^{nz}. \tag{5.75}$$

To this end, the Case I ($\alpha_1\neq 0$) and the two subcases of it corresponding to $\beta_1\neq 0$ and $\beta_1=0$ which were named as "Case I; Subcase I" and "Case I;

Subcase II," respectively, have been completed. Further proceeding of the procedure requires the reconsideration of the system (5.33)–(5.35) for the case $\alpha_1 = 0$. In the series of "main cases," this case is designated as "Case II ($\alpha_2 = 0$)."

Case II ($\alpha_2 = 0$)

With the substitution $\alpha_2 = 0$, the system (5.33)–(5.35) admits the (non-trivial) solution of the form

$$\alpha_4 = -\alpha_2,\ \alpha_5 = \alpha_3 - \alpha_2,\ \alpha_6 = -2\alpha_2,\ \alpha_7 = -2\alpha_2 + \alpha_3, \tag{5.76}$$

where α_2 and α_3 are the free variables, hence arbitrary. Substituting

$$-2\alpha_2 = m \text{ and } \alpha_3 = B, \tag{5.77}$$

the new variables, constructed in the same way as did in the previous cases, come out to be

$$\xi = \mathrm{e}^{-Bx} z,\ \ \eta = \mathrm{e}^{\frac{m}{2}x} y,\ \ \psi = \mathrm{e}^{\frac{m}{2}x} F(\xi, \eta),\ \ \phi = \mathrm{e}^{\left(B + \frac{m}{2}\right)x} G(\xi, \eta). \tag{5.78}$$

The wall velocities also involve the exponential functions and come out of the form

$$u_w = \mathrm{e}^{mx} F_w(\xi),\ \ w_w = \mathrm{e}^{(B+m)x} G_w(\xi). \tag{5.79}$$

With the aid of these new variables, the original system (5.26)–(5.28) transforms to the following new system involving two independent variables:

$$\begin{aligned} &m\left(\frac{\partial F}{\partial \eta}\right)^2 - \frac{m}{2} F \frac{\partial^2 F}{\partial \eta^2} - \frac{\partial G}{\partial \xi}\frac{\partial^2 F}{\partial \eta^2} + \frac{\partial G}{\partial \eta}\frac{\partial^2 F}{\partial \xi \partial \eta} \\ &\quad - B\xi\left(\frac{\partial F}{\partial \eta}\frac{\partial^2 F}{\partial \xi \partial \eta} - \frac{\partial F}{\partial \xi}\frac{\partial^2 F}{\partial \eta^2}\right) = \nu \frac{\partial^3 F}{\partial \eta^3}, \end{aligned} \tag{5.80}$$

$$\begin{aligned} &(B+m)\frac{\partial F}{\partial \eta}\frac{\partial G}{\partial \eta} - \frac{m}{2} F \frac{\partial^2 G}{\partial \eta^2} - \frac{\partial G}{\partial \xi}\frac{\partial^2 G}{\partial \eta^2} + \frac{\partial G}{\partial \eta}\frac{\partial^2 G}{\partial \xi \partial \eta} \\ &\quad - B\xi\left(\frac{\partial F}{\partial \eta}\frac{\partial^2 G}{\partial \xi \partial \eta} - \frac{\partial F}{\partial \xi}\frac{\partial^2 G}{\partial \eta^2}\right) = \nu \frac{\partial^3 G}{\partial \eta^3}, \end{aligned} \tag{5.81}$$

$$\left.\begin{array}{llll} \frac{\partial F}{\partial \eta} = F_w(\xi),\ \ \frac{\partial G}{\partial \eta} = G_w(\xi),\ \ \frac{m}{2}F - B\xi\frac{\partial F}{\partial \xi} + \frac{\partial G}{\partial \xi} = 0, & \text{at} & \eta = 0 \\ \frac{\partial F}{\partial \eta} = 0,\ \ \frac{\partial G}{\partial \eta} = 0, & \text{at} & \eta = \infty \end{array}\right\}. \tag{5.82}$$

In order to eliminate ξ from the system (5.80)–(5.82), one again requires to follow the same procedure as was performed in Case I. It is worth noting that the names of the variables in (5.80)–(5.82) are, however, exactly the same as they are in (5.40)–(5.42), but are entirely different, in actual. Therefore, for the sake of doing mathematics the similarity in their symbolic names can be utilized in order to avoid

the replication of similar things. In this way, staying limited to their symbolic names, we employ the group (5.43) to the above system (5.80)–(5.82). Transforming Eqs. (5.80)–(5.82) to the form of new variables, defined in Eq. (5.43), and imposing the restriction of invariance, one is finally left with the system of following linear equations:

$$2\beta_2 - 2\beta_3 = \beta_1 + 2\beta_2 - \beta_3 - \beta_4 = 3\beta_2 - \beta_3, \tag{5.83}$$

$$2\beta_2 - \beta_3 - \beta_4 = \beta_1 + 2\beta_2 - 2\beta_4 = 3\beta_2 - \beta_4, \tag{5.84}$$

$$\beta_2 - \beta_3 = -\beta_5,\ \beta_2 - \beta_4 = -\beta_6,\ \beta_1 - \beta_4 = -\beta_3. \tag{5.85}$$

Following the previous practice, let us decide to eliminate the variable ξ for which two cases arise regarding the zero and nonzero character of β_1. The cases $\beta_1 \neq 0$ and $\beta_1 = 0$ shall be referred to as the Subcase I and Subcase II, respectively. In the perspective of Case II ($\alpha_1 = 0$), they shall finally be referred to as "Case II; Subcase I" for $\alpha_1 = 0$ & $\beta_1 \neq 0$ and "Case II; Subcase II" for $\alpha_1 = 0$ & $\beta_1 = 0$.

Case II; Subcase I ($\alpha_1 = 0;\ \beta_1 \neq 0$)
Interestingly, the system (5.83)–(5.85) is the same as (5.47)–(5.49). Utilization of the assumption $\beta_1 \neq 0$ in the system (5.83)–(5.85) produces the same non-trivial solution as given in Eq. (5.53) with $\frac{\beta_2}{\beta_1}$ as an arbitrary constant. Therefore, the construction of new variables follows immediately from Eq. (5.54) and the expressions of the wall velocities are also exactly the same as given in Eq. (5.55). Thus, the new variables in this case read as

$$\zeta = \xi^{\frac{n-1}{2}}\eta,\quad F(\xi,\eta) = \xi^{\frac{n-1}{2}} f(\zeta),\quad G(\xi,\eta) = \xi^{\frac{n+1}{2}} g(\zeta), \tag{5.86}$$

and the wall velocities come out to be

$$F_w(\xi) = a\xi^{n-1},\quad G_w(\xi) = b\xi^n, \tag{5.87}$$

with a and b serving as (pure) constants having suitable dimensions. In terms of new variables, Eqs. (5.80) and (5.81) take the form

$$(m - B(n-1))f'^2 - \frac{1}{2}(m - B(n-1))ff'' - \left(\frac{n+1}{2}\right)gf'' + (n-1)f'g' = vf''', \tag{5.88}$$

$$(m - B(n-1))f'g' - \frac{1}{2}(m - B(n-1))fg'' - \left(\frac{n+1}{2}\right)gg'' + ng'^2 = vg''', \tag{5.89}$$

and the boundary conditions (5.82), with the aid of Eq. (5.87), transform as

$$\left.\begin{array}{llll} f' = a, \;\; g' = b, \;\; \frac{1}{2}(m - B(n-1))f + \left(\frac{n+1}{2}\right)g = 0, & \text{at} & \zeta = 0 \\ f' = 0, \;\; g' = 0, & \text{at} & \zeta = \infty \end{array}\right\}. \tag{5.90}$$

Combination of Eq. (5.86) with Eq. (5.78) and of Eq. (5.87) with Eq. (5.79) gives, respectively, the unified form of the similarity variables and the associated wall velocities, as

$$\zeta = z^{\frac{n-1}{2}} e^{\frac{1}{2}(m-B(n-1))x} y, \;\; \psi = z^{\frac{n-1}{2}} e^{\frac{1}{2}(m-B(n-1))x} f(\zeta), \;\; \phi = z^{\frac{n+1}{2}} e^{\frac{1}{2}(m-B(n-1))x} g(\zeta), \tag{5.91}$$

and

$$u_w = a z^{n-1} e^{(m-B(n-1))x}, \;\; w_w = b z^n e^{(m-B(n-1))x}. \tag{5.92}$$

It is evident that the system (5.88)–(5.90) is in the self-similar form and can also be recovered by applying the transformation (5.91) directly to the system (5.26)–(5.28).

Case II; Subcase II ($\alpha_1 = 0, \;\; \beta_1 = 0$)

The choice $\beta_1 = 0$ is the same as that in the case "Case I; Subcase II." Therefore, the system of linear Eqs. (5.83)–(5.85), at $\beta_1 = 0$, recovers to the same results as given in Eq. (5.62). Consequently, the new variables in the present case are exactly the same as those constructed in Eq. (5.65), in symbolic sense. Just to avoid any confusion, we prefer to write here the new variables of the present case given by

$$\zeta = e^{\frac{n}{2}\xi} \eta, \;\; F(\xi, \eta) = e^{\frac{n}{2}\xi} f(\zeta), \;\; G(\xi, \eta) = e^{\frac{n}{2}\xi} g(\zeta), \tag{5.93}$$

which are, of course, of the same form as given in Eq. (5.65), but are entirely different (from 5.65) in physical sense because of the different definitions of ξ and η in these two cases. Similarly, the wall velocity profiles of this case, given by

$$F_w(\xi) = a e^{n\xi}, \;\; G_w(\xi) = b e^{n\xi}, \tag{5.94}$$

are also similar to those given in Eq. (5.66), in symbolic sense. According to the variables defined in Eq. (5.93) and the wall velocities given in Eq. (5.94), the system (5.80)–(5.82) readily transforms to the form

$$m f'^2 - \frac{m}{2} f f'' - \frac{n}{2} g f'' + n f' g' - Bn\xi \left(f'^2 - \frac{1}{2} f f'' \right) = v f''', \tag{5.95}$$

$$(B + m) f' g' - \frac{m}{2} f g'' - \frac{n}{2} g g'' + n g'^2 - Bn\xi \left(f' g' - \frac{1}{2} f g'' \right) = v g''', \tag{5.96}$$

with

$$\left.\begin{array}{llll} f' = a, & g' = b, & \frac{1}{2}(m - Bn\xi)f + \frac{1}{2}ng = 0, & \text{at} \quad \zeta = 0 \\ f' = 0, & g' = 0, & & \text{at} \quad \zeta = \infty \end{array}\right\}. \tag{5.97}$$

Again, similar to the case "Case I; Subcase II" the system (5.95)–(5.97) is not free from the previous variable ξ. Choosing $B = 0$, the self-similar system for the present case furnishes as

$$mf'^2 - \frac{m}{2}ff'' - \frac{n}{2}gf'' + nf'g' = vf''', \tag{5.98}$$

$$mf'g' - \frac{m}{2}fg'' - \frac{n}{2}gg'' + ng'^2 = vg'''. \tag{5.99}$$

$$\left.\begin{array}{llll} f' = a, & g' = b, & mf + ng = 0, & \text{at} \quad \zeta = 0 \\ f' = 0, & g' = 0 & & \text{at} \quad \zeta = \infty \end{array}\right\}. \tag{5.100}$$

Unification of Eqs. (5.93) and (5.78) gives the complete set of similarity variables (under the assumption $B = 0$)

$$\zeta = \mathrm{e}^{\frac{1}{2}(mx+nz)}y, \quad \psi = \mathrm{e}^{\frac{1}{2}(mx+nz)}f(\zeta), \quad \phi = \mathrm{e}^{\frac{1}{2}(mx+nz)}g(\zeta), \tag{5.101}$$

due to which Eqs. (5.26)–(5.28) can directly be transformed to the system (5.98)–(5.100) in a single step. Combination of Eqs. (5.94) and (5.79) gives the final form of the velocity functions (after substituting $B = 0$)

$$u_w = a\mathrm{e}^{mx+nz}, \quad w_w = b\mathrm{e}^{mx+nz}. \tag{5.102}$$

In the above calculations, the self-similar equations of the generalized three-dimensional flow, due to the bidirectional motion of the flexible continuous sheet, have been furnished. The utilized group theoretical approach splits itself into four separate cases and produces different self-similar systems for each case. Normally, in a case, when there is only one variable to be eliminated, as in the two-dimensional case, Sect. 5.1, two types of the wall velocity function are obtained, namely the power-law (given in Eq. 5.14) and the exponential form (given in Eq. 5.20). The nonzero case of the scaling exponent of the leaving variable results in the power-law wall velocity, and the vanishing value of such scaling exponent produces the exponential form of the wall velocity in order to end up with a self-similar system. In other words, this can also be rephrased as that these two cases corresponding to zero and nonzero character of the scaling variable promise to end up with a self-similar system provided that the wall velocities must follow either exponential form or the power-law form, respectively. From here, it can easily be perceived that if the self-similar solution to the boundary-layer equations exists, the wall velocities (or reference velocities) must follow either power-law or exponential form, in general. The converse of this does, however, not apply in general. This is because the self-similarity of the involved partial

differential equations is strictly associated with the requirement of their reduction to the ordinary differential equations, free from the previous variables completely. From Eqs. (5.68)–(5.69) and Eqs. (5.95)–(5.96), it is obvious that the power-law or exponential form of the wall velocities did not guarantee the self-similarity of the whole system. Thus, in general, the requirement of the wall velocities to follow the power-law or exponential forms is the first ingredient and the requirement of reduction of the governing system of *pdes* to an equivalent system of *odes* by eliminating the previous variables completely is the second ingredient. These two fundamental ingredients of self-similarity are actually executed due to the similarity transformations. Hence, the appropriate wall velocity functions (power-law or exponential) and the suitable similarity transformations along with the condition of thorough elimination of the previous variables from the transformed system in new variables ensure the self-similarity of the boundary-layer equations. If any one of these ingredients is not fully achieved, the self-similarity cannot be guaranteed.

Finally, regarding the forms of wall the velocity functions in the perspective of self-similarity, it is concluded that wall velocities can never take any form other than the power-law or exponential ones. Neither a linear combination of the two families nor a linear combination of any two particular entities of the same family can be taken, in general, in order to obtain the self-similar solution. For example, the self-similar solution exists for the famous Falkner–Skan [9] equation if the potential flow follows the power-law form, i.e., $u_\infty(x) = ax^m$. The value $m = 0$ recovers the Blasius [17] case $u_\infty(x) = U_0 = \text{const.}$, while the value $m = 1 (u_\infty(x) = ax)$ recovers the wedge flow. It is well known that the similarity solution exists in these two cases. However, there is no self-similar solution for the combination of these two, that is, when the potential velocity is a combination of the two $(u_\infty(x) = U_0 \pm ax)$. This type of potential flow is particular to the famous Howarth's [18] non-similar flow.

In the currently treated three-dimensional flow, there were two variables x & z to be eliminated. In this case too, there were two choices for the wall velocities to follow, namely the power-law and the exponential one. In this case, the product of the two families has appeared as another possible form of the wall velocities as can be seen in Eqs. (5.61), (5.75), (5.92), and (5.102). This is because of the fact that the variables have been eliminated successively, and the exponential and the power-law cases of the descendent variables are automatically combined with either the exponential or the power-law cases of the preceding elimination. That is, the power-law in x has been combined by the power-law in z (Eq. 5.61) and exponential in z (Eq. 5.75); similarly, exponential wall velocity in x has been combined with the power-law in z (Eq. 5.92) and exponential in z (Eq. 5.102). Thus, the wall velocity functions defined in Eqs. (5.61), (5.75), (5.92), and (5.102) define the criterion of self-similarity for the wall velocities in three-dimensional flow due to a moving continuous flat surface. If the wall velocities deviate from the forms given in these equations, the self-similarity is not guaranteed.

5.3 Axially Symmetric Flow

In the previous two sections, the planner cases of two- and three-dimensional flows near the flat surfaces have been considered. In the case of axially symmetric flows, the solid surface of interest would be the solid body of revolution either flat or non-flat. In the case of non-flat surfaces, the surface curvature imparts significant effects on the flow characteristics within the boundary-layer. Consequently, the surface curvature also plays an important role while determining the self-similar wall velocities. A long, slim continuous cylinder is a trivial example of the body of revolution involving surface curvature. On the other hand, the circular flat disk is the example where the surface involves no curvature besides being an axially symmetric body of revolution. Thus, the circular cylinder and the circular disk shall be the objects of our interest in this section. Different from the previous two planner cases, some important facts shall be revealed regarding the cylinder and the disk geometries in view of the similarity criterion because of the axially symmetric nature of these flows.

5.3.1 Moving Cylinder

Consider a long continuous solid cylinder, having symmetry about the z-axis, immersed in a viscous and incompressible fluid and moving with velocity $u = u_w(z)$ in the steady state. The circular cylinder might be of constant as well as of variable cross section. Therefore, in general, the radius of the cylinder is taken as $R(z)$, varying in z. The schematic of the flow and the chosen system of coordinates is shown in Fig. 5.3. The governing equations in this case are the same as (2.13) and (2.14) subject to the boundary condition

$$\left.\begin{array}{lll} u = u_w(z),\ v = 0, & \text{at} & r = R(z) \\ u = 0, & \text{at} & r = \infty \end{array}\right\}. \tag{5.103}$$

Introducing the stream function of the form

$$u = \frac{1}{r}\frac{\partial \psi}{\partial r},\quad v = -\frac{1}{r}\frac{\partial \psi}{\partial z}, \tag{5.104}$$

due to which Eq. (2.13) satisfies identically and Eq. (2.14) transforms to

$$\frac{1}{r}\frac{\partial \psi}{\partial r}\frac{\partial^2 \psi}{\partial r \partial z} + \frac{1}{r^2}\frac{\partial \psi}{\partial r}\frac{\partial \psi}{\partial z} - \frac{1}{r}\frac{\partial \psi}{\partial z}\frac{\partial^2 \psi}{\partial r^2} = \nu\left[\frac{1}{r^2}\frac{\partial \psi}{\partial r} - \frac{1}{r}\frac{\partial^2 \psi}{\partial r^2} + \frac{\partial^3 \psi}{\partial r^3}\right]. \tag{5.105}$$

The procedure of finding the self-similarity criterion in this case is the same as implemented in the previous two sections. We, therefore, assume a one-parameter

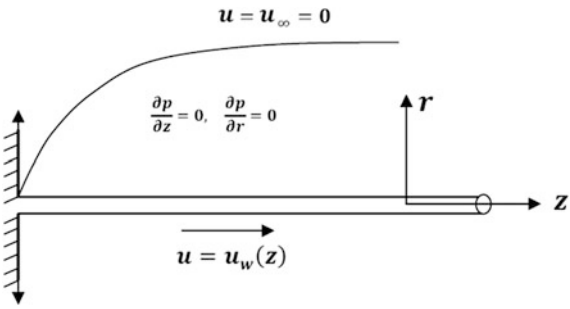

Fig. 5.3 Axisymmetric flow and the associated system of coordinate shown schematically

group of scaling transformations for the variables involved in Eqs. (5.105) and (5.103), of the form

$$\bar{z} = k^{\alpha_1} z, \quad \bar{r} = k^{\alpha_2} r, \quad \bar{\psi} = k^{\alpha_3} \psi, \quad \bar{u}_w = k^{\alpha_4} u_w, \quad \bar{R} = k^{\alpha_5} R. \tag{5.106}$$

The restriction of invariance of the governing system under the group of scalings will be imposed in order to get a system of linear equations in the scaling exponents. The non-trivial solution of this system will lead toward the construction of new variables. In view of the boundary-layer character, the leaving variable must be z. Accordingly, the two cases arise regarding the zero and nonzero character of the scaling exponent α_1. The details of determining the new variables have been omitted in order to avoid the repetition of previously exercised steps. Therefore, the similarity variables for the case $\alpha_1 \neq 0$ are given directly as

$$\eta = r z^{\frac{m-1}{2}}, \quad \psi = z f(\eta). \tag{5.107}$$

The wall velocity and the cylinder radius come out of the form

$$u_w = a z^m, \quad R(z) = R_0 z^{\frac{1-m}{2}}, \tag{5.108}$$

where R_0 denotes the fixed reference radius of the cylinder corresponding to the case $m = 1$.

With the help of transformation (5.107), Eq. (5.105) transforms as

$$m\left(\frac{f'}{\eta}\right)^2 - \frac{f}{\eta}\left(\frac{f''}{\eta} - \frac{f'}{\eta^2}\right) = \nu \frac{1}{\eta}\frac{d}{d\eta}\left(\eta \frac{d}{d\eta}\left(\frac{f'}{\eta}\right)\right), \tag{5.109}$$

and boundary conditions (5.103), in view of Eqs. (5.107)–(5.108), take the form

$$\left.\begin{array}{lll} f' = aR_0, \ f = 0, & \text{at} & \eta = R_0 \\ f' = 0, & \text{at} & \eta = \infty \end{array}\right\}. \tag{5.110}$$

Equations (5.109) and (5.110) are completely free from the previous variables; therefore, they can be regarded as self-similar. Consequently, Eq. (5.107) contributes as the similarity transformations to this case.

Equation (5.108) contains interesting information regarding the similarity criterion of this case. The power-law wall velocity has been obtained for the case $\alpha_1 \neq 0$ as it has also happened in the previous two sections. The different thing in this case is the involvement of z in the expression of R for $m \neq 1$. For $m = 1$, one is left with the linear wall velocity case (see Eq. 5.108) for which the radius of cylinder stays fixed. Corresponding to the other values of m, the particular construction of η does not allow the radius of the cylinder to stay constant. This means that the nonlinear stretching of the cylinder is possible only if the cylinder radius does not stay constant but follows the power-law form (defined in Eq. 5.108), analogous to the boundary-layer thickness. The boundary-layer thickness in the nonlinear stretching flow varies as $z^{\frac{1-m}{2}}$ which actually guides the body contour of the axially symmetric body of revolution to follow the same law, i.e., $z^{\frac{1-m}{2}}$. This simply reflects that the similarity solution is possible for the power-law velocities if the cylindrical surface does also vary in the same manner as does the boundary-layer thickness; otherwise, the solution must be non-similar. Another, worth noting, difference between the planner and the axisymmetric flows is the case of constant wall velocity. In the case of moving sheet, the self-similar Sakiadis flow is recovered immediately, by taking $m = 0$, without imposing any restriction on the sheet's thickness. On the other hand, the self-similar solution is, though recovered, in the cylinder case for $m = 0$ but with a compromise on the thickness of cylinder. If one forces the cylinder's radius to be constant (for $m = 0$), the self-similarity is lost and the classical Sakiadis' non-similar flow due to a moving continuous cylinder is recovered. This was in fact the reason behind the utilization of approximate integral method by Sakiadis to his (non-similar) flow. Very few audiences are aware of the fact that Sakiadis started the cylinder case with the non-similar flow. Hence, the radius of the cylinder can be made to stay constant (only) if the cylinder is being stretched with linear velocity, in order to ensure the existence of self-similar solution. In this way, the case of moving cylinder is much more interesting in comparison with the two-dimensional case and needs to be explored completely. So far, the available literature concerning the continuous cylinder is strictly limited to the cases $m = 0$ and $m = 1$, only.

In the case $\alpha_1 = 0$, the exponential forms of wall velocity and the cylinder radius are obtained, which are given by

$$u_w = a\mathrm{e}^{mz}, \quad R(z) = R_0\mathrm{e}^{-\frac{m}{2}z}. \tag{5.111}$$

The corresponding similarity variables are constructed as

$$\eta = r\mathrm{e}^{\frac{m}{2}z}, \quad \psi = f(\eta), \tag{5.112}$$

which transform Eq. (5.105) to the form

$$m\left(\frac{f'}{\eta}\right)^2 = \nu\frac{1}{\eta}\frac{\mathrm{d}}{\mathrm{d}\eta}\left(\eta\frac{\mathrm{d}}{\mathrm{d}\eta}\left(\frac{f'}{\eta}\right)\right). \tag{5.113}$$

The boundary conditions (5.103), in view of Eqs. (5.111)–(5.112), transform as

$$\left.\begin{array}{lll} f' = aR_0 & \text{at} & \eta = R_0 \\ f' = 0, & \text{at} & \eta = \infty \end{array}\right\}. \tag{5.114}$$

Thus in the case of continuous cylinder too, the power-law and exponential forms are the ultimate wall velocities in order for the existence of self-similar solution. This fact will also be proved in Chap. 10 while modeling the non-similar flows. Regarding the nonlinear stretching/shrinking of the cylinder, the curvilinear system of coordinates as considered in Chap. 10 is recommended. The conventional cylindrical system of coordinates, however, creates certain ambiguities in the mathematical formulation.

5.3.2 *Radial Motion of Flexible Disk*

Consider a flexible flat circular disk of infinite radius immersed in an incompressible viscous fluid. The disk geometry and the associated system of coordinates are shown in Fig. 5.4. Following the notation convention practiced in the existing literature, particular to the disk flow, r is taken as the radial coordinate and z is taken as the axial coordinate where u and w denote the velocity components along these axes, respectively. The disk is being stretched or shrunk in the radial direction with a velocity $u_w(r)$ as shown in Fig. 5.4. Because of no involvement of any circular motion, the angular component of velocity is zero. Therefore, the suitable velocity vector for this flow in the steady-state form reads as

$$\boldsymbol{V} = [u(r,z), 0, w(r,z)], \tag{5.115}$$

due to which the governing equations of this flow are the same as given in Eqs. (2.15) and (2.16). The appropriate boundary conditions read as

$$\left.\begin{array}{llll} u = u_w(r), & w = 0, & \text{at} & z = 0 \\ u = 0, & & \text{at} & z = \infty \end{array}\right\}. \tag{5.116}$$

Introducing the stream function $\psi(r,z)$ which is related to the velocity components as

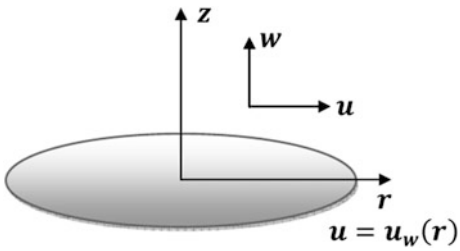

Fig. 5.4 Disk geometry and the chosen system of coordinates

$$u = \frac{1}{r}\frac{\partial}{\partial z}(r\psi), \quad w = -\frac{1}{r}\frac{\partial}{\partial r}(r\psi). \tag{5.117}$$

Because of Eq. (5.117), the equation of continuity (2.15) is satisfied identically and Eq. (2.16) takes the form

$$\frac{\partial\psi}{\partial z}\frac{\partial^2\psi}{\partial r\partial z} - \frac{\psi}{r}\frac{\partial^2\psi}{\partial z^2} - \frac{\partial\psi}{\partial r}\frac{\partial^2\psi}{\partial z^2} = \nu\frac{\partial^3\psi}{\partial z^3}. \tag{5.118}$$

The group theoretical procedure will be employed to Eqs. (5.118) and (5.116) in order to find the self-similarity criterion for this flow. The variables involved in this system are r, z, ψ and u_w for which the scaling group reads as

$$\bar{r} = k^{\alpha_1} r, \quad \bar{z} = k^{\alpha_2} z, \quad \bar{\psi} = k^{\alpha_3}\psi, \quad \bar{u}_w = k^{\alpha_4} u_w. \tag{5.119}$$

The substitution of Eq. (5.119) into the system (5.118) and (5.116) subject to the condition of invariance under (5.119) gives rise to a system of simultaneous algebraic equations, similar to the previous problems. In this case, we decide to eliminate r due to which two cases arise for the values of α_1, namely $\alpha_1 \neq 0$ and $\alpha_1 = 0$. In the case $\alpha_1 \neq 0$, the similarity variables so constructed are (by omitting the details of their derivation)

$$\eta = r^{\frac{m-1}{2}} z, \quad \psi = r^{\frac{m+1}{2}} f(\eta), \tag{5.120}$$

which successfully transform Eq. (5.118) to the self-similar form, given by

$$mf'^2 - \left(\frac{m+3}{2}\right) ff'' = \nu f''', \tag{5.121}$$

subject to the restriction that the wall velocity must follow the power-law form defined by

$$u_w = ar^m. \tag{5.122}$$

Accordingly, the boundary conditions (5.116) transform as

$$\left.\begin{array}{lll} f' = a, \ f = 0, & \text{at} & \eta = 0 \\ f' = 0, & \text{at} & \eta = \infty \end{array}\right\}. \tag{5.123}$$

Thus, Eqs. (5.121) and (5.123) are in self-similar form based on the condition that the wall velocity must follow the power-law form given in Eq. (5.122).

In the case $\alpha_1 = 0$, the group theoretical procedure ends up with the transformations involving exponential form, such as

$$\eta = \mathrm{e}^{\frac{m}{2}r} z, \quad \psi = \mathrm{e}^{\frac{m}{2}r} f(\eta), \tag{5.124}$$

with the wall velocity following the exponential form, given by

$$u_w = a\mathrm{e}^{mr}. \tag{5.125}$$

Utilization of the transformations (5.124) transforms Eq. (5.118) to the form

$$mf'^2 - \frac{1}{r} ff'' - \frac{m}{2} ff'' = \nu f'''. \tag{5.126}$$

Obviously, the variable r has not been eliminated completely from the equation after the utilization of Eq. (5.124). This simply reflects that the transformations (5.126) cannot transform the Eq. (5.118) to the self-similar form and implies that the self-similar solution is not possible in this case. Thus, in the case of circular disk, the similarity solutions are limited to the power-law case only and the exponential wall velocities fail to produce the self-similar solution. The mathematical reason behind this fact is the appearance of r as a variable coefficient in the second term of Eq. (5.126) which is impossible to eliminate.

5.4 Restriction on Wall Suction/Injection

This has already been explored in the previous sections that the self-similar solutions are the limited solutions and are possible only if the wall velocities follow certain particular forms. In the case of cylinder, the radius of the cylinder also undergoes certain restrictions in addition to the wall velocities in order to ensure the self-similarity. The similar situation persists for the cases when one also takes into account the wall suction/injection in the boundary-layer. This section is devoted to the determination of those particular wall suction/injection profiles which do not break the self-similarity of the considered flow.

Corresponding to the two-dimensional and three-dimensional cases, the normal wall velocity shall be denoted by $v_w(x)$ and $v_w(x, z)$, respectively. Being a function of x and (x, z), the wall velocities $v_w(x)$ and $v_w(x, z)$ serve as variable quantities in

the governing system. Similar to the other variable quantities, either dependent or independent, the considered groups of scalings shall be appended by another scaling transformation of the variable v_w. In doing so, the obtained system of linear equations (due to the restriction of invariance) will also be increased by one more equation resulting from the boundary condition $v = v_w$ at $y = 0$ in Sects. 5.1 and 5.2. Consequently, the non-trivial solution of the system of such algebraic equations in scaling exponents will also include the solution for the scaling exponent of v_w which will subsequently be utilized in the construction of corresponding new variables.

Particular to Sects. 5.1 and 5.2, the scaling group for v_w could be taken of the form

$$\bar{v}_w = k^{\gamma} v_w, \tag{5.127}$$

where γ denotes the scaling exponent. Combining Eq. (5.127) with the group (5.8) and following the subsequent procedure executed in Sect. 5.1, the system (5.11) is appended by an additional linear equation of the form

$$\alpha_1 - \alpha_3 = -\gamma, \tag{5.128}$$

which, for the case $\alpha_1 \neq 0$, admits the solution

$$-\frac{\gamma}{\alpha_1} = \frac{\alpha_2}{\alpha_1}. \tag{5.129}$$

In view of Eq. (5.14), the wall velocity $v_w(x)$ comes out of the form

$$v_w(x) = \mathrm{d}x^{\frac{m-1}{2}}, \tag{5.130}$$

where d denotes a pure constant having suitable dimensions. The positive and negative values of d characterize the injection and suction velocities, respectively, while $d = 0$ designates no suction or injection at the wall. It is important to note that the power-law form of the wall velocity (given in Eq. 5.14) does also require the normal wall velocity to follow the same (power-law) form in order to ensure the self-similarity. The same is the case with exponential wall velocity (5.20) which requires the suction/injection velocity also to follow the exponential form, given by

$$v_w(x) = \mathrm{d}\mathrm{e}^{\frac{m}{2}x}. \tag{5.131}$$

The trend follows similarly in Sect. 5.2 where the suction/injection velocity not only follows the power-law and exponential forms but also is a product of the two. The details have, however, been omitted completely for the sake of brevity. Corresponding to the every case of Sect. 5.2, the suction/injection velocity has been obtained as follows:

Case I; Subcase I

$$v_w(x,z) = \mathrm{d}x^{\frac{m-1}{2}-B\left(\frac{n-1}{2}\right)}z^{\frac{n-1}{2}}, \tag{5.132}$$

Case I; Subcase II

$$v_w = \mathrm{d}x^{\frac{m-1}{2}}\mathrm{e}^{\frac{n}{2}z}, \tag{5.133}$$

Case II; Subcase I

$$v_w(x,z) = \mathrm{d}\mathrm{e}^{\frac{1}{2}(m-B(n-1))x}z^{\frac{n-1}{2}}, \tag{5.134}$$

Case II; Subcase II

$$v_w(x,z) = \mathrm{d}\mathrm{e}^{\frac{1}{2}(mx+nz)}. \tag{5.135}$$

Accordingly, the corresponding boundary conditions at the wall also modify as

$$\frac{1}{2}(m+1-B(n-1))f(0) + \frac{n+1}{2}g(0) = -d, \tag{5.136a}$$

$$\left(\frac{m+1}{2}\right)f(0) + \frac{n}{2}g(0) = -d, \tag{5.136b}$$

$$\frac{1}{2}(m-B(n-1))f(0) + \frac{n+1}{2}g(0) = -d, \tag{5.136c}$$

$$\frac{1}{2}(mf(0)+ng(0)) = -d, \tag{5.136d}$$

which, respectively, refer to the cases "Case I; Subcase I," "Case I; Subcase II," "Case II; Subcase I," and "Case II; Subcase II." The corresponding boundary conditions of the two-dimensional case can also be recovered from Eq. (5.136a)–(5.136d).

The cases of axially symmetric flow due to continuous cylinder or circular flexible disk follow in the similar manner. In the case of continuous cylinder, when the surface velocity obeys the power-law profile the second condition in Eq. (5.110) at $\eta = R_0$ modifies as

$$f = -\mathrm{d}R_0. \tag{5.137}$$

In the case of circular flexible disk, the second condition in Eq. (5.124) at $\eta = 0$ modifies as

$$\frac{m+3}{2} f(0) = -d, \tag{5.138}$$

where the wall velocity obeys power-law profile.

By the end of this chapter, the criterion of self-similarity for the planner and the axisymmetric cases has in general been derived. The wall velocities, other than the derived ones, will make the flow non-similar. The power-law, exponential, and a product of the two have been discovered for the three-dimensional flow, whereas the exponential wall velocity has been extended for various powers of the already known exponential wall law in the two-dimensional case. Regarding the axisymmetric flow due to moving cylinder, the nonlinear and exponential stretching or shrinking have been discovered. The case of linear stretching or shrinking has been extended to the nonlinear one in the case of circular flexible disk. In what follows, the determination of self-similarity criterion regarding the wall velocities in the above-named flow situations has completely been discovered.

References

1. B.C. Sakiadis, Boundary-layer behavior on continuous solid surfaces: II. The boundary-layer on a continuous flat surface. AIChE **7**(2), 221–225 (1961)
2. L.J. Crane, Flow past a stretching sheet. Z. Angew. Math. Phys. **21**, 645–647 (1970)
3. W.H.H. Banks, Similarity solution of the boundary-layer equations for a stretching wall. J. Mecanique Theorique et Appliquee **2**(3), 375–392 (1983)
4. E. Magyari, B. Keller, Heat and mass transfer in the boundary layers on an exponentially stretching continuous surface. J. Phys. D Appl. Phys. **32**(5), 577–585 (1999)
5. C.Y. Wang, The three-dimensional flow due to a stretching surface. Phys. Fluids **27**, 1915–1917 (1984)
6. C.Y. Wang, Fluid flow due to a stretching cylinder. Phys. Fluids **31**, 466–468 (1988)
7. T. Fang, Flow over a stretchable disk. Phys. Fluids 19(1–4), 12805 (2007)
8. M. Miklavcic, C.Y. Wang, Viscous flow sue to a shrinking sheet. Quart. Appl. Math. **64**(2), 283–290 (2006)
9. V.M. Falkner, S.W. Skan, Some approximate solutions of the boundary-layer equations. Phil. Mag. **12**, 865–896 (1931)
10. H.S. Takhar, A.J. Chamkha, G. Nath, Unsteady three-dimensional MHD-boundary-layer flow due to the impulsive motion of a stretching surface. Acta Mech. **146**, 59–71 (2001)
11. C.Y. Wang, Stretching of surface in a rotating fluid. ZAMP **39**, 177–185 (1988)
12. I.C. Liu, H.H. Wang, Y.F. Peng, Flow and heat transfer for three-dimensional flow over an exponentially stretching surface. Chem. Eng. Comm. **200**, 253–268 (2013)
13. F.K. Moore, Three-dimensional compressible laminar boundary-layer flow. NASA TN 2279 (1951)
14. T. Geis, "Similar" three-dimensional boundary-layers. NASA TT F-30 (1961)
15. G.W. Bluman, S.C. Anco, in *Symmetry and Integration Methods for Differential Equations* (Springer, Berlin, 2002)

16. W.F. Ames, in *Nonlinear Partial Differential Equations in Engineering* (Academic Press, Cambridge, 1965)
17. H. Blasius, Grenzschichten in Flüssigkeiten mit kleiner Reibung. Z. Math. u. Phys. **56**, 1–37 (1908)
18. L. Howarth, On the solution of the laminar boundary layer equations. Proc. Roy. Soc. Lond. A **164**, 547–579 (1938)

Chapter 6
Viscous Flow Due to Accelerated/Decelerated Stretching Surfaces

The criterion of self-similarity regarding the stretching or shrinking wall velocities has been determined in the previous chapter including the cases of two-dimensional, three-dimensional, and axially symmetric flows. The so-determined particular power-law and exponential wall velocities have been observed to be responsible for the existence of self-similarity in the above-named flows. As a matter of fact, the governing equations in this chapter are the ordinary differential equations (due to the self-similarity) which have been solved numerically using the MATLAB built-in package, commonly known as bvp4c. In this regard the self-similar systems obtained in the previous chapter shall be made dimensionless in order to facilitate the flow analysis. The ranges of the power-law or exponential index regarding the existence of solution and the regions of multiple solutions have also been identified in some cases. In some appropriate cases the already published results have also been reconfirmed and the previously ignored cases have also been pointed out as well. It is particularly emphasized that the correct understanding of the stretching or shrinking sheet flows can only be ensured when the accelerated or retarded behavior of the wall velocities is taken into account. The more intense realization of the importance of this fact will be experienced in Chap. 7 while discussing the shrinking sheet flow.

6.1 Two-Dimensional Case

The simplest case among the three major categories considered in Chap. 5 is the case of two-dimensional flow. Because of this reason it has been considered first for the discussion of boundary-layer flow due to the stretching surfaces. Two independent self-similar systems have been derived for this case corresponding to the power-law and exponential wall velocities. Before we start discussion on the flow governed by these systems, it is appropriate to first normalize them. The

A. Mehmood, *Viscous Flows*, Mathematical Engineering,
DOI 10.1007/978-3-319-55432-7_6

normalization of these systems is not difficult but requires some care. The careful handling of this procedure results in the correct dimensionless similarity transformations, especially in the case of shrinking sheet flow. We consider the power-law case first for which the similarity transformations are given in Eq. (5.14).

Let us write the similarity variable and the velocity functions in the form

$$\eta = Ax^{\frac{m-1}{2}}y, \quad u = ax^m f'(\eta), \quad v = -\frac{a}{A}x^{\frac{m-1}{2}}\left(\left(\frac{m+1}{2}\right)f + \left(\frac{m-1}{2}\right)\eta f'\right). \tag{6.1}$$

The constant A is unknown to be determined having suitable dimensions such that η is finally dimensionless, a is also a constant (as described in Chap. 5) having suitable dimensions such that ax^m finally has the dimensions of velocity; the ratio a/A in the expression of v arose due to the equation of continuity (5.2) by satisfying it identically. The substitution of Eq. (6.1) into Eq. (5.3) results in the self-similar equation of the form

$$mf'^2 - \left(\frac{m+1}{2}\right)ff'' = \frac{\nu A^2}{a}f''', \tag{6.2}$$

which is the same as Eq. (5.15) with the coefficient of f''' modified by a little. Equation (6.2) could be in dimensionless form if the dimension of the ratio $\frac{\nu A^2}{a}$ is equal to 1. At this stage, before moving any further, it is very much important to incorporate the character of the constant a, first. This step is very much important and is usually ignored, especially in the shrinking sheet problems. Notice that, if $a > 0$, then there is no need to stop here, but when $a < 0$, it is then quite necessary to incorporate the sign of a here, in order to end up with correct dimensionless similarity transformations and hence the equation also. In all the cases, considered in Chap. 5, the positive values if $a(a > 0)$ refer to the stretching surface, whereas the negative values of a $(a < 0)$ refer to the shrinking surface. In this way it seems better to write $a = \pm\bar{a}$ where $\bar{a} > 0$ have the same dimensions as does the constant a. By doing so Eq. (6.2) modifies as

$$mf'^2 - \left(\frac{m+1}{2}\right)ff'' = \pm\frac{\nu A^2}{\bar{a}}f'''. \tag{6.3}$$

Equation (6.3) can be made completely dimensionless if one chooses $A = \sqrt{\bar{a}/\nu}$. With this particular choice of A Eq. (6.3) reads in dimensionless form as

$$mf'^2 - \left(\frac{m+1}{2}\right)ff'' = \pm f''', \tag{6.4}$$

where the "+" and "−" signs refer, respectively, to the stretching and shrinking surface cases. In this way Eq. (6.1) also modifies as

$$\eta = \sqrt{\bar{a}/\nu}x^{\frac{m-1}{2}}y, \quad u = ax^m f'(\eta),$$
$$v = \pm\left[-\sqrt{\bar{a}\nu}x^{\frac{m-1}{2}}\left\{\left(\frac{m+1}{2}\right)f + \left(\frac{m-1}{2}\right)\eta f'\right\}\right],$$

or

$$\eta = \sqrt{\frac{\pm u_w(x)}{\nu x}}y, \quad u = u_w(x)f'(\eta),$$
$$v = \pm\left[-\sqrt{\frac{\pm u_w(x)\nu}{x}}\left\{\left(\frac{m+1}{2}\right)f + \left(\frac{m-1}{2}\right)\eta f'\right\}\right], \tag{6.5}$$

where $u_w(x)$ is the power-law wall velocity given in Eq. (5.14). Utilization of similarity transformations (6.5) into boundary conditions (5.4) results in the dimensionless boundary condition, given by

$$\left.\begin{array}{lll} f' = 1, & f = 0, & \text{at}\,\eta = 0 \\ f' = 0, & & \text{at}\,\eta = \infty \end{array}\right\} \tag{6.6}$$

which is though the same as Eq. (5.16), but the variables involved here are now in dimensionless form.

The system of Eqs. (6.4)–(6.6) constitutes the dimensionless self-similar system for the two-dimensional flow, either the sheet is being stretched or shrunk following the power-law wall velocities. Similarly, the self-similar system (5.20)–(5.22), corresponding to the exponential wall laws, reads in dimensionless form as

$$\eta = \sqrt{\frac{\pm u_w(x)}{\nu L}}y, \quad u = u_w(x)f'(\eta), \quad v = \pm\left[-\frac{m}{2}\sqrt{\frac{\pm u_w(x)\nu}{L}}(f + \eta f')\right], \tag{6.7}$$

$$m\left(f'^2 - \frac{1}{2}ff''\right) = \pm f''', \tag{6.8}$$

$$\left.\begin{array}{lll} f' = 1, & f = 0, & \text{at}\,\eta = 0 \\ f' = 0, & & \text{at}\,\eta = \infty \end{array}\right\} \tag{6.9}$$

where $u_w(x) = \pm\bar{a}e^{\frac{mx}{L}}$. The coefficient of skin-friction in these two cases is calculated as

$$C_f = \frac{2\tau_w}{\rho u_w(x)^2}, \quad \text{where } \tau_w = \mu\left.\frac{\partial u}{\partial y}\right|_{y=0}. \tag{6.10}$$

The utilization of Eqs. (6.5) and (6.7) in Eq. (6.10) gives the dimensionless form of the skin-friction coefficient corresponding to the power-law and exponential wall velocities, respectively, as

$$\left.\begin{aligned} &\sqrt{\frac{\pm u_w(x)x}{4\nu}}C_f = f''(0) \\ &\text{and} \\ &\sqrt{\frac{\pm u_w(x)L}{\nu}}C_f = f''(0) \end{aligned}\right\}. \tag{6.11}$$

The second boundary condition at $\eta = 0$, in Eqs. (6.6) and (6.9), modifies to

$$f(0) = \pm\left[-\frac{\mathrm{d}}{\sqrt{\bar{a}\nu}}.\frac{2}{m+1}\right], \quad \text{and} \quad f(0) = \pm\left[-\frac{\mathrm{d}}{\sqrt{\bar{a}\nu}}.\frac{2\sqrt{L}}{m}\right], \tag{6.12}$$

respectively, when the wall suction or injection is also taken into account. In the case of stretching sheet flow, "+" sign will be considered, and in the case of shrinking sheet flow, "−" sign will be selected in either of the above systems. Since, in this chapter, we are particularly interested in the stretching sheet flows, the consideration of "−" sign will stay pending till the next chapter.

Equations (6.4) and (6.6) have extensively been studied for the "+" sign case, and the corresponding range of values of m regarding the existence and uniqueness of the solution has also been determined in literature. Such ranges have been reported by van Gorder et al. [1] which were further corrected by Paullet and Previte [2], subsequently. According to Paullet and Previte the claim of uniqueness of solution made by van Gorder et al. is limited to the interval $0 \leq m \leq \infty$ and infinitely many solutions exist for the values $-\frac{1}{3} < m < 0$; where the values $m \leq -\frac{1}{3}$ do not admit any solution bearing the character $f(\eta) > 0$ and $f''(\eta) < 0$ for all $\eta > 0$. This fact has also been confirmed in the current numerical computations. The velocity graphs are plotted in Fig. 6.1 against η for different values of m. It can be seen in this figure that upon increasing the values of m the boundary-layer thickness decreases gradually by limiting the variations in velocity to a thinner and thinner region close to the wall. In this thin region the velocity varies rapidly by starting with the wall velocity value and approaches asymptotically to the potential velocity. For the increasing values of m the flow remains adhered to the wall and exhibits strong boundary-layer character. For the decreasing values of m the boundary-layer becomes thicker and thicker and tends to be blown away, more particularly, when m decreases with negative values. This effect can also be confirmed from Table 6.1 where the values of the skin-friction coefficient can be seen approaching zero as $m \to -1/3$. Upon further decreasing the value of m by crossing $m = -1/3$ the equation seizes of producing the results. This is actually in accordance with the generally known fact about the boundary-layer flows that the boundary-layer establishes in the accelerated flow and blows away in the retarded

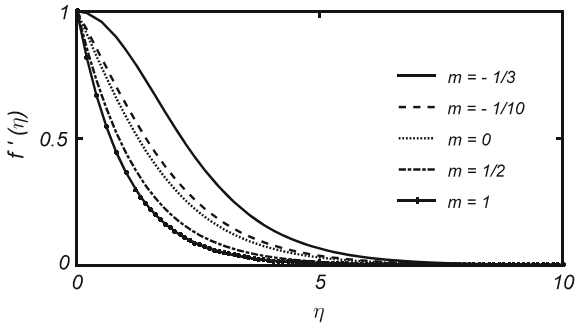

Fig. 6.1 Velocity profile corresponding to the stretching sheet flow

Table 6.1 Values of $-f''(0)$ for $a > 0$ for different m

	$-f''(0)$	
m	Power-law	Exponential
−1/3	0.0000	
−1/5	0.23426	
−1/10	0.35026	
0	0.44375	
1/10	0.52353	0.2870
1/2	0.77037	0.6409
1	1.00000	0.9064
2	1.34846	1.2818
5	2.06894	2.0267
10	2.89607	2.8662

flow situations. In physical point of view, when $u_w(x) > 0$, the positive values of m correspond to the accelerated wall velocities, whereas the negative values of m correspond to the retarded wall velocities. This finally designates the considered cases, corresponding to $m > 0$ and $m < 0$, as the accelerated and decelerated flows, respectively.

The graphs of the wall velocity function $u_w(x)(a > 0)$ against x in the accelerated $(m > 0)$ and decelerated $(m < 0)$ cases are shown in Fig. 6.2. At our opinion the designation of the stretching or shrinking wall velocity as accelerated or decelerated is of fundamental importance in the understanding of boundary-layer flow due to moving continuous surfaces.

The importance of the plots given in Fig. 6.2 will further be realized while studying the shrinking sheet flow in the next chapter. Thus, Fig. 6.1 finally reveals that the stretching sheet flow is suitable to be studied for the accelerated wall velocity (especially, in the absence of wall suction) because for the retarded wall velocity the boundary-layer separates at $m = -1/3$ and needs some assistance (such as suction) for its survival at further smaller values of m. Continuing the analysis of stretching sheet flow it can further be realized from Fig. 6.1 that the retarded wall velocity assists the flow until $m = -1/3$, whereas this value is $m = -0.091$ in the Falkner-Skan flow. This simply reflects that the moving surface

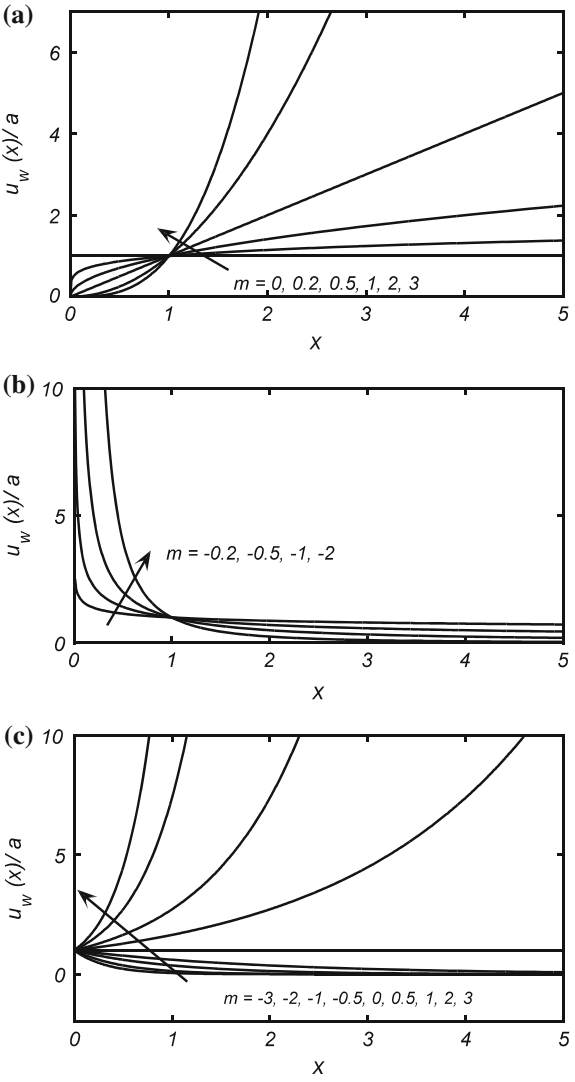

Fig. 6.2 **a** Power-law accelerated wall velocities ($m > 0$), **b** power-law decelerated wall velocity ($m < 0$), **c** accelerated and decelerated exponential wall velocities

boundary-layers assist the flow for some further retarded velocities as compared to the Falkner-Skan boundary-layers. This is simply because of the reason that the skin-friction in the moving surface boundary-layers is greater than those due to potential flow past a finite surface. In the simple cases, namely, the Blasius and the Sakiadis, the skin-friction is 66% greater in Sakiadis flow as compared to the Blasius flow. The variation of the skin-friction coefficient with respect to m is shown in Fig. 6.3 where the graph of $-f''(0)$ has been shown as an increasing function of m. Multiplicity of solution in this case has already been proved for the values $-1/3 < m < 0$ by Paullet and Previte [2] which is, however, not a topic of interest, here.

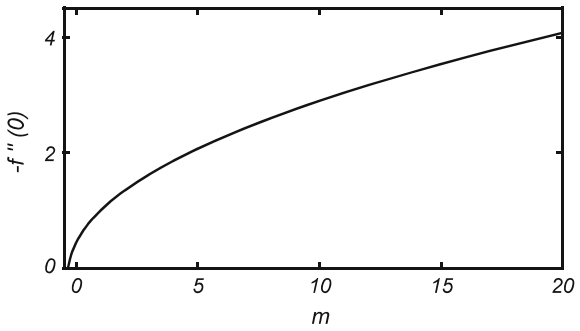

Fig. 6.3 Coefficient of wall skin-friction plotted against m

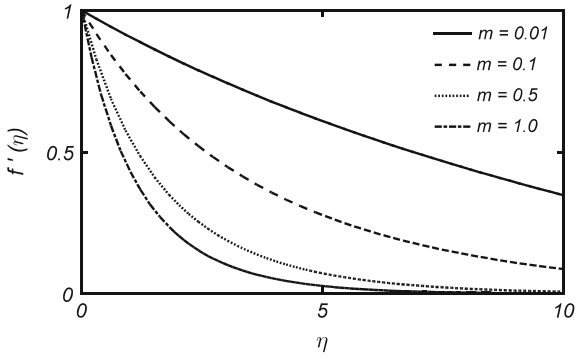

Fig. 6.4 Velocity profile of the exponentially stretching sheet

The velocity profile of the exponentially stretching sheet case is plotted in Fig. 6.4. Qualitatively, similar behavior of the velocity profile is observed as seen, previously, in the power-law case, corresponding to the increasing values of m. However, the boundary-layer thickness is significantly smaller in this case in comparison with the power-law case. The velocity graphs (see Fig. 6.4) tend to become linear as one assumes the values of m smaller and smaller by keeping $m > 0$. This can readily be observed from Eq. (6.8) that the inertial part of the momentum equation minimizes to be negligible as $m \to 0$, by staying positive.

Consequently, the inertial forces vanish out and the creeping flow situation is reached which does not obey the boundary-layer behavior. Notice that as $m \to 0$ the wall velocity $u_w(x) = \bar{a}e^{\frac{mx}{L}}$ becomes constant, but self-similar Eq. (6.8) does not reduce to the Sakiadis flow (Eq. 1.2). However, the Sakiadis flow is immediately recovered from Eq. (6.4) for the limit $m \to 0$ where the power-law velocity $u_w(x) = \bar{a}x^m$ also recovers the Sakiadis wall velocity as $m \to 0$. This actually reveals that the Sakiadis flow is a special case of the power-law class and exponential wall laws do not recover the constant wall velocity case any way. The values of the skin-friction coefficient for the exponential stretching case are also listed in Table 6.1 from where it is clear that the magnitude of skin-friction coefficient decreases gradually as m approaches to 0; this fact can also be confirmed from

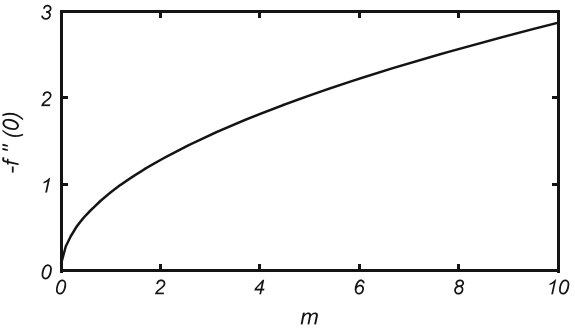

Fig. 6.5 Coefficient of skin-friction in the exponentially stretching sheet case

Fig. 6.5. Particular to this case it can, in general, be stated that the solution[1] exists for $0 < m < \infty$ with an exception of very small neighborhood of m at $m = 0$. On the other hand no solution exists at all for $m < 0$ in this case. That is, different from the power-law wall velocities, the exponential wall velocities do not tolerate the retarded flow any way.

6.2 Three-Dimensional Case

It has already been observed, in Chap. 5, that the similarity criterion for the three-dimensional flow due to a moving continuous sheet involves not only the power-law and exponential wall velocities but also a product of the two where the wall expressions involve power-law as well as the exponential forms simultaneously. Because of this reason the three-dimensional case had further been splitted into four different cases in the course of developing the self-similar equations. The non-dimensionalization of all such cases has been carried out (here) in the same manner as it has already been done in Sect. 6.1. After omitting the details of the procedure, the self-similar systems corresponding to the four classified cases read as:

"Case I; Subcase I"

$$\left.\begin{aligned} \eta &= \sqrt{\frac{\mathrm{Sgn}(a)u_w(x,z)}{\nu x}}\,y, \quad u = u_w(x,z)f'(\eta), \quad \lambda w = \frac{\mathrm{Sgn}(a)}{\mathrm{Sgn}(b)}\,w_w(x,z)g'(\eta), \\ v &= -\frac{\mathrm{Sgn}(a)}{2}\sqrt{\frac{\mathrm{Sgn}(a)u_w(x,z)\nu}{x}}\Big[\,(m+1-B(n-1))f+(m-1-B(n-1))\eta f' \\ &\qquad\qquad +(n+1)g+(n-1)\eta g'\,\Big] \end{aligned}\right\}, \tag{6.13}$$

[1]The "solution" here means the solution obeying the boundary-layer character.

$$(m - B(n-1))f'^2 - \left(\frac{m+1}{2} - B\left(\frac{n-1}{2}\right)\right)ff'' - \left(\frac{n+1}{2}\right)gf'' + (n-1)f'g' = \mathrm{Sgn}(a)f''', \tag{6.14}$$

$$(m - 1 - B(n-1))f'g' - \left(\frac{m+1}{2} - B\left(\frac{n-1}{2}\right)\right)fg'' - \left(\frac{n+1}{2}\right)gg'' + ng'^2 = \mathrm{Sgn}(a)g''', \tag{6.15}$$

subject to the boundary conditions

$$\left.\begin{array}{lll} f' = 1, \quad g' = \dfrac{\mathrm{Sgn}(b)}{\mathrm{Sgn}(a)}\lambda, \quad \frac{1}{2}(m+1-B(n-1))f + \frac{1}{2}(n+1)g = 0, & \text{at } \eta = 0 \\ f' = 0, \quad g' = 0, & \text{at } \eta = \infty \end{array}\right\}, \tag{6.16}$$

where $\lambda = |b|/|a|$ is the dimensionless ratio of the magnitudes of the two stretching rates. In all the subsequent cases the definitions of n, u, and w shall stay the same as defined in Eq. (6.13) subject to the consideration of appropriate definitions of $u_w(x, z)$ and $w_w(x, z)$ in accordance with the considered particular cases, whereas the normal component of velocity, v, will vary in all such cases.

"Case I; Subcase II"

$$v = -\frac{\mathrm{Sgn}(a)}{2}\sqrt{\frac{\mathrm{Sgn}(a)u_w(x,z)}{x}}[(m+1)f + (m-1)\eta f' + n(g + \eta g')], \tag{6.17}$$

$$mf'^2 - \left(\frac{m+1}{2}\right)ff'' - \frac{n}{2}(gf'' - 2f'g') = \mathrm{Sgn}(a)f''', \tag{6.18}$$

$$(m-1)f'g' - \left(\frac{m+1}{2}\right)fg'' - \frac{n}{2}(gg'' - g'^2) = \mathrm{Sgn}(a)g'''. \tag{6.19}$$

The boundary conditions in this case are the same as given in Eq. (6.16) except the condition on v at $\eta = 0$ which modifies as

$$\frac{1}{2}((m+1)f + ng) = 0, \quad \text{at} \quad \eta = 0. \tag{6.20}$$

In this case the self-similar wall velocities read as

$$u_w(x,z) = ax^m e^{\frac{nz}{L}}, \quad w_w(x,z) = bx^{m-1} e^{\frac{nz}{L}}, \tag{6.21}$$

where L denotes the appropriate characteristic length in the z-direction.

"Case II; Subcase I"
In this case the definition of η changes by a little as

$$\eta = \sqrt{\frac{\mathrm{Sgn}(a)u_w(x,z)}{vL}}y, \tag{6.22}$$

where the variable x in the denominator in (in Eq. 6.13) has been replaced by L. The velocity component v reads, in this case, as

$$v = -\frac{\mathrm{Sgn}(a)}{2}\sqrt{\frac{\mathrm{Sgn}(a)u_w(x,z)v}{L}}[(m - B(n-1))(f + \eta f') + (n+1)g + (n-1)\eta g'], \tag{6.23}$$

$$(m - B(n-1))\left(f'^2 - \frac{1}{2}ff''\right) - \left(\frac{n+1}{2}\right)gf'' + (n-1)f'g' = \mathrm{Sgn}(a)f''', \tag{6.24}$$

$$(m - B(n-1))\left(f'g' - \frac{1}{2}fg''\right) - \left(\frac{n+1}{2}\right)gg'' + ng'^2 = \mathrm{Sgn}(a)g''', \tag{6.25}$$

with

$$(m - B(n-1))f + (n+1)g = 0, \quad \text{at} \quad \eta = 0. \tag{6.26}$$

"Case II; Subcase II"
In this case η is exactly the same as given in (6.22), but the normal velocity component becomes of the form

$$v = -\frac{\mathrm{Sgn}(a)}{2}\sqrt{\frac{\mathrm{Sgn}(a)u_w(x,z)v}{L}}[m(f + \eta f') + n(g + \eta g')], \tag{6.27}$$

$$mf'^2 - \frac{m}{2}ff'' - \frac{n}{2}\left(gf'' - 2f'g'\right) = \mathrm{Sgn}(a)f''', \tag{6.28}$$

$$mf'g' - \frac{m}{2}fg'' - \frac{n}{2}\left(gg'' - 2g'^2\right) = \mathrm{Sgn}(a)g''', \tag{6.29}$$

with

$$\frac{1}{2}(mf + 2ng) = 0, \quad \text{at } \eta = 0. \tag{6.30}$$

In view of the available literature the three-dimensional flow is almost unexplored at the most. Only the power-law and the exponential forms of the wall velocity have been considered with the limited scope. Wang [3] was the first who considered steady three-dimensional flow due to a stretching sheet in two lateral directions. He assumed the linear wall velocities of the form

$$u_w = ax, \quad w_w = bz,$$

and introduced the similarity variable $\eta = \sqrt{a/\nu}y$. This particular form of the stretching velocities is already included in the case "Case I; Subcase I" and can readily be recovered by choosing $m = n = 1$. All those cases corresponding to other values of m and n are still pending, particularly the cases, when the wall velocities follow power-law in the two variables simultaneously. According to the current notation the Wang's stretching velocities can also be written as $u_w(x, z) = ax^1z^0$ and $w_w(x, z) = bx^0z^1$. Regarding the exponential wall laws the self-similar solution was introduced by Liu et al. [4] by assuming the exponential stretching velocities in the two lateral directions. The exponential wall laws and the resulting self-similar system introduced by [4] can readily be recovered from Eqs. (6.27)–(6.29) by choosing $m = n = 1$, and the corresponding boundary conditions can be recovered from Eq. (6.30). For the exponential case too, the cases corresponding to the other values of m and n different from zero are still pending. Thus, the explored cases of power-law and exponential wall velocities have only been explored for $m = n = 1$ which are also included in the present cases, namely "Case I; Subcase I" and "Case II; Subcase II," respectively. Besides these two cases, the cases "Case I; subcase II" and "Case II; subcase I" are totally unexplored and have never been studied earlier to the best of our knowledge. Thus, in total, the three-dimensional flow due to a stretching or shrinking sheet has not been studied completely yet and requires extensive investigations in order to discover its all cases. At this stage the author, however, refrains to engage in the solution of the above four systems corresponding to the said four classified cases. It certainly seems impossible to report their complete analysis by considering the cases of all values of m and n and their particular ranges regarding the existence/non-existence and uniqueness/non-uniqueness in detail within a single section of this chapter. This has therefore been left to the interested audience to get involved into this interesting class of three-dimensional boundary-layers and explore the unknown cases. The aim of the author, particular to this section, is just to introduce the dimensionless self-similar modeling of three-dimensional flow due to the moving continuous flat sheet.

6.3 Axially Symmetric Case

In the previous chapter the axially symmetric flow has also been considered for the continuous cylinder and for the flexible circular disk. In the case of cylinder the self-similar solution exists for both the power-law and the exponential wall velocities.

The case of disk is, however, restricted to the power-law wall profiles only. Because of different flow geometries the discussion of axially symmetric case has further been splitted into two subsections.

6.3.1 Continuous Stretching Cylinder

The self-similar system in this case has been given in Eqs. (5.107)–(5.110) where the wall velocity and the cylinder's surface vary following the power-law form. The said self-similar system in dimensionless form reads as

$$\eta = \sqrt{\frac{\pm u_w(z)}{\nu z}}r, \quad u = u_w \frac{1}{\eta} f'(\eta), \quad v = \pm\left[-\sqrt{\frac{\pm u_w(z)\nu}{z}}\left(\frac{1}{\eta}f + \frac{m-1}{2}f'\right)\right], \tag{6.31}$$

$$m\left(\frac{f'}{\eta}\right)^2 - \frac{f}{\eta}\left(\frac{f''}{\eta} - \frac{f'}{\eta^2}\right) = \pm\frac{1}{\eta}\frac{\mathrm{d}}{\mathrm{d}\eta}\left(\eta\frac{\mathrm{d}}{\mathrm{d}\eta}\left(\frac{f'}{\eta}\right)\right), \tag{6.32}$$

$$\left.\begin{array}{ll} f' = Re_{R_0}, \quad f = 0, & \text{at } \eta = Re_{R_0} \\ f' = 0, & \text{at } \eta = \infty \end{array}\right\}, \tag{6.33}$$

where $Re_{R_0} = \sqrt{\pm aR_o^2/\nu}$ is the Reynolds number based on the fixed reference radius R_o of the cylinder. With this particular definition, the Reynolds number actually characterizes the curvature of the cylinder's surface. Here the selection of "+" and "−" sign on the RHS of Eq. (6.32) is particular to the stretching or shrinking cylinder cases, respectively. Equation (6.32) involves several divisions by η and its integral powers, with most of the terms of it, which obviously makes it somewhat complex, mathematically. Boundary conditions (6.33) also involve Re_{R_0} which also seems inconvenient regarding the numerical integration process and the mathematical compactness, as well. Equations (6.32) and (6.33) can, however, be recasted into a simple form having domain from 0 to ∞ by eliminating the variable coefficients from the inertial part of Eq. (6.32) and the Reynolds number Re_{R_0} from the boundary conditions by introducing the new variable $\bar{\eta}$ as

$$\bar{\eta} = \frac{\eta^2 - Re_{R_0}^2}{2Re_{R_0}}. \tag{6.34}$$

Consequently, system (6.32)–(6.33) simplifies to (after dropping the bars)

$$mf'^2 - ff'' = \pm[(1 + 2\kappa\eta)f'']', \tag{6.35a}$$

$$\left.\begin{array}{ll} f' = 1, & f = 0, \quad \text{at } \eta = 0 \\ f' = 0, & \text{at } \eta = \infty \end{array}\right\}, \tag{6.35b}$$

where $\kappa = 1/Re_{R_0}$ denotes the curvature parameter. Equation (6.35a) reduces to the system developed by Wang [5] for the linear stretching case by choosing $m = 1$. The studies conducted by Grubka and Bobba [6], Munawar et al. [7, 8], and Butt et al. [9] can also be recovered by substituting $m = 1$ in the present system when the additional assumptions considered by [6–9] are ignored. When the surface suction or injection is also taken into account the second boundary condition in Eq. (6.35b) at $\eta = 0$ modifies as

$$f(0) = \pm\left(-\frac{\mathrm{d}}{\sqrt{av}}\right), \tag{6.36}$$

where the wall suction/injection velocity also follows the power-law form given by

$$v_w = \mathrm{d}z^{\frac{m-1}{2}}. \tag{6.37}$$

The constant d is the dimensionless constant and designates the normal wall velocity as wall suction or injection corresponding to its "−ve" or "+ve" values, respectively, whereas the selection of "+" or "−" sign on RHS in Eq. (6.36) refers to the stretching or shrinking cases, respectively.

The other values of m different from unity correspond to the nonlinear power-law stretching of the cylinder. Corresponding to these values of m the cylinder's shape also varies due to which the cylinder may be regarded as of variable thickness.

The shapes of the cylinder's surface corresponding to different values of m are shown in Fig. 6.6a–d. The other family of cylinders for which the similarity solutions are possible belongs to those whose body contours follow the exponential form. This happens when the wall velocity function does follow the exponential wall law given in Eq. (5.111), corresponding to which the self-similar system is given in Eqs. (5.112)–(5.114).

Following the previously exercised steps the self-similar system for this case reads as

$$mf'^2 = \pm[(1 + 2\kappa\eta)f'']', \tag{6.38a}$$

$$\left.\begin{array}{ll} f' = 1, & \text{at } \eta = 0 \\ f' = 0, & \text{at } \eta = \infty \end{array}\right\}. \tag{6.38b}$$

The variable shapes of the cylinder's surface governed by the exponential radius function, given in Eq. (5.111), are plotted in Fig. 6.7a–d.

Notice that the above self-similar modeling corresponding to the cylinder's shapes generated by the functions $R(z) = R_0 z^{\frac{1-m}{2}}$ and $R_0 \mathrm{e}^{-\frac{m}{2L}z}$ seems to really valid to

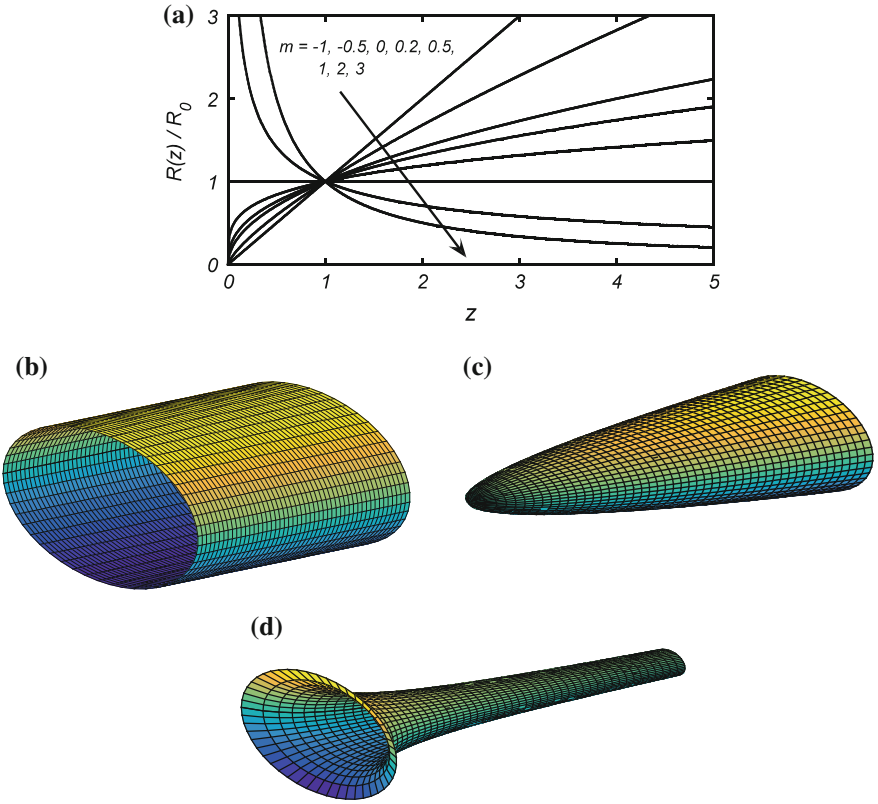

Fig. 6.6 **a** Body contours of the cylinder's surface corresponding to various values of m, **b** cylinder of constant radius obtained at $m = 1$, **c** cylinder (paraboloid) obtained at $m = 0$, **d** cylinder having infinite opening at the orifice obtained at $m = 2$

all those shapes generated by these functions. However, the situation is not that general, in actual. The current modeling is, however, restricted to the bodies whose longitudinal curvature is not that significant rather deems to be negligible. The longitudinal curvature κ_l is given by

$$\kappa_l = \frac{\frac{\mathrm{d}^2 R(z)}{\mathrm{d}s_l^2}}{1 - \left(\frac{\mathrm{d}R(z)}{\mathrm{d}s_l}\right)^2} \approx \frac{\mathrm{d}^2 R(z)}{\mathrm{d}s_l^2}, \tag{6.39}$$

where $1 - \left(\frac{\mathrm{d}R(z)}{\mathrm{d}s_l}\right)^2 \approx 1$ and s_l denotes the longitudinal arc length variable. This fact has further been explained in Sect. 10.1 of Chap. 10. Thus, the current analysis corresponds only to those shapes of the cylinder's surface for which $\frac{\mathrm{d}^2 R(z)}{\mathrm{d}s_l^2} \approx 0$. In Sect. 10.1, it will be shown that the self-similarity criterion is quite hard to

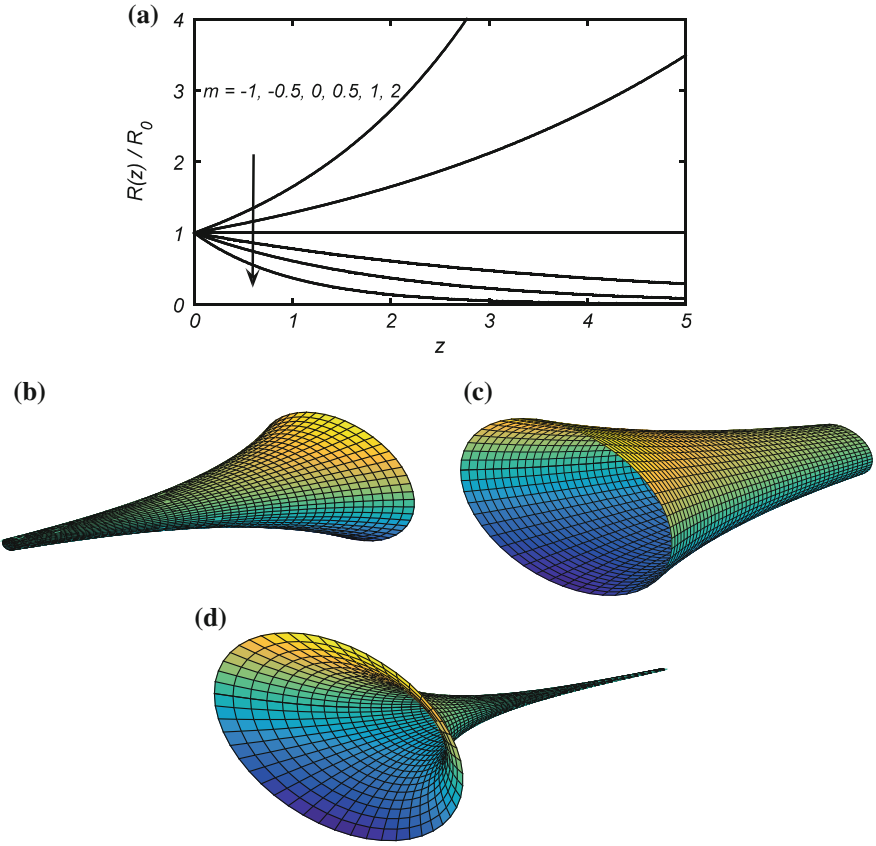

Fig. 6.7 **a** Body contours of the cylinder's surface whose cross section varies exponentially, **b** cylinder's surface whose radius varies exponentially; obtained at $m = -1$, **c** exponentially varying cylinder obtained at $m = 0.5$, **d** shape of the cylinder having large opening at the orifice

determine for very slender shapes of the cylinder or the bodies of revolution. In Eq. (5.108) the value $m = 1$ recovers the case of cylinder of uniform thickness; $m = 0$ a paraboloid of revolution; and $m = -1$ a circular cone. The positive values of $m(> 1)$ (in Eq. 5.108) correspond to the shapes having infinite opening at the orifice $(x = 0)$ and squeeze continuously downstream. Similar is the situation for $m > 0$ with the exponential surface shapes; in this case the opening of the cylinder stays, however, finite at the orifice.

In view of the wall velocity forms given in Eqs. (5.108) and (5.111) the values $m < 0$ correspond to the retarded wall velocities in either case. The power-law stretching case has been observed to survive till $m \to -1^+$; at $m = -1$ the coefficient of skin-friction becomes zero and turns positive for values $m < -1$. Such an intelligent solution of the present problem denies the possibility of the forms associated with the values $m < -1$ in the case of power-law stretching of the

cylinder. Similarly, in the case of exponential stretching, the coefficient of wall skin-friction turns positive, immediately, upon taking $m<0$ after attaining the value $f''(0) = 0$ at $m = 0$. In this case the retarded wall velocities completely fail in establishing the boundary-layer flow any way. Another reason behind this fact is the role of transverse curvature of the particular cylindrical shapes associated with these values of $m(< -1)$. For such cylinders the radius near the orifice does not stay very larger than the thickness of the boundary-layer there; rather, the boundary-layer thickness becomes of the order of cylinder's radius. Such a situation is actually not covered by the current equations. The velocity graphs for different values of m are plotted in Figs. 6.8 and 6.9 corresponding to the power-law and exponential cases, respectively. Clearly, the boundary-layer thickness increases and the skin-friction decreases upon reducing the values of m. This can simply be attributed to the retarded nature of the wall velocities for decreasing values of m. As the values of $m \to -1^+$ for $\kappa = 0.2$, the velocity curve approaches to attain the S-shape which is ultimately attained at $m = -1$ in the power-law case, as shown in Fig. 6.8. The situation is quite similar in the case of exponential wall velocity also. Upon increasing the values of m the flow establishes in the boundary-layer, and for decreasing values of m the boundary-layer thickness starts to grow. However, the so-called S-shape is not attained at $m = 0$, in this case, besides the vanishing behavior of the skin-friction coefficient. This is because of the reason that the sufficiently small values of m actually kill the inertial part of the momentum equation, in self-similar form, thus resulting in no boundary-layer behavior for these values of m. In this case too, the boundary-layer thickness decreases and the boundary-layer stays attached with the cylinder's surface for the accelerated wall velocities. This in turn causes to increase the surface skin-friction in the case of accelerated wall velocities.

The effects of the transverse curvature parameter κ are also shown in Figs. 6.10 and 6.11 where the velocity profiles have been plotted for various values of κ. Evidently, the velocity gradients near the wall increase upon increasing the surface transverse curvature parameter, κ in both the figures.

Close to the wall the velocity starts with the sharp gradients, for increasing values of κ, and immediately starts to decrease subsequently onward whereby causing the graphs to cross over the others. Consequently, the velocity dies out slowly in the upper part of the boundary-layer, thus increasing the boundary-layer thickness. The effects of curvature parameter are, however, more pronounced in the power-law case as compared to the exponential case.

The variation of the coefficient of skin-friction with respect to the parameters m and κ is shown in Figs. 6.12 and 6.13 for the considered two cases. The numerical values of the coefficient of skin-friction are also listed in Table 6.2. Increased values of the surface skin-friction corresponding to the large surface curvature reveal the assistive role of surface curvature toward the prevention of flow separation. Such assistance is actually provided by the favorable pressure gradient in the flows past a finite flat body. This fact has also been observed by Probstein and Elliott [10] for the bodies of revolution of finite lengths. With this observation the

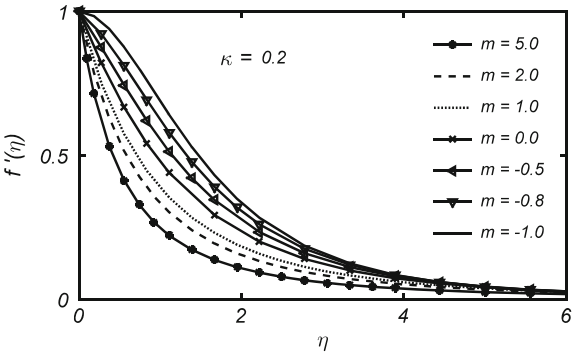

Fig. 6.8 Velocity profile in the power-law stretching case

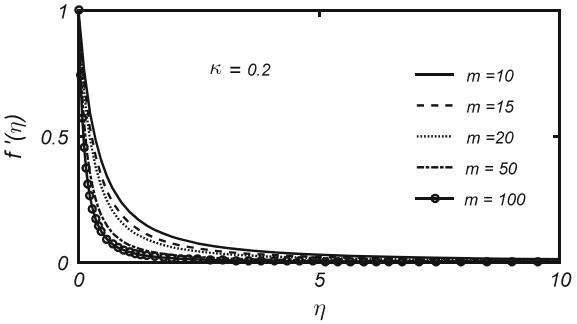

Fig. 6.9 Velocity profile in the exponential stretching case

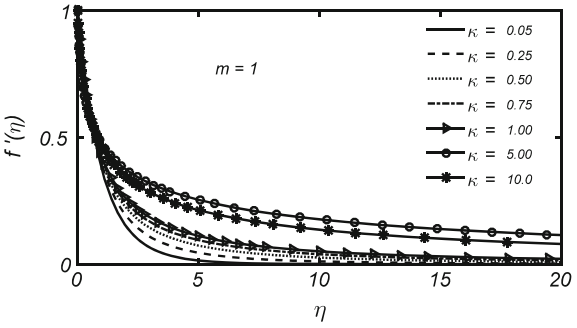

Fig. 6.10 Effects of surface curvature on the velocity profile (power-law case)

retarded flow cases for $m < -1$ and $m < 0$ corresponding to the power-law and exponential wall laws, respectively, can be made to survive to some extent, by taking sufficiently large values of κ.

It is therefore possible to find the ranges of admissible values of m (in both cases) corresponding to every value of κ; however, this has not been done in the present analysis. Another supportive agent in the case of retarded flow is the wall suction velocity. For the values $m < -1$ or $m < 0$ the solutions are also possible to make exist with the introduction of sufficient wall suction at the cylinder's surface in these two cases.

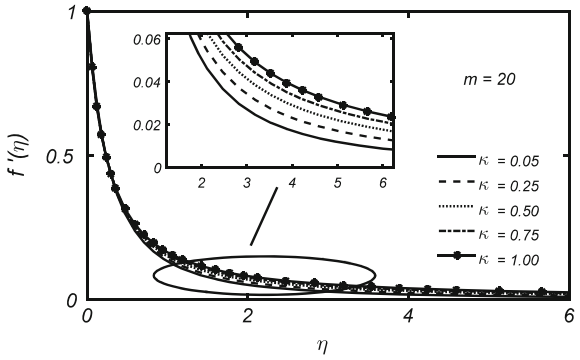

Fig. 6.11 Variation in velocity profiles for different κ (exponential case)

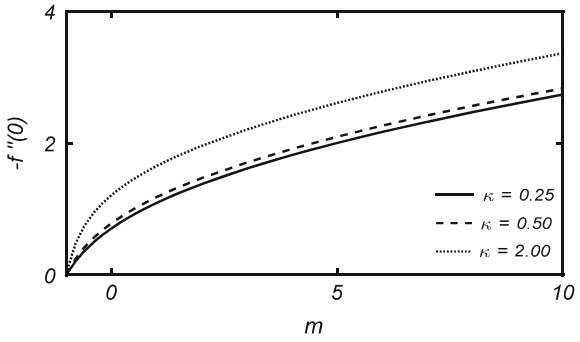

Fig. 6.12 Effects of curvature parameter on the skin-friction coefficient (power-law case)

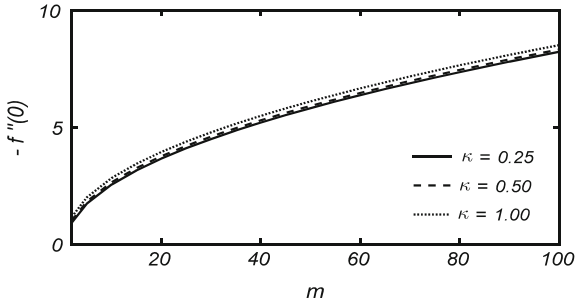

Fig. 6.13 Coefficient of skin-friction for different values of κ (exponential case)

6.3.2 *Radially Stretching Disk*

In the case of radially stretching circular disk the self-similar solution is possible for the power-law stretching velocity only, as determined in the second last section of Chap. 5. The admissible wall velocity has been described in Eq. (5.122), and the corresponding self-similar system is given by Eqs. (5.121) and (5.123), while the corresponding similarity variables have been defined in Eq. (5.120). This self-similar system has also been non-dimensionalized in the same manner as it is

Table 6.2 Values of $-f''(0)$ for different m and κ (power-law stretching cylinder)

	$-f''(0)$		
m	$\kappa = 0.25$	$\kappa = 0.5$	$\kappa = 2.0$
10	2.7336	2.8290	3.3596
7	2.3224	2.4172	2.9393
5	2.0001	2.0940	2.6077
3	1.6120	1.7042	2.2047
1	1.0905	1.1778	1.6486
0	0.7056	0.7826	1.2078
−0.2	0.6057	0.6779	1.0832
−0.4	0.4925	0.5576	0.5576
−0.8	0.2021	0.2373	0.4698
−1.0	0.0000	0.0000	0.0172

done in the previous sections of this chapter. The similarity variables in the dimensionless form are, therefore, given by

$$\begin{aligned} \eta &= \sqrt{\frac{\pm u_w(r)}{\nu r}} z, \quad u = u_w(r) f'(\eta), \\ v &= \pm \left[-\sqrt{\frac{\pm u_w(r)}{r}} \nu \left(\frac{m+3}{2} f + \frac{m-1}{2} \eta f' \right) \right], \end{aligned} \tag{6.40}$$

due to which governing Eqs. (5.121) and (5.123) take the form

$$m f'^2 - \left(\frac{m+3}{2} \right) f f'' = \pm f''', \tag{6.41}$$

and

$$\left.\begin{aligned} f' &= 1, \quad f = 0, \quad \text{at } \eta = 0 \\ f' &= 0, \quad\quad\quad \text{at } \eta = \infty \end{aligned}\right\}, \tag{6.42}$$

respectively. Equation (6.41) can further be recasted in a more compact form given by

$$\frac{2m}{m+3} f'^2 - f f'' = \pm f''', \tag{6.43}$$

which is obtained due to the scaling of η by $\sqrt{\frac{m+3}{2}}$. It must be noted that such a scaling in η must always be compensated by the same scaling in $f(\eta)$, as in the Falkner-Skan case. Because of this scaling of η Eq. (6.43) has taken the form similar to the two-dimensional equation given in Eq. (5.17) with a little difference in the coefficient of f'^2. Equation (5.17) and (6.4) are the alternative forms of each

other in the two-dimensional stretching sheet flow. Equivalently, Eq. (6.43) does also own the same form with a slightly modified coefficient. It, therefore, seems reasonable to not solve Eq. (6.43) again but to recover its solution from the known solution of (6.4), derived in Sect. 6.1. This can easily be done by first naming the coefficients of the two equations as

$$\beta_1 = \frac{2m}{m+1}, \quad \text{and} \quad \beta_2 = \frac{2m}{m+3}. \tag{6.44}$$

In the two-dimensional case the corresponding ranges of existence and uniqueness and non-uniqueness of the solution of Eq. (5.17) or (6.4) are already known and mentioned in Sect. 6.1. It has, there, been concluded that the solution is possible for the values $-1<\beta_1<2$ whereby infinitely many solutions exist for $-1<\beta_1<0$ and no solution at all for $\beta_1<-1$ (see Paullet and Previte [2]). Corresponding to these ranges of β_1 the respective ranges of m are: $0\le m<\infty$, $-\frac{1}{3}<m<0$ and $m<-1/3$ which, respectively, correspond to the existence of unique solution, infinitely many solutions, and no solution at all, respectively. Since Eqs. (6.43) and (5.17) are of the same form, the above ranges of β_1 are, therefore, also applicable to β_2 without any change. Thus, Eq. (6.43) also admits a unique solution if $\beta_2 \in (0,2)$, infinite many solutions if $\beta_2 \in (-1,0)$, and no solution when $\beta_2<-1$. Corresponding to these ranges of β_2 the respective ranges of values of m (in the stretching disk case) for which Eq. (6.43) admits a unique solution, many solution, and no solution are obtained due to Eq. (6.44) as $0\le m<\infty$, $-1<m<0$ and $m<-1$, respectively. With the availability of these ranges it is now possible to explore the disk case completely without solving Eq. (6.43). The above ranges can also be confirmed by noting that $\beta_2 \equiv \beta_1$ if m is replaced by $3m$ in the expression of β_2. Thus, in the disk case it can directly be obtained from the two-dimensional case by replacing m by $3m$ in the two-dimensional solution. Therefore, the solution in the disk case is possible if $-\frac{1}{3}<3m<\infty$ or $-1<m<\infty$, which is the same as determined above. This lowest initial value of m in the disk case, beyond which no solution exists, is absolutely correct and has also been confirmed numerically. The corresponding velocity graphs are shown in Fig. 6.14 where the velocity curves can obviously be seen approaching the typical S-shape as $m \to -1^+$; the same fact can also be conformed from Fig. 6.15 where the coefficient of skin-friction can be seen dying out at $m=-1$. Clearly, for increasing values of m the coefficient of skin-friction increases and the boundary-layer thickness decreases (see Figs. 6.14 and 6.15).

In order to further ensure the above-mentioned fact the two equations, namely the two-dimensional and the disk flow, have been solved independently, and the results are listed in Table 6.3.

Clearly, the values of m for which the (disk) Eq. (6.43) recovers the two-dimensional results are a multiple of 3 of the corresponding values of m in the two-dimensional case. Hence, the value of m for which the two equations produce the same results is a multiple of 3 (for the disk case) of the values independently chosen

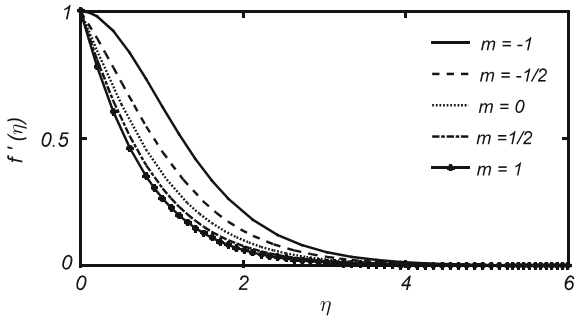

Fig. 6.14 Velocity profile for different m (stretching disk case)

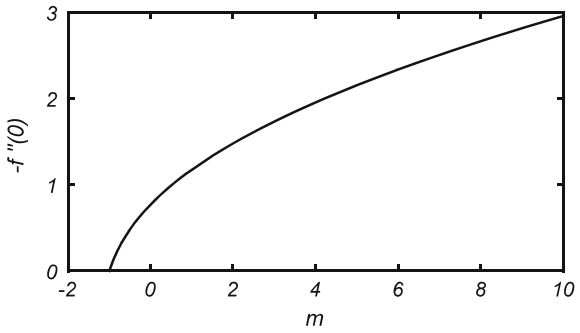

Fig. 6.15 Coefficient of skin-friction plotted against m (stretching disk case)

Table 6.3 Equivalence of the two-dimensional and the disk cases

Two-dimensional case		The disk case	
m	$\left(\frac{m+1}{2}\right)^{-1/2} f''(0)$	$\left(\frac{m+3}{2}\right)^{-1/2} f''(0)$	m
0	0.6276	0.6276	0
1/5	0.7668	0.7668	3/5
1/3	0.8299	0.8299	1
1	1.0000	1.0000	3
3	1.1486	1.1486	9
−1/7	0.4645	0.4645	−3/7
−1/5	0.3704	0.3704	−3/5
−1/21	0.5816	0.5816	−1/7

in the two-dimensional case. This is the reason due to which minimum value of $m = -1/3$ (in the two-dimensional case) has been prolonged to $m = -1$ in the disk case. This means that a situation which arises for a particular value of m in the two-dimensional case does also appear in the disk case but at the value $3m$. Therefore, Eq. (5.17) is equally applicable to the two-dimensional and the axisymmetric disk flows simultaneously. This actually means that the disk case need not to be studied separately; rather, it is already included in the two-dimensional case. It seems worth mentioning that the reported graphs have been plotted by solving Eqs. (6.41) and (6.42) numerically.

In view of the above discussion this can finally be concluded that the disk flow owns exactly the same character as does the two-dimensional sheet flow. After having explored the two-dimensional flow in full detail there lefts nothing behind to be studied in the disk flow, regarding the mathematics concerned. However, in physical point of view the value $\beta_2 = -1$ refers to the value $m = -1$ of the stretching exponent. In comparison with the two-dimensional flow the power-law retarded velocity has further been extended to the value $m = -1$ in the disk case. This means that the axial symmetry allows for the further retarded velocities as compared to the planner geometry.

In light of the above-mentioned facts it is important to note that such a comparison and resemblance between the two-dimensional and the disk cases have never been pointed out to the best of our knowledge. These observations, noted above, became actually possible due to the availability of Eqs. (6.41) or (6.43) in the form of m which motivates one to compare it with Eq. (5.17). Because of the non-availability of the self-similar formulation, for the general case of power-law stretching of the disk, it has extensively been studied by number of researchers without making any connection with the two-dimensional case. However, the studies related to the rotating stretchable disk do not find any such resemblance with the two-dimensional flow. Therefore, the above discussion is strictly restricted to the case when the circular component of velocity is absent in the disk flow. The two-dimensional solution does not apply to the stretching disk case if the flow is three-dimensional because of the rotation of the outer fluid or that of the disk itself.

When the disk surface is assumed to be porous and wall suction or injection is permissible, then the second condition in Eq. (6.42) at $\eta = 0$ modifies as

$$f(0) = \pm\left(-\frac{\mathrm{d}}{\sqrt{av}} \cdot \frac{2}{m+3}\right), \tag{6.45}$$

which, in view of above discussion, is also of the similar form as the first condition of Eq. (6.12), corresponding to the two-dimensional case.

6.4 Surface Texture

In the previous three sections the self-similar flows have been studied in view of the admissible wall velocities both the lateral and normal components by considering the surface of interest as flat except in the case of cylinder. In the special case of constant cross section the cylinder can still not be regarded as flat but enters in the category of flat surface bodies in a sense that such a stretching cylinder maintains constant thickness as do the other flat surfaces such as the sheet or the disk. In Sect. 6.3.1 it has been seen, in the nonlinear stretching case, that the cylinder fails to maintain the constant cross section throughout its length and the existence of self-similarity requires the variable thickness of it. On the other hand, the stretching sheet or the disk did not lose the property of constant thickness either being

stretched nonlinearly or exponentially. A natural question arises, what happens to the self-similarity conditions if the thickness of the stretching surface is not kept constant? Does the similarity solution persist or the similarity breaks down? The answer to this question does also come from Chap. 5 where the similarity criterion of all the considered flows has been demonstrated in view of the wall velocities. As a rule of thumb, it is easy to guess that the variable thickness of the non-flat body can be of the power-law form or of the exponential form as is evident from the cylinder case. With this discussion, we shall restrict ourself to the two-dimensional case only and will left the three-dimensional and the disk cases to the reader as they follow in the same manner.

Similar to the cylinder case let us denote the non-flat surface of the two-dimensional sheet as $S(x)$ where x is the variable due to which the thickness of the sheet varies (schematic diagram is shown in Fig. 6.16). By doing so, another variable does enter to governing system (5.2)–(5.4) or (5.6)–(5.7) where the boundary conditions at $y = 0$ in Eq. (5.7) have been shifted at $y = S(x)$. Consequently, the scaling group (5.8) will include one more scaling $\bar{S}(x) = k^{\alpha_s} S$ of the variable $S(x)$ which contributes another equation $\alpha_2 = \alpha_s$ to system (5.11) admitting the solution $\frac{\alpha_s}{\alpha_1} = \frac{1-m}{2} (\alpha_1 \neq 0)$ and $\alpha_s = -\frac{m}{2} (\alpha_1 = 0)$. The subsequent construction of the new variables results in the following two forms of the variable surface thickness function

$$S(x) = Kx^{\frac{1-m}{2}} \quad \text{and} \quad S(x) = K\mathrm{e}^{-\frac{m}{2}x}, \tag{6.46}$$

where K is a constant having suitable dimensions not necessarily the same in the two definition. The values of K actually scale the surface gradients, and the values $K > 1$ correspond to the surfaces having great curvature.

Governing Eqs. (5.2)–(5.4) have been obtained under the boundary-layer assumptions and the pressure gradient term $\frac{\partial p}{\partial x}$ has been ignored, there, because of the flat surface texture. If the surface texture involves considerably large surface gradients, then the assumption $\frac{\partial p}{\partial x} = 0$ remains no more valid. Therefore, Eq. (6.46) is applicable only to those situations where the surface curvature is small. The utilization of the dimensionless similarity variable η defined in (Eq. 6.5) reduces the surface conditions from $y = S(x)$ to $\eta = Re_K$ where $Re_K = \sqrt{aK^2/\nu}$ is the Reynolds number based on the surface gradient parameter K. This Reynolds number is of the same form as does the Re_{R_0} based on the fixed cylinder's radius R_0 in Sect. 6.3.1. The rest of the things, corresponding to the variable thickness of the sheet case, follow exactly in the same manner as have already been done in Sect. 6.3.1 for the case of cylinder. The two-dimensional flow due to the stretching sheet of variable thickness following the power-law wall velocity profile has already been studied by Fang et al. [11] where they have discussed the curvature effects on the velocity and skin-friction. Dual solutions have also been reported for an interval of values of m having finite length. The mathematics follows the similar in the case of exponentially varying surface thickness also. Following similar

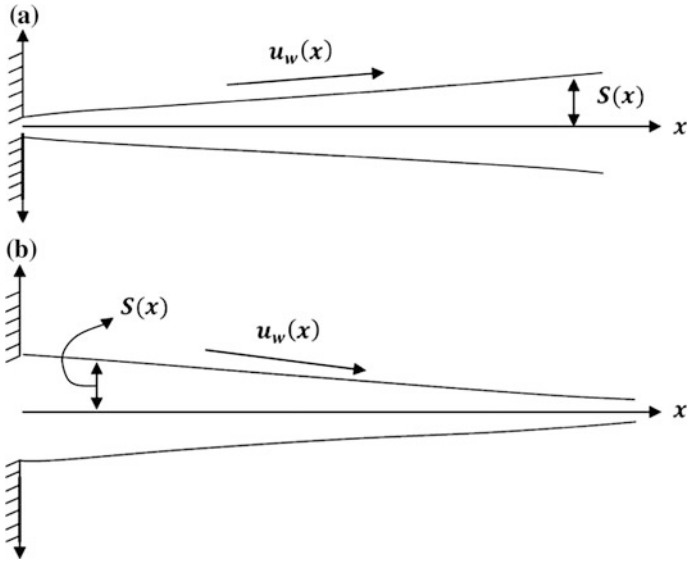

Fig. 6.16 **a–b** Variable thickness of the sheet shown schematically

procedure one can also find the variable surface shapes for the three-dimensional and the disk cases accordingly.

Finally, at the end, it seems better to give a brief summary of the facts discussed throughout this chapter. It has finally been concluded that the stretching surface flows do not experience any problem, regarding their existence, in the case of accelerated wall velocities, whereas the uniqueness of the solution vanishes out in the case of retarded wall velocities. Particular to the stretching surfaces, the accelerated wall velocities correspond to the values $m > 0$ and the decelerated wall velocities refer to the values $m < 0$. It should, however, be remembered that the two-dimensional and the disk problems do not admit solution for all negative values of m but in some limited intervals in the left neighborhood of $m = 0$. For such negative values of m the solutions are observed to be non-unique rather, uncountable. In the plots, given in this chapter, the second or other multiple solutions have intentionally been discarded and only those solutions have been reported which are meaningful in the physical sense. In Sect. 6.3.2 it has been concluded that the solution of stretching disk problem is already included in the two-dimensional case which can immediately be recovered by a suitable scaling of the values of m in the two-dimensional case. Similar to the wall velocities, the self-similarity does persist for the non-flat surfaces also provided; the surface texture follows either power-law or exponential forms in accordance with the wall velocities. Section 6.4, in the continuation of the topics considered in Chap. 5, completes the course of determination of self-similarity criterion for the flows due to moving continuous surfaces in view of their wall velocities and the surface textures of the moving continuous surfaces.

References

1. R.A. van Gorder, K. Vajravalu, F.T. Akyildiz, Existence and uniqueness results for a non-linear differential equation arising in viscous flow over a nonlinearly stretching sheet. Appl. Math. Lett. **24**, 238–242 (2011)
2. J.E. Paullet, J.P. Previte, Comment on "Existence and uniqueness results for a nonlinear differential equation arising in viscous flow over a nonlinearly stretching sheet". Appl. Math. Lett. **25**, 1114–1117 (2012)
3. C.Y. Wang, The three-dimensional flow due to a stretching surface. Phys. Fluids **27**, 1915–1917 (1984)
4. I.C. Liu, H.H. Wang, Y.F. Peng, Flow and heat transfer for three-dimensional flow over an exponentially stretching surface. Chem. Eng. Comm. **200**, 253–268 (2013)
5. C.Y. Wang, Fluid flow due to a stretching cylinder. Phys. Fluids **31**, 466–468 (1988)
6. J. Grubka, K.M. Bobba, Heat transfer characteristics of a continuous stretching surface with variable temperature, J. Heat Transf.-Trans. ASME, **107**, 248–250 (1985)
7. S. Munawar, A. Mehmood, A. Ali, Time-dependent flow and heat transfer over a stretching cylinder. Chin. J. Phys. **50**(5), 828–848 (2012)
8. S. Munawar, N. Saleem, A. Mehmood, Entropy production in the flow over a swirling stretchable cylinder. Thermophy. Aeromech. **23**(3), 435–444 (2016)
9. A.S. Butt, A. Ali, A. Mehmood, Numerical investigation of magnetic field effects on entropy generation in viscous flow over a stretching cylinder embedded in a porous medium. Energy **99**, 237–249 (2016)
10. R.F. Probstein, D. Elliott, The transverse curvature effect in compressible axially symmetric laminar boundary-layer flow. J. Aero. Sci. **23**, 208–224 (1956)
11. T. Fang, J. Zhang, Y. Zhong, Boundary layer flow over a stretching sheet with variable thickness, Appl. Math. Comp. **218**, 7241–7252 (2012)

Chapter 7
Viscous Flow Due to the Shrinking Surfaces

In the preceding chapter, attention has particularly been given to the viscous flows due to stretching continuous surfaces only. This chapter is therefore particularly devoted to the shrinking sheet/surface flows. However, honestly speaking, the shrinking surface case does not own any great potential which could require a separate chapter for its consideration. In reality the title of the preceding chapter was better to be ended by the phrase "motion of continuous surfaces" instead of "stretching surfaces," and the cases of shrinking surfaces were also appropriate to be appended to the respective sections of the stretching surface flows. Even with the realization of these facts, we are still forced to devote a separate complete chapter to this flow case. The reason behind this is the existing huge volume of archived literature on the shrinking surface flow, which can safely be regarded incorrect based upon the incorrect mathematical formulation and inappropriate handling of the problem. Because of such mishandling, the involved authors obtained wrong results which subsequently forced them to device unrealistic and non-physical reasoning for the explanation and justification of such wrong results. It is now generally perceived that the shrinking sheet/surface problems do not admit a solution in the absence of any wall suction. On the basis of their wrong analyses, most of the involved authors claimed that the shrinking surface problems offer more nonlinear phenomena in comparison with the stretching surface flows besides the fact that they are also governed by, almost, the same equations as do the flows due to stretching surfaces. Such conclusions are absolutely wrong and have nothing to do with the shrinking surface problems. The erroneousness of these facts and their correction has been presented in the coming sections.

The biggest misfortune with the shrinking surface problems is the general acceptance of the existing wrong self-similar formulation and hence the wrong results by the audience concerning this topic. This resulted in the immediate adaptations of the available wrong results by most of the researchers working in this field. Consequently, a huge number of wrong publications have so far been contributed to the pool of archived literature which is continuously going on increasing

A. Mehmood, *Viscous Flows*, Mathematical Engineering,
DOI 10.1007/978-3-319-55432-7_7

by every passing year. This mistake has so widely been spread that it has now become absolute because of the availability of authentic published literature on the back of it. The appropriate venue for the correction of this mistake was actually the same forum where the first wrong result, on this topic, was published. The author has already tried this option, but the editor simply refused by saying that the reviewers are against the publication of this correction. However, the comments of the reviewers have never been shared with the author despite his several requests to the editor concerned and even the all editorial board members. Having experiencing such a bad response and knowing the intensity of the growing fundamental mistake, the author finds this chapter as a great opportunity for the description of the erroneousness of the existing literature on this topic and for the presentation of correct mathematical formulation and hence the correct analysis and the results of this problem.

7.1 An Overview of Existing Literature

The criterion of self-similarity for the variable wall velocities u_w and w_w has already been determined in Chap. 5 for various flow situations. In view of the definitions of the obtained wall velocities, the flow is designated as due to a stretching surface if the lateral wall velocities are positive (for example $u_w > 0$, in the two-dimensional case), and the flow is designated as shrinking surface flow if the wall velocities are negative, that is $u_w < 0$. Such a flow was introduced by Miklavcic and Wang [1] where they considered a three-dimensional flow due to linear bilateral stretching of the porous flexible sheet. In view of the coordinate system chosen in Sect. 2.1.3, the boundary conditions of [1] read as

$$u_w = -u_{\text{ref}}(x), \quad w_w = -(\bar{m}-1)w_{\text{ref}}(z), \quad v_w = -V, \quad \text{at } y = 0, \tag{7.1}$$

where

$$u_{\text{ref}}(x) = ax \quad \text{and} \quad w_{\text{ref}}(z) = az \tag{7.2}$$

The constant $a(>0)$ involved in above wall velocities was designated as the constant shrinking rate in [1]. Therefore, the wall velocities (7.2), with $a(>0)$, can simply be regarded as stretching wall velocities. However, the presence of "−" sign in Eq. (7.1) makes these wall velocities, overall, negative by providing a reason for their designation as shrinking wall velocities. The factor $(\bar{m}-1)$ serves as an on/off switch corresponding to $\bar{m} = 2$ or $\bar{m} = 1$, respectively. The similarity variables introduced by Miklavcic and Wang [1] are given by

$$\eta = \sqrt{\frac{a}{\nu}}y, \frac{u}{u_{\text{ref}}(x)} = f'(\eta), \frac{w}{w_{\text{ref}}(x)} = (m-1)f'(\eta), v = -\sqrt{a\nu}\bar{m}f(\eta), \tag{7.3}$$

due to which they obtained the self-similar governing equation of the form

$$f'^2 - \bar{m}ff'' = f''', \tag{7.4}$$

subject to the boundary conditions

$$f'(0) = -1, f(0) = \frac{V}{\bar{m}\sqrt{av}} \equiv s, f'(\infty) = 0. \tag{7.5}$$

Corresponding to the value $\bar{m} = 1$, Eq. (7.4) becomes exactly the same as Eq. (6.4) (for $m = 1$; and with the selection of "+" sign on right-hand side) which corresponds to the two-dimensional stretching sheet flow. The similarity transformations (7.3) are also those valid for the stretching sheet flow; see for instance Eq. (6.5). Thus, so far, it has been obvious that the similarity transformations (Eq. 7.3) and the self-similar equation (Eq. 7.4), derived originally for the shrinking sheet flow, are actually those governing the stretching sheet flow. The only difference between the stretching and shrinking sheet flow, due to the formulation in [1], is of the boundary condition

$$f'(0) = -1, \tag{7.6}$$

where the "−" sign has appeared on the RHS of Eq. (7.6) which gets vanished for the stretching sheet case. Thus, according to the formulation proposed in [1], the only difference between the self-similar systems governing the stretching sheet or shrinking sheet flow is the absence or presence of "−" sign on the RHS of Eq. (7.6), respectively.

After solving the system (7.4) and (7.5), Miklavcic and Wang [1] concluded that the solution to this problem does not exist at all unless an adequate suction is allowed at the shrinking surface. The authors of [1] ended their paper by stating that "the shrinking sheet studied in this paper offers a wealth of nonlinear fluid phenomena." With such a claim of nonexistence and nonlinear phenomena owned by Eqs. (7.4) and (7.5), the shrinking sheet flow attracted number of researchers who immediately got involved with these equations in order to investigate the existence and uniqueness of such flows. On the other hand, several other researchers got also involved with this problem by considering the heat-mass transfer and other physical assumptions, such as the impact of magnetic field or the role of porous medium. In all such studies, the contributing authors definitely obtained wrong results which lead them to make the false conclusions justified by non-physical reasoning. The reason behind such a false conclusions is that the shrinking sheet problem has neither been formulated correctly nor been studied in the perspective of correct physics of this flow. The elaboration of this fact will stay pending till Sect. 7.5.

Despite the presence of more than hundred peer-reviewed research papers on the shrinking surface flow, the author intentionally refrains from citing any or few of them. At the author's opinion, citing few of them is as bad as ignoring the most of

them. The reference [1] has also been cited with great regret, but it was unavoidable. Otherwise, it was not possible to move on this topic anyway.

7.2 Erroneousness of the Existing Shrinking Sheet Results

The misfortune with the shrinking sheet flow is twofold, as concluded in the above section: First one is the erroneous nature of the self-similar modeling (7.3)–(7.5), and the second, and perhaps more important one is the improper handling. Erroneousness of the system (7.3)–(7.5) persists because of the wrong selection of reference velocity in the process of non-dimensionalization. In Eq. (7.3) the velocity components u and w have been normalized due to the reference velocities $u_{\text{ref}}(x)$ and $w_{\text{ref}}(z)$, respectively. Similarly the definitions of η and v have also been furnished because of the reference velocity $u_{\text{ref}}(x)$. But actually the correct reference velocities in this case are u_w and w_w (see Chap. 6) that is "$-u_{\text{ref}}(x)$" and "$-w_{\text{ref}}(z)$" instead of "$u_{\text{ref}}(x)$" and "$w_{\text{ref}}(z)$," respectively. Because of this reason the "$-$" sign appearing on the right-hand side of the first two boundary conditions in Eq. (7.1) have not been removed in the self-similar boundary conditions (7.5). If the correct reference velocities "$-u_{\text{ref}}(x)$" and "$-w_{\text{ref}}(z)$" are utilized, the mentioned "$-$" sign in the indicated boundary condition in Eq. (7.5) gets vanished by turning it into the form $f'(0) = 1$, which is the same as for the stretching sheet flow. Consequently, a negative sign appears on the right-hand side of Eq. (7.4) with the term f''' by making it "$-f'''$", instead. This fact has also been explained by Batchelor [2] in his book while discussing the boundary-layer flow past a flat plate.

As we stated above, the second misfortune with this problem is that, it has never been studied in view of its correct physics. Only one aspect of the shrinking sheet flow has so far been explored at the most, which is the flow due to a "retarded shrinking sheet," and the accelerated aspect of the shrinking sheet flow has totally been ignored. This is the reason due to which the accelerated or decelerated designation of the stretching or shrinking velocities has particularly been emphasized throughout this Book.

7.3 Accelerated/Decelerated Shrinking Wall Velocities

Consider the unidirectional stretching/shrinking of the sheet defined by

$$u_w(x) = ax^m, \tag{7.7}$$

where m is the stretching/shrinking exponent and a is the constant stretching/shrinking rate. Corresponding to $a > 0$, $u_w(x)$ denotes the stretching of the wall, whereas $a < 0$ denotes the shrinking of the surface. The wall velocity (6.7) has already been plotted in Fig. 6.2 for the stretching sheet case corresponding to

several values of m. From this figure, it is clear that for +ve values of $m, u_w(x)$ increases as x increases, representing the accelerated wall velocity. On the other hand, for negative values of m, the wall velocity $u_w(x)$ decreases as one moves along the stretching sheet referring to the decelerated nature of the wall velocity. Now in the shrinking sheet case, the direction of motion of the sheet has been reversed to the direction of motion of the stretching sheet, that is, in the −ve x-direction. Because of this fact, the wall velocity is designated as accelerated when $m<0$ and decelerated when $m>0$ as depicted in Fig. 7.1. As one moves in the −ve x-direction, the velocity magnitude increases for $m<0$ (see Fig. 7.1a, d) and decreases for $m>0$ (see Fig. 7.1b, c). Therefore, the flow studied in [1] is actually retarded in nature because of the form of considered shrinking wall velocity having positive exponents of x and z in Eq. (7.2).

This is a common character of the boundary-layers that the boundary-layer flow is assisted by the accelerated reference velocity which actually makes the boundary-layer to stay attached with the solid surface, whereas the retarded reference velocities, being unable to assist the flow, separate the boundary-layer from the solid surface creating a wake behind the point of separation and causing a reverse flow, subsequently. This fact is commonly known as the phenomena of separation. Another well-known fact in the theory of boundary-layers is that, the occurrence of separation can simply be delayed or the separating boundary-layer can easily be made to stay attached with the solid surface by the introduction of sufficient wall suction at the solid surface. In actual, the coefficient of wall skin-friction, gradually, becomes smaller and smaller in the separating boundary-layer and ultimately becomes zero, i.e., $f''(0)=0$, at the point of separation.

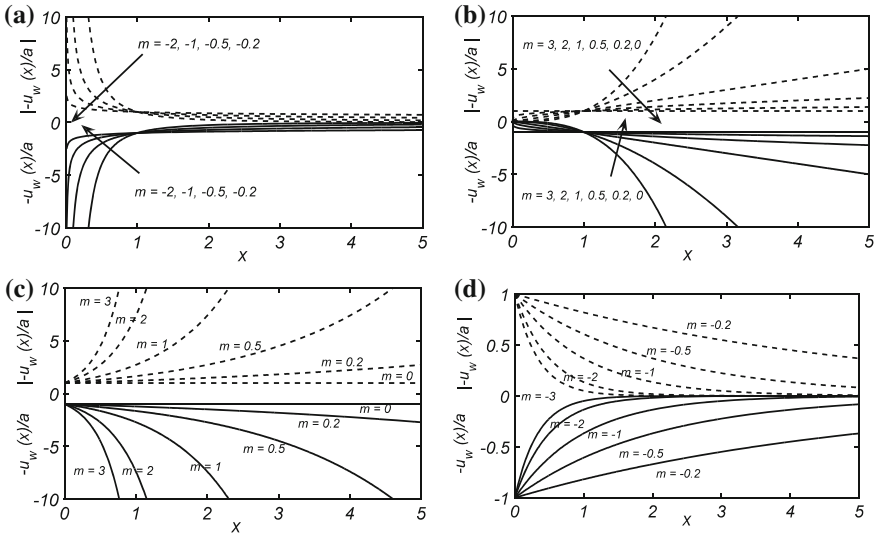

Fig. 7.1 Shrinking wall velocities for different m: **a**, **b** power-law wall velocity, **c**, **d** exponential wall velocity

The introduction of sufficient suction at the wall surface prevents the value of $f''(0)$ from becoming zero due to which the boundary-layer stays attached to the solid surface. The same does actually happen in the case of decelerated shrinking sheet (for $m = 1$) considered by Miklavcic and Wang [1]. In this case too, the flow can obviously be made to exist if sufficient amount of suction is introduced at the solid surface; and the same has been done and concluded in [1]. However, because of ignoring the correct nature of the shrinking wall velocity, the authors, in the last paragraph of [1], argued that the stretching of the sheet "induces far-field suction toward the sheet, while the shrinking sheet would cause a velocity away from the sheet." "Thus from physical grounds, vorticity of the shrinking sheet is not confined within a boundary-layer, and the flow is unlikely to exist unless adequate suction on the boundary is imposed." These false arguments actually lead them to draw the wrong conclusion of nonexistence of solution for the shrinking sheet flow which was further agreed upon by the subsequent authors.

On the basis of above-mentioned limited and wrong analyses pertaining to the shrinking surface problems, it has generally been perceived that the shrinking sheet flow is far more difficult from the stretching sheet flow and exhibits dramatic changes. Such a conclusion is totally misleading, because the correct analysis of the shrinking sheet flow based on the correct self-similar modeling has never been made. Such a correct analysis reveals that, in general, the flow behavior is similar to the stretching sheet flow, qualitatively. The difference between the two flows is only of quantitative nature which is quite natural. A detailed discussion on the shrinking sheet flow is given in Sect. 7.5.

7.4 Correct Self-similar Formulation

The problem with the existing self-similar formulation of the shrinking sheet flow is basically the wrong selection of reference velocity for the purpose of non-dimensionalization, as pointed out in Sect. 7.2. The criterion for the self-similar wall velocities for these flows is the same as it is for the case of stretching surfaces as derived in Chap. 5. Thus the self-similar solution exists, for a shrinking surface flow, if the wall velocity follows either power-law or exponential form. For the sake of simplicity, the two-dimensional case is preferred to be discussed here for the purpose.

The corresponding self-similar wall velocities in this case read as $u_w = ax^m$ and $u_w = ae^{mx}$, corresponding to the power-law and exponential forms, respectively. Particular to the shrinking sheet case, we choose to say $a = -\bar{a}$; $\bar{a} > 0$. With this substitution, Eq. (6.1) takes the form

$$\eta = Ax^{\frac{m-1}{2}}y, \quad u = -\bar{a}x^m f'(\eta), \quad v = \frac{\bar{a}}{A}x^{\frac{m-1}{2}}\left(\left(\frac{m+1}{2}\right)f + \left(\frac{m-1}{2}\right)\eta f'\right), \quad (7.8)$$

Hence, Eq. (6.4) becomes

$$mf'^2 - \left(\frac{m+1}{2}\right)ff'' = -f''', \tag{7.9}$$

with the restriction that $A = \sqrt{\bar{a}/\nu}$. The utilization of this value of A in Eq. (7.8) results in

$$\eta = \sqrt{\frac{\bar{a}x^m}{\nu x}}, \quad u = -\bar{a}x^m f'(\eta), \quad v = \sqrt{\frac{\bar{a}x^m \nu}{x}}\left[\left(\frac{m+1}{2}\right)f + \left(\frac{m-1}{2}\right)\eta f'\right].$$

Notice that, particular to this case, $u_w = -\bar{a}x^m$. Because of this form of $u_w(x)$ the above equation can also be rewritten as

$$\eta = \sqrt{\frac{-u_w(x)}{\nu x}}, \quad u = u_w(x)f'(\eta), \quad v = \sqrt{\frac{-u_w(x)\nu}{x}}\left[\left(\frac{m+1}{2}\right)f + \left(\frac{m-1}{2}\right)\eta f'\right]. \tag{7.10}$$

Consequently, the boundary condition $u = u_w(x) = -\bar{a}x^m$ at $y = 0$ simplifies to $f'(0) = 1$ carrying no "−" sign with 1 (on RHS), whereas Eq. (7.9) carries a −ve sign with the term f''' on right-hand side, as pointed out in Sect. 7.2. Evidently, Eqs. (7.9) and (7.10) are exactly in accordance with the Batchelor's comment, in this regard. Note that Eqs. (7.9) and (7.10) can directly be obtained from Eqs. (6.4) and (6.5) by selecting the −ve sign among the "±" signs. Thus the dimensionless self-similar systems presented in Chap. 6 include both the cases, namely, the stretching and shrinking surface cases. Equations (7.9) and (7.10) thus finally prove the erroneousness of the existing (due to [1]) self-similar dimensionless formulation of the shrinking surface flows by endorsing the claim made in the start of this Chapter, in this regard. The same follows in the case of exponential wall law and the three-dimensional and axisymmetric cases.

7.5 Viscous Flow Due to an Accelerated/Decelerated Shrinking Sheet

In Sect. 7.2, the error in the shrinking surface flows was designated to be twofold; first was concerned with the mathematical formulation, while the second was related to the insufficient analysis of the flow. The mathematical error has been fixed in the preceding section, while the correct flow analysis will be presented here. In doing so, attention will only be focused to the two-dimensional flow again because of its simple nature. The cases of power-law and exponential wall velocities, for this flow, have been investigated in full detail. In the two cases, power-law or exponential shrinking velocities, the boundary conditions are the same as those

valid for the stretching sheet flow given in Eq. (6.6). The governing self-similar equations in dimensionless form for the said two cases are Eqs. (7.9) and (6.8), respectively, with the selection of "−" sign among the "±" signs on the right-hand side.

Corresponding to the power-law shrinking case, the dimensionless velocity $f'(\eta)$ has been plotted against η for several values of m in Fig. 7.2. Our analysis shows that for $m > 0$ no solution exists, but for $m < 0$ the solution seems to exist but does not obey the boundary-layer character. Such a trend continues if one further decrease the values of m till $m = -1$. However, it is noted that at $m = -0.99$ the solution does not differ from the solution at $m = -1$ by any large. Therefore, the value $m = -0.99$ has been taken as the maximum threshold beyond which the shrinking sheet flow does not exist. Although the shrinking velocity is accelerated for $-0.99 < m < 0$ and $f''(0) \neq 0$, still the velocity profile fails to exhibit the boundary-layer character. Actually, it seems that, for $-0.99 < m < 0$, the wall velocity is too weak to be insufficient to cause a boundary-layer flow in the adjacent fluid. Thus the solution does not exist for $m > -0.99$ in the case of power-law shrinking of the sheet. In contrast, the stretching sheet flow also survives for the retarded wall velocities till $m > -1/3$ in the power-law case. This gives an obvious clue regarding the weaker coefficient of skin-friction for the shrinking sheet flow in comparison with the stretching sheet flow corresponding to the same magnitude of stretching/shrinking exponent $|m|$. This fact can readily be confirmed from Table 7.1 where the values of $f''(0)$ have been listed for the two cases. The identification of the range $m < -0.99$ for the existence of solution to the shrinking sheet case is based upon numerical investigations and can further be refined. A rigorous mathematical analysis can provide the exact value of m beyond which the solution does not exist; involving in such a task is, however, not the objective of this chapter. Upon further decreasing the values of $m(< -1)$, the solution follows the boundary-layer character in a more pronounced manner as shown in Fig. 7.2 without exhibiting any unusual behavior. In qualitative sense, their behavior is exactly the same as in the case of stretching sheet flow. But quantitatively, they do slightly differ from the stretching sheet flow. This fact can also be confirmed by comparing the values of $f''(0)$ in Table 7.1, once again. The variation of $f''(0)$ against m, obtained due to correct formulation, is also given in Fig. 7.4.

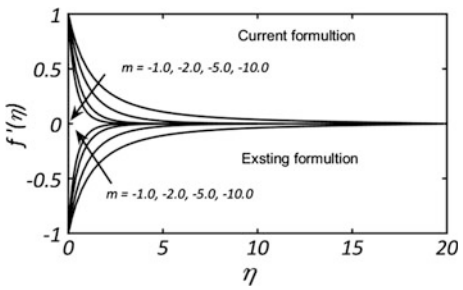

Fig. 7.2 Velocity profile for power-law shrinking sheet

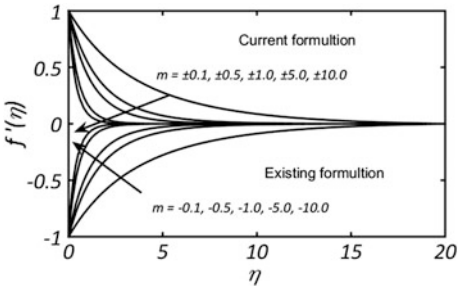

Fig. 7.3 Velocity profile for exponentially stretching/shrinking sheet

Table 7.1 Values of $f''(0)$ for power-law and exponential shrinking sheet cases due to the current and existing formulations

m	Current formulation			Existing formulation	
	$u_w = \bar{a}x^m$ $(-1/3 \leq m \leq 10)$	$u_w = \pm\bar{a}e^{\frac{mx}{L}}$ $(m \gtrless 0)$	$u_w = -\bar{a}x^m$ $(m \leq -1)$	$u_w = -\bar{a}e^{\frac{mx}{L}}$ $(m < 0)$	$u_w = -\bar{a}x^m$ $(m \leq -1)$
−1/3	−0.00000				
−1/5	−0.23426				
−1/10	−0.35026				
0.0	−0.44375	−0.00200		0.00200	
±1/10	−0.52353	−0.28662		0.28662	
±1/2	−0.77037	−0.64092		0.64092	
±1.0	−1.00000	−0.90638	−0.81651	0.90638	0.81651
±2.0	−1.34846	−1.28183	−1.21603	1.28183	1.21603
±5.0	−2.06894	−2.02673	−1.98473	2.02673	1.98473
±10.0	−2.89607	−2.86630	−2.83648	2.86630	2.83648

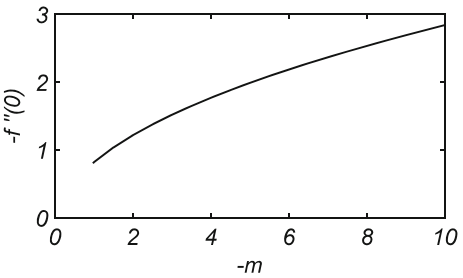

Fig. 7.4 Variation of $-f''(0)$ against m (power-law case)

The availability of correct formulation does allow for making an interesting observation here. The present (correct) Eqs. (7.9) and (6.6) can also be recovered from those of Miklavcic and Wang [1] (7.4 and 7.5) by replacing f by $-f$ in (7.4) and (7.5); taking $\bar{m} = 1$ and $s = 0$. This means that due to the existing formulation due to [1], the velocity $-f'(\eta)$ has actually been studied instead of $f'(\eta)$. This simply reverts the things in opposite to the actual situation. Because of this reason, the graphs obtained due to the existing (wrong) formulation are the mirror images

of those plotted due to the (present) correct formulation (see Fig. 7.2). From here it is also possible to deny the nonexistence of the solution to this case, even due to the existing wrong formulation, without the presence of adequate wall suction, as claimed by Miklavcic and Wang [1]. Clearly, their Eqs. (7.4) and (7.5) do admit the physically deemed meaningful solution for the values $m \leq -1$ in the absence of any wall normal velocity. The same fact can also be confirmed from Table 7.1 by comparing the values of $f''(0)$ due to the two formulations. The magnitude of the values of $f''(0)$ is exactly the same (due to the two formulations) but is opposite in sign.

In the preceding discussion, it has been observed that the shrinking sheet flow is similar to the stretching sheet flow in qualitative sense but differ quantitatively. The situation is quite more favorable in the case when the shrinking wall velocity obeys the exponential form. In contrast to the exponentially stretching sheet flow, which exists for $m > 0$, the shrinking sheet flow exists for $m < 0$. In this case, corresponding to the accelerated wall velocity $(m < 0)$, the governing self-similar system of shrinking sheet flow comes out to be exactly the same as for the exponentially stretching sheet flow $m > 0$. Consequently, the shrinking sheet flow follows exactly the same behavior, in toto, as does the stretching sheet flow in the case of exponential wall velocity. The graphs of the velocity profiles are given in Fig. 7.3 corresponding to different values of m. Clearly, the stretching and shrinking cases exhibit the same behavior (qualitatively) when $|m|$ is taken the same for these flows. It is also observed that as $|m|$ increases, the graphs exhibit the boundary-layer character more clearly which is in accordance with the fact observed in the accelerated flows; that is, upon increasing the values of $|m|$ the layer thickness decreases and the skin-friction increases at the wall (see Figs. 7.3 and 7.5). Figure 7.5 depicts that the magnitude of $f''(0)$ increases with $|m|$, and this increase is more pronounced for smaller values of $|m|$. In this case too, the results due to wrong formulation have also been plotted in the lower part of Fig. 7.3 where the resulting graphs are again the mirror images of the corresponding correct graphs (Fig. 7.4).

In view of the above flow analysis, it can now easily be realized that the shrinking sheet flow has never been studied in accordance with the correct physics. Furthermore, the claims of exhibition of dramatic changes by this flow have also been falsified due to the above analysis. The so-called dramatic changes and the

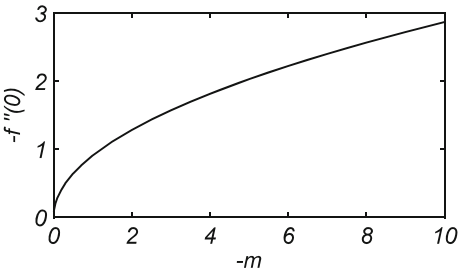

Fig. 7.5 Variation of $-f''(0)$ against m (exponential shrinking)

exhibition of "more nonlinear" phenomena attributed, particularly, to the shrinking sheet flow can also be experienced for the stretching sheet flow (e.g., power-law case) by taking the value of $m < -1/3$. The stretching sheet problem does not admit any solution for $m < -1/3$ as does the shrinking sheet problem for $m > -0.99$ (in the power-law case). Therefore, it can finally be concluded that the facts which had generally been admitted about the shrinking sheet flow are actually based upon the improper handling and incomplete analysis of the shrinking sheet flow. Studying only one aspect of this flow, namely, the retarded flow due to a shrinking sheet (by taking $m > 0$, only) had been a consequence of losing the correct physics of this flow.

7.6 Axially Symmetric Flow

Two axially symmetric flows have been considered in this section, namely, due to the shrinking continuous cylinder and the radially shrinking circular disk. For these two cases the non-dimensionalization of the corresponding self-similar systems has already been given Chap. 6. It has also been observed in Sect. 6.3 that the disk problem needs not to be studied separately rather the results for this case can readily by recovered from the two-dimensional case. It has also been found that any situation appearing in the two-dimensional flow, corresponding to some particular value m^* (say) of m, does also exist in the disk case for the value $m = 3m^*$. Because of this important fact, the shrinking disk problem also needs not be studied separately, rather it can be discovered from the results of the respective two-dimensional case, directly. In the preceding section, it is found that the shrinking sheet flow exists for $m \leq -0.99$ and that for $m > -0.99$ the solution does not obey the boundary-layer behavior. Consequently, in the disk case, the solutions must start at $m = 3 \times (-0.99) = -2.97$ and persist for all $m < -2.97$, whereas for $m > -2.97$ the solution must not obey the boundary-layer character. In order to seek further authentication of this fact, the above values $(m \leq -2.97)$ have also been confirmed by solving Eq. (6.41) subject to the boundary condition (6.42) by selecting the "−" sign with f'''. The obtained velocity curves are shown in Fig. 7.6 corresponding to the power-law case, whereas the exponential wall velocity is not admitted by the self-similar disk flow. From Fig. 7.6 it is clear that for larger values of $|m|$ the boundary-layer flow is established more and more by confining itself in a very thin region close to the shrinking disk. The reason behind this is the accelerated nature of the shrinking wall velocity (for $m < 0$) for which the solution is shown to exist without requiring any suction or injection at the shrinking surface. The values $-2.97 < m < 0$, though negative have, however, been discarded because the solution in this range does not fully exhibit the characteristics of boundary-layer flow. The asymptotic behavior of the velocity plots is observed to be dis-satisfactory in this range of values of m. Near the value $m = -2.97$, the solutions are quite sensitive and the numerical infinity is significantly large. Although the solution does converge, the asymptotic behavior near the edge of the boundary-layer is delayed quite long, for

these values of m. Since the threshold value $m = -2.97$ has been determined due to the two-dimensional solution. Therefore, any correction in the threshold value of two-dimensional case (i.e., $m = -0.99$) will lead to the further correction to the value $m = -2.97$, in the disk case.

Similar to the stretching cylinder case, the shrinking cylinder case has only been studied for the linear wall velocity, in the existing literature. According to the existing formulation, the shrinking wall velocity in the cylinder case has also been constructed by putting a "−" sign with the stretching wall velocity. Since the available literature on the stretching cylinder is strictly limited to the linear stretching case. Therefore, the shrinking case of cylinder is also limited to the linear wall law only. In this way, the accelerated cases of the power-law and exponentially shrinking cylinder have, so far, not been considered, similar to the two-dimensional case. According to the correct self-similar modeling, as explained previously, Eqs. (6.35) and (6.38) govern the shrinking cylinder flow with the selection of "−" sign among "±" on the right-hand sides of Eqs. (6.35a) and (6.38a) corresponding to the power-law and exponential shrinking velocities, respectively. In this case too, the solution does not exist in the case of retarded wall velocities (i.e., $m > 0$), similar to the previous two cases. Because of the presence of surface curvature parameter κ, the so-called threshold value of m (say m^*), which bifurcates the domain of m into two parts corresponding to the regions of existence and nonexistence of the solution is not unique. This threshold value m^* bears continuous dependence upon the curvature parameter and changes upon varying the values of κ. For large values of κ, the threshold value $|m^*|$ is small and vice versa. Again in this case, it is not possible for the author to report the threshold values of m corresponding to every value of κ as we already pointed out in the previous chapter.

Our numerical solution shows that within the admissible range of values of m, the numerical infinity is significantly large for small values of $|m|$ despite the convergence of the solution. Therefore, sufficiently large values of $|m|$ have been considered while plotting the graphs in this case. The flow behavior, in general, is somehow similar to that as it is in the stretching cylinder case. The boundary-layer thickness decreases upon increasing the values of $|m|$ (see Fig. 7.7). Consequently, the skin-friction increases as shown in Fig. 7.8. The increasing values of κ also contribute to increase the coefficient of skin-friction (see Fig. 7.8), thus assisting the flow in the weak wall velocity situations. Some numerical values of the coefficient of skin-friction corresponding to different values of m and κ are also listed in

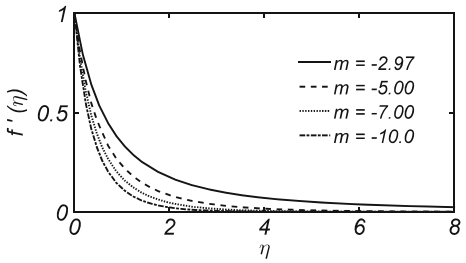

Fig. 7.6 Velocity profile for shrinking disk

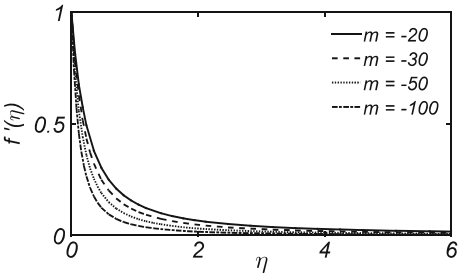

Fig. 7.7 Velocity profile for shrinking cylinder at $\kappa = 0.3$

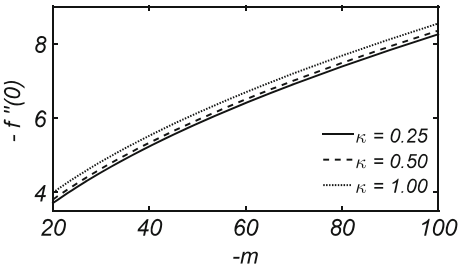

Fig. 7.8 $-f''(0)$ plotted against m for shrinking cylinder

Table 7.2 Values of $-f''(0)$ at different m and κ for power-law shrinking cylinder case

$-m$	$-f''(0)$		
	$\kappa = 0.25$	$\kappa = 0.5$	$\kappa = 1.0$
20	3.7139	3.8101	3.9968
25	4.1489	4.2455	4.4334
30	4.5416	4.6385	4.8271
40	5.2378	5.3351	5.5248
50	5.8498	5.9474	6.1384
70	6.9115	7.0093	7.2017
80	7.3846	7.4825	7.6752
100	8.2490	8.3470	8.5401

Table 7.2. This assisting role of κ is exactly the same as observed in the stretching cylinder case in the previous chapter. The effect of κ on the velocity profiles within the boundary-layer is also the same as in the stretching cylinder case; very close to the wall the velocity decreases upon increasing κ, and soon after, the curves cross over the others and die out slowly in the upper part of the boundary-layer (see Fig. 7.9).

Similar behavior is observed in the exponential shrinking case and the results have been depicted in Figs. 7.10, 7.11, and 7.12. Despite the difference in threshold values of m, from those of power-law shrinking case, the qualitative behavior of the current two cases (the power-law and exponential shrinking of the disk) is, however, exactly the same, in qualitative sense. Moreover, the flow behavior in the present exponentially shrinking cylinder case is also the same as in the corresponding case of

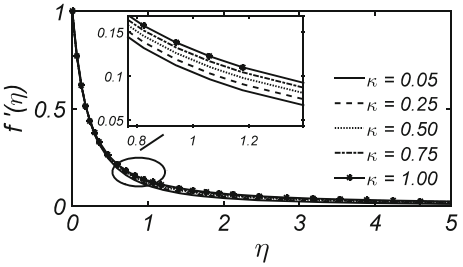

Fig. 7.9 Velocity for different κ for power-law shrinking cylinder at $m = -30$

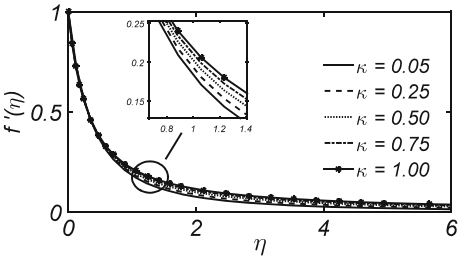

Fig. 7.10 Velocity at different κ for exponentially shrinking cylinder at $m = -10$

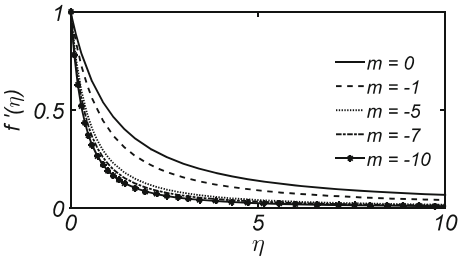

Fig. 7.11 Velocity profile of exponentially shrinking cylinder at $\kappa = 0.2$

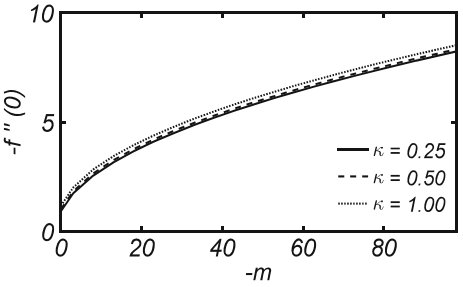

Fig. 7.12 Values of $-f''(0)$ plotted against m for different κ

exponentially stretching cylinder case. This fact again denies the exhibition of any "dramatic" behavior of the shrinking surface flow in comparison with the stretching surface flow. The reason behind this fact is the consideration of correct flow equations and the appropriate values of m in the shrinking surface cases.

Table 7.3 Values of $-f''(0)$ at different m and κ for exponentially shrinking cylinder

$-m$	$-f''(0)$		
	$\kappa = 0.25$	$\kappa = 0.5$	$\kappa = 1.0$
0	0.9117	1.0001	1.1661
3	1.7304	1.8234	2.0003
8	2.5477	2.6427	2.8253
18	3.6578	3.7542	3.9413
28	4.4962	4.5933	4.7820
38	5.1987	5.2956	5.4860
48	5.8149	5.9125	6.1038
68	6.8821	6.9798	7.1723
88	7.8031	7.9007	8.0940
98	8.2245	8.3222	8.5157

Variation in velocity due to κ and m is shown in Figs. 7.10 and 7.11, respectively. The behavior of coefficient of skin-friction in view of the variation of m and κ follows the same as observed in the power-law shrinking case. Numerical values of the coefficient of skin-friction for various values of m and κ are listed in Table 7.3. The solution in the shrinking cylinder case can also be made to exist for $m > 0$ provided a sufficient amount of suction/injection is introduced at the cylinder's surface.

References

1. M. Miklavcic, C.Y. Wang, Viscous flow sue to a shrinking sheet. Quart. Appl. Math. **64**(2), 283–290 (2006)
2. G.K. Batchelor, *An Introduction to the Fluid Dynamics* (Cambridge University Press, Cambridge, 1967)

Chapter 8
Unsteady Flow Due to the Stretching/Shrinking Surfaces

The preceding three chapters have strictly been restricted to the cases of steady viscous flows due to the motion of continuous surfaces. The similarity criterion has been established for such flows regarding the rectangular and axisymmetric flow geometries. So far, attention has not been given to the unsteady flows of this category regarding the existence of self-similarity, in this book. The determination of the self-similarity criterion for unsteady flows follows in the same manner as has already been practiced in Chap. 5. However, just to remind, it is restated here in order to proceed the current discussion further. Mathematically, any boundary-layer flow can be self-similar provided that the number of independent variables involved can be reduced to one so that the governing partial differential equations can be reduced to ordinary ones by staying invariant under the scaling transformations utilized for this purpose. The elimination of the time variable t follows in the same manner as does the elimination of spatial "slack" variables. However, interesting situation arises, in the unsteady flows, while reducing the auxiliary data to the new variables. In all the previous problems, we had been lucky enough because the investigated problems did not contain any auxiliary data corresponding to the leaving slack variable(s). However, the unsteady problems considered in this chapter do essentially involve the initial condition at $t = 0$ or $t < 0$.

Due to the unsteady boundary-layers, the time variable t also serves as the slack variable and eventually leaves the system while constructing the new (similarity) variables. The only surviving variable is the normal space variable in these flows too. Consequently, all the original auxiliary data, either initial or the boundary conditions, have finally to be represented in the form of boundary conditions (only) defined (most probably) at the ends of the new spatial domain corresponding to the new similarity variable running across the boundary-layer. This means that the elimination of t could only be possible if either the casted initial condition can fully be represented by any one of the (transformed) boundary conditions of the system or the problem does not involve the initial condition at all. This fact necessitates the utilization of the concept of ill- or well-posedness of any initial or boundary value problem because the criterion of the self-similarity depends strongly upon it. For an

A. Mehmood, *Viscous Flows*, Mathematical Engineering,
DOI 10.1007/978-3-319-55432-7_8

ill-pose problem, there are three possibilities; (i) the problem is non-similar, (ii) the problem is self-similar and admits a unique similarity, and (iii) the problem is self-similar but admits many similarity variables. The situation is, however, limited for the well-posed problems. The well-posed problems can either be non-similar or self-similar admitting the unique similarity. The unsteady flows, having prescribed initial data, do fall into this category; thus limiting the pool of unsteady self-similarity solutions in the boundary-layer flows. The importance of the initial condition and its coalition with (at least one) boundary condition for the existence of self-similarity will be explained in the following section.

This chapter includes the case of two-dimensional and axisymmetric boundary-layer flows due to moving continuous surfaces. The corresponding self-similarity criterion has been determined and discussed in detail in Sect. 8.1. The procedure follows the same for the three-dimensional case also. Two-dimensional unsteady flow due to the stretching or shrinking sheet is discussed in Sect. 8.2 and the cases of cylinder and disk in Sect. 8.3.

8.1 Criterion of Self-similarity

8.1.1 Two-Dimensional Case

Consider the two-dimensional boundary-layer flow due to a moving continuous flat surface started impulsively at time $t = 0$. The steady case of this flow has already been considered in Sect. 5.1, and the flow schematic is shown in Fig. 5.1. The difference between the present case and that considered in Sect. 5.1 is only the impulsive start of the surface motion where other flow assumptions are the same in these two cases. In view of the above assumptions, the boundary-layer equations in this case are obtained from the system (2.10)–(2.12), by

$$\frac{\partial u}{\partial x} + \frac{\partial v}{\partial y} = 0, \tag{8.1}$$

$$\frac{\partial u}{\partial t} + u\frac{\partial u}{\partial x} + v\frac{\partial u}{\partial y} = \nu\frac{\partial^2 u}{\partial y^2}, \tag{8.2}$$

subject to the initial and boundary conditions

$$u(x, y, t) = 0, \quad \text{at } t = 0, \ \ \forall x, y, \tag{8.3}$$

and

$$\left.\begin{array}{ll} u(x, y, t > 0) = u_w(x, t), v(x, y, t > 0) = 0, & \text{at } \ y = 0 \\ u(x, y, t > 0) = 0, & \text{at } \ y = \infty \end{array}\right\}, \tag{8.4}$$

respectively. The criterion of self-similarity of the above system is determined following the same procedure as executed in Sect. 5.1 by introducing the scaling in time of the form

$$\bar{t} = k^{\alpha_0} t, \tag{8.5}$$

to the group of scalings (5.8). Consequently, the system (5.11) includes one more equation due to the term $\frac{\partial u}{\partial t}$ in Eq. (8.2) and modifies as

$$\alpha_0 + \alpha_2 - \alpha_3 = \alpha_1 + 2\alpha_2 - 2\alpha_3 = 3\alpha_2 - \alpha_3, \alpha_2 - \alpha_3 = -\alpha_4. \tag{8.6}$$

Obviously, the inclusion of a new equation to the system (5.11) will cause to further restrict the simultaneous solution of the system (5.11) which will, in turn, cause to reduce the number of self-similar solutions produced by the system (5.11). This fact is going to be confirmed in the next few steps.

Note that Eq. (8.2) involves three independent variables, which are to be reduced to one by the elimination of t and x. Since, the group consisting of Eqs. (5.8) and (8.5) involves one parameter, the elimination of t and x follows successively in two steps. The elimination of t generates two cases regarding the nonzero and zero character of α_0.

Case I $(\alpha_0 \neq 0)$
In this case the new variables are constructed as

$$\xi = xt^{-(n+1)}, \eta = yt^{-1/2}, \psi = t^{n+\frac{1}{2}} F(\xi, \eta), u_w(x,t) = t^n F_w(\xi), \tag{8.7}$$

which transform the system (8.2)–(8.4) to the form

$$n\frac{\partial F}{\partial \eta} + \left(\frac{\partial F}{\partial \eta} - (n-1)\xi\right)\frac{\partial^2 F}{\partial \xi \partial \eta} - \left(\frac{1}{2}\eta + \frac{\partial F}{\partial \xi}\right)\frac{\partial^2 F}{\partial \eta^2} = \nu \frac{\partial^3 F}{\partial \eta^3}, \tag{8.8}$$

$$\left.\begin{array}{ll} \frac{\partial F}{\partial \eta} = F_w(\xi), \frac{\partial F}{\partial \xi} = 0, & \text{at } \eta = 0 \\ \frac{\partial F}{\partial \eta} = 0, & \text{at } \eta = \infty \end{array}\right\}. \tag{8.9}$$

The definition of η given in Eq. (8.7) reflects that at $t = 0$ or $y = \infty$; $\eta = \infty$. This means that the initial condition defined in Eq. (8.3) (at $t = 0$) and the boundary condition at $y = \infty$ in Eq. (8.4) shall be represented by a single boundary condition at $\eta = \infty$. Such a restriction, arose, due to the particular form of the similarity variable η which, in fact, requires the initial condition (at $t = 0$) and the boundary condition (at $y = \infty$) to coalesce. Fortunately, the initial condition (8.3) and the boundary condition (8.4) at $y = \infty$ have the forms which allow them to coalesce. If, for example, any one of them was different from zero prohibiting them to coalesce, the similarity transformations (8.7) were not possible to construct. The impact of absence of initial condition will be discussed a bit later.

The elimination of ξ from the system (8.8) and (8.9) requires the once more utilization of one-parameter scaling group of the form

$$\bar{\xi} = k^{\beta_1}\xi, \bar{\eta} = k^{\beta_2}\eta, \bar{F} = k^{\beta_3}F, \bar{F}_w = k^{\beta_4}F_w. \tag{8.10}$$

The substitution of group (8.10) and the condition of invariance of the system (8.8)–(8.9) gives rise to the linear system of equations in $\beta_i (i = 1, \ldots, 4)$ as

$$\beta_2 - \beta_3 = \beta_1 + 2\beta_2 - 2\beta_3 = 3\beta_2 - \beta_3, \beta_2 - \beta_3 = -\beta_4. \tag{8.11}$$

Based on the elimination of ξ, two cases arise for the zero and nonzero character of β_1. Similar to Chap. 5, the successive elimination of t and x requires to organize the procedure of group-theoretic approach into the form of major cases and subcases. Thus, following the analogy of Sect. 5.2, we proceed in the same fashion.

Case I; Subcase I $(\alpha_0 \neq 0,\ \beta_1 \neq 0)$
The system (8.11) admits a non-trivial solution (for $\beta_1 \neq 0$) due to which the new variables are constructed as

$$\zeta = \eta, F = \xi f(\zeta), F_w(\xi) = a\xi, \tag{8.12}$$

which successfully eliminate the variable ξ from Eqs. (8.8) and (8.9). Consequently, Eq. (8.8) transforms to an ordinary differential equation of the form

$$(f' - 1)f' - \left(\frac{1}{2}\zeta + f\right)f'' = vf''', \tag{8.13}$$

subject to the boundary conditions

$$\left.\begin{array}{ll} f' = a,\ f = 0, & \text{at } \zeta = 0 \\ f' = 0, & \text{at } \zeta = \infty \end{array}\right\}. \tag{8.14}$$

The unified similarity transformations which transform Eqs. (8.2)–(8.4) directly to the system (8.13)–(8.14), are obtained by combining Eqs. (8.7) and (8.12) as

$$\zeta = yt^{-\frac{1}{2}}, \psi = xt^{-\frac{1}{2}}f(\zeta), u_w(x,t) = \frac{ax}{t}. \tag{8.15}$$

Case I; Subcase II $(\alpha_0 \neq 0, \beta_1 = 0)$
Consideration of the value $\beta_1 = 0$ leads to the trivial solution of the system (8.11) which denies the possibility of any new variables at all. Consequently, the self-similarity does not exist in this case.

Case II $(\alpha_0 = 0)$
The system (8.6) admits a non-trivial solution after the substitution of $\alpha_0 = 0$, due to which the new variables are constructed as

$$\xi = x\mathrm{e}^{-nt}, \eta = y, \psi = \mathrm{e}^{nt}F(\xi,\eta), u_w(x,t) = \mathrm{e}^{nt}F_w(\xi). \tag{8.16}$$

It is important to note that the above definition of η does not involve the variable t, meaning that the initial condition (8.3) is impossible to coalesce with the boundary condition (8.4) at $y = \infty$. Thus the process of reducing the variables in the system (8.1)–(8.4) with the surety of its invariance cannot be proceeded any further. However, if for instance, the initial condition (8.3) is ignored then the ongoing process may be continued provided the transformation (8.16) eliminates t from Eq. (8.2) completely. With the aid of Eq. (8.16), Eqs. (8.2) and (8.4), respectively, take the form

$$n\frac{\partial F}{\partial \eta} + \left(\frac{\partial F}{\partial \eta} - n\xi\right)\frac{\partial^2 F}{\partial \xi \partial \eta} - \frac{\partial F}{\partial \xi}\frac{\partial^2 F}{\partial \eta^2} = v\frac{\partial^3 F}{\partial \eta^3}, \tag{8.17}$$

and

$$\left.\begin{array}{ll} \frac{\partial F}{\partial \eta} = F_w(\xi), \frac{\partial F}{\partial \xi} = 0, & \text{at } \eta = 0 \\ \frac{\partial F}{\partial \eta} = 0, & \text{at } \eta = \infty \end{array}\right\}, \tag{8.18}$$

where the previous variables have completely been removed. Notice that, with the availability of the initial condition (8.3) the problem stands well-posed in time and admits only one similarity transformation as did in the previous case (case I) and no similarity in the present case at all. This is in accordance with the facts which we already have mentioned some earlier. The reduction of Eqs. (8.2) and (8.4) to the form (8.17) and (8.18), respectively, is a consequence of the ill-posed nature of the problem which has been "switched on" with the exclusion of the initial condition (8.3); in the following cases the initial condition (8.3) will continue to stay ignored.

Further elimination (of ξ) is straightforward for which the system of linear equations is the same as Eq. (8.11). Two cases are essential regarding the zero and nonzero character of β_1 here.

Case II; Subcase I $(\alpha_0 = 0, \beta_1 \neq 0)$
The assumption $\beta_1 \neq 0$ results in the construction of new variables given by

$$\zeta = \eta, F = \xi f(\zeta), F_w(\xi) = a\xi, \tag{8.19}$$

which transform the system (8.17)–(8.18) to the form

$$f'^2 - ff'' = vf''', \tag{8.20}$$

$$\left.\begin{array}{ll} f' = a, f = 0, & \text{at } \zeta = 0 \\ f' = 0, & \text{at } \zeta = \infty \end{array}\right\}, \tag{8.21}$$

by eliminating the variable ξ, completely. The case "Case II; Subcase II $(\alpha_0 = 0, \beta_1 = 0)$" is similar to the case "Case I; Subcase II" resulting in no new

variables at all. The transformations (8.16) and (8.19) can be combined to get the unified transformations of the form

$$\zeta = y, \psi = xf(\zeta), u_w(x,t) = ax, \tag{8.22}$$

which are the same as for the case of steady flow due to linear stretching or shrinking of the wall. The reason behind such an "unexpected" result, for the unsteady equation, is the removal of initial condition (8.3) from the auxiliary data (8.3)–(8.4). Thus with the presence of (8.3) the problem turns well-posed in time and admits only one similarity, namely, Eq. (8.15) ("Case I; Subcase I") or no similarity at all ("Case II").

From Eq. (8.15) it is clear that the wall velocity $u_w(x,t)$ is linear in x and does not admit the general power-law profile. This means that the self-similar solution to this case is possible if the sheet is being stretched or shrunk linearly. Other self-similar wall velocities, admitted in the steady flow, have simply been killed by the unsteady nature of the flow.

8.1.2 Axially Symmetric Case

In this category of boundary-layer flows, caused because of the stretching or shrinking of a continuous surface, the axisymmetric flow occurs in the case of cylinder or the disk. The self-similarity criterion for the two-dimensional unsteady flow near the stretching or shrinking sheet has been determined in Sect. 8.1.1 where it is seen that the similarity in time ultimately kills the spatial similarity corresponding to the nonlinear and exponential wall velocities leaving behind the linear wall law only [see for example Eq. (8.15)]. The same pattern follows in the case of axially symmetric flows, namely the cylinder or the disk cases. It will be seen that the similarity in time is only possible if the cylinder or the disk is being stretched or shrunk linearly. No self-similar solution is possible for nonlinear or exponential wall velocities in the unsteady case.

Following the procedure presented in the last section, one readily finds that the self-similar system corresponding to the stretching or shrinking cylinder having impermeable surface reads as

$$\zeta = rt^{-1/2}, u = \frac{zt^{-\frac{1}{2}}}{r} f'(\zeta), v = -\frac{1}{r} f(\zeta), \tag{8.23}$$

$$-\frac{1}{2}\left(\frac{f'}{\zeta} + f''\right) + \left(\frac{f'}{\zeta}\right)^2 - \frac{f}{\zeta}\left(\frac{f''}{\zeta} - \frac{f'}{\zeta^2}\right) = v\frac{1}{\zeta}\frac{d}{d\zeta}\left(\zeta\frac{d}{d\zeta}\left(\frac{f'}{\zeta}\right)\right), \tag{8.24}$$

subject to the boundary conditions

$$\left.\begin{array}{ll} f' = aR_0, f = 0, & \text{at } \zeta = R_0 \\ f' = 0, & \text{at } \zeta = \infty \end{array}\right\}. \tag{8.25}$$

The admitted wall velocity u_w comes out of the form

$$u_w(z,t) = \frac{az}{t}. \tag{8.26}$$

Notice that the term on right-hand side of Eq. (8.24) is the same as it is in Eq. (5.109) (for the self-similar steady flow), whereas the left-hand side of Eq. (5.109) (with the restriction $m = 1$) has been appended by the first two terms appearing in the left-hand side of Eq. (8.24). The mentioned two terms are actually the contribution of the non-steady convective term appearing in Eq. (2.14). The boundary conditions (8.25) are, however, the same as they are in the steady case for $m = 1$; see Eq. (5.110).

An interesting feature, quite particular to the cylinder case, is that the self-similarity solutions are impossible due to a stretching or shrinking cylinder of constant thickness except in the cases of linear stretching or shrinking wall velocities. In Chap. 6, it has already been seen that the nonlinear or exponential wall velocities are permissible only if the thickness of the cylinder also varies in the similar manner (that is following the power-law or exponential form) as does the wall velocity. Such a variable nature of the cylinder radius is also derived due to the self-similarity in time in the unsteady case. Interestingly, the similarity in time exists only for the linear wall velocity, when the radius stays constant spatially, but requires the time dependent swallowing of the cylinder surface in the unsteady case. In this way, the above self-similar system (8.23)–(8.26) is only valid if the cylinder radius varies in time as

$$R(z,t) = R_0 t^{1/2}. \tag{8.27}$$

The fundamental reason behind this fact is that the boundary-layer thickness varies in time $\delta \sim \sqrt{t}$ in the unsteady case of stretching/shrinking cylinder [see Eq. (8.23)]. The existence of self-similarity to this case requires the cylinder's radius also to vary in the same manner as does the boundary-layer thickness. This fact has also been identified in Chap. 6 for the respective steady flow case.

The requirement of linear wall velocity for the existence of self-similarity in time continues to persist in the case of disk flow also. The stretching or shrinking wall velocity in the case of disk comes out to be of the form

$$u_w(r,t) = \frac{ar}{t}, \tag{8.28}$$

admitting the similarity transformations

$$\zeta = zt^{-1/2}, u = rt^{-1}f'(\zeta), w = -2t^{-1/2}f(\zeta), \tag{8.29}$$

due to which Eq. (2.15) is satisfied identically and Eq. (2.16) reduces to the form

$$(f' - 1)f' - 2\left(\frac{1}{2}\zeta + f\right)f'' = vf''', \tag{8.30}$$

subject to the boundary conditions

$$\left.\begin{array}{ll} f' = a, f = 0, & \text{at } \zeta = 0 \\ f' = 0, & \text{at } \zeta = \infty \end{array}\right\}. \tag{8.31}$$

Again in this case too, the unsteady term in Eq. (2.16) has contributed the terms $-f' - \zeta f''$ on the LHS of Eq. (8.30) where the rest of the equation is that applicable to the steady flow due to linearly stretching or shrinking disk. The stretching and shrinking character, of the cylinder or the disk, is characterized by the positive and negative values of the constant a appearing in Eqs. (8.26) and (8.28), respectively.

8.2 Two-Dimensional Unsteady Self-similar Flow

8.2.1 Stretching Sheet Flow

In the previous section, it has been determined that in the case of two-dimensional unsteady flow the wall velocity must be of the form $u_w(x,t) = \frac{ax}{t}$ and the corresponding self-similar system is that given in Eqs. (8.13)–(8.14). Before solving this system, it is convenient to cast it into dimensionless form first. The procedure of non-dimensionalization exercised in Chap. 6 will be followed here. Proceeding that way, the similarity transformations (8.15) in dimensionless form read as

$$\zeta = \sqrt{\frac{\pm u_w(x,\tau)}{vx}}y, u = u_w(x,\tau)f'(\zeta), v = \pm\left[-\sqrt{\frac{\pm u_w(x,\tau)v}{x}}f(\zeta)\right], \tag{8.32}$$

and the wall velocity takes the form

$$u_w(x,\tau) = \frac{ax}{\tau}; \quad \tau = at, \tag{8.33}$$

where $a > 0$ corresponds to a linear stretching whereas $a < 0$ denotes the linear shrinking of the sheet. Accordingly, Eqs. (8.13) and (8.14) also modify as

$$(f' - (\pm 1))f' - \left(\frac{\pm\zeta}{2} + f\right)f'' = \pm f''', \tag{8.34}$$

$$\left.\begin{array}{ll} f' = 1, f = 0, & \text{at } \zeta = 0 \\ f' = 0, & \text{at } \zeta = \infty \end{array}\right\}. \tag{8.35}$$

The form adopted in Eq. (8.32) has intentionally been given in order to make the similarity transformations of the unsteady case compatible with the similarity transformation of the steady case. Furthermore, it also provides an opportunity for making an important note here. Because of Eqs. (8.1) and (8.32) is satisfied identically, and Eq. (8.2) transforms as

$$\left(\frac{t}{u_w}\frac{\partial u_w}{\partial t} + t\frac{\partial u_w}{\partial x}f'\right)f' - \frac{1}{2}\zeta f'' + \frac{t}{u_w}\left(v\frac{\partial u}{\partial y}\right) = f'''. \tag{8.36}$$

The assumption of unidirectional flow $(v = 0)$ and constant wall velocity $(u_w(x,t) = U_0)$ reduces the above Eq. (8.36) to the form

$$f''' + \frac{1}{2}\zeta f'' = 0, \tag{8.37}$$

subject to the boundary conditions [from Eq. (8.4)]

$$\left.\begin{array}{ll} f' = 1, f = 0, & \text{at } \zeta = 0 \\ f' = 0, & \text{at } \zeta = \infty \end{array}\right\}, \tag{8.38}$$

which is the famous Stokes' first problem. This shows that the current self-similar formulation is a generalization of the corresponding unidirectional flow situation which can easily be recovered from the current one. Another worth noting fact is the resemblance among the unidirectional and two-dimensional cases regarding the development of boundary-layer with respect to time. The definition of ζ in Eq. (8.32), in view of Eq. (8.33), reads as

$$\zeta = \frac{y}{\sqrt{vt}}. \tag{8.39}$$

This means that, in the two-dimensional case too, the boundary-layer thickness varies $(\delta \sim \sqrt{vt})$ in the same way as for the unidirectional case [Stokes' first problem, Eq. (3.3)].

Due to Eq. (8.32) the coefficient of skin-friction reads in this case as

$$\frac{1}{2}\sqrt{Re_x}C_f = \sqrt{\tau}f''(0), \tag{8.40}$$

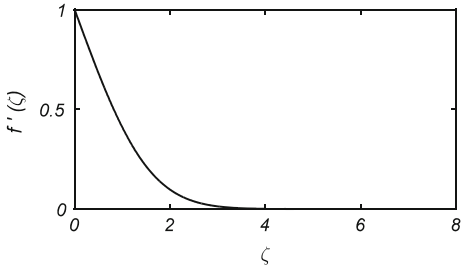

Fig. 8.1 Velocity profile for unsteady stretching sheet flow

where $Re_x = ax^2/v$ is the local Reynolds number. The velocity graph in this case is shown in Fig. 8.1, and the coefficient of skin-friction has been plotted against τ in Fig. 8.2. Clearly, the velocity dies out asymptotically, exhibiting the boundary-layer character. The penetration depth in this case is $\eta_\infty = 3.7714$, which is 72% greater than that $(\eta_\infty = 2.190)$ in the Stokes' first problem. The penetration depth has been calculated when the velocity in the boundary-layer becomes 99% of the external potential velocity. Figure 8.2 depicts that the coefficient of skin-friction intends to attain the steady state as the time increases. Qualitatively, the behavior is the same as for the unidirectional flow.

Such an unsteady self-similar flow is not new for the stretching sheet flow; rather it had already been studied by several authors since long. Devi et al. [1] considered three-dimensional unsteady flow due to a linearly stretching sheet in two lateral directions. They considered the wall velocities of the form (according to current system of coordinates)

$$u_w = ax(1 - \lambda^*\tau)^{-1}, w_w = bz(1 - \lambda^*\tau)^{-1}, \tag{8.41}$$

where λ^* is a pure constant and is commonly known as the unsteadiness parameter in literature. In such a way τ is restricted to be smaller than unity. Consequently, the constant λ^* appears as a coefficient of the linear terms on the left-hand side of Eq. (8.13). According to the running practice, the effects of the so-called unsteady parameter are usually studied on the velocity profile and the wall skin-friction. However, the factor $(1 - \lambda^*\tau)^{-1}$ appearing in Eq. (8.41) is analogous to the factor τ^{-1} appearing in Eq. (8.33). Thus the two forms can be regarded equivalent and used for further flow analysis.

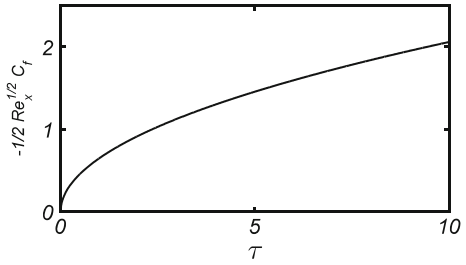

Fig. 8.2 Coefficient of skin-friction against τ for unsteady stretching sheet

8.2.2 Shrinking Sheet Flow

The system (8.34)–(8.35) governs the shrinking sheet flow if one chooses "−" sign among the "±" signs on both sides of the Eq. (8.34). By doing so the resulting system does not admit any solution at all. The reason is that, with the choice $a<0$, the wall velocity given in (8.33) represents retarded shrinking velocity (in x) due to the +ve value of the power-law index m (i.e., $m = 1$). In Chap. 7, it has already been explained that the shrinking sheet problems do admit meaningful solution only in the case of accelerated wall velocities. The existence of a physically meaningful solution in the current case is possible if the shrinking sheet is permeable and the normal wall velocity is different from zero that is $v_w(x,\tau) \neq 0$. The criterion of self-similarity determined in Sect. 8.1.1 recommends the following form of normal wall velocity

$$v_w = d\tau^{-1/2}, \tag{8.42}$$

so that the self-similarity in time persists as described in Eqs. (8.32) and (8.33). Following the dimensionless form of the similarity transformations given in Eq. (8.32), the second boundary condition at $\zeta = 0$ in Eq. (8.35) modifies as

$$\pm f(0) = -s, \tag{8.43}$$

where $s = d/\sqrt{av}$ is the dimensionless parameter representing the normal flow velocity. Notice that the positive values of d correspond to the constant wall injection, whereas the negative values of d indicate the constant wall suction as evident from Eq. (8.42).

It is observed that the system (8.34)–(8.35) after taking the condition (8.43) into consideration with the selection of "−" sign among "±" signs in the Eqs. (8.34) and (8.43) does admit a meaningful solution for sufficiently large values of $|s|$. The current analysis indicates the existence of some critical value s_c of s corresponding to which the solution exists when $s<s_c$, whereas the existence of any physical solution for $s > s_c$ is not confirmed. Staying on the safe side, the value $s = -3$ has been chosen in the light of current numerical solution. However, a rigorous mathematical analysis of this problem would reveal the correct threshold value of s. It is also observed that the second solution does also exist in this case but has not been captured intentionally. The velocity graphs in this case have been plotted in Fig. 8.3 against ζ for different values of the parameter s. It can be observed that the strong suction velocity assists the flow in following the boundary-layer behavior.

The impact of wall suction on the coefficient of wall skin-friction has also been shown in Fig. 8.4. Clearly, the skin-friction increases by increasing the magnitude of s which in turn makes the boundary-layer to stay attached with the shrinking surface, thus preventing the separation to occur. Some numerical values of $f''(0)$ corresponding to different values of the parameter s are given in Table 8.1.

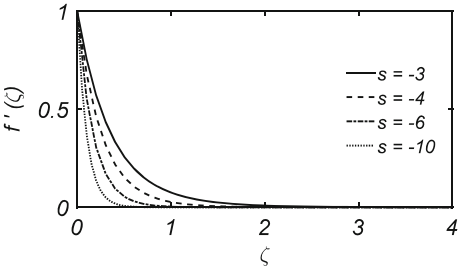

Fig. 8.3 Velocity profile for unsteady shrinking sheet case

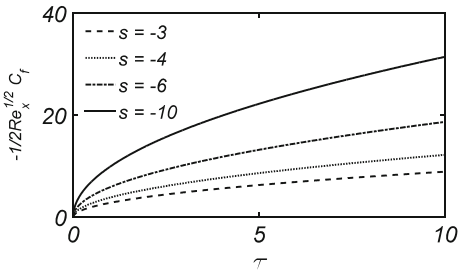

Fig. 8.4 Coefficient of skin-friction against τ for shrinking sheet flow

The form of the normal wall velocity (8.42) is also applicable to the stretching sheet flow where the "+" sign must be selected among "±" signs in Eq. (8.43).

8.3 Axially Symmetric Unsteady Self-similar Flow

The similarity criterion for the unsteady axially symmetric cases, namely the cylinder and the disk, has already been determined in Sect. 8.1. So far it has also been realized that these two axially symmetric flows do not have any thing common. However, the disk case finds great resemblance with the two-dimensional case as shown in the previous two chapters. Being different in nature, the cylinder and the disk cases are therefore analyzed separately for the unsteady case also.

8.3.1 The Cylinder Case

The corresponding self-similar system (8.24)–(8.25) in dimensionless form reads as

$$-\frac{\pm 1}{2}\left(\frac{f'}{\zeta}+f''\right)+\left(\frac{f'}{\zeta}\right)^2-\frac{f}{\zeta}\left(\frac{f''}{\zeta}-\frac{f'}{\zeta^2}\right)=\pm\frac{1}{\zeta}\frac{\mathrm{d}}{\mathrm{d}\zeta}\left(\zeta\frac{\mathrm{d}}{\mathrm{d}\zeta}\left(\frac{f'}{\zeta}\right)\right), \tag{8.44}$$

Table 8.1 Values of $-f''(0)$ for different s in the unsteady shrinking sheet flow

s		$-f''(0)$
−3		2.4115
−4		3.5930
−5		4.6846
−6		5.7414
−7		6.7804
−8		7.8090
−9		8.8309
−10		9.8482

subject to the conditions

$$\left.\begin{array}{ll} f' = Re_{R_0}, f = 0, & \text{at } \zeta = Re_{R_0} \\ f' = 0, & \text{at } \zeta = \infty \end{array}\right\}, \tag{8.45}$$

where the similarity transformations (8.23) in dimensionless form are furnished as

$$\zeta = \sqrt{\frac{\pm u_w}{\nu z}} r, u = \frac{u_w}{\zeta} f'(\zeta), v = \pm\left[-\sqrt{\frac{\pm u_w \nu}{z}} \frac{1}{\zeta} f(\zeta)\right]. \tag{8.46}$$

Similar to the steady case, presented in Sect. 6.3, the domain of interest $Re_{R_0} \leq \zeta < \infty$ can again be transformed to $[0, \infty)$ due to the transformation (6.34). The utilization of Eq. (6.34) in the system (8.44)–(8.45) transforms it to the form (after dropping the bars)

$$(f' - (\pm 1))f' - \left(\frac{\pm 1}{2\kappa}(1 + 2\kappa\zeta) + f\right) f'' = \pm[(1 + 2\kappa\zeta)f'']', \tag{8.47}$$

$$\left.\begin{array}{ll} f' = 1, f = 0, & \text{at } \zeta = 0 \\ f' = 0, & \text{at } \zeta = \infty \end{array}\right\}. \tag{8.48}$$

The steady flow equation of this case Eq. (6.35) can immediately be recovered from this system by ignoring the contribution of temporal the local acceleration on the left-hand side of Eq. (8.47).

The system (8.47)–(8.48) is solved (by considering "+" sign among "±" signs) for different values of the curvature parameter κ for which the velocity profiles have been plotted in Fig. 8.5. The small values of κ correspond to small surface curvature for which the circular cylindrical surface becomes flatter and flatter due to which the flow resembles with the planner case for sufficiently small values of κ. This fact can easily be confirmed from Fig. 8.5 where the boundary-layer thickness is not that large as is for the value $\kappa > 1$. As κ increases the boundary-layer thickness also starts to grow as a consequence of the presence of surface curvature. This, ultimately, results in a continuous decrease in the wall skin-friction. It has, however, been

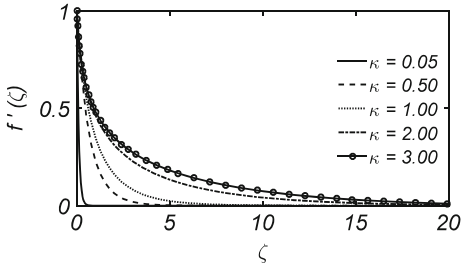

Fig. 8.5 Velocity profile of unsteady cylinder case for different κ

Table 8.2 Coefficient of skin-friction for different κ for unsteady cylinder flow

κ		$-f''(0)$
0.05		10.0990
0.10		5.1927
0.20		2.8531
0.40		1.8261
0.50		1.6563
1.00		1.4281
1.10		1.4241
1.14		1.4241
1.143		1.4242
1.15		1.4243
1.50		1.4497
2.00		1.5244
3.00		1.7167
4.00		1.9230
5.00		2.1302

observed that after certain critical value κ_c of κ the decreasing trend of values of skin-friction coefficient turns to increasing on with increasing values of κ. According to the present numerical solution, this value reads as $\kappa_c = 1.14$. The existence of multiple solutions for certain values of κ has also been observed but has not been reported here.

The coefficient of skin-friction in this case also varies (with time) in the same way as did in the previous two cases presented in the Sect. 8.2 and therefore have not been plotted here again. The values of $f''(0)$ for different values of κ are, however, listed in Table 8.2 and plotted in Fig. 8.6.

The system (8.47)–(8.48) does not allow any solution when the selection of "−" sign is made among "±" signs on the RHS of Eq. (8.47). Evidently [see Eq. (8.26)], the current wall velocity corresponds to the retarded linear shrinking case for which the solution is not possible as has already been discussed in the two-dimensional case. The solution can, however, be made to exist with the allowance of sufficient wall suction or injection at the cylinder's surface. If this is to be done, one must choose the normal wall velocity of the form

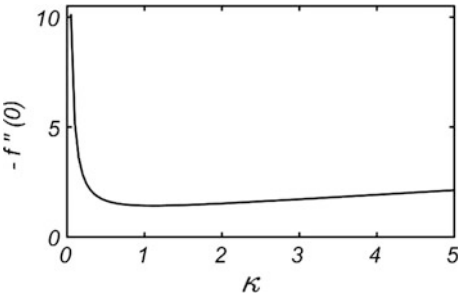

Fig. 8.6 Coefficient of skin-friction of unsteady cylinder case against κ

$$v_w(z,\tau) = d\tau^{-1/2}, \tag{8.49}$$

which in dimensionless form reads as

$$\pm f(0) = -\frac{d}{\sqrt{av}}. \tag{8.50}$$

The solution to this case has intuitionally been dropped in order to avoid the repetition of similar results.

8.3.2 The Disk Case

The dimensionless form of Eqs. (8.29)–(8.31) is given by

$$\zeta = \sqrt{\frac{\pm u_w}{vr}}z, u = u_w f'(\zeta), w = \pm\left[-2\sqrt{\frac{\pm u_w v}{r}}f(\zeta)\right], \tag{8.51}$$

$$(f' - (\pm 1))f' - 2\left(\frac{\pm 1}{2}\zeta + f\right)f'' = \pm f''', \tag{8.52}$$

and

$$\left.\begin{array}{ll} f' = 1, f = 0, & \text{at } \zeta = 0 \\ f' = 0, & \text{at } \zeta = \infty \end{array}\right\}, \tag{8.53}$$

where the wall velocity is given is Eq. (8.28) which is also of the same form as it was in all the previous cases. In the case of stretching disk, the system (8.52)–(8.53) admits a physically meaningful solution, whereas it seizes to produce any solution in the case of shrinking disk. Similar to the previous cases the solution can, however, be made to exist if the normal wall velocity is permissible. Within the framework of above self-similar system, such a normal wall velocity must be of the form

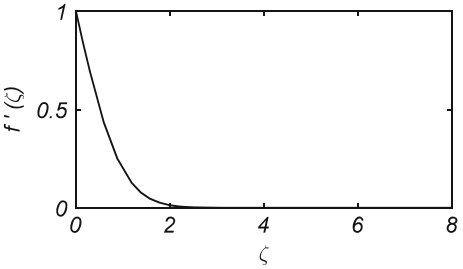

Fig. 8.7 Velocity profile for unsteady stretching disk flow

$$w_w(r,\tau) = d\tau^{-1/2}, \tag{8.54}$$

which in dimensionless form reads as

$$\pm f(0) = -\frac{d}{\sqrt{av}}. \tag{8.55}$$

The velocity graph, in the stretching case, is plotted in Fig. 8.7 for which the coefficient of skin-friction is $f''(0) = -1.0647$. The unsteady case of the stretching or shrinking disk is special in some sense which makes it unique among the family of stretching or shrinking disk flows. In the steady-state case, discussed in Chap. 6, it was finally concluded that the disk flow can directly be recovered from the steady two-dimensional flow by replacing "m" by "$3m$" in the two-dimensional solution. This conclusion fails in the unsteady case because both in the two-dimensional and in the disk flows the wall velocity follows linear law ($m = 1$ only) and does not allow for any other value of m. This prevents one from any manipulation of the constant coefficients of the equations (corresponding to the said problems) as it was possible in the steady-state case in order to recover the solution of disk case from the two-dimensional one by replacing "m" by "$3m$." In the present form the coefficients of Eqs. (8.52) and (8.34) are entirely different and are impossible to manipulate. Because of this, solution of one case cannot be recovered from the solution of the other. Therefore, different from the steady flow, the unsteady disk flow is worth investigation independent of the two-dimensional flow.

Reference

1. C.D.S. Devi, H.S. Takhar, G. Nath, Unsteady, three-dimensional, boundary-layer flow due to a stretching surface. Int. J. Heat Mass Transf. **29**(12), 1996–1999 (1986)

Part III
Non-similar Flows

Chapter 9
Two-Dimensional Non-similar Flows

In the foregoing chapters, we had strictly been limited to the self-similar flows due to moving continuous surfaces of different geometries. Despite the devoted efforts spent in the previous part, it is yet a matter of reality that the class of self-similar solutions in all the considered cases is very restricted being strictly limited to the power-law and the exponential wall velocities. In particular applications, the situations, in general, need not to follow the power-law or exponential wall velocities only. In such circumstances, the wall velocity functions are free to adopt any differentiable from other than the power-law and the exponential forms. Such classes of velocity functions are really very large in comparison with the self-similar ones and have a great potential to cover almost all the other possible wall velocities occurring in technological applications. Corresponding to all other forms of the wall velocity functions, the flow will essentially be non-similar in nature. In view of the available literature on the boundary-layers due to moving continuous surfaces, no significant efforts have so far been spent in this direction. In this regard, the current part of this book is of great importance where we intend to introduce the non-similar flows due to moving continuous surfaces. In Chaps. 9 and 10, the spatial non-similarity in the planner two-dimensional and the axially symmetric cases has been considered, respectively, whereas the temporal non-similarity is considered in Chap. 11.

9.1 Non-similar Governing Equations

The previously considered governing system (5.2)–(5.4) for the two-dimensional self-similar flows is equally applicable to the case of non-similar flows considered in this section. Different from the self-similar flows, the variable wall velocity $u_w(x)$ neither does obey the power-law nor the exponential form in this case. Such a violation of the self-similarity criterion is actually responsible for the *non-similar* designation of the current viscous flows. With this breaking of the similarity

A. Mehmood, *Viscous Flows*, Mathematical Engineering,
DOI 10.1007/978-3-319-55432-7_9

criterion, the velocity function $u_w(x)$ is free to assume any other form falling out of the scope of similarity wall velocities. Such other forms are finally charged by a partial differential equation to be solved, instead of ordinary differential equation, for the non-similar flows.

Till the third quarter of the last century, the non-similar flows had been thought to be difficult to handle because of the limited availability of high-performance computing machines. This restriction has now been elevated completely because of the availability of cheap but high-performance computing machines as a consequence of the advent of modern technology. On the other hand, the tremendous developments in the CFD have now made the solution of non-similar equations equally that easy as does the solution of *odes*.

The non-similar formulation of the governing system (5.2)–(5.4) comes directly from the self-similar formulation with the consideration that $\frac{\partial f}{\partial x} \not\equiv 0$, whereas in the self-similar flows $\frac{\partial f}{\partial x} \equiv 0$. In this way, the similarity transformations (6.5) do also work in the non-similar case but with the modified form of the stream function ψ, given by

$$\psi = \sqrt{u_w(x)\nu x} f(x, \eta), \tag{9.1}$$

where only "+" sign has been considered in the transformation (6.5) which corresponds to the stretching sheet flow only. The case of shrinking wall velocities follows, however, in the similar way and has been discarded in this discussion. Because of Eqs. (6.5) and (9.1), the governing system (5.2)–(5.4) transforms to

$$\frac{x}{u_w}\frac{\mathrm{d}u_w}{\mathrm{d}x}\left(\frac{\partial f}{\partial \eta}\right)^2 - \frac{1}{2}\left(1 + \frac{x}{u_w}\frac{\mathrm{d}u_w}{\mathrm{d}x}\right) f\frac{\partial^2 f}{\partial \eta^2} + x\left(\frac{\partial f}{\partial \eta}\frac{\partial^2 f}{\partial \eta \partial x} - \frac{\partial^2 f}{\partial \eta^2}\frac{\partial f}{\partial x}\right) = \frac{\partial^3 f}{\partial \eta^3}, \tag{9.2}$$

$$\left.\begin{array}{ll} \frac{\partial f}{\partial \eta} = 1, f = 0, & \text{at } \eta = 0 \\ \frac{\partial f}{\partial \eta} = 0, & \text{at } \eta = \infty \end{array}\right\}. \tag{9.3}$$

In this case, the coefficient of skin-friction comes out of the form

$$\frac{1}{2}\sqrt{Re_x} C_f = \left.\frac{\partial^2 f}{\partial \eta^2}\right|_{\eta=0}; \; Re_x = \frac{u_w x}{\nu}. \tag{9.4}$$

It is worth noting here that the first two terms on the left-hand side of Eq. (9.2) own the variable coefficients involving $\frac{x}{u_w}\frac{\mathrm{d}u_w}{\mathrm{d}x}$ which is a function of x, in general. However, situations do exist, for example: $u_w(x) = ax^m$, when the coefficient $\frac{x}{u_w}\frac{\mathrm{d}u_w}{\mathrm{d}x}$ becomes a pure constant. In such situations, the last two terms, involving differentiation w.r.t. x on the left-hand side of Eq. (9.2), do not contribute any more. Consequently, the *pde* turns to an *ode*, thus representing the self-similar situation. Therefore, Eq. (9.2) can also be regarded as a generalization of the self-similar

Eq. (6.4) for the stretching sheet case which certainly reduces to Eq. (6.4) when the variable coefficients become constant. Particular to the case considered in this section, the non-similarity comes due to the wall velocity only. Equation (9.2) can further be recasted in a relatively simpler form, given by

$$2\frac{\xi}{u_w}\frac{\mathrm{d}u_w}{\mathrm{d}\xi}\left(\frac{\partial f}{\partial \eta}\right)^2 - f\frac{\partial^2 f}{\partial \eta^2} + 2\xi\left(\frac{\partial f}{\partial \eta}\frac{\partial^2 f}{\partial \eta \partial \xi} - \frac{\partial^2 f}{\partial \eta^2}\frac{\partial f}{\partial \xi}\right) = \frac{\partial^3 f}{\partial \eta^3}, \tag{9.5}$$

where the utilized change of variables reads as

$$\mathrm{d}\xi = \rho^2 \nu u_w(x)\mathrm{d}x, \quad \mathrm{d}\eta = \frac{\rho u_w(x)}{\sqrt{2\xi}}\mathrm{d}y, \quad \psi(x,y) = \sqrt{2\xi} f(\xi,\eta). \tag{9.6}$$

The coefficient of skin-friction and the momentum and displacement thicknesses in terms of the variables (9.6) take the form

$$C_f = \frac{\tau_w}{\frac{1}{2}\rho u_w^2} = \mu\sqrt{\frac{2}{\xi}}\frac{\partial^2 f}{\partial \eta^2}\bigg|_{\eta=0}, \tag{9.7}$$

$$\theta = \frac{\sqrt{2\xi}}{\rho u_w}\int_0^\infty u^2 \mathrm{d}\eta, \tag{9.8}$$

and

$$\delta^* = \frac{\sqrt{2\xi}}{\rho u_w}\int_0^\infty u\,\mathrm{d}\eta, \tag{9.9}$$

respectively.

9.2 Accelerated/Decelerated Non-similar Flows

All differentiable forms of $u_w(x)$, in addition to the power-law and exponential ones, are admissible by the system (9.2)–(9.3). However, the power-law and exponential wall velocities shall not be considered here because, with these forms of the wall velocity, system (9.2)–(9.3) reduces to the self-similar form, as mentioned earlier. Even with the exclusion of self-similar wall velocities, the family of non-similar wall velocities is still too large. It is therefore impossible to mention all such forms here and hence to analyze all of them. However, as an example, the Howarth's [1] (like) wall velocity of the form

$$u_w(x) = U_0 \pm ax, \tag{9.10}$$

is considered where U_0 denotes the constant wall velocity and a is a positive constant. The "+" sign refers to the accelerated wall velocity, while the "−" sign governs the retarded wall law.

Physically, the wall velocity (9.10) is a linear combination of the translating velocity and the linear stretching or shrinking velocity corresponding to the "+" or "−" sign, respectively. Thus, the shrinking sheet flow, being retarded in nature, is vulnerable to the separation phenomena, whereas the stretching sheet flow would involve no separation at all because of accelerated nature of it. With the selection of "−" sign in Eq. (9.10), it has been calculated that the coefficient of skin-friction decreases continuously till $x^*_{sep.} = 0.42$, where it becomes zero and changes its sign further onward to $x^*_{\text{sep.}}$. This fact has been depicted in Fig. 9.1 where the velocity graph tends to attain *S*-shape with increasing values of x^* till $x^*_{\text{sep.}} = 0.42$, where the velocity graph achieves the *S*-shape and the velocity curve shows the presence of point of inflection in it. The coefficient of wall skin-friction is shown plotted against x^* in Fig. 9.2 where the function $f''(x^*)$ can be seen hitting zero at $x^*_{\text{sep.}} = 0.42$. Due to Eqs. (9.6) and (9.10), the variables x^* and ξ are related as

$$\xi = \rho^2 \nu (1 \pm a x^*) x^*, \tag{9.11}$$

where $x^* = x/L$ with L denoting suitable characteristic length in the x-direction.

The numerical values of skin-friction coefficient listed in Table 9.1 correspond to different values of x^*. In comparison with the Howarth's retarded flow [1], the separation has been delayed by 250% in the present case. The reason behind this is the increased wall skin-friction in the moving continuous sheet flows as compared to the sheets of fixed length. Therefore, the increased wall friction thus assists the boundary-layer flow to survive a quite longer in the infinite continuous wall cases in comparison with the finite wall cases.

The stretching sheet case of the current non-similar flow involves no such trouble because of its accelerating nature. Upon advancing along the moving sheet in increasing x^*-direction, the flow establishes more and more by confining itself to a narrower region near the moving continuous wall. The velocity graphs of this case

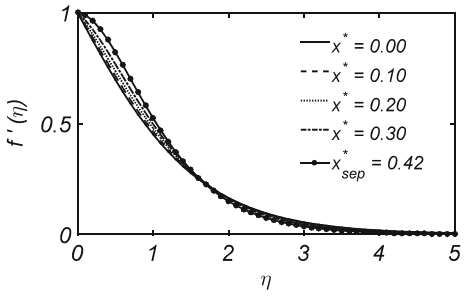

Fig. 9.1 Velocity graphs at different x^* locations

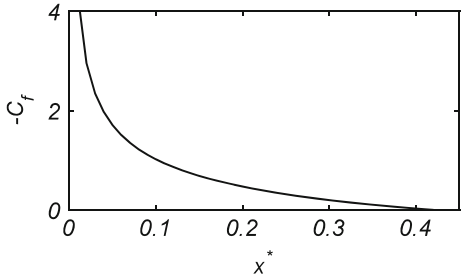

Fig. 9.2 Variation of coefficient of skin-friction while x^* approaches the separation point

Table 9.1 Dimensionless wall shear values

	$-\frac{\tau_w}{\rho U_0^2} Re_L^{1/2}$	
x^*	Shrinking case	Stretching case
0.01	4.3134	4.5644
0.05	1.7091	2.2704
0.1	1.0206	1.8139
0.15	0.6859	1.6566
0.2	0.4717	1.5912
0.25	0.3174	1.5670
0.3	0.1992	1.5653
0.35	0.1052	1.5771
0.38	0.0575	1.5886
0.40	0.0288	1.5977
0.42	0.0022	1.6078

are shown plotted in Fig. 9.3 where the velocity graphs can be seen decreasing upon increasing the values of x^*. Consequently, the coefficient of skin-friction increases as shown in Fig. 9.4 with x^*, thus avoiding the occurrence of flow separation. The numerical values of the coefficient of skin-friction have also been listed in Table 9.1 at different x^*-stations. The above-reported results have been obtained due to Eq. (9.5) subject to the boundary conditions (9.3).

For the two-dimensional and axially symmetric non-similar boundary-layer equations, the famous Keller-Box Method is the appropriate numerical tool which

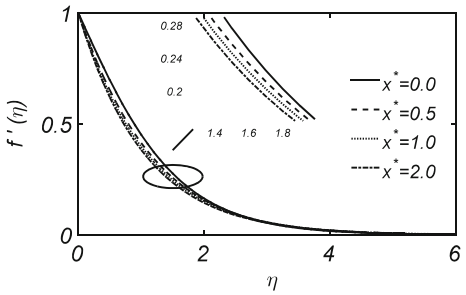

Fig. 9.3 Velocity profile for the accelerated case

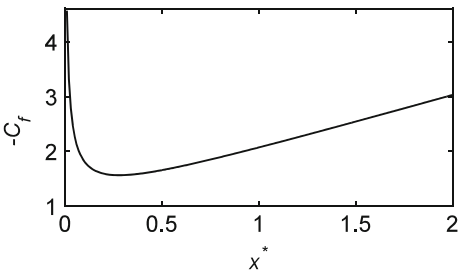

Fig. 9.4 Coefficient of skin-friction plotted against x^* (accelerated case)

Table 9.2 Accuracy of the method for Howarth's flow: dimensionless wall shear values

	$\frac{\tau_w}{\rho U_0^2} Re_L^{1/2}$	
x^*	Present method	Howarth's [1]
0.0125	2.742	2.739
0.0250	1.773	1.772
0.0375	1.310	1.309
0.0500	1.011	1.011
0.0625	0.790	0.790
0.0750	0.612	0.613
0.0875	0.458	0.459
0.1000	0.314	0.315
0.1125	0.163	0.163
0.1200	0.002	0.000

Table 9.3 Grid independence in ξ by fixing $\Delta\eta = 0.1$ and numerical infinity equal to 8.0

No. of points	$x^*_{\text{sep.}}$	$-\frac{\tau_w}{\rho U_0^2} Re_L^{1/2}$
15	0.42	0.0029
22	0.42	0.0026
43	0.42	0.0022
61	0.42	0.0022
85	0.42	0.0023
141	0.42	0.0023
422	0.421	0.0010

converges unconditionally. An introduction to this method has already been given in Sect. 4.2.2. The current solution has also been obtained because of this method. The accuracy of the utilized numerical procedure was first ensured by solving the famous Howarth's retarded flow. A comparison of the results obtained due to the current procedure with those of Howarth's [1] has been given in Table 9.2. Clearly, the current solution is in appreciable agreement with the Howarth's solution [1]. This authenticates our numerical procedure and allows for the integration of Eq. (9.5) with the aid of it. The grid independence check has also been applied to the current numerical procedure, and the results have been shown in Tables 9.3 and 9.4.

Table 9.4 Grid independence in η by taking numerical infinity equal to 8.0

	$\Delta\xi = 0.01$		$\Delta\xi = 0.001$	
No. of points	$x^*_{\text{sep.}}$	$-\frac{\tau_w}{\rho U_0^2} Re_L^{1/2}$	$x^*_{\text{sep.}}$	$-\frac{\tau_w}{\rho U_0^2} Re_L^{1/2}$
17	0.42	0.0016	0.421	0.0003
81	0.42	0.0022	0.421	0.0010
161	0.42	0.0024	0.421	0.0011
801	0.42	0.0024	0.421	0.0011

The data presented in these tables show that the current solution is independent of the grid for appropriate selection of the step sizes in ξ- and η-directions.

Normally, owing to the boundary-layer behavior, relatively big step sizes in ξ do produce the correct results, but regarding the capturing of separation point, the current analysis reveals that the dense grid provides the much better approximation in comparison with the coarse one. After several runs, the results reported in Table 9.1 were calculated by choosing $\Delta\xi = 0.01$ and $\Delta\eta = 0.1$ and taking (the numerical infinity) $\eta_\infty = 8.0$.

Reference

1. L. Howarth, On the solution of the laminar boundary layer equations. Proc. Roy. Soc. London A **164**, 547–579 (1938)

Chapter 10
Axially Symmetric Non-similar Flows

The axially symmetric non-similar flow due to a moving continuous body of revolution has relatively longer history than the self-similar flow of this type. The axisymmetric flow due to a uniformly translating cylinder of constant cross-section was first formulated by Sakiadis himself [1]. Interestingly, the equations so developed for this flow (Eqs. (10.3) and (10.4a) of [1]) did not admit a self-similar solution at all. The fundamental reason behind such an "unexpected" behavior of Eqs. (10.3) and (10.4a) of [1] can easily be identified due to Chap. 5 where the criterion of self-similarity for this case has been derived. Equation (5.108) shows that the circular cylinder must allow a variable cross-section in order to admit a similarity solution for the constant wall velocity case. That is, a cylinder of constant cross-section is unable to admit a self-similar solution if the wall velocity is kept constant. Sakiadis [2] realized this fact and obtained an approximate non-similar solution to this problem using the integral method. Thus, in the very beginning of the study of moving cylinder boundary-layers, Sakiadis had to tackle a non-similar problem in contrast to the continuous flat surface for which the Sakiadis flow admits a self-similar solution. In this way, the moving cylinder case turns out to be richer in physics as well as mathematics in comparison with the moving flat surface case.

The involvement of the transverse curvature in the governing equations of cylinder case makes the solution of these equations a bit more challenging in comparison with the equivalent non-similar equations of the moving flat surface. The boundary-layer thickness increases significantly with the increase of curvature parameter which requires a considerable time for a single run in the numerical computations. However, on the other hand, the approximate analytic solution, such as the series solution or the solution due to some integral method, has been observed to be very cheap in time and efforts, especially the integral method solution. This might be the fact because of which Sakiadis avoided the numerical and the series solution procedures and opted for the integral method in his first pioneering paper [2] on this particular flow. Amazingly, his integral method, based on the selection of appropriate velocity ansatz, though very cheap in time and efforts, produced quite good approximation to the quantities of physical interest

A. Mehmood, *Viscous Flows*, Mathematical Engineering,
DOI 10.1007/978-3-319-55432-7_10

such as the boundary-layer thickness and, the momentum and the displacement areas. Sakiadis [2] utilized a logarithmic profile (Eq. (10.5a) of [2]) in his integral method in order to make his results applicable at the downstream locations. Such a logarithmic profile was first proposed by Glauert and Lighthill [3] in the calculation of axisymmetric boundary-layers near a long slim cylinder of finite length. Sakiadis also observed that, contrary to the continuous flat surface, the quartic profile does not satisfy the surface boundary condition in the case of cylinder. However, at the leading edge where the cylinder radius $R_0 \gg \delta$ (the boundary-layer thickness), it satisfies the boundary conditions in limiting sense. Consequently, the results due to quartic profile are limited to a little leading edge neighborhood and deem un-applicable at the downstream locations where the boundary-layer thickness grows significantly and violates the restriction $R_0 \gg \delta$; in such a region, the transverse curvature effects are in fact significant.

The worth mentioning significant contributions regarding the calculation of transverse curvature effects on a cylinder of finite length are due to Seban and Bond [4], Glauert and Lighthill [3], Curle [5], Probstein and Elliot [6] and Stewartson [7]. Kelly [8] introduced important numerical corrections to the Seban and Bond's series solution valid for the interval $0.001 < (\delta/R_0)^2 < 0.04$ (where $\delta = \sqrt{\frac{\nu x}{U_\infty}}$ denotes the Blasius boundary-layer thickness). Glauert and Lighthill [3] utilized the Pohlhausen method [9] and a power-series method to extend the results of [4, 7] for significantly large values of the curvature parameter δ/R_0. Their results were further refined by Curle [5] where he computed few more terms of the approximating series. The studies on the curvature effects due to a moving continuous cylinder in the non-similar flow are due to Sakiadis [2] and Crane [10] only, to the best of our knowledge. Crane [10] revisited the Sakiadis flow [2] and concluded that the flow resembles the two-dimensional case in the vicinity of leading edge and at the far downstream locations the boundary-layer decays algebraically instead of exponentially. However, close to the cylinder's surface he confirmed the logarithmic behavior of velocity in accordance with the Glauert and Lighthill [3].

The advent of modern technology and the availability of high-performance computing machines have now made it possible to go for the numerical solution of such important and complex problems. The famous finite difference schemes have been observed to work well for the computation of such non-similar flows. Important contributions in this regard can be seen in Refs. [11–22].

10.1 Governing Equations

The similarity criterion determined in the case of cylinder (in Chap. 5) requires the variable radius of the cylinder in the cases of power-law and exponential wall velocities with an exception of the case of linear wall velocity. Thus, for a continuous slim cylinder the flow will be non-similar whenever the aforementioned criterion is not fulfilled by the wall velocity and the cylinder radius, simultaneously.

The boundary-layer equations presented in Sect. 2.1.4, corresponding to the axially symmetric case, have been derived in terms of typical system of cylindrical coordinates. In Chap. 6, it was, however, realized that such a formulation is, somewhat, inconvenient because of the description of surface boundary conditions at $y = R$ instead of $y = 0$. In order to avoid such an inconvenience, it seems, therefore, desirable to formulate the governing equations in terms of curvilinear coordinates (x, y, θ) shown in Fig. 10.1. The function $r_0(x)$[1] denotes the variable radius of the body of revolution, x stands for the curvilinear variable in the longitudinal direction starting from the stagnation point, y is the surface normal coordinate, and θ denotes the circular coordinate.

For a viscous flow coming on to the smooth axisymmetric body of revolution (shown in Fig. 10.1), the variations in the flow within the boundary-layer along the circumference are assumed to be zero. Therefore, the resulting flow is similar to two-dimensional flow in nature. The corresponding boundary-layer equations for an incompressible steady flow come out of the form (for details, the reader is referred to follow Ref. [18])

$$\frac{\partial}{\partial x}(ru) + \frac{\partial}{\partial y}(rv) = 0, \tag{10.1}$$

$$u\frac{\partial u}{\partial x} + v\frac{\partial u}{\partial y} = -\frac{1}{\rho}\frac{\partial p}{\partial x} + \nu\frac{1}{r}\frac{\partial}{\partial y}\left(r\frac{\partial u}{\partial y}\right), \tag{10.2}$$

where u and v denote the x- and y-components of the velocity vector and r is defined by

$$r(x, y) = r_0(x) + y\cos\alpha(x). \tag{10.3}$$

The absence of any potential flow will make the term $\frac{\partial p}{\partial x} = 0$. However, for the bodies involving significant transverse curvature the second component of the Navier–Stokes equations yields $\frac{1}{\rho}\frac{\partial p}{\partial y} \approx \frac{u^2}{R}$, where R is the radius of curvature; otherwise (for moderate surface curvature), it is usually taken equal to zero (i.e., $\frac{\partial p}{\partial y} \approx 0$).

Corresponding to the bodies having fixed radius $r_0(x) = \text{const.}$, the angle $\alpha = 0$ which makes $r \equiv y$ in Eq. (10.3) by aligning x with the body axis. In this case, Eqs. (10.1)–(10.2) reduce to the form

$$u\frac{\partial u}{\partial x} + v\frac{\partial u}{\partial r} = \frac{\nu}{r}\frac{\partial}{\partial r}\left(r\frac{\partial u}{\partial r}\right), \tag{10.4a}$$

[1]Particular to this formulation, the radius of the cylinder will be denoted by $r_0(x)$ from now to onwards.

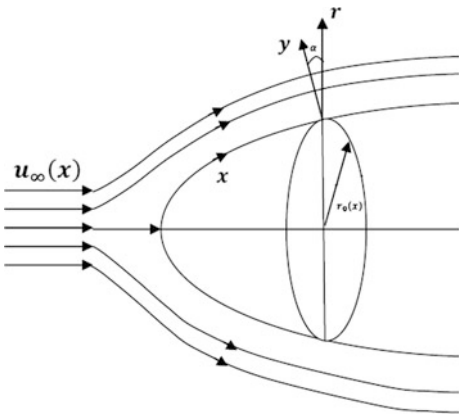

Fig. 10.1 Curvilinear system of coordinates on a body of revolution

$$\frac{\partial(ru)}{\partial x} + \frac{\partial(rv)}{\partial r} = 0, \tag{10.4b}$$

which are identical to Eqs. (2.13)–(2.14) after replacing x by z. In the cases when the body radius is significantly large, such that the previously mentioned condition is resolved that is, $\delta/r_0 \ll 1$, meaning no transverse curvature effects at all. The $r(x, y)$ then becomes independent of y in Eq. (10.3) leading to significant simplification in Eq. (10.2) by reducing it to the form

$$u\frac{\partial u}{\partial x} + v\frac{\partial u}{\partial y} = v\frac{\partial^2 u}{\partial y^2}. \tag{10.5a}$$

Accordingly, $r(x, y)$ is replaced by $r_0(x)$ (due to Eq. 10.3) in the equation of continuity (10.1) to give

$$\frac{\partial}{\partial x}(r_0 u) + \frac{\partial}{\partial x}(r_0 v) = 0. \tag{10.5b}$$

The above momentum Eq. (10.5a) for axisymmetric case is exactly the same as for the two-dimensional case or the disk case, but the continuity Eq. (10.5b) is different from that of two-dimensional case. Equations (10.4a)–(10.5a) are exactly those as utilized by Boltze [23] for the axisymmetric flows around the bodies of revolution in his dissertation. These equations apply, for example, to the cases of circular cylinder in cross-flow and circular disk, respectively. This is the reason because of which the famous Mangler's transformations (see for details [24]) transform the axisymmetric equations, involving small transverse curvature, to an equivalent system of two-dimensional form.

For small transverse curvature, when $\frac{\delta}{r_0} \ll 1$ but is also not of the order of unity, Mangler introduced the change of variables as (see for instance [24])

$$d\bar{x} = \left(\frac{r_0}{L}\right)^2 dx, \quad d\bar{y} = \frac{r_0}{L} dy, \tag{10.6}$$

where L denotes a characteristic length. Accordingly, the dependent variables were also updated but have not been mentioned here. Corresponding to the system (10.1)–(10.3), the condition for δ/r_0 to be less than unity, though not so small to be negligible, cannot be guaranteed to be fulfilled in general. That is, cases may occur when δ/r_0 might be of the order of unity, thus making the utility of Eq. (10.6) questionable. This issue was resolved by Probstein and Elliott [6] by generalizing the typical Mangler's transformations (10.6), by leaving their first part unaltered, as

$$d\bar{x} = \left(\frac{r_0}{L}\right)^2 dx, \quad d\bar{y} = \frac{r(x,y)}{L} dy, \tag{10.7}$$

due to which

$$\bar{x} = \frac{1}{L^2}\int r_0^2(x)dx \text{ and } \bar{y} = \frac{1}{L}\int r(x,y)dy = \left(\frac{r_0}{L} + \frac{\cos\alpha}{2L}y\right)y. \tag{10.8}$$

Introducing the stream functions $\psi(x,y)$ such that

$$ru = \frac{\partial\psi}{\partial y}, \quad rv = -\frac{\partial\psi}{\partial x}, \tag{10.9}$$

and utilizing the change of variables (10.7) to obtain the partial derivatives in terms of new variables as

$$\left.\begin{array}{l} \frac{\partial}{\partial x} = \left(\frac{r_0}{L}\right)^2 \frac{\partial}{\partial \bar{x}} + \frac{\partial \bar{y}}{\partial x}\frac{\partial}{\partial \bar{y}} \\ \frac{\partial}{\partial y} = \left(\frac{r}{L}\right)\frac{\partial}{\partial \bar{y}} \end{array}\right\}, \tag{10.10}$$

Equation (10.1) is satisfied identically, and the velocity components u and v transform as

$$u = \bar{u}, \quad v = \frac{r_0^2}{rL}\left(\bar{v} - \left(\frac{L}{r}\right)^2 \frac{\partial \bar{y}}{\partial x}\bar{u}\right), \tag{10.11a}$$

where

$$\frac{\partial\bar{\psi}}{\partial\bar{y}} = \bar{u} \text{ and } \frac{\partial\bar{\psi}}{\partial\bar{x}} = -\bar{v} \text{ with } \psi = L\bar{\psi}. \tag{10.11b}$$

Consequently, Eq. (10.2) transforms to the form

$$\bar{u}\frac{\partial \bar{u}}{\partial \bar{x}} + \bar{v}\frac{\partial \bar{u}}{\partial \bar{y}} = \nu \frac{\partial}{\partial \bar{y}}\left[(1+t)^2 \frac{\partial \bar{u}}{\partial \bar{y}}\right], \tag{10.12}$$

by noting that

$$\left(\frac{r}{r_0}\right)^2 = 1 + \frac{2L\cos\alpha}{r_0^2 \bar{y}}. \tag{10.13}$$

The parameter t stands for the transverse curvature parameter and is defined as

$$t = -1 + \sqrt{1 + \frac{2\cos\alpha}{L}\left(\frac{L}{r_0}\right)^2 \bar{y}}. \tag{10.14}$$

For $t = 0$, Eq. (10.12) reduces to the two-dimensional form including no transverse curvature effects. Equation (10.12) can be non-dimensionalized with the availability of appropriate reference velocity and the characteristic length. The reference length in this case is the boundary-layer thickness $\delta = \sqrt{\frac{\nu \bar{x}}{u_{\mathrm{ref}}(\bar{x})}}$, where $u_{\mathrm{ref}}(\bar{x})$ is the reference velocity. In this way, the dimensionless variables are defined as

$$\eta = \sqrt{\frac{u_{\mathrm{ref}}(\bar{x})}{\nu \bar{x}}}\bar{y}, \quad \bar{\psi} = \sqrt{u_{\mathrm{ref}}(\bar{x})\nu \bar{x}} f(\bar{x}, \eta), \tag{10.15}$$

due to which Eq. (10.12) transforms to a third-order partial differential equation with variable coefficients of the form

$$\begin{aligned} &\frac{\bar{x}}{u_{\mathrm{ref}}}\frac{\mathrm{d}u_{\mathrm{ref}}}{\mathrm{d}\bar{x}}\left(\frac{\partial f}{\partial \eta}\right)^2 - \frac{1}{2}\left(1 + \frac{\bar{x}}{u_{\mathrm{ref}}}\frac{\mathrm{d}u_{\mathrm{ref}}}{\mathrm{d}\bar{x}}\right) f\frac{\partial^2 f}{\partial \eta^2} - \frac{\partial}{\partial \eta}\left[(2+t)t\frac{\partial^2 f}{\partial \eta^2}\right] \\ &\quad = \frac{\partial^3 f}{\partial \eta^3} + \bar{x}\left(\frac{\partial f}{\partial \bar{x}}\frac{\partial^2 f}{\partial \eta^2} - \frac{\partial f}{\partial \eta}\frac{\partial^2 f}{\partial \bar{x}\partial \eta}\right). \end{aligned} \tag{10.16}$$

The non-similar Eq. (10.16) is equally applicable to the self-similar flows also, provided the variable coefficients of the terms on left-hand side become pure constants. This in turn seems to provide the criterion of self-similarity to these cases associated strictly with the simultaneous solution of the system

$$\frac{\bar{x}}{u_{\mathrm{ref}}}\frac{\mathrm{d}u_{\mathrm{ref}}}{\mathrm{d}\bar{x}} = \text{const. and } (2+t)t = \text{const.} \tag{10.17}$$

Probstein and Elliott [6] investigated the above system in detail and showed that if either $u_{\mathrm{ref}}(x) = ax^m$ and $r_0(x) = R_0 x^{\frac{1-m}{2}}$ or $u_{\mathrm{ref}} = a\mathrm{e}^{mx}$ and $r_0(x) = R_0 \mathrm{e}^{-2mx}$, the system (10.17) is satisfied identically under the restriction that $\cos\alpha \approx 1$. Thus, the allowable forms of the reference velocity and the body radius, due to Eq. (10.17),

came out of the power-law or exponential form as derived in Chap. 5. Equation (10.16) transforms to the self-similar forms

$$mf'^2 - ff'' = [(1 + 2\kappa\eta)f'']', \tag{10.18}$$

and

$$(m-1)f'^2 = [(1 + 2\kappa\eta)f'']', \tag{10.19}$$

corresponding to the power-law and exponential reference velocities, respectively. The variable η in both of the above equations has been scaled by a factor of $\frac{1}{\sqrt{2-m}}$. For all other forms of the reference velocity irrespective to the form of $r_0(x)$, the flow will be non-similar and represented by Eq. (10.16) in full. Even in the cases when the reference velocity does follow the power-law or exponential form but not the body radius, the flow will again be non-similar governed by the complete non-similar Eq. (10.16).

In the case of a disk, Eq. (10.5a) serves as the governing system with the condition $r_0 \equiv x$. In order to make it compatible with the notation used for the disk problem in the previous chapters, we decide to replace x by r; y by z and v by w in the above-named system. In this way, the governing system comes out to be

$$\frac{\partial}{\partial r}(ru) + \frac{\partial}{\partial z}(rw) = 0, \tag{10.20}$$

$$u\frac{\partial u}{\partial r} + w\frac{\partial u}{\partial z} = \nu\frac{\partial^2 u}{\partial z^2}. \tag{10.21}$$

Similar to the previous two cases, namely, the two-dimensional and the axisymmetric non-similar flows, the non-similar formulation for the disk flow also comes directly from the corresponding self-similar one. Introduction of the new variables of the form (in view of Eq. 6.40)

$$\eta = \sqrt{\frac{u_{\text{ref}}(r)}{\nu r}}z, \quad \psi = \sqrt{u_{\text{ref}}(r)\nu r}f(r,\eta), \tag{10.22}$$

transforms the momentum Eq. (10.21) to the non-similar form

$$\frac{r}{u_{\text{ref}}}\frac{\mathrm{d}u_{\text{ref}}}{\mathrm{d}r}\left(\frac{\partial f}{\partial \eta}\right)^2 - \frac{1}{2}\left(3 + \frac{r}{u_{\text{ref}}}\frac{\mathrm{d}u_{\text{ref}}}{\mathrm{d}r}\right)f\frac{\partial^2 f}{\partial \eta^2} = \frac{\partial^3 f}{\partial \eta^3} + r\left(\frac{\partial^2 f}{\partial \eta^2}\frac{\partial f}{\partial r} - \frac{\partial f}{\partial \eta}\frac{\partial^2 f}{\partial \eta \partial r}\right), \tag{10.23}$$

and satisfies the equation of continuity (10.20) identically. The stream function ψ, defined in Eq. (10.22), is related to the velocity components as

$$ru = \frac{\partial}{\partial z}(r\psi), \quad -rw = \frac{\partial}{\partial r}(r\psi). \tag{10.24}$$

10.2 The Cylinder Case

Particular to the axisymmetric boundary-layers, the problems presented in this book have been considered in view of two specific geometries, namely the cylinder and the disk, as mentioned previously. Although the curvature effects have also been studied in the self-similar flow due to the moving cylinder in Chap. 6, the important role of the curvature parameter $\delta/r_0(x)$ will be realized in the non-similar flows considered in this section. In view of curvature effects, the above-mentioned two cases of the axisymmetric flow can, however, be categorized as the axisymmetric flows with and without surface curvature, respectively. It seems fruit full to recall that the non-similarity in the case of a cylinder may arise when either of the wall velocity or the cylinder radius follows the power-law or exponential form but essentially not the other, or when both are free to adopt any other form. In such situations, the transverse curvature plays a significant role within the boundary-layer and causes to increase the boundary-layer thickness quite significantly. The study of curvature effects corresponding to all non-similar wall velocities and all cylinder shapes is, obviously, impossible to conduct as a general case here. Therefore, the problems presented in this section are just of exemplary nature. Their selection has been made by making an analogy with the corresponding non-similar flow in planner case. In these problems, the cylinder radius is kept constant $(r_0(x) = R_0)$ and the surface is assumed to move either uniformly or with accelerated/decelerated velocities.

10.2.1 Sakiadis Flow

As a first example, the classical Sakiadis problem of a moving cylinder is considered for which the flow is non-similar, as mentioned in the start of this chapter. Sakiadis [2] assumed a continuous slim cylinder of infinite length moving uniformly along its axis. Because of the absence of flow self-similarity, the governing partial differential equations with variable coefficients, as derived in previous section, do not allow for any simplification at all. Sakiadis determined an approximate solution to this problem due to the Karman–Pohlhausen integral method. Benefiting from the results reported by Glauert and Lighthill [3], Sakiadis decided to choose the logarithmic velocity profile in his integral method for the laminar case.

The integral momentum equation used by Sakiadis is given in Eq. (2.29), and the logarithmic profile utilized by Sakiadis is of the form

$$\frac{u}{u_w} = 1 - \frac{1}{\beta(z)} \ln\left(1 + \frac{r}{R_0}\right), \tag{10.25}$$

where $\beta(z)$ is an unknown function of z whose dependence upon z represents the non-similarity in the assumed velocity profile. The substitution of above velocity ansatz into Eq. (2.29) yields

$$\frac{\mathrm{d}}{\mathrm{d}z} \int_0^\beta \left[R_0 u_w \mathrm{e}^x \left(1 - \frac{x}{\beta}\right)\right]^2 \mathrm{d}x = \frac{\nu u_w}{\beta}, \tag{10.26}$$

where x is related to r by the relation $r = R_0(\mathrm{e}^x - 1)$. The simplification of Eq. (10.26) results in the form of curvature parameter $\frac{1}{4}\xi = \sqrt{\frac{\nu z}{u_w R_0^2}}$ as

$$\xi^2 = 8 \int_0^\beta \left[\beta\left(1 + \mathrm{e}^{2\beta}\right) + \left(1 - \mathrm{e}^{2\beta}\right)\right] \frac{\mathrm{d}\beta}{\beta^2}. \tag{10.27}$$

The coefficient of total drag and the displacement area come out of the form

$$\frac{L}{R_0} D = \frac{\Theta}{\pi R_0^2} \text{ and } \frac{\bar{\delta}^*}{\pi R_0^2} = \frac{1}{\pi R_0^2} \int_0^\infty \frac{u}{u_w} 2\pi(R_0 + r)\mathrm{d}r = -\frac{1}{2\beta}\left(1 + 2\beta - \mathrm{e}^{2\beta}\right), \tag{10.28}$$

where D denotes the total drag and $\Theta/\pi R_0^2$ denotes the dimensionless momentum area, defined by

$$\frac{\Theta}{\pi R_0^2} = \frac{1}{\pi R_0^2} \int_0^\infty \left(\frac{u}{u_w}\right)^2 2\pi(R_0 + r)\mathrm{d}r = -\frac{1}{2\beta}\left(2(1 + \beta) + \frac{1 - \mathrm{e}^{2\beta}}{\beta}\right). \tag{10.29}$$

Once the values of β are obtained by integrating Eq. (10.27), it is then straight forward to calculate the momentum area, the coefficient of total drag and the displacement area from the above equations. Based on this integral method, Sakiadis generated a table of values of the quantities of physical interest such as the boundary-layer thickness and the momentum and displacement areas for sufficiently large values of the curvature parameter ξ. It was observed that all the three quantities increase by increasing the surface curvature parameter. An important observation, particular to the cylinder case, is that all the three quantities decrease (in magnitude) for small values of ξ and after a critical value of ξ, they start to increase continuously. In such a course of analysis, the momentum area is observed to have the lowest of the minimum, whereas the displacement area achieves the greatest of the maximum values among the three quantities. The values reported by Sakiadis

Table 10.1 Sakiadis' integral solution

$\log(\xi)$	$\log(\Theta/\pi R_0^2)$	$\log(\bar{\delta}^*/\pi R_0^2)$	$\log(\delta/R_0)$
−3.0880	−3.4770	−3.3009	−3.3009
−2.7869	−3.1759	−2.9997	−2.9998
−2.0873	−2.4760	−2.2996	−2.2999
−1.7856	−2.1739	−1.9971	−1.9978
−1.0807	−1.4662	−1.2864	−1.2901
−0.7724	−1.1540	−0.9706	−0.9781
−0.0113	−0.3599	−0.1437	−0.1879
0.3757	0.0774	0.3413	0.2351
0.8781	0.7160	1.0934	0.8054
1.2945	1.3226	1.8200	1.2807
1.6939	1.9632	2.5700	1.7291
2.0926	2.6428	3.3428	2.1685
2.4941	3.3539	4.1342	2.6047
2.8933	4.0888	4.9340	3.0397
3.3076	4.8415	5.7446	3.4742
3.7184	5.6078	6.5621	3.9086
4.1325	6.3849	7.3849	4.3429

for the said three quantities have been listed in Table 10.1 for several values of the curvature parameter ξ.

The curvature effects can best be visualized if the present results are compared with those of the flat plate case. In this regard, the ratios of the physical quantities of interest corresponding to the present case with those of the flat plate case are found to be use full.

Such ratios have, respectively, been determined for the drag coefficient, the pumping action and the boundary-layer thickness defined as

$$\frac{D}{D_f} = \frac{2\left(\Theta/\pi R_0^2\right)}{C_\Theta \xi}, \frac{q}{q_f} = \frac{2\left(\bar{\delta}^*/\pi R_0^2\right)}{C_{\bar{\delta}^*}\xi}, \frac{\delta}{\delta_f} = \frac{4(\delta/R_0)}{C_\delta \xi},$$

where the quantities in the numerator correspond to the continuous cylinder whereas those in the denominator and subscripted by "f" correspond to the continuous flat plate.

The values of the ratios have been calculated due to Table 10.1 and are listed in Table 10.2. For smaller values of ξ, all the ratios yield 1.0 and for increasing values of ξ the ratios cross the value 1.0 and depart further on wards. This shows that for smaller values of ξ, when the surface curvature is small, the cylinder case resembles with the two-dimensional case. But for significantly large values of ξ, the above quantities of interest are greater in the cylinder case as compared to the flat plate case. The Sakiadis flow due to a moving cylinder can also be dealt numerically because of the availability of efficient numerical methods and the high-performance computing machines.

Table 10.2 Ratios of the quantities of interest: cylinder case to flat plate case

$\log(\xi)$	D/D_f	q/q_f	δ/δ_f
−3.0880	1.000	1.000	1.000
−2.7869	1.000	1.000	1.000
−2.0873	1.001	1.001	1.001
−1.7856	1.002	1.002	1.002
−1.0807	1.008	1.0017	1.008
−0.7724	1.017	1.034	1.017
−0.0113	1.097	1.204	1.087
0.3757	1.232	1.508	1.181
0.8781	1.686	2.681	1.381
1.2945	2.613	5.475	1.582
1.6939	4.553	12.27	1.771
2.0926	8.693	29.05	1.945
2.4941	17.73	71.28	2.106
2.8933	37.89	176.8	2.256
3.3076	88.73	446.6	2.397
3.7184	189.8	1139.4	2.530
4.1325	437.9	2919.5	2.651

The non-similar formulation of the cylinder case has already been derived in Eqs. (10.15)–(10.16). However, analogous to the flat plate case, the non-similar formulation of the cylinder case can also be obtained due to the similarity transformations (Eq. 6.31) by assuming the dimensionless stream function also depending upon z in addition to the variable r. Various equivalent transformations, in this regard, are available in the literature among which any one can be replaced by the other without any mathematical error. The transformations developed by Probstein and Elliott [6] and Hayes and Probstein [25] as reported by Cebeci and Smith [17] based upon the typical Mangler transformation are, however, the more general and mathematically compact. Therefore, the author is more inclined toward those developed by Cebeci and Smith [17]. However, particular to the Sakiadis flow, the formulations developed by Seban and Bond [4] and Curle [5] shall be utilized in order to make the reader familiar with these too. Afterward, in the next part of this section, corresponding to accelerated/decelerated flows, the aforementioned formulation due to [6, 25] and [17] will be utilized. Based on [4], Curle [5] utilized the following change of variables

$$\xi = \sqrt{\frac{2\nu z}{u_w R_0}}, \quad \eta = \sqrt{\frac{u_w}{2\nu z}} \frac{r^2 - R_0^2}{2R_0} \tag{10.30}$$

The velocity components in terms of stream function are given as

$$ru = \frac{\partial \psi}{\partial r}, \quad rv = -\frac{\partial \psi}{\partial z}, \tag{10.31}$$

where the stream function is defined as

$$\psi = \sqrt{2u_w v z} R_0 f(\xi, \eta). \tag{10.32}$$

It is important to mention here that the formulation developed by [6, 25] and hence [17] utilizes the curvilinear coordinates defined in Fig. 10.1, whereas the transformations (10.30) utilized by Seban & Bond and Curle are particular to the typical cylindrical system of coordinates. Because of Eqs. (10.30)–(10.32), Eq. (2.13) is satisfied identically, whereas Eq. (2.14) transforms to the non-similar form, given by

$$0\left(\frac{\partial f}{\partial \eta}\right)^2 - f\frac{\partial^2 f}{\partial \eta^2} = \frac{\partial}{\partial \eta}\left((1+2\xi\eta)\frac{\partial^2 f}{\partial \eta^2}\right) + \xi\left(\frac{\partial^2 f}{\partial \eta^2}\frac{\partial f}{\partial \xi} - \frac{\partial f}{\partial \eta}\frac{\partial^2 f}{\partial \eta \partial \xi}\right). \tag{10.33}$$

The boundary conditions (2.27) with $v_w \equiv 0$ transform in terms of new variables as

$$\left.\begin{array}{ll} \frac{\partial f}{\partial \eta} = 1, f = 0, & \text{at } \eta = 0 \\ \frac{\partial f}{\partial \eta} = 0, & \text{at } \eta = \infty \end{array}\right\}. \tag{10.34}$$

Important quantities of physical interest such as the coefficient of wall skin-friction, the momentum and displacement areas are defined as

$$C_f = \frac{\tau_w}{\frac{1}{2}\rho u_w^2} = \sqrt{\frac{2v}{u_w z}}\frac{\partial^2 f}{\partial \eta^2}\bigg|_{\eta=0}, \tag{10.35}$$

$$\frac{\Theta}{\pi R_0^2} = \frac{1}{\pi R_0^2}\int_{R_0}^{\infty}\left(\frac{u}{u_w}\right)^2 2\pi r \mathrm{d}r = 2\xi\int_0^{\infty} f'^2 d\eta, \tag{10.36}$$

and

$$\frac{\bar{\delta}^*}{\pi R_0^2} = \frac{1}{\pi R_0^2}\int_{R_0}^{\infty}\frac{u}{u_w} 2\pi r \mathrm{d}r = 2\xi f(\infty), \tag{10.37}$$

respectively.

The system (10.33)–(10.34) has been solved numerically with the use of famous Keller-Box finite difference scheme. The current solution is tabulated in Table 10.3 and is compared with the Sakiadis' integral solution in Fig. 10.2. Clearly, the integral solution matches quite well with the current numerical solution for small

Table 10.3 Numerical solution of Sakiadis flow

$\log(\xi)$	$\log(\Theta/\pi R_0^2)$	$\log(\bar{\delta}^*/\pi R_0^2)$	$\log(\delta/R_0)$
−3.5229	−3.4235	−3.1634	−3.6734
−3.2218	−3.1224	−2.8622	−3.3724
−2.5376	−2.4379	−2.1770	−2.6881
−2.2366	−2.1365	−1.8748	−2.3871
−1.5317	−1.4288	−1.1603	−1.6822
−1.2240	−1.1176	−0.8406	−1.3745
−0.4628	−0.3225	0.0265	−0.6133
−0.0758	0.1137	0.5488	−0.2263
0.4266	0.7442	1.3258	0.2760
0.8430	1.3155	1.9701	0.6924
1.2424	1.9075	2.6328	1.0918
1.6411	2.5095	3.2810	1.4902
2.0426	3.3371	4.3494	1.8902
2.3432	4.0370	5.0496	2.2972
2.8561	4.7662	5.8195	2.7055
3.2669	5.5224	6.6501	3.1164
3.6810	6.2929	7.5238	3.5304

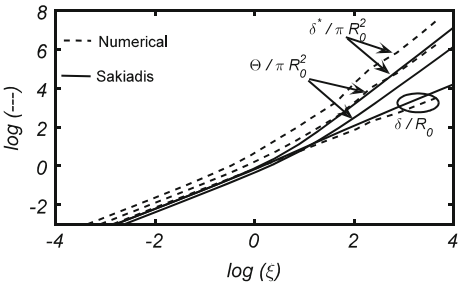

Fig. 10.2 Comparison between the numerical solution and the Sakiadis' integral solution

values of ξ and deviates downstream from the numerical solution. Qualitatively, the Sakiadis' solution is in accordance with the present numerical solution. However, the difference between the two solutions is not quite large which does not deny the acceptability of the Sakiadis' solution. For such a quite acceptable (approximate) solution, the credit not only goes to Sakiadis alone but also to the Glauert and Lighthill who identified the logarithmic profile for the cylinder case. This reflects that the velocity profile utilized by Sakiadis, the logarithmic one, proved itself to be the appropriate choice for this case. The graphs of the velocity profile are plotted against η for different values of the curvature parameter ξ and are shown in Fig. 10.3. Upon increasing the values of ξ, the velocity curves become steep and steep showing large velocity gradients near the solid surface and extend till far away from the cylinder causing to increase the boundary-layer thickness, significantly.

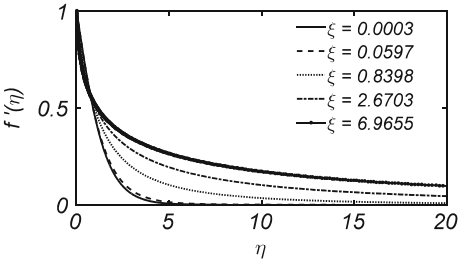

Fig. 10.3 Velocity profile obtained due to numerical solution of Sakiadis flow

10.2.2 Accelerated/Decelerated Flow

The accelerated/decelerated nature of the wall velocity does characterize the accelerated/decelerated nature of the flow within the boundary-layer. Such types of wall velocities are not governed by a unique mathematical function but are diverse in actual. Therefore, we shall restrict our self to the form represented in a linear combination of uniform translation and uniform stretching/shrinking as given in Eq. (9.10). The accelerated/decelerated character of the wall velocity will be distinguished by the selection of "+" or "−" sign as did in the previous chapter. Similar to the Sakiadis' non-similar flow, the accelerated/decelerated non-similar flow can equally be studied due to Eq. (10.16) or following the formulation (10.30)–(10.33). Accordingly, the variable coefficients of Eq. (10.33) shall be modified and the 0 coefficient of the first term on LHS of Eq. (10.33) will turn out to be nonzero of the form $\frac{\xi}{u_w}\frac{\mathrm{d}u_w}{\mathrm{d}\xi}$. These "modified" variable coefficients actually incorporate the role of variable wall velocity into the governing system.

This has already been mentioned, in the previous part of this section, that the non-similar formulation due to [6, 25] and [17] will be utilized in the study of non-similar flow due to accelerated/decelerated wall velocities. It has already been seen that the transformations (10.30) are typical to the equations developed in terms of conventional cylindrical system of coordinates where the surface boundary conditions are defined at $r = R$ instead of $r = 0$. To avoid this deficiency and to incorporate the transverse curvature effects more conveniently, the curvilinear system of coordinates is introduced in Sect. 10.1 to reach Eq. (10.16). Further niceties to the formulation developed in Sect. 10.1 were contributed by Cebeci and Smith [17] due to which the definitions of ξ, η and ψ are modified as

$$\mathrm{d}\xi = \rho^2 \nu u_w \left(\frac{r_0}{L}\right)^2 \mathrm{d}x, \quad \mathrm{d}\eta = \frac{\rho u_w r}{\sqrt{2\xi}L}\mathrm{d}y, \quad \psi(x,y) = \sqrt{2\xi}Lf(\xi,\eta), \tag{10.38}$$

where the velocity components are related to ψ as

$$r\rho u = \frac{\partial \psi}{\partial y}, \quad r\rho v = -\frac{\partial \psi}{\partial y}. \tag{10.39}$$

In view of Eqs. (10.38)–(10.39), the equation of continuity (10.1) satisfies identically and Eq. (10.2) results in the following non-similar equation:

$$\frac{2\xi}{u_w}\frac{\mathrm{d}u_w}{\mathrm{d}\xi}\left(\frac{\partial f}{\partial \eta}\right)^2 - f\frac{\partial^2 f}{\partial \eta^2} = \frac{\partial}{\partial \eta}\left((1+\Lambda\eta)\frac{\partial^2 f}{\partial \eta^2}\right) + 2\xi\left(\frac{\partial^2 f}{\partial \eta^2}\frac{\partial f}{\partial \xi} - \frac{\partial f}{\partial \eta}\frac{\partial^2 f}{\partial \eta \partial \xi}\right), \tag{10.40}$$

where $\Lambda = \frac{2L}{R_0}\frac{\sqrt{2\xi}}{\rho u_w} = 2\sqrt{\frac{2\kappa\bar{\xi}}{\bar{u}_w^2}}$; $\mathrm{d}\bar{\xi} = \bar{u}_w \mathrm{d}x^*$, and $x^* = \frac{ax}{U_0}$. Equation (10.40) includes all the terms of Eq. (10.33) with modified coefficients where the first term on the LHS of Eq. (10.40) was zero in Eq. (10.33) due to the constant wall velocity. Such a great resemblance between Eqs. (10.33) and (10.40), obtained due to the different formulations, actually proves the equivalence of the two formulations. Therefore, the results due to one formulation can easily be shifted to the other one in view of Eqs. (10.3), (10.32) and (10.38). In the subsequent analysis, we substitute $\bar{u}_w = 1 \pm x^*$ where κ has been chosen to be equal to 0.25. The "+" and "−" signs in the expression of $\bar{u}_w$ refer, respectively, to the accelerated and decelerated cases. The boundary conditions in dimensionless form for this case are the same as given in Eq. (10.34). The physical quantities of interest such as the coefficient of wall skin-friction, the momentum and displacement thicknesses in terms of the new variables read as

$$C_f = \frac{\tau_w}{\frac{1}{2}\rho u_w^2} = \mu\sqrt{\frac{2R_0^2}{\xi L^2}\frac{\partial^2 f}{\partial \eta^2}}\bigg|_{\eta=0}, \tag{10.41}$$

$$\theta = \frac{\sqrt{2\xi L^2}}{\rho R_0 u_w}\int_0^\infty u^2 \mathrm{d}\eta, \tag{10.42}$$

and

$$\delta^* = \frac{\sqrt{2\xi L^2}}{\rho R_0 u_w}\int_0^\infty u \mathrm{d}\eta, \tag{10.43}$$

respectively.

The system (10.40) and (10.34) has also been solved numerically through Keller-Box method. The graphical results are shown in Figs. 10.4, 10.5, 10.6 and 10.7. For the accelerated case, the flow behavior is similar to the corresponding flat plate case in the sense that no separation occurs. In this case too, velocity graphs become steeper near the cylinder surface and extend far away from the cylinder upon moving in the downstream direction, thus confirming the significant increase

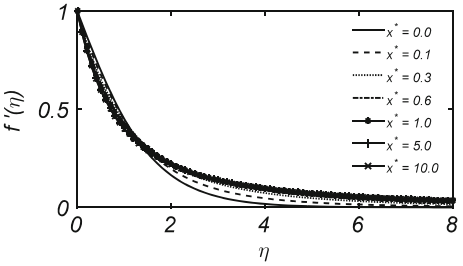

Fig. 10.4 Accelerated velocity profile at different longitudinal locations

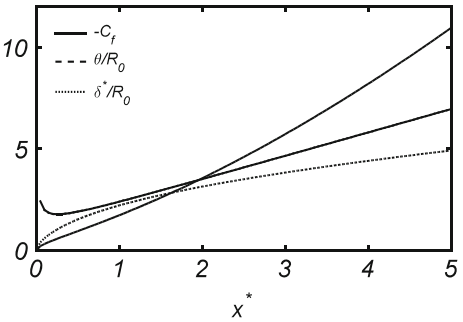

Fig. 10.5 Numerical results for quantities of interest plotted against x^*

in the boundary-layer thickness (see Fig. 10.4). The coefficient of skin-friction, corresponding to the accelerated case, is also plotted against the variable x^* and depicted in Fig. 10.5. Clearly, the skin-friction first decreases for very small values of x^* and at a certain critical value of x^* it seizes to decrease and start increasing monotonically, afterward. The graphs of the momentum and displacement thicknesses are plotted in Fig. 10.5. Both the thicknesses grow as one moves in the downstream direction along the cylinder. Numerical values of the coefficient of skin-friction, momentum and displacement thicknesses have also been generated at various longitudinal locations and are listed in Table 10.4.

The case of retarded flow due to a moving cylinder is also similar to that of corresponding moving plate in the sense that it also involves the flow separation. The point of separation is noted to be $x^*_{\text{sep}} = 0.495$ where the value $f''(x^*, 0)$ becomes of the order 10^{-3}. The numerical code, however, does not seize to producing results, and the solution does converge till the values of x^* grow almost up to the order of unity. The velocity profile is shown to be separated at the value $x^*_{\text{sep}} = 0.495$ by plotting the velocity curves at different values of the variable x^* as shown in Fig. 10.6. The coefficient of skin-friction is plotted in Fig. 10.7 which shows that the skin-friction decreases continuously and eventually becomes zero at $x^*_{\text{sep}} = 0.495$ which is, in fact, the point of separation. The graphs of the momentum and displacement thicknesses are also plotted in Fig. 10.7. In this case too, both the thicknesses increase in the downstream direction, but the rate of increase in this case is quite less than that of the accelerated case, depicted in Fig. 10.5. The

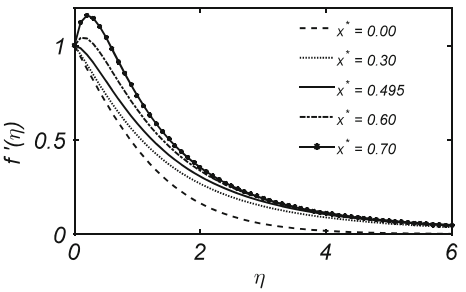

Fig. 10.6 Velocity profile of the retarded case exhibiting the flow separation at $x^* = 0.495$

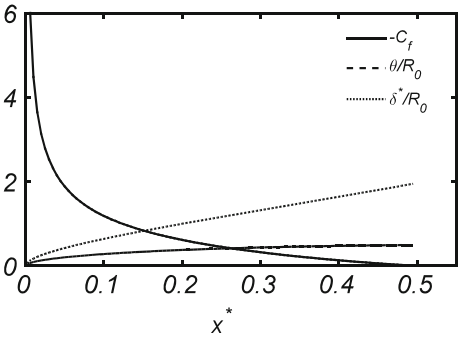

Fig. 10.7 Physical quantities of interest plotted against x^*

Table 10.4 Numerical results for the accelerated and decelerated cases

x^*	$\bar{u}_w = 1 - x^*$			$\bar{u}_w = 1 + x^*$		
	$-\frac{\tau_w}{\rho U_0^2} \mathrm{Re}_{R_0}^{1/2}$	θ	δ^*	$-\frac{\tau_w}{\rho U_0^2} \mathrm{Re}_{R_0}^{1/2}$	θ	δ^*
0.01	4.4803	0.0894	0.1708	4.7355	0.0906	0.1704
0.02	3.1386	0.1268	0.2502	3.5018	0.1303	0.2488
0.05	1.8820	0.2000	0.4212	2.4628	0.2140	0.4145
0.1	1.1832	0.2784	0.6373	2.0151	0.3183	0.6149
0.2	0.6135	0.3761	0.9749	1.8095	0.4899	0.9148
0.3	0.3205	0.4358	1.3111	1.7995	0.6942	1.2742
0.4	0.1296	0.4735	1.6362	1.8010	0.6459	1.1517
0.45	0.0566	0.4861	1.7973	1.8510	0.7975	1.3528
0.48	0.0182	0.4920	1.8956	1.9100	0.9184	1.4958
0.49	0.0062	0.4937	1.9287	1.9182	0.9336	1.5127
0.495	0.0004	0.4945	1.9415	1.9223	0.9412	1.5211
1.00				2.4273	1.7419	2.3491
2.00				3.5596	3.6177	3.4218
3.00				4.7216	5.8476	4.2155
4.00				5.8909	8.3935	4.3869
5.00				7.0628	11.223	5.4491

numerical values of the coefficient of skin-friction and the two thicknesses are also listed in Table 10.4.

10.3 The Disk Case

The axially symmetric viscous flow involving no transverse curvature effects is governed by Eq. (10.5a), in terms of curvilinear coordinates. Equations (2.15)–(2.16) for the steady case, developed in conventional cylindrical system of coordinates, can immediately be recovered from Eq. (10.5a) and are given in Eqs. (10.20)–(10.21). As pointed out in the previous section, that Eq. (10.21) is exactly the same as that of two-dimensional flow and the disk case differs only in equation of continuity from the two-dimensional flow. Furthermore, while studying the self-similar disk flow in Chaps. 6 and 7, it has already been discovered that the stretching/shrinking disk flow needs not to be studied separately, rather the results of this case can immediately be recovered from those of two-dimensional case with certain manipulation in the values of m. This fact can also be realized here again that the non-similar flow due to a stretching or shrinking disk is governed by the same equation as does the two-dimensional flow but with certain modification in the coefficients of the equation. Such a modification in the variable coefficients does also find some analogy with the corresponding self-similar two-dimensional and disk flows and can be identified by comparing the governing equation of self-similar and non-similar cases of two-dimensional and disk flows. The non-similar equation in the disk case reads as

$$\frac{r}{u_w}\frac{\mathrm{d}u_w}{\mathrm{d}r}\left(\frac{\partial f}{\partial \eta}\right)^2 - \frac{1}{2}\left(3 + \frac{r}{u_w}\frac{\mathrm{d}u_w}{\mathrm{d}r}\right) f\frac{\partial^2 f}{\partial \eta^2} = \frac{\partial^3 f}{\partial \eta^3} + r\left(\frac{\partial^2 f}{\partial \eta^2}\frac{\partial f}{\partial r} - \frac{\partial f}{\partial \eta}\frac{\partial^2 f}{\partial r \partial \eta}\right). \quad (10.44)$$

The boundary conditions, however, stay the same as given in Eq. (9.3) or (10.34). The variables used in the above equation do also come directly from the similarity transformations of the respective flow, given by

$$\eta = \sqrt{\frac{u_w}{\nu r}}z, \quad \psi = \sqrt{u_w \nu r} f(r, \eta), \quad (10.45)$$

where the velocity functions are related to the stream function by the relations defined in Eq. (10.24).

All the wall velocities other than the self-similar one can be considered in this case. The accelerated/decelerated wall velocities considered in the previous sections (but not limited to those) can also be utilized here. Because of the great similarity of the disk flow with that of two-dimensional flow, Eq. (10.44) has not been solved for any case here, just to avoid the repetition of similar results.

References

1. B.C. Sakiadis, Boundary-layer behavior on continuous solid surface: I. Boundary-layer equations for two-dimensional and axisymmetric flow. AIChE **7**(1), 26–28 (1961)
2. B.C. Sakiadis, Boundary-layer behavior on continuous solid surfaces: III. The boundary-layer on a continuous cylindrical surface. AIChE **7**(3), 467–472 (1961)
3. M.B. Glauert, M.J. Lighthill, The axisymmetric boundary layer on a long thin cylinder. Proc. R. Soc. Lond. A **230**, 188–203 (1955)
4. R.A. Seban, R. Bond, Skin-friction and heat-transfer characteristics of a laminar boundary layer on a cylinder in axial incompressible flow. J. Aeronuat. Sci. **18**, 671 (1951)
5. S.N. Curle, Calculation of the axisymmetric boundary layer on a long thin cylinder. Proc. R. Soc. Lond. A, Math. Phys. Sci. **372**(1751), 555–564 (1980)
6. R.F. Probstein, D. Elliott, The transverse curvature effect in compressible axially symmetric laminar boundary-layer flow. J. Aeronaut. Sci. **23**, 208–224 (1956)
7. K. Stewartson, The asymptotic boundary layer on a circular cylinder in axial incompressible flow. Q. Appl. Math. **3**, 113–122 (1955)
8. H.R. Kelly, A note on the laminar boundary layer on a circular cylinder in axial incompressible flow. J. Aeronaut. Sci. **21**, 643 (1954)
9. K. Pohlhausen, Zur näherungsweisen Integration der Differentialgleichung der laminaren Reibungsschicht. ZAMM **1**, 252–268 (1921)
10. L.J. Crane, Boundary layer flow on a circular cylinder moving in a fluid at a rest. ZAMP **23**, 201–212 (1972)
11. T.Y. Na, *Computational Methods in Engineering Boundary Value Problems* (Academic Press, 1979)
12. H.B. Keller, in *A New Difference Scheme for Parabolic Problems*, ed. by J. Bramble. Numerical Solution of Partial Differential Equations, II (Academic Press, New York, 1970)
13. H.B. Keller, T. Cebeci, Accurate numerical methods for boundary-layer flows-I. Two-dimensional laminar flows. AIAA J. **10**, 1193 (1971)
14. H.B. Keller, T. Cebeci, Accurate numerical methods for boundary-layer flows-II. Two-dimensional turbulent flows. AIAA J. **10**, 1193 (1972)
15. T. Cebeci, H.B. Keller, in *On the Computation of Unsteady Boundary Layers*. Recent Research on Unsteady Boundary Layers (IUTAM Symp. 1971), vol. I (Les Presses de I' Universitė Laval, Quebee, Canada), p. 1082
16. T. Cebeci, H.B. Keller, in *Laminar Boundary Layers with Assigned wall Shear*. Proceedings of International Conference on Numerical Methods Fluid Dynamics, 3rd edn. Lecture Notes in Physics, vol. 19 (Springer-Verlag, Berlin and New York, 1973)
17. T. Cebeci, A.M.O. Smith, *Analysis of Turbulent Boundary Layers* (Academic Press Inc. 1974)
18. T. Cebeci, P. Bradshaw, *Momentum Transfer in Boundary Layers* (Hempshere Publishing Company, 1977)
19. M.N. Bui, T. Cebeci, Combined free and forced convection on vertical slender cylinders. J. Heat Transf.-Trans. ASME **107**, 476–478 (1985)
20. T. Cebeci, J. Qasim, Free convective heat transfer from slender cylinders subject to uniform heat flux. Lett. Heat Mass Transf. **1**, 159–162 (1974)
21. T.Y. Na, I. Pop, Flow and heat transfer over a longitudinal circular cylinder moving in parallel or reversely to a free stream. Acta Mech. **118**, 185–195 (1996)
22. H.T. Lin, Y.P. Shih, Laminar boundary layer heat transfer along static and moving cylinders. J. Chin. Int. Eng. **3**, 73–79 (1980)
23. E. Boltze, Grenzschichten an Rotationskörpern. Diss. Göttingen, 1908
24. P.H. Denke, in *A matric Method of Structural Analysis*. The Proceedings of the Second U.S. National Congress of Applied Mechanics, 1952
25. W.D. Hayes, R.F. Probstein, *Hypersonic Flow Theory* (Academic Press, New York, 1959)

Chapter 11
Time-Dependent Non-similarity

In the previous Part, it has already been seen that the concept of *similarity* is not particular to the space variables only but is also equally applicable to the time variable. Owing to the physical and mathematical meanings of similarity, the criterion of self-similarity in time for stretching/shrinking surfaces has been derived in Chap. 8. Interestingly, the spectrum of self-similar unsteady flows due to the stretching or shrinking surfaces is very limited which in turn signifies the diversity of the non-similar flows to the unsteady case. Even being a very restricted family, the self-similar unsteady flows have widely been studied in the literature, whereas the non-similar unsteady flows have not been investigated on such a large scale. The reason behind this is again the nature of governing non-similar equations which are in fact the partial differential equations as they usually are in the case of spatial non-similarity. It is, however, a matter of fact that the temporal non-similarity does not pose a severe challenge as does the spatial non-similarity. In most of the cases, it is too light to be resolvable analytically, because of the homotopy analysis method (HAM) or the other series methods, etc., with great accuracy. In numerical computations, the straightforward finite difference schemes work well without requiring the use of Newton's method for the subsequent linearization of the nonlinear difference equations as is utilized in the Keller-Box scheme. Gaussian elimination procedure serves sufficiently for the solution of so-obtained simultaneous difference equations. Such analytic or numerical techniques shall be utilized in the coming Sections by considering some particular types of the surface velocity.

11.1 Two-Dimensional Unsteady Non-similar Flows

The cases of two- and three-dimensional flows follow the same non-similar formulation. Therefore, the preference shall be given the two-dimensional flows because of their mathematical simplicity in comparison with the three-dimensional flows. In the unsteady flows, caused due to uniform stretching/shrinking of the

A. Mehmood, *Viscous Flows*, Mathematical Engineering,
DOI 10.1007/978-3-319-55432-7_11

continuous surfaces, the strength of mathematical difficulty in the non-similar flows depends mostly upon the nature of the wall velocity assumed. In Chap. 8, it was determined that the temporal similarity is admitted only for the linear stretching or shrinking of the sheet when the wall velocity is inversely proportional to t, i.e., $u_w = \frac{ax}{t}$ or $u_w = \frac{ax}{1+\gamma t}$. All other forms of the wall velocity yield non-similar flows. The other source of non-similarity in time is the auxiliary data, that is, the initial and the boundary conditions. In Chap. 8, it was also realized that for a well-posed problem, the initial condition (essentially) and at least one of the boundary conditions must coalesce in order to establish the self-similarity. If the auxiliary data do not allow any such coalescing, then the establishment of self-similarity is impossible. Thus, if the wall velocity does not follow the above-mentioned forms or the auxiliary data do not allow any coalescing of the initial and boundary condition(s), the similarity solution will never be permissible. In all such situations, the temporal non-similarity is deemed unavoidable.

Temporal non-similarity may occur in both the spatially self-similar and non-similar flows. In this Chapter, we shall, however, restrict ourselves to the case of spatially self-similar flows. In such flows, the original three variables (x, y, t) shall be reduced to two due to suitable mixing of the original variables. The reduction of variables, in two-dimensional flow, from three (x, y, t) to two may occur in two ways: If the new variable is constructed due to x and t of the form x/t, then the solutions are usually called *pseudo-steady*; and if the three variables (x, y, t) are reduced to two by any other way, then the solutions are called *semi-similar*. In all those cases, where the spatial similarity is admissible, the similarity variable η is already constructed due to y and x, thus allowing no combination of the form x/t for the new variable. In such flows, the governing unsteady problem is eventually transformed to a partial differential equation admitting self-similarity in x and y but no similarity in time. Such a solution falls into the above-mentioned category of semi-similar solutions. A simple example from this category is the unsteady Crane's flow where the flat sheet is started impulsively to be stretching linearly in x-direction. In this case, the governing equations are given in Eqs. (2.10) and (2.11) (with $w = 0$) and the initial and boundary conditions are of the form

$$\left.\begin{array}{l} \text{at } t \le 0: \ u = v = 0, \forall x, y \\ \text{at } t > 0: \ \left\{\begin{array}{l} u = ax, v = 0, \quad \text{at} \quad y = 0 \\ u = 0, \quad \text{at} \quad y = \infty \end{array}\right. \end{array}\right\}. \tag{11.1a}$$

Sometimes they are also casted into the form

$$\left.\begin{array}{l} \text{at } t < 0: \ u = v = 0, \ \forall\, x, y \\ \text{at } t \ge 0: \ \left\{\begin{array}{l} u = ax, \ v = 0, \quad \text{at} \quad y = 0 \\ u = 0, \quad \text{at } y = \infty \end{array}\right. \end{array}\right\} \tag{11.1b}$$

which in a limiting sense $t \to 0$ is equivalent to (11.1a), that is, $t \to 0^+, u \to ax; t \to 0^-, u \to 0$. However, Eq. (11.1a) will be considered in the

coming analysis. In Eq. (11.1a), the wall velocity shows linear stretching of the wall in x-direction for which the similarity variables are given due to (Chap. 6) by

$$\eta = \sqrt{\frac{a}{\nu}}y, \frac{u}{ax} = f'(\eta), \tag{11.2}$$

in the steady flow situation. These new variables completely eliminate the previous variables from the governing equation, thus reducing it to the self-similar form. The consideration of unsteadiness in this case makes the variable t to appear in the equation of motion. Now, if the wall velocity does follow the form given in Eq. (8.15), then the flow is self-similar while non-similar otherwise. The non-similar or semi-similar formulation of the problem considered in this Section requires a proper extension of the similarity transformations (11.2). Initially, such problems had been investigated due to two different formulations particular to the small time or large time situations. Finally, a unified transformation, valid for small time as well as large time, was introduced by Williams and Rhyne [1]. A thorough discussion on this issue is given in the following paragraph.

The literature available on unsteady flow past the surfaces of finite length is very much rich and authentic, because of the pioneering contributions of the legends of the boundary-layer theory, in comparison with the literature on impulsively started continuous surfaces. Since the history of unsteady flows, caused either due to impulsively started continuous bodies or the bodies of finite length, goes back to the classical Rayleigh's problem, in the Rayleigh's problem the flow is developed in a stationary fluid due to the impulsive (uniform) motion of the bounding wall due to which the vorticity transports from the moving wall to the ambient fluid with the passage of time. After a while, when sufficient time has elapsed, the flow becomes fully developed within a finite thin region near the wall beyond which the ambient situation persists without any change. Such a situation is usually referred to as the establishment of steady state. Because of the above illustration, the boundary-layer seems to grow in time, which actually the case is, and is given by $\delta_R \sim \sqrt{\nu t}$, thus providing a natural length scale to this flow. Such an availability of appropriate length scale makes it possible to construct the new similarity variable $\eta_R = y/\sqrt{\nu t}$ in order to transform the governing partial differential equation of the Rayleigh's problem to an equivalent ordinary differential equation.

On the other hand, an exact similarity solution to the steady two-dimensional case does also exist which is commonly known as the Blasius solution. How the normal length scale δ_R (of Rayleigh's problem) could be utilized in the Blasius flow which is steady in nature. In this case, the boundary-layer thickness develops in streamwise direction (by staying independent of time) due to the presence of external potential flow. Therefore, the time t in the expression of Rayleigh's boundary thickness δ_R could be replaced by x/u_{ref} by interpreting it as the time required by a fluid particle to reach a distance x. In this way, the length scale δ_R modifies to $\delta_{FS} \sim \sqrt{\frac{\nu x}{u_{\text{ref}}}}$ to be utilized in the construction of similarity variable $\eta_{FS} = y\sqrt{\frac{u_{\text{ref}}}{\nu x}}$ of this flow. In this case, u_{ref} denotes the external reference velocity

of the Blasius or the Falkner–Skan type. The subscripts R and FS are particular to the Rayleigh problem and the Falkner–Skan flow, respectively. Thus, in the case of two-dimensional unsteady flow over a finite plate, the Rayleigh's solution and the Blasius or Falkner–Skan solution serve as the initial and final solutions, respectively.

By utilizing the above-named initial and final solutions, the unsteady flow past a wedge has been formulated by several researchers. Because of the availability of similarity variables, that is, $\eta_R = y/\sqrt{\nu t}$ and $\eta_{FS} = y\sqrt{\frac{u_e}{\nu x}}$, two separate formulations have been developed referring to the small time and large time solutions. While doing so, the time has been non-dimensionalized as $\tau = \frac{u_{\text{ref}} t}{x}$. Because of the variables η_R and τ, the resulting formulation agrees well with the Rayleigh's solution for small time but does not match the Falkner–Skan solution for large time. Similarly, the formulation due to η_{FS} and τ fits very well to the Falkner–Skan solution for large τ but deviates from the Rayleigh's solution for small τ. The reason behind this fact is that the so-obtained non-similar equations change their character as τ increases (starting) from 0 and crosses the value $\tau = 1$. Consequently, the transformation serving appropriate for small τ diverges for large τ and the vice versa. This fact was first pointed out by Stewartson [2] in 1951. This issue was finally resolved by Williams & Rhyne [1] by determining a unified formulation which reduces to η_R and τ (formulation) for small τ and $\eta_{FS}\&\tau$ (formulation) for large τ. In doing so, the semi-infinite time domain of τ has been collapsed to closed interval $[0, 1]$ which in fact facilitates in the numerical integration of the governing equations. The new time variable constructed by Williams and Rhyne [1] is given by

$$\xi = 1 - \mathrm{e}^{-\frac{u_{\text{ref}} t}{x}},$$

according to which, $\xi \to 0$ as $\frac{u_{\text{ref}} t}{x} \to 0$ and $\xi \to 1$ as $\frac{u_{\text{ref}} t}{x} \to \infty$. Thus, the steady-state Falkner–Skan solution appears at the end of the new time interval $(\xi = 1)$, and the Rayleigh's solution is recovered at the start of the time interval, that is, at $\xi = 0$. For detailed derivation of such a semi-similar (non-similar) solution, the reader is referred to follow [1].

The transformation developed by Williams and Rhyne has frequently been used in the study of unsteady laminar flows over continuous surfaces or surfaces of finite length (see for instance [3–7] and the references there in). Thus, for the unsteady Crane's flow, the steady similarity transformations (11.2) extend to the semi-similar form as

$$\eta = \sqrt{\frac{a}{\nu\xi}}y,\ \psi = \sqrt{a\nu\xi}\, x f(\xi, \eta),\ \xi = 1 - \mathrm{e}^{-\tau};\ \tau = at, \tag{11.3}$$

due to which the equation of continuity is satisfied identically and the momentum equation takes the form

$$\xi\left(\left(\frac{\partial f}{\partial \eta}\right)^2 - f\frac{\partial^2 f}{\partial \eta^2}\right) = \frac{\partial^3 f}{\partial \eta^3} + \frac{1}{2}(1-\xi)\eta\frac{\partial^2 f}{\partial \eta^2} - \xi(1-\xi)\frac{\partial^2 f}{\partial \eta \partial \xi}, \tag{11.4}$$

subject to the boundary conditions

$$f(0,\xi) = 0, \left.\frac{\partial f}{\partial \eta}\right|_{\eta=0} = 1, \quad \text{and} \left.\frac{\partial f}{\partial \eta}\right|_{\eta=\infty} = 0. \tag{11.5}$$

Clearly, at $\xi = 0$, Eq. (11.4) recovers the Rayleigh's problem, and at $\xi = 1$, it reduces to the self-similar Crane's equation. As evident from their name, semi-similar, such flows do not depart far away from the self-similar solution. Only in a small neighborhood of $\xi = 0$, the solution undergoes temporal transition and finally achieves the steady-state self-similar solution corresponding to the large values of ξ. Because of this fact, the level of (mathematical) difficulty in these "non-similar" problems is not that severe as it is in the case of spatially non-similar problems. These problems can easily be solved by usual finite difference schemes. Asymptotic analytic solutions are also possible due to the conventional asymptotic expansion (in ξ) or due to the homotopy methods. The homotopy analysis method, in particular, works very well with these problems without taking enough long time or facing the issues of convergence. In contrast, the spatially non-similar equations are quite hard to solve with such asymptotic series solution methods such as HAM or HPM.

System (11.4) and (11.5) has been solved analytically due to HAM procedure, and the results have been depicted in Figs. 11.1 and 11.2. The velocity profile can be seen plotted against η at different values of the time variable ξ. For small values of ξ, transition from the Raleigh's solution to that of Crane's can be seen quite obvious upon increasing the values of ξ. For sufficiently large values of ξ, the flow is shown fully developed in the steady state with no further dependence upon time. The coefficient of wall skin-friction modifies in this case as

$$Re_x^{1/2} C_f = \xi^{-1/2}\left.\frac{\partial^2 f}{\partial \eta^2}\right|_{\eta=0}, \tag{11.6}$$

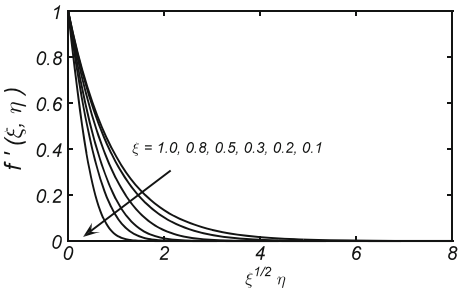

Fig. 11.1 Velocity profile against η for different ξ

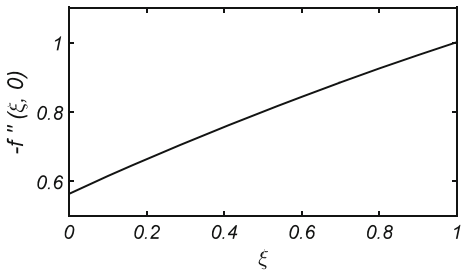

Fig. 11.2 Velocity gradient function at $\eta = 0$ plotted against ξ

where $Re_x = ax^2/v$ is the local Reynolds number. The values of $f''(\xi, 0)$ have been plotted in Fig. 11.2 where the wall velocity gradient can be seen increasing rapidly in the transition time period and stabilizing, afterward, for large values of time.

The same problem was first considered by Wang et al. [8] for the impulsively started stretching sheet. They utilized the usual similarity transformations introduced by Crane for the steady case (Eq. 11.2) and obtained an asymptotic solution for small and large time and a numerical solution as a whole. Their, so-reduced, semi-similar equation appeared in the form

$$\frac{\partial^2 f}{\partial \eta \partial \xi} + \left(\frac{\partial f}{\partial \eta}\right)^2 - f\frac{\partial^2 f}{\partial \eta^2} = \frac{\partial^3 f}{\partial \eta^3}, \tag{11.7}$$

which differs mainly, from Eq. (11.4), in the important Rayleigh's term (second term on the right-hand side). The first term on the left-hand side of Eq. (11.7) seems to stay dominant for small time values, but the contribution of the remaining two terms on the left-hand side, representing the convective acceleration, has also not been restricted to the large time values as has been done in Eq. (11.4). The basic reason behind this fact is the utilization of the transformation group $\eta_{FS}\&\tau$ as we explained previously. On the other hand, Pop and Na [9] also considered the same problem by utilizing the other similarity group, namely the $\eta_R\&\tau$. Consequently, they obtained an equation of form (11.4) with a bit different coefficient given by

$$4at\left(-f\frac{\partial^2 f}{\partial \eta^2} + \left(\frac{\partial f}{\partial \eta}\right)^2\right) = \frac{\partial^3 f}{\partial \eta^3} + 2\eta\frac{\partial^2 f}{\partial \eta^2} - 4t\frac{\partial^2 f}{\partial \eta \partial t}. \tag{11.8}$$

Clearly, for small values of time $(t \to 0)$, Eq. (11.8) recovers the Rayleigh's solution, but for large values of time, the last two terms on the right-hand side of Eq. (11.8) do not seem to vanish out in order to recover the Crane's solution. Thus, in order to find a solution which is uniformly valid for all time, the Williams & Rhyne's transformations (11.3) are observed to be the perfect choice.

11.1.1 Oscillatory Stretching of the Sheet

Continuing with the semi-similar solutions, there are several other forms of the wall velocities for which the resulting equations are semi-similar. A general criterion in this regard is the admissibility of spatial self-similarity by the problem. This can only be ensured when the spatial dependence of the wall velocity follows either the power-law or exponential form as derived in Chap. 5. The problem considered in the above discussion, namely the unsteady Crane's flow, follows the power-law wall velocity with an impulsive start. Another generalization of the Crane's flow is to take the oscillatory stretching rate of the uniform stretching velocity in the form

$$u_w(x,t) = (a\cos\omega t)x.$$

Such a wall velocity was considered by Wang [10] for which he utilized the similarity transformation of form (11.2) and introduced the dimensionless time of the form $\tau = \omega t$. In this case too, he obtained the transformed equation of form (11.7) given by

$$St\,\frac{\partial^2 f}{\partial\eta\partial\tau} + \left(\frac{\partial f}{\partial\eta}\right)^2 - f\frac{\partial^2 f}{\partial\eta^2} = \frac{\partial^3 f}{\partial\eta^3}, \tag{11.9}$$

with a perturbation parameter St representing the frequency of oscillations. The parameter St is defined as the ratio of oscillations' frequency to the amplitude of oscillations which is commonly referred as the Strouhal number, that is, $St = \omega/a$. Large values of St correspond to high-frequency oscillations with very small amplitude. Owing to the physical justification of this behavior, Wang obtained perturbation solution for large values of St. However, a quite exact analytic or numerical solution of Eq. (11.9) which is uniformly valid for small and large values of the Strouhal number is possible to obtain with the aid of commonly used HAM or finite difference schemes. Abbas et al. [11] considered sinusoidal oscillations in the stretching rate of a linearly stretching flat sheet immersed in a non-Newtonian viscoelastic fluid[1] under the influence of uniform magnetic field. They utilized the same transformations as did the Wang [10], that is, Eq. (11.2) by appending $\tau = \omega t$ to it and obtained the semi-similar system of the form

$$St\,\frac{\partial^2 f}{\partial\eta\partial\tau} + \left(\frac{\partial f}{\partial\eta}\right)^2 - f\frac{\partial^2 f}{\partial\eta^2} + M^2\frac{\partial f}{\partial\eta} = \frac{\partial^3 f}{\partial\eta^3} + K\left(s\frac{\partial^4 f}{\partial\eta^3\partial\tau} + 2\frac{\partial f}{\partial\eta}\frac{\partial^3 f}{\partial\eta^3} - \left(\frac{\partial^2 f}{\partial\eta^2}\right)^2 - f\frac{\partial^4 f}{\partial\eta^4}\right), \tag{11.10}$$

[1]The non-Newtonian fluids are not a topic of concern here. This problem has been chosen to report just because of the flow assumptions and solution procedure regardless of the nature of fluid.

subject to the boundary conditions

$$\left.\frac{\partial f}{\partial \eta}\right|_{\eta=0} = \sin\tau,\ f(0,\tau) = 0,\ \left.\frac{\partial f}{\partial \eta}\right|_{\eta=\infty} = 0,\ \left.\frac{\partial^2 f}{\partial \eta^2}\right|_{\eta=\infty} = 0. \tag{11.11}$$

Ignoring the physical nature of the parameters M, K and s, they have simply been considered as pure constants. The authors of [11] obtained a purely analytic solution to the system (11.10)–(11.11), with the aid of HAM, which is uniformly valid for small and large values of St. They also obtained an efficient numerical solution to the same system based on the finite difference scheme and reported a comparison of the two solutions. It is demonstrated (in [11]) that the analytic HAM solution produces sufficiently accurate approximation in order to meet the numerical one. A listing of numerical values of the skin-friction coefficient is given in Table 11.1 for various values of the involved physical parameters.

The problems presented under this head are though semi-similar but differ by a little in the level of difficulty from those considered in this Section prior to this head, corresponding to the impulsively started sheet. In such problems, the boundary conditions stay fixed and the time variable needs to be manipulated only in the governing equations, whereas, in the problems corresponding to the oscillatory rate of stretching, the boundary conditions also modify at every next time step. However, the solution procedure in both the aforementioned cases stays less hectic than those involving the spatial non-similarity, dealt in the previous two Chapters.

Table 11.1 Values of the coefficient of skin-friction due to [11]

K	s	M	$\tau = 1.5\,\pi$	$\tau = 5.5\,\pi$	$\tau = 9.5\,\pi$
0.0	1.0	12.0	11.678656	11.678707	11.678656
0.2			5.523296	5.523371	5.523257
0.5			−3.899067	−3.899268	−3.899162
0.8			−11.674383	−11.676506	−11.676116
1.0			−15.617454	−15.624607	−15.624963
0.2	0.5		5.322161	5.322193	5.322173
	1.0		5.523296	5.523371	5.523257
	2.0		6.087060	6.087031	6.087156
	3.0		6.769261	6.768992	6.769294
	4.0		7.497932	7.406924	7.496870
	5.0		8.232954	8.229085	8.228996
	1.0	5.0	2.323502	2.323551	2.323548
		7.0	3.278018	3.278005	3.278123
		9.0	4.197624	4.197771	4.197733
		12.0	5.423296	5.523371	5.523257
		15.0	6.791323	6.791301	6.791278

11.2 Axially Symmetric Unsteady Non-similar Flows

The unsteady non-similar flow due to a stretching disk follows similarly to the two-dimensional case because of the previously determined similarity between the disk flow and the two-dimensional flow. The case of a stretching cylinder follows also in a, somehow, similar manner but with a little difference in the governing equations because of the presence of transverse curvature parameter. Different from the planner case, the axisymmetric unsteady flow has not been studied any frequently. In this case too, the analogy of semi-similarity persists in the cases when the spatial dependence of the wall velocity follows the similarity criterion of the corresponding self-similar flow. As a consequence of it, the resulting equations also come out of the similar form as did in the previous planner cases. For an unsteady Crane's flow due to an impulsively started stretching cylinder, the governing equations are those given in Eqs. (2.13) and (2.14) subject to the initial and boundary conditions

$$\left.\begin{array}{l} \text{at } t \leq 0: \; u = v = 0, \; \forall \, z, r \\ \text{at } t > 0: \; \left\{ \begin{array}{ll} u = az, \; v = 0, & \text{at } r = R \\ u = 0, & \text{at } r = \infty \end{array} \right. \end{array} \right\}. \tag{11.12}$$

The so-called semi-similarity transformations of this problem come directly in a combination of the similarity transformations of the corresponding self-similar steady flow and those of the famous Rayleigh's problem following the Williams and Rhyne's [1] formulation. The similarity transformations for the steady case are given in Chap. 6 in dimensionless form. In view of these transformations, the similarity variables for the present unsteady problem are constructed (due to [1]) as

$$\eta = \frac{r^2 - R^2}{2R}\sqrt{\frac{a}{\nu\xi}}, \; \psi = \sqrt{a\nu\xi}\, Rzf\,(\xi, \eta), \; \xi = 1 - e^{-\tau}; \tau = at. \tag{11.13}$$

The stream function $\psi\,(r, z, t)$ is related to the velocity components u and v as $ru = \frac{\partial \psi}{\partial r}, rv = -\frac{\partial \psi}{\partial z}$ due to which the equation of continuity (Eq. 2.13) is satisfied identically and Eq. (2.14) transforms as

$$\begin{aligned} \xi\left(\left(\frac{\partial f}{\partial \eta}\right)^2 - f\frac{\partial^2 f}{\partial \eta^2}\right) &= \frac{\partial}{\partial \eta}\left[\left(1 + 2\kappa\sqrt{\xi}\eta\right)\frac{\partial^2 f}{\partial \eta^2}\right] \\ &\quad + (1 - \xi)\left(\frac{1}{2}\eta\frac{\partial^2 f}{\partial \eta^2} - \xi\frac{\partial^2 f}{\partial \eta \partial \xi}\right) \end{aligned} \tag{11.14}$$

Similar to Eq. (11.4), the above equation also recovers the Rayleigh's flow at $\xi = 0$ and the steady (Crane's) flow due to a uniformly stretching cylinder at $\xi = 1$. Based upon this reasoning, the solution of Eq. (11.14) is equally applicable to the

small time as well as to the large time scenarios. The boundary conditions in terms of transformed variables are given by

$$f(0,\xi)=0,\ \left.\frac{\partial f}{\partial \eta}\right|_{\eta=0}=1,\ \left.\frac{\partial f}{\partial \eta}\right|_{\eta=\infty}=0. \tag{11.15}$$

This problem has already been studied in detail by Munawar et al. [12] including the heat transfer phenomena for the cases of prescribed surface temperature (PST) and prescribed heat flux (PHF). Analytic and numerical solutions were obtained due to the HAM and the finite difference numerical scheme, respectively. The HAM solution for the dimensionless stream function is obtained in the form of the series [12]

$$f(\xi,\eta)=\sum_{k=0}^{\infty}\sum_{m=0}^{\infty}\sum_{l=0}^{\infty}\alpha_{m,l}^{k}\xi^{k}\eta^{l}\mathrm{e}^{-m\eta},$$

where the $\alpha_{m,l}^{k}$ are the constant coefficient of the series and m,l,k are the involved indices. The initial solution and the linear operator were chosen of the form

$$f_0(\xi,\eta)=1-\mathrm{e}^{-\eta}\quad\text{and}\quad L=\frac{\partial}{\partial\eta^3}-\frac{\partial}{\partial\eta},$$

respectively.

In the numerical solution, the authors of [12] utilized the finite difference scheme by approximating the partial derivatives by the finite differences of the form

$$\frac{\partial f}{\partial\bar{\eta}}=\frac{f_{j+1}-f_{j-1}}{2\Delta\bar{\eta}},\frac{\partial^2 f}{\partial\bar{\eta}^2}=\frac{f_{j+1}-2f_j+f_{j-1}}{(\Delta\bar{\eta})^2},$$
$$\frac{\partial^3 f}{\partial\bar{\eta}^3}=\frac{f_{j+2}-3f_{j+1}+3f_j-f_{j-1}}{(\Delta\bar{\eta})^3},\frac{\partial f}{\partial\xi}=\frac{f_{j+1}-f_j}{\Delta\xi}$$

where $\bar{\eta}=\frac{1}{1+\eta}$ which transforms the semi-infinite spatial domain $[0,\infty)$ to a bounded interval $[0,1]$ in order to facilitate the numerical computations. The accuracy of the two solutions is shown in Table 11.2 where the analytic and numerical results reported by [12] have been compared. An excellent agreement can be seen in the two solutions. The velocity graphs for different values of the time variable τ are shown in Fig. 11.3. Analogous to Fig. 11.1, with the passage of time the flow develops within the boundary-layer and attains the steady state for sufficiently large values of τ. The coefficient of skin-friction in this case is given by

$$\frac{1}{2}Re_xC_f=\frac{1}{\xi}\left.\frac{\partial^2 f}{\partial\eta^2}\right|_{\eta=0}. \tag{11.16}$$

Table 11.2 Comparison between the analytic and numerical solutions for different values of the curvature parameters κ and ξ, at the 13th-order Padé approximation

$f''(0,\xi)$				
κ	HAM results $\xi = 0.2$	Numerical results $\xi = 0.2$	HAM results $\xi = 0.4$	Numerical results $\xi = 0.4$
0.0	−0.65611	−0.65652	−0.74578	−0.74578
0.2	−0.69813	−0.69910	−0.80232	−0.80251
0.5	−0.75824	−0.75816	−0.88255	−0.88260
1.0	−0.85228	−0.85233	−1.00695	−1.00713
1.5	−0.94979	−0.94983	−1.12328	−1.12331
2.0	−1.02509	−1.02515	−1.42200	−1.42200

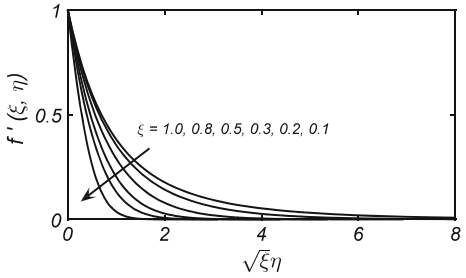

Fig. 11.3 Velocity profile at different ξ values

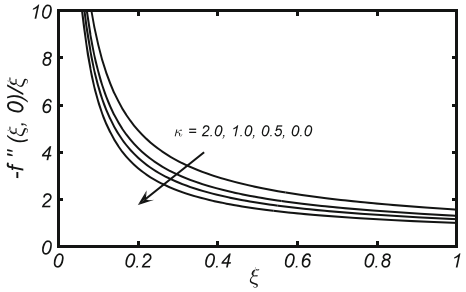

Fig. 11.4 Coefficient of skin-friction against ξ for different κ

The variation of $\frac{1}{2}Re_xC_f$ against ξ for different values of the curvature parameter κ is shown in Fig. 11.4. Obviously, the skin-friction varies quite rapidly for small values of time τ and stabilizes for sufficiently large values of time. The transition time is that which is taken by the impulsively started fluid in establishing the fully developed flow within the boundary-layer. The results of heat transfer phenomena have intentionally been disregarded, and the interested reader is referred to follow Ref. [12] in this regard.

11.2.1 The Case of Oscillatory Stretching

The case of oscillatory stretching rate of the linear stretching velocity of the cylinder's surface, for which the steady flow admits a self-similar solution, follows also in the same manner as does the corresponding planner case. In this case, the rate of stretching is assumed to be a periodic function of sin or cos as considered in the previous Section. Different from the previous case, the oscillatory rate of stretching wall velocity may also be taken as

$$u_w(z,t) = a(1+\epsilon\, cos\, \omega t)z. \tag{11.17}$$

This particular form of the wall velocity has also been investigated by Munawar et al. [13]. In this case, the momentum Eq. (2.14) comes out of the form

$$\left(\frac{\partial f}{\partial \eta}\right)^2 - f\frac{\partial^2 f}{\partial \eta^2} = \kappa \frac{\partial}{\partial \eta}\left((1+\eta)\frac{\partial^2 f}{\partial \eta^2}\right) - St\frac{\partial^2 f}{\partial \eta \partial \tau}, \tag{11.18}$$

and the equation of continuity (2.13) satisfies identically. The so-called semi-similarity transformations, as utilized by [13], read as

$$\eta = \left(\frac{r}{R}\right)^2 - 1,\ \psi = azR^2 f(\eta,\tau),\ \tau = \omega t, \tag{11.19}$$

due to which the boundary conditions in terms of new variables are given by

$$\left.\frac{\partial f}{\partial \eta}\right|_{\eta=0} = 1+\epsilon cos\, \tau, f(0,\tau) = 0,\ \left.\frac{\partial f}{\partial \eta}\right|_{\eta=\infty} = 0, \tag{11.20}$$

where ϵ denotes the amplitude of oscillations; for $\epsilon = 0$ (no oscillations), the case of steady flow is recovered. The coefficient of skin-friction in view of Eq. (11.19) takes the form

$$\frac{1}{2}Re_x C_f = \left.\frac{\partial^2 f}{\partial \eta^2}\right|_{\eta=0}. \tag{11.21}$$

The variation of velocity and the skin-friction coefficient due to the varying values of the Strouhal number and the parameter ϵ have been depicted in Figs. 11.5, 11.6, 11.7, 11.8, and 11.9. Clearly, upon increasing the values of amplitude parameter, the velocity increases and the amplitude of oscillations in the skin-friction graphs increases. Similar trend persists for the increasing values of the Strouhal number also. Development of the flow, for initial values of time, can obviously be seen in Figs. 11.8 and 11.9 where the coefficient of skin-friction undergoes rapid variations for small time values and established afterward.

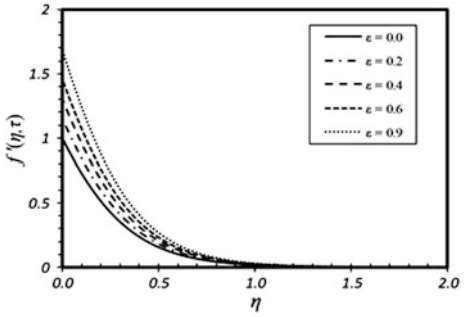

Fig. 11.5 Velocity graph against η for different ϵ

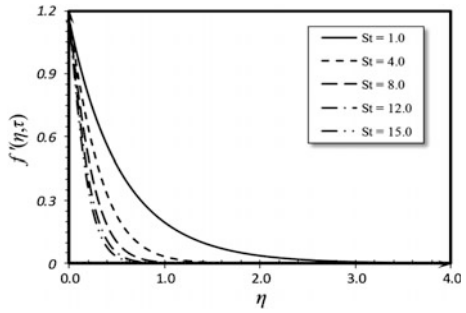

Fig. 11.6 Effect of Strouhal number *St* on velocity profile

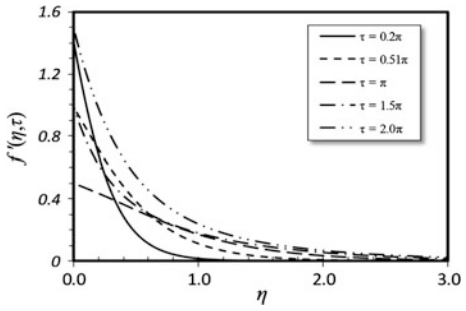

Fig. 11.7 Velocity graph at different time values

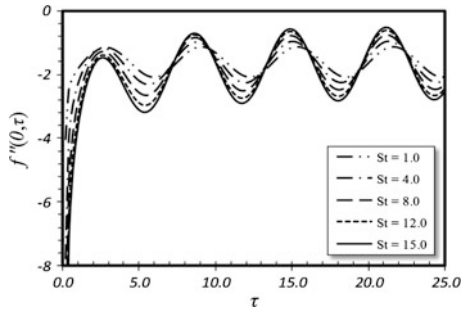

Fig. 11.8 Variation of skin-friction against τ corresponding to various values of *St*

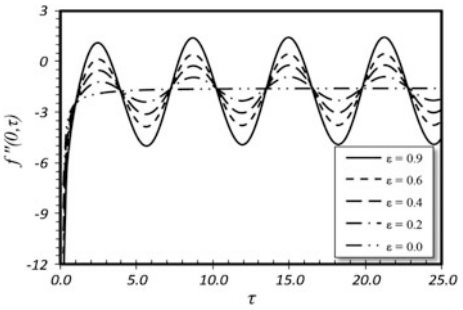

Fig. 11.9 Impact of amplitude parameter ϵ on the skin-friction profile

To all the problems, considered in this Chapter, the name "non-similar" flows has repeatedly been referred, whereas the literature recognizes them as the semi-similar flows. The reason behind their designation as semi-similar is that they do not depart far away from the similarity solution and finally attain the steady-state self-similar solution, particularly in the impulsively started cases. However, besides such a physical nobility, their governing equations never ever allow the reduction of three independent variables to one (the self-similar solution). Because of such a non-reducible nature of their associated manifold, they fail to fulfill the criterion of self-similarity, in general. This is the fundamental reason due to which they have been referred as the time-dependent non-similar flows. However, it has also been stated several times, in this Chapter, that these time-dependent non-similar flows are not that severe and challenging as do the spatially non-similar flows. Therefore, besides calling them the semi-similar flows, it must not be confused that they are not non-similar. Actually, they are non-similar, but the passive nature of temporal non-similarity does not take them far away from the spatially self-similar solution due to which they are commonly known as the semi-similar solutions.

References

1. J.C. Williams III, T.B. Rhyne, Boundary-layer development on a wedge impulsively set into motion. SIAM J. Appl. Math. **38**(2), 215–224 (1980)
2. K. Stewartson, On the impulsive motion of a flat plate in a viscous fluid. Quart. J. Mech. App. Math. **4**, 182–198 (1951)
3. H. Xu, S.J. Liao, Series solution of unsteady magnetohydrodynamic flows of non-Newtonian fluids caused by an impulsively stretching plate. J. Non-Newtonian Fluid Mech. **129**, 46–55 (2005)
4. S.J. Liao, An analytic solution of unsteady boundary-layer flow caused by an impulsively stretching plate. Commun. Nonlinear Sci Numer. Simulat. **11**(3), 326–339 (2006)
5. A. Mehmood, A. Ali, Unsteady boundary-layer flow due to an impulsively started moving plate. Proc. Inst. Mech. Eng. Part G: J. Aero Eng. 221, 385–390 (2007)
6. A. Mehmood, A. Ali, H.S. Takhar, T. Shah, Unsteady three-dimensional MHD boundary-layer flow due to impulsive motion of a stretching surface (Acta Mech. 146, 59–71, 2001), Acta Mech. 199, 241–249 (2008)

7. I. Ahmad, M. Sajid, T. Hayat, M. Ayub, Unsteady axisymmetric flow of a second-grade fluid over a radially stretching sheet. Comput. Math. Appl. **56**(5), 1351–1357 (2008)
8. C.Y. Wang, Q. Du, M. Miklavcic, C.C. Chang, Impulsive stretching of a surface in a viscous fluid. SIAM J. Appl. Math. **57**(1), 1–14 (1997)
9. I. Pop, T.Y. Na, Unsteady flow past a stretching sheet. Mech. Res. Commun. **23**(4), 413–422 (1996)
10. C.Y. Wang, Nonlinear streaming due to the oscillatory stretching of a sheet in a viscous fluid. Acta Mech. **72**, 261–268 (1988)
11. Z. Abbas, Y. Wang, T. Hayat, M. Oberlack, Hydromagnetic flow in a viscoelastic fluid due to the oscillatory stretching surface. Int. J. Non-Linear Mech. **43**, 783–793 (2008)
12. S. Munawar, A. Mehmood, A. Ali, Time-dependent flow and heat transfer over a stretching cylinder. Chin. J. Phys. **50**(5), 828–848 (2012)
13. S. Munawar, A. Mehmood, A. Ali, Unsteady flow of viscous fluid over the vascillate stretching cylinder. Int. J. Numer. Methods Fluids **70**, 671–681 (2012)

Part IV
Turbulent Flows

Chapter 12
Turbulent Flow Due to Moving Continuous Surfaces

The turbulent flow due to moving continuous surfaces is another aspect of the viscous boundary-layers in addition to the laminar flows presented in the previous two parts. The literature on turbulent boundary-layer flows due to the moving (translating) or stretching surfaces is, literally, very few and is strictly limited to the uniformly moving plate and the slim continuous cylinder cases only. These flows were also considered by Sakiadis in his pioneering papers [1, 2] on this topic. In comparison with the laminar flows of this class, the turbulent flows are almost completely unknown to the best of our knowledge. After the historic initiative of Sakiadis, the idea had not been progressed, so far, by the subsequent investigators in the case of turbulent flows. Ultimately, this created a huge gap between the laminar and the turbulent flows of this class. The present chapter focuses particularly on the turbulent flow due to the translating or stretching continuous surfaces. Sakiadis [1, 2] considered the turbulent flow due to a uniformly moving flat plate and a long slim continuous cylinder of constant cross section. In Sect. 12.1, the Sakiadis' turbulent flow in the said two cases is being presented while the Crane's turbulent flow, namely due to the stretching sheet and the stretching cylinder, has been considered in Sect. 12.2. Approximate analytic solution in all the four cases has been obtained due to the integral method approach.

12.1 Turbulent Sakiadis Flow

12.1.1 Two-Dimensional Case

The two-dimensional laminar boundary-layer flow of an incompressible viscous fluid is governed by Eqs. (2.10)–(2.11) (with $w \equiv 0$) where the right-hand side involves the derivative of the laminar shear stress only. In the turbulent two-dimensional flows too, the governing system [Eqs. (2.10)–(2.11)] stays the

A. Mehmood, *Viscous Flows*, Mathematical Engineering,
DOI 10.1007/978-3-319-55432-7_12

same but with a modified right-hand side. The shear stress, of turbulent flow, does not follow the simple Newton's law of viscosity (only) but involves an additional contribution due to the turbulent eddies. The description of such turbulent eddies is not any straightforward and requires their appropriate modeling. Therefore, different describing models for the turbulent Reynolds stresses have been developed, in this regard. The selection of appropriate turbulent model depends strongly upon the nature of flow, under investigation. Based upon empirical data, the turbulent shear stresses have been modeled in terms of physical boundary-layer parameters and such empirical models have their general acceptability having the capacity of producing sufficiently accurate results. Nevertheless, the numerical or theoretical solution of a turbulent flow always requires a comparison with the experiment in order to state a concrete conclusion about the studied particular flow. Unfortunately, the Sakiadis' turbulent flow has never been studied experimentally to the best of our knowledge. Because of this hindrance, it has always been impossible to compare the theoretical results with any experimental data.

The current theoretical analysis compromises of an approximate integral method solution for various power-law velocity profiles. More clear and authentic picture of these flows will stay pending until the availability of experimental data for these flows.

Approximate solution

The momentum integral equation for a two-dimensional Sakiadis flow is given in Eq. (2.26). For laminar flows, the wall shear stress $(\tau_{x,0})$ simply follows the Newton's law of viscosity, whereas, for turbulent flows, it requires appropriate modeling. Based on the Blasius law of friction, the famous so-called wall law of the pipe flow is equally valid for the two-dimensional case also and is given by

$$\tau_{x,0} = \rho V_{\alpha}^2, V_{\alpha} = 0.150 u_w^{7/8} \left(\frac{\nu}{\delta}\right)^{1/8}, \tag{12.1}$$

where V_{α} denotes the friction velocity. The momentum and displacement thicknesses in this case are defined as

$$\theta = \int_0^{\delta} \left(\frac{u}{u_w}\right)^2 \mathrm{d}y, \tag{12.2}$$

and

$$\delta^* = \int_0^{\delta} \frac{u}{u_w} \mathrm{d}y, \tag{12.3}$$

respectively. The momentum integral Eq. (2.26) can also be rewritten in terms of momentum thickness as

$$\frac{\mathrm{d}}{\mathrm{d}x}\left(u_w^2\theta\right) = \frac{\tau_{x,0}}{\rho}. \tag{12.4}$$

Sakiadis utilized the famous power-law velocity profile of the form

$$\frac{u}{u_w} = 1 - \left(\frac{y}{\delta}\right)^{\frac{1}{n}}, \tag{12.5}$$

in his integral method and chose to use the value $n = 7$. The substitution of Eq. (12.5) in momentum integral Eq. (12.4), for $n = 7$, results in a first-order ordinary differential equation in $\delta(x)$, of the form

$$\frac{1}{36}\frac{\mathrm{d}\delta}{\mathrm{d}x} = 0.0225 Re_\delta^{-1/4}, \tag{12.6}$$

where $Re_\delta = \frac{u_w \delta}{\nu}$ is the Reynolds number based on the boundary-layer thickness $\delta(x)$. The integration of Eq. (12.6) yields

$$\frac{\delta}{x} = 1.01002 Re_x^{-1/5}. \tag{12.7}$$

The availability of $\delta(x)$ helps in furnishing the other quantities of interest such as the momentum and displacement thicknesses and the coefficient of wall skin-friction which are calculated as

$$\frac{\theta}{x} = 0.028056 Re_x^{-1/5}, \tag{12.8}$$

$$\frac{\delta^*}{x} = 0.126225 Re_x^{-1/5}, \tag{12.9}$$

and

$$C_f = 0.044890 Re_x^{-1/5}, \tag{12.10}$$

respectively.

It is a generally observed fact that the velocity profile in the turbulent boundary-layer becomes fuller upon increasing the flow Reynolds number. In the same manner, the power-law velocity profile given in Eq. (12.5) becomes fuller upon increasing the power-law index n, such as $n = 8, 9$ or 10. In view of the available experiences with the power-law velocity profile, it has now generally been admitted that the 1/7th power-law profile approximates well for the turbulent Reynolds numbers immediately next to the transition region and gives poor approximation for moderate and higher values of the turbulent Reynolds number. The 1/8th or 1/9th power-law profiles fit quite well to the experimental data for

moderate Reynolds numbers, that is, of the order of 10^7 or 10^8 and the 1/10th power-law profile for the turbulent Reynolds numbers of the order of 10^9 and 10^{10} as is also observed in the case of rotating disk flow. In what follows, the Sakiadis' integral solution seems to be limited to small turbulent Reynolds numbers and requires to be improved for moderate and higher turbulent Reynolds numbers. In this regard, the values 8, 9, and 10 of the power-law index "n" have also been considered and the results for physical quantities of interest have been furnished in the following.

To include the results for other values of n (i.e., $n = 8, 9$ & 10), the general 1/nth power-law profile, given in Eq. (12.5), is utilized. In doing so, Eq. (12.6) modifies as

$$\frac{\mathrm{d}\delta}{\mathrm{d}x} = 0.0225 C_{1/n}^{-1} Re_{\delta}^{-1/4}, \tag{12.11}$$

which integrates to give

$$\frac{\delta}{x} = 0.05745 C_{1/n}^{-4/5} Re_x^{-1/5}, \tag{12.12}$$

where $C_{1/n} = 1 - 2A + B; A = \frac{n}{n+1}, B = \frac{n}{n+2}$. Consequently, Eqs. (12.8)–(12.10) do also modify and, respectively, read as

$$\frac{\theta}{x} = 0.05745 (C_{1/n}^{-1} Re_x)^{-\frac{1}{5}}, \tag{12.13}$$

$$\frac{\delta^*}{x} = 0.05745 \frac{(1-A)}{C_{1/n}} (C_{1/n}^{-1} Re_x)^{-\frac{1}{5}}, \tag{12.14}$$

$$C_f = 0.09192 (C_{1/n}^{-1} Re_x)^{-\frac{1}{5}}, \tag{12.15}$$

The Sakiadis' solution for 1/7th profile is also contained in the results given in Eqs. (12.12)–(12.15) and can readily be recovered by substituting $n = 7$ (see Table 12.1). The above results for 1/nth power-law profile are summarized in Table 12.1 and have also been compared to the case of surface of finite length. The boundary-layer thickness for continuous surface is quite larger than that of surface of finite length. Because of this fact, the coefficient of skin-friction is smaller for continuous surface in comparison with the finite surface. The momentum thicknesses in the two cases are, however, comparable, but the displacement thicknesses of the two cases differ by large from each other.

The velocity curves for $n = 7, 8, 9$ & 10 are plotted in Fig. 12.1 showing that the velocity becomes fuller upon increasing the power-law index n. The boundary-layer, momentum and displacement thicknesses, and the coefficient of skin-friction are plotted in Figs. 12.2, 12.3, 12.4, and 12.5 against the longitudinal

Table 12.1 Comparison between the continuous and the finite surface cases

	$1/n$	$\frac{\delta}{x} Re_x^{1/5}$	$\frac{\theta}{x} Re_x^{1/5}$	$\frac{\delta^*}{x} Re_x^{1/5}$	$C_f Re_x^{1/5}$
Continuous surface	1/7	1.01002	0.0280562	0.1262253	0.0448900
	1/8	1.20742	0.0268317	0.134158	0.0429307
	1/9	1.41769	0.0257761	0.141769	0.0412418
	1/10	1.64031	0.0248531	0.149119	0.0397650
Finite surface	1/7	0.3700	0.0360	0.0460	0.0576
	1/8	0.3983	0.0354	0.0442	0.0566
	1/9	0.4260	0.0350	0.0430	0.0557
	1/10	0.4526	0.0343	0.0411	0.0549

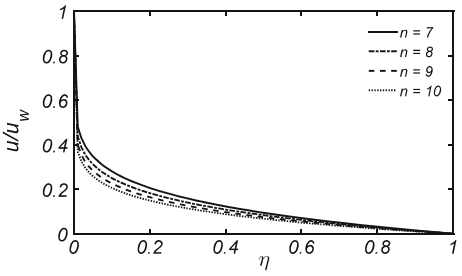

Fig. 12.1 Power-law velocity profile

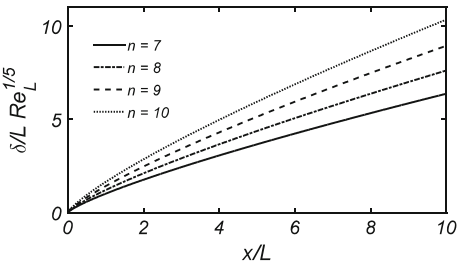

Fig. 12.2 Variation of boundary-layer thickness in x

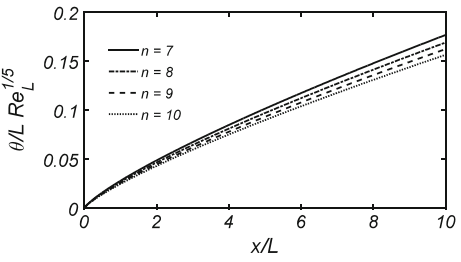

Fig. 12.3 Momentum thickness plotted against x

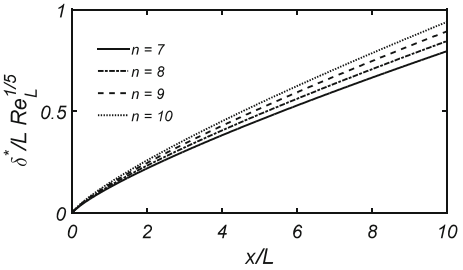

Fig. 12.4 Dependence of displacement thickness upon x

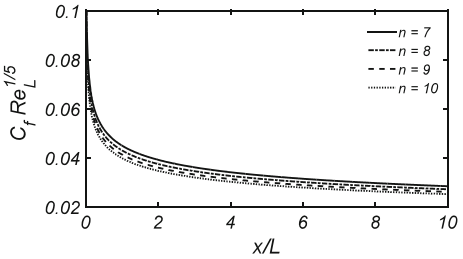

Fig. 12.5 Coefficient of local skin-friction plotted against x

variable x. The three thicknesses, namely the boundary-layer, the momentum, and the displacement ones grow almost linearly as one progresses in the downstream direction.

The consequence of the growing boundary-layer thickness is the decrease in the wall skin-friction coefficient at downstream locations. Furthermore, the momentum thickness decreases and the displacement thickness increases upon increasing the values of n.

12.1.2 The Cylinder Case

The turbulent flow due to a moving continuous cylinder was also investigated by Sakiadis [2] himself with the aid of integral method. He utilized the same 1/7th power-law profile of the continuous flat plate in this case too. Unfortunately, Sakiadis failed in obtaining physically reliable results in this case. However, the method developed by him involves great mathematical beauty and allows a direct comparison with the results of corresponding flat surface case. The momentum integral equation applicable to this case is given in Eq. (2.29) (for a permeable surface), and in the case of impermeable surface, the normal wall velocity must be taken equal to zero, that is, $v_w = 0$. Following the previous case, Eq. (2.29) (with $v_w = 0$) can also be rewritten as

$$\frac{\mathrm{d}}{\mathrm{d}z}\left(u_w^2 R\theta\right) = R\frac{\tau_{z,0}}{\rho}, \tag{12.16}$$

where R denotes the radius of the infinite cylinder and θ denotes the momentum thickness given by

$$\theta = \int_R^\delta \left(\frac{u}{u_w}\right)^2 r\mathrm{d}r,$$

which for the cylinder of constant radius $R = R_0$ reads as

$$\theta = \int_{R_0}^\delta \left(\frac{u}{u_w}\right)^2 r\mathrm{d}r.$$

The momentum area, in this case, is obtained due to the momentum thickness as

$$\Theta = \pi\left[(R_0+\theta)^2 - R_0^2\right].$$

The famous wall law of the pipe flow, given in Eq. (12.1), is assumed to be applicable in this case too for the approximation of wall shear stress. The utilization of the 1/7th power-law profile of the form given in Eq. (12.5) transforms Eq. (12.16) to the form

$$\frac{\mathrm{d}}{\mathrm{d}z}\left[\delta\left(\frac{1}{36}+\frac{1}{120}\frac{\delta}{R_0}\right)\right] = 0.0225\left(\frac{\delta}{z}\right)^{-1/4} Re_z^{-1/4}. \tag{12.17}$$

Integration of above equation results in a nice mathematics which allows a direct comprises between the present case and the case of the corresponding flat continuous surface. Equation (12.17) integrates to give

$$\left[\frac{\delta}{z}\left(1+0.167\frac{\delta}{R_0}\right)\right] = 1.01002\left(\frac{\delta}{z}\right)^{-1/4} Re_z^{-1/4},$$

or

$$\frac{\delta}{R_0} = \lambda\phi^{4/5}, \tag{12.18}$$

where $\phi = \left(\frac{z}{R_0}\right)^{5/4} Re_z^{-1/4}$ and λ comes out to be the ratio of cylinder's boundary-layer thickness to that of the flat-plate case, that is, $\lambda = \delta/\delta_p$. The calculated values of ϕ, due to Eq. (12.18), give the ratio of the boundary-layer thickness of the present case to the flat-plate case. For particularly chosen values of

Table 12.2 Values of λ obtained due to 1/7th power-law profile

$\phi^{\frac{1}{5}}$	λ
0	1.000
0.5	0.987
1.0	0.891
1.5	0.682
2.0	0.500
2.5	0.371
3.0	0.281
3.5	0.220
4.0	0.177
5.0	0.122
6.0	0.088
7.0	0.068

ϕ, the corresponding values of λ are listed in Table 12.2. Contrary to the laminar case, the calculated boundary-layer thickness in the cylinder case comes out to be less thick than that of the flat-plate case (see Table 12.2), which is of course incorrect. In actual, the boundary-layer thickness in the cylinder case is larger than the corresponding flat-plate case because of the presence of surface curvature. This fact has also been observed in the self-similar and non-similar flows on a continuous cylinder in the previous two parts. Such a flaw in the present results forbade one from the further analysis.

The ratio of the surface drag of the two cases, namely the cylinder and the flat plate, is given by

$$\frac{D}{D_p} = \left(1 + 0.152\frac{\delta}{R_0}\right)\phi, \tag{12.19}$$

which is also underpredicted by the present method (see Table 12.3). Sakiadis held responsible, however, partly, to the utilized 1/7th power-law profile for such incorrect results.

The generalization of the Sakiadis' results for the 1/*n*th power-law profile is also obtained by utilizing the general power-law profile given in Eq. (12.5). The momentum integral Eq. (12.16), after the utilization of Eq. (12.5), results in the following form

$$\frac{\mathrm{d}}{\mathrm{d}z}\left[\delta\left(K_1 + \frac{1}{2}K_2\frac{\delta}{R_0}\right)\right] = 0.0225\left(\frac{\delta}{z}\right)^{-1/4} Re_z^{-1/4}, \tag{12.20}$$

where $K_1 = -2(A - B - C), K_2 = AD^{-1} - 4D; C = \frac{B}{n}, D = \frac{n}{2n+1}$.

Integration of Eq. (12.20) again results in the form of ratio of two boundary-layer thicknesses, as before, that is,

Table 12.3 Ratio of the surface drag predicted by 1/7th power-law profile

$\phi^{\frac{1}{5}}$	D/D_p
0	1.00
0.5	1.00
1.0	1.01
1.5	1.05
2.0	1.11
2.5	1.18
3.0	1.25
3.5	1.33
4.0	1.40
5.0	1.54
6.0	1.65
7.0	1.75

$$K_1 \frac{\delta}{z}\left(1+\frac{5}{9}\frac{K_2}{K_1}\frac{\delta}{R_0}\right) = 0.028125\left(\frac{\delta}{z}\right)^{-1/4} Re_z^{-1/4},$$

or

$$\frac{\delta}{R_0} = \lambda_{1/n}\phi^{4/5}, \tag{12.21}$$

where $\lambda_{1/7} \equiv \lambda$. The values of the ratio $\lambda_{1/n}$ are listed in Table 12.4 for different values of ϕ corresponding to various values of the power-law index n. Evidently, the 1/8th,…,1/10th profiles also fail to predict the correct results as the ratio $(\lambda_{1/n})$ quickly becomes less than 1. However, the ratio is observed to stay greater than 1 a little bit longer for greater values of n in comparison with the smaller values of n.

Table 12.4 Summarized results for various values of n in the axisymmetric case

$\phi^{1/5}$	$\lambda_{1/n}$			
	$n = 7$	$n = 8$	$n = 9$	$n = 10$
0.0	1.009988	1.207380	1.417506	1.640247
0.5	1.001619	1.195741	1.401729	1.619465
1.0	0.902676	1.062546	1.227275	1.397360
1.5	0.697155	0.803691	0.909795	1.017103
2.0	0.508408	0.578480	0.647087	0.715591
2.5	0.375222	0.423967	0.471305	0.518745
3.0	0.285203	0.320999	0.355611	0.390268
3.5	0.223301	0.250739	0.277202	0.303691
4.0	0.179422	0.201166	0.222104	0.243059
5.0	0.123252	0.137952	0.152080	0.166218
6.0	0.090121	0.100778	0.111012	0.121252
7.0	0.068961	0.077076	0.084876	0.092655

This indicates the requirement of some major modification in the integral method for the turbulent flow on a continuous cylinder.

12.2 Turbulent Crane's Flow

The turbulent (Crane's) flow due to a stretching continuous surface either in the two-dimensional planer case or axially symmetric case is the subject of this Section. After the Sakiadis' pioneering work, the turbulent flow due to moving continuous surfaces has never been considered to the best of our knowledge. Besides the fundamental nature of these flows, they still require proper attention by the theorists and the experimentalists for their complete understanding and further exploration.

At this point, the author takes the privilege to express that the modern developments in CFD and the commercialization of research have forced the new entering scientists and the engineers to get involved in the commercially sponsored research. Consequently, the topics of fundamental research kept on being ignored with the passage of time and now they have totally become "outdated." Following the engineers, the theorists and more particularly the Mathematicians and the Physicists have also been involved in such a CFD-based research by ignoring the mathematical/theoretical development of the field. With the continued practice of this trend, a time may come when the new generation will totally be unaware of the fundamental topics and tools of research in fluid dynamics. In what follows, the big lose will definitely be borne by the Mathematics. Therefore, this is a time when the competent researchers in the field of fluid dynamics must also spend their efforts on the theoretical research especially on mathematical methods in order to make the new generations well aware of the advanced research bearing a strong connection with its essential fundamental basis. Because of these reasons, the famous Sakiadis and Crane's flows must be given proper attention by the experimentalists as well as theorists in order to develop appropriate theoretical procedures regarding their investigation. The axially symmetric flow of a moving or stretching cylinder, as considered in the previous and the current sections, respectively, reveals the scarce of the availability of the authentic data and thus the handicapping of the theoretical procedures.

In the following, the turbulent viscous flow due to a stretching sheet and a stretching cylinder is considered. The previously utilized integral method has again been employed here by using general power-law velocity profile. The presented results are, however, not any authentic rather misleading in the cylinder case, but nevertheless have been reported for the purpose of motivation.

12.2.1 Stretching Sheet

The turbulent flow due to a stretching sheet is also governed by the same equation [Eq. (2.26)] as utilized in the previous section. The pipe law of friction velocity [Eq. (12.1)] is also assumed applicable here. In view of these assumptions, the momentum integral equation [Eq. (2.26)] after the substitution of self-similar 1/*n*th power-law profile takes the form

$$C_{1/n}\frac{1}{x^2}\frac{\mathrm{d}}{\mathrm{d}x}\left(x^2\delta\right) = 0.0225\,Re_{\delta}^{-1/4}. \tag{12.22}$$

Equation (12.22) admits a solution of the power-law form given by

$$\frac{\delta}{x} = K_{1/n}^{\delta}\,x^{\alpha_e-\frac{3}{5}}\,Re_x^{-1/5}, \tag{12.23}$$

where $K_{1/n}^{\delta}$ and α_e are pure dimensionless constants and are given by

$$K_{1/n}^{\delta} = 0.022375\,C_{1/n}^{-4/5}, \quad \text{and} \quad \alpha_e = \frac{3}{5}. \tag{12.24}$$

Corresponding to various values of n, the values of $K_{1/n}^{\delta}$ are shown in Table 12.5.

Because of these values given in Eq. (12.24), Eq. (12.23) finally furnishes as

$$\frac{\delta}{x} = 0.022375(C_{1/n}^4\,Re_x)^{-\frac{1}{5}}. \tag{12.25}$$

With the aid of Eq. (12.25), the expressions of the momentum and displacement thicknesses and of the wall skin-friction coefficient are furnished as

$$\frac{\theta}{x} = 0.022375(C_{1/n}^{-1}\,Re_x)^{-\frac{1}{5}}, \tag{12.26}$$

$$\frac{\delta^*}{x} = 0.022375(1-A)(C_{1/n}^4\,Re_x)^{-\frac{1}{5}}, \tag{12.27}$$

Table 12.5 Values of the constant coefficient [defined in Eq. (12.24)] for various n in the Crane's flow

1/*n*	$K_{1/n}^{\delta}$	
	Two-dimensional	Axisymmetric
1/7	0.393461	0.320875
1/8	0.47036	0.381278
1/9	0.552268	0.444873
1/10	0.638992	0.511402

Table 12.6 Summarized results for turbulent stretching sheet flow

$1/n$	$\frac{\delta}{x} Re_x^{1/5}$	$\frac{\theta}{x} Re_x^{1/5}$	$\frac{\delta^*}{x} Re_x^{1/5}$	$C_f Re_x^{1/5}$
1/7	0.393461	0.0109295	0.0491827	0.0568182
1/8	0.470360	0.0104524	0.0522622	0.0543382
1/9	0.552268	0.0100412	0.0552268	0.0522006
1/10	0.638992	0.0096817	0.0580902	0.0503314

$$C_f = 0.116345(C_{1/n}^{-1} Re_x)^{-\frac{1}{5}}, \tag{12.28}$$

respectively. The above results are summarized in the form of a Table for various values of n in Table 12.6.

12.2.2 Stretching Cylinder

The case of uniformly stretching cylinder follows similarly as does the case of uniformly translating cylinder considered in the previous Section. After the substitution of $1/n$th power-law velocity profile given in Eq. (12.5), the governing momentum integral equation [Eq. (12.16)], in view of Eq. (12.1), takes the form

$$2K_1\left(1+\frac{1}{2}\frac{z}{\delta}\frac{\mathrm{d}\delta}{\mathrm{d}z}+\frac{1}{2}\frac{z}{R}\frac{\mathrm{d}R}{\mathrm{d}z}\right)+K_2\frac{\delta}{R}\left(1+\frac{z}{\delta}\frac{\mathrm{d}\delta}{\mathrm{d}z}\right)=0.0225\left(\frac{\delta}{z}\right)^{-5/4}Re_z^{-1/4}. \tag{12.29}$$

The above equation follows a solution of the form

$$\frac{\delta}{R_0}=K_{1/n}^{\delta}\left(\frac{z}{R_0}\right)^{m_1}Re_{R_0}^{-1/5}, \tag{12.30}$$

under the restriction that the radius R of the cylinder must also follow the same form as does the boundary-layer thickness, that is,

$$\frac{R}{R_0}=\left(\frac{z}{R_0}\right)^{m_2}Re_{R_0}^{-1/5}. \tag{12.31}$$

The constant $K_{1/n}^{\delta}$ and the exponents m_1 and m_2, appearing in Eqs. (12.30)–(12.31), are pure dimensionless constants. In this case, it is found that $m_1 = m_2 = 3/5$, and $K_{1/n}^{\delta}$satisfies the following equation:

$$K_1+\frac{1}{2}K_2K_{1/n}^{\delta}=0.007031\left(K_{1/n}^{\delta}\right)^{-5/4}. \tag{12.32}$$

Table 12.7 Summarized results for the turbulent stretching cylinder flow

$1/n$	$\frac{\delta}{z} Re_z^{1/5}$	$\frac{\Theta}{\pi z^2} Re_z^{2/5}$	$\frac{\bar{\delta}^*}{\pi z^2} Re_z^{2/5}$	$C_f Re_z^{1/5}$
1/7	0.320875	0.018684	0.087083	0.059790
1/8	0.381278	0.017896	0.093280	0.057267
1/9	0.444873	0.017219	0.099391	0.055100
1/10	0.511402	0.016630	0.1050436	0.053214

The values of $K_{1/n}^{\delta}$ corresponding to different values of n are listed in Table 12.5. Important quantities of physical interest such as the boundary-layer thickness, momentum and displacement areas, and the coefficient of wall skin-friction are given by

$$\frac{\delta}{z} = K_{1/n}^{\delta} Re_z^{-\frac{1}{5}},$$

$$\frac{\Theta}{\pi z^2} = 2\left(K_1 + \frac{1}{2} K_2 K_{1/n}^{\delta}\right) K_{1/n}^{\delta} Re_z^{-\frac{2}{5}},$$

$$\frac{\bar{\delta}^*}{\pi z^2} = \left((2 - 2A) + (1 - 2D) K_{1/n}^{\delta}\right) K_{1/n}^{\delta} Re_z^{-\frac{2}{5}},$$

$$C_f = 0.045 \left(K_{1/n}^{\delta}\right)^{-\frac{1}{4}} Re_z^{-\frac{1}{5}}.$$

Corresponding to the various values of the power-law index n, the results are summarized in Table 12.7.

References

1. B.C. Sakiadis, Boundary-layer behavior on continuous solid surfaces: II the boundary-layer on a continuous flat surface. AIChE **7**(2), 221–225 (1961)
2. B.C. Sakiadis, Boundary-layer behavior on continuous solid surfaces: III the boundary-layer on a continuous cylindrical surface. AIChE **7**(3), 467–472 (1961)